Doctoral Dissertation (Shinshu University)

A study on power generation from low grade heat using Organic Rankine Cycle system in Thailand

March 2018

SORAWIT SONSAREE

Sorawit Sonsaree: *A study on power generation from low grade heat using Organic Rankine Cycle system in Thailand*, Doctoral Dissertation, March 2018

SUPERVISORS:
Kiyoshi Tanaka
Tatsunori Asaoka
Somchai Jiajitsawat
Hernán Aguirre

Dedicated to my family,

Who has always been with me in happiness and sadness.

ABSTRACT

An Organic Rankine Cycle (ORC) system has been widely applied for power generation from low-temperature heat sources such as solar energy, geothermal, biomass, wasted heat from industrial processes, etc. However, this technology is less applicable for the heat source having temperature below 70 °C due to a combination of market and technical barriers. Moreover, there are only a few designed to utilize lower-temperature heat supplies on a small-scale ORC power generation. ***Chapter 1*** introduces a concept and scope of this thesis. ***Chapter 2*** describes the theoretical of the main components of the proposed systems are: solar water heating system (SWHS), vapor compression heat pump (VCHP), gas engine-driven heat pump (GEHP), absorption heat transformer (AHT), and Organic Rankine Cycle (ORC) systems. ***Chapter 3***, 19 fluids were investigated to find the suitable working fluid for an ORC system and a VCHP system. The operating conditions of the ORC system were power output of 60 kW_{th}, ORC evaporating temperature was in a range of 60 to 100 °C and ORC condensing temperature of 35 °C. Moreover, isentropic efficiencies of pump and turbine were 80 and 85%, respectively. It was found that the suitable working fluid for the ORC system is R-365mfc, R-245ca, R-245fa, and R-1234zez, due to they gave low mass flow rate, low evaporating pressure and high thermal efficiency. In addition, it low global warming potential (GWP), toxicity, and non-flammable. For the VCHP system, the operating conditions were cooling capacity of 10 kW, VCHP evaporator temperature was set at 60 °C, required of hot water temperature is around 70 to 90 °C. Moreover, isentropic efficiency of compressor, degree of superheating and sub-cooling is 80%, and 5 °C, respectively. It was found that the suitable working fluid of the VCHP system is R-365mfc due to its low maximum pressure for the heat pump compressor and the highest value of COP for supplying heat at around 70 to 90 °C.

Chapter 4 analyzes the low-heat upgrading technologies for ORC Power Generation; three upgrading technologies for recovering industrial waste heat (IWH) to work in conjunction with ORC generation are evaluated and compared. These three systems: (i) Vapor compression heat pump (VCHP), (ii) Gas engine-driven heat pump (GEHP), and (iii) Absorption heat transformer (AHT), are mathematically modeled considering a thermal capacity of 250 kW for all three systems. For VCHP and GEHP, the working fluid is R-365mfc, while the AHT uses H_2O-LiBr. In each combination, a 20 kW_e ORC power generator with R-245fa as working fluid is connected. The results were found that, the VCHP system was considered the most suitable in terms of its compactness, and simplicity in installation, operation and maintenance. According to economic analysis, when the temperature of heat source is around 63 °C, VCHP-ORC also achieves the lowest levelized cost of electricity (LCOE), followed by AHT-ORC and GEHP-ORC, respectively.

Chapter 5 simulates the performance of the VCHP-ORC power system while the wasted industrial heat is available and upgraded by solar water heating system (SWHS). In this Chapter, simulates the performance of the VCHP system modeled in *Chapter 4* and integrated with the ORC system supplied by the low-grade IWH upgraded by the SWHS for

power generation; the supplied heat to the system is at temperature below 70 °C. A SWHS and a VCHP are used to boost up the heat. A 400 kW thermal capacity VCHP, with R-365mfc as the working fluid, is used to rise the heat from IWH and SWHS before supplying to a 60 kW_e ORC power generator with R-245fa from KOBELCO Company. Three types of solar collectors were used to generate heat: flat-plate, heat pipe evacuated-tube and compound parabolic concentrator (CPC). Between 300 and 700 units of each type of the collectors were connected in parallel. The system is mathematically modeled and simulated to evaluate the net power output, the CO_2 emission, and the LCOE. Six industrial areas consist of, Chiang Mai, Bangkok, Ratchaburi, Songkhla, Nakhon Ratchasima, and Chon Buri, that represent the north, central, west, south, north-east and east part of Thailand, respectively. Their weather data was taken for the simulations. The simulation results showed that the system produced high electricity when the number of the collectors is increased. Moreover, the system located in Chiang Mai produced the highest amount of electricity with the lowest LCOE.

Chapter 6 area where the only heat source is a SWHS were considered, particularly the case which would make the use of heat boosters lose their effectiveness. This was done taking into account that a system that only requires solar collectors, which are more common in Thailand, would be more interesting for the Department of Alternative Energy Development and Efficiency (DEDE) of Ministry of Energy, and reduce the barrier from its implementation. In this Chapter, evaluate a small-scale solar Organic Rankine Cycle (SORC) power system with temperature below 100 °C; the system performance was analyzed based on two capacities for the ORC system with R-245fa (20 and 60 kW_e) combined in four different configurations with three types of stationary solar collectors (Flat-plate, evacuated-tube and CPC solar collectors). The testing configuration consists of solar collectors between 100 and 1200 units integrated with one, two, and three units of a 20 kW_e ORC system, and one unit of a 60 kW_e ORC system. This system was mathematically modeled and simulated to obtain the optimal flow rate of hot water for the maximum power output, the minimum CO_2 emission, and the LCOE. The weather data from Bangkok chosen as a representative city in the central part of Thailand was used for simulations. The study results were presented according to power output and environment impact based on each model, type, and the number of the employed collectors. The simulation results show that, with the same number of solar collectors, the system can produce the highest power output, when the system combined with the CPC collectors. In terms of the economic analysis, LCOE of a 60 kW_e ORC system has the lowest value in case of taking 950 units of evacuated-tube solar collectors without initial investment of the collectors into consideration. In addition to that, LCOE of the system has the lowest value in case of considering 900 units of the same collectors with initial investment of them.

ACKNOWLEDGEMENTS

First of all I would like to thank to my parents, Manu and Somris, my wife, Dujdow, my sons, Poohwarit, and my aunts Maitree and Samran for their ever helps and supports, especially in difficult moments.

Next, I wish to express my sincere gratitude and appreciation to my supervisor Professor Kiyoshi Tanaka for admitting me into the doctoral program. I would like to thank to all my co-supervisors, Tatsunori Asaoka, Hernán Aguirre, and Somchai Jiajitsawat from Energy Research and Promotion Center, Faculty of Science, Naresuan University, Thailand for their advice, encouragement, or even proofreading of my research papers during the work.

I would also like to express my gratitude to the dissertation committee, Professor Henmi Nobuhiko from Department of Mechanical Systems Engineering, Faculty of Engineering, Shinshu University and Professor Hiroyuki Kumano from Department of Mechanical Engineering, Aoyama Gakuin University. Thanks to all researchers in my field, who answered my emails and provided their papers with free of charge.

Last but not least, I would like to thank to Keiko Nishizawa, Ms Watanabe for assisting me for all paper work. Thanks to the Japanese language teachers of Matsumoto and Nagano campus for their patience and kindness in teaching me Japanese language. I kindly appreciate my friends: Sattaya Yimprasert, Yeoh Tze Wei, Hugo Monzon, Jaime Alberto Sandoval Gálvez, and William Tan for their encouragement and support during my studies.

Finally, I would like to gratefully acknowledge the financial support from the Japanese Government Scholar ship program – Monbukagakusho from October 2014 – March 2018.

CONTENTS

LIST OF TABLES

LIST OF FIGURES

NOMENCLATURE

A_{Coll}	:	Solar collector area (m^2)
c_p	:	The specific heat (kJ/kg-K)
C	:	Cost (USD)
COP	:	Coefficient of performance
E	:	The equation of time (in minutes)
$E_{Annual\ Net\ Power}$	:	The annual net power (kWh/Year)
$F_R U_L$	:	Overall heat transfer coefficient (W/m^2-K)
$F_R(\tau\alpha)_e$	:	Optical efficiency
G_{SC}	:	Solar constant (W/m^2)
h	:	Enthalpy (kJ/kg)
H	:	The daily total radiation (MJ/m^2-day)
HTF	:	Heat transfer fluid
H_d	:	The daily total diffuse radiation (MJ/m^2-day)
H_o	:	Radiation on a horizontal surface
i_d	:	The real debt interest rate (%)
I	:	The hourly total radiation (W/m^2)
I_b	:	The hourly beam radiation (W/m^2)
I_d	:	The hourly diffuse radiation (W/m^2)
I_T	:	The hourly total solar radiation on the sloped surface (W/m^2)
k	:	The annual insurance rate (%/Year)
$LCOE$	:	The levelized cost of electricity (USD/kWh)
L_{loc}	:	The longitude of the location (Degree)
L_{st}	:	The standard meridian for the local time zone (Degree)
$\dot{m}$	:	The mass flow rate (kg/s)
M	:	The mass or the volume of water in the thermal storage tank (kg or m^3)
n	:	The day of the year ($1 \leq n \leq 365$)
N_{Series}	:	Number of collectors in series connection
P	:	Pressure (kPa)
q	:	Energy input (kW)
$\dot{Q}$	:	Heat transfer rate (kW_{th})
$\dot{Q}_s$	:	The total heat capacity for a cycle operating (kW_{th})
r_d	:	Ratio of hourly diffuse to daily diffuse radiation
r_t	:	Ratio of hourly total to daily total radiation
R	:	Refrigerant
R_b	:	Ratio of beam radiation on tilted surface to that on horizontal surface
t	:	Time

T	:	Temperature (°C)
UA	:	Overall coefficient of heat loss (W/K)
v	:	Specific volume (m^3/kg)
W	:	Work input (kW)
X	:	Concentration (%)
Y	:	The depreciation period in year (Year)

Greek symbols

$\emptyset$	:	Latitude (Degree)
δ	:	Declination angle (Degree)
β	:	Slope (Degree)
γ	:	Surface azimuth angle (Degree)
ω	:	Hour angle (Degree)
ω_s	:	Sunset hour angle (Degree)
θ	:	Angle of incidence (Degree)
θ_z	:	Zenith angle (Degree)
ρ_g	:	Ground reflectance
η_{Coll}	:	Solar Collectors Efficiency (%)
Δ	:	Rang or step
ε	:	Effectiveness (%)

Subscript and superscript

Abs	:	Absorber
AHT	:	Absorption heat transformer system
Amb	:	Ambient
Aux	:	Auxiliary heater
Avg	:	Average
$Coll$	:	Solar collectors
$Comp$	:	Compressor
$Comb$	:	Combustion
$Cond$	:	Condenser
el	:	Electrical energy
$Evap$	:	Evaporator
ge	:	Gas engine
Gen	:	Generator
$GEHP$	:	Gas engine-driven heat pump system
HS	:	Heat source
HX	:	Heat exchanger
i	:	Inlet
$invest$	:	Investment cost
IHE	:	Internal heat exchanger
$isen$	:	Isentropic process
L	:	Load

LHV	:	Low heating value
$Loss$	:	Heat loss
max	:	Maximum
min	:	Minimum
ME	:	Mechanical
MO	:	Motor
N	:	Number of collectors
o	:	Outlet
ORC	:	Organic Rankine Cycle system
$O\&M$	:	Operation and maintenance
p	:	Pump
r	:	Refrigerant
ref	:	Reference
S	:	Start
sp	:	Solution pump
ST	:	Storage tank
STD	:	Standard
t	:	Time
Tur	:	Turbine
th	:	Thermal energy
U	:	Stop using time
$VCHP$	:	Vapor compression heat pump system
w	:	Water
WH	:	Waste heat
$a, A, B, C, D, E, F, G, H$	:	Position in the cycle
$1-10$	:	Position in the cycle

1

Introduction

1.1 Background

In recent years world's energy demand is in the continuous growth as the economy develops. A concrete example is the higher fuel consumption required for today's activity and living standards [1]. From 2006 to 2015, global energy consumption as reported by BP Energy was increased from 11.3×10^9 to 13.1×10^9 TOE [2]. In 2035 a growth of the consumption is expected by 34 percent [3]. For Thailand, its total energy consumption is expected to increase around 40.5 percent by 2036, as compared to the 2015 data [4], with the industrial sector having the highest share of 36.6 percent when comparing by economic sector [5]. In industrial processes, 60 percent of the heat released to the environment has a temperature lower than 230 °C, which indicates potential of heat recovery [6-10]. Unfortunately, this low-temperature heat cannot be directly supplied to a steam Rankine cycle system for power generation since the generation is less profitable when the heat source temperature is lower than 340 °C [9], however with an Organic Rankine Cycle (ORC) system the electrical generation is possible [11-14].

An ORC system operates as the steam Rankine cycle system, but the system utilizes organic refrigerants instead of water. These refrigerants vapor lower temperature and pressure as compared to the water [15]. This system is proved to be one of the most reliable and efficient scalable thermodynamic solutions for converting low-temperature thermal sources that can be configured to meet variable project demands [16] or it can be implemented in the form of regionalized lower-capacity power plants [17, 18], in the range of few kW_e to tens of MW_e. In addition, ORC technology has several other advantages such as autonomous and straightforward operation, low-maintenance, and long lifetime (> 20 years). Accordingly, ORC system has become sharply attractive for small-sized power plants with the low-temperature heat source. From current literature [19-22], the ORC is a well-proportioned low-temperature sources technology that can generate electrical work. The technology is less applicable to the sources below 70 ºC due to a combination of economic and technical barriers [17, 23-25], resulting in a large amount of heat from industrial processes is disposed into the environment. Moreover, there are only a few designs that combine the use of lower temperature thermal energy supplies and small-scale ORC systems. For instance, a very small-scale ORC system for power generation with the capacity lower than 20 kW_e [26, 27], and large-scale if higher than 250 kW_e [28]. Which, these capabilities are not suitable to be applied to regionalized small-scale thermal power plants.

Solar energy is one of renewable energy resources used for power generation. Thailand considered as one of countries has the high solar radiation intensity with an average total and direct normal solar radiation of 18.0 MJ/m^2-day [29] as shown in Figure 1-1 (a) and in the range of 1350 – 1400 kWh/m^2-Year [30, 31], as shown in Figure 1-1 (b), respectively. However, some solar energy technologies such as Concentrating Solar Power (CSP) are not applicable because it require direct normal radiation of 1500 kWh/m^2-Year. Therefore, most applications are limited to low-to-medium temperature hot water production, mostly consumed by hospitals, hotels, and some industries, etc. From 2008 – 2015, the Department of Alternative Energy Development and Efficiency (DEDE) of the Ministry of Energy in Thailand had promoted solar water heating system (SWHS) combined with wasted heat from industrial processes or condensing units of the air conditioner, etc. [32]. Moreover, total 182 systems with 46,498 m^2 of solar collectors were installed in hotels, factories, ranch, hospitals, colleges, residential areas and office buildings, with the ratios presented in Figure 1-2. Also, an Alternative Energy Development Plan (AEDP2015) from DEDE by 2036 the target is 9.2 million-m^2 of government-sponsored installations of solar collectors for SWHS used in hot water production [4].

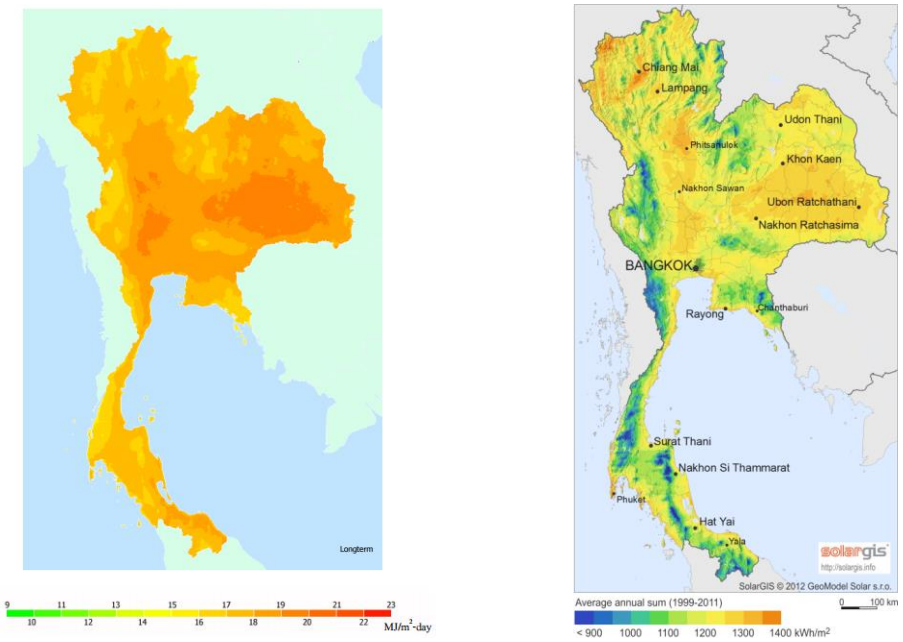

(a) Average total solar radiation (MJ/m^2-day) [29]

(b) Direct normal solar radiation (kWh/m^2) [33]

Figure 1-1 Potential of solar radiation in Thailand

As mentioned above, such system could promote the use of low-heat renewable heat sources like solar energy, or be used to take advantage of the available industrial waste heat. In particular, there is the added benefit that can help industries reduce their energy intensity while increasing the efficiency of the processes [34], and reduce pollutant (greenhouse gas emission (GHG), and thermal pollution) as well minimize thermal population. Then, to enhancing the low-temperature heat source with temperature lower 70 °C, to achieve the high-temperature heat sink or heat reservoir with the temperature equal to or higher than 70 °C, is inviting in the small-scale ORC power generation.

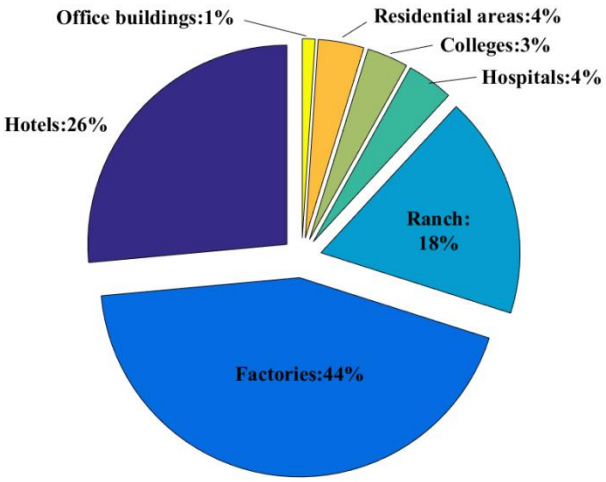

Figure 1-2 Ratios of solar collectors installed between 2008 – 2015 in Thailand

In this research, low-temperature heat source consisting of waste heat from industrial process heat and SWHS already installed in factories was proposed and investigated for a small-scale ORC power generation. The ORC capacity recorded was between 20 and 60 kW_e, and thus it was also proposed for regionalized small-scale thermal power plants due to its suitability. The *First part* shown in Chapter 4 discussed heat-boosting technologies, as efficient and energy conservation technology, which present unique advantages for environmental protection and energy usage [35]. The said technologies can raise the low-temperature heat source from low-grade industrial waste heat (IWH) to high-temperature heat sink or heat reservoir. The present study sought to mathematically model and analyze three different heat-boosting technologies: vapor compression heat pump (VCHP), gas engine-driven heat pump (GEHP), and absorption heat transformer (AHT) systems, which are used to increase low-temperature heat before supplying it to the ORC power generation for economic reasons and mitigation of environmental impact. The main components of the combination system as shown in Figure 1-3 are heat boosting technology (VCHP, GEHP, and AHT), ORC power generation, and thermal storage tank. In the system operation, waste heat from an industrial process, with prescribed quantity and quality, is stored in thermal storage tank one. The heat grade is then augmented by any of the proposed heat boosters to an equal to or higher temperature heat and is later stored in the heat reservoir/thermal storage tank two. After that, the heat from the thermal storage tank two is supplied to the ORC system to generate electricity.

The *Second part* shown in Chapter 5 considered situations apart from the SWHS in place *(the SWHS were already installed)*. It considered low-grade waste heat product of industrial processes with temperature lower than 70 °C. This part of the study mathematically modeled and analyzed an ORC power generation from low-grade IWH combined with SWHS by using the VCHP system as a heating booster. The main components of the combination system (as shown in Figure 1-4) are solar collectors, VCHP system, ORC power generation, and a thermal storage tank. In the system operation, during *the daytime* low-grade IWH at constant quality and quantity is used to increase or maintain the outlet temperature of hot water from the ORC system *(Point: A)* before supplying it to the solar collectors for hot water

production. In this step, if the outlet hot water temperature from solar collectors *(Point: B)* is equal to or higher than 70 °C, the heat is directly supplied to the ORC system for power generation. If not, the temperature is increased by the VCHP system to an equal to or higher temperature and is later stored in the heat reservoir/thermal storage tank. After that, the heat from the thermal storage tank is supplied to the ORC system to generate electricity. During *the nighttime*, low-grade IWH at the same quantity and quality is provided directly to the VCHP system where the temperature is increased before supplying it to the ORC power generation.

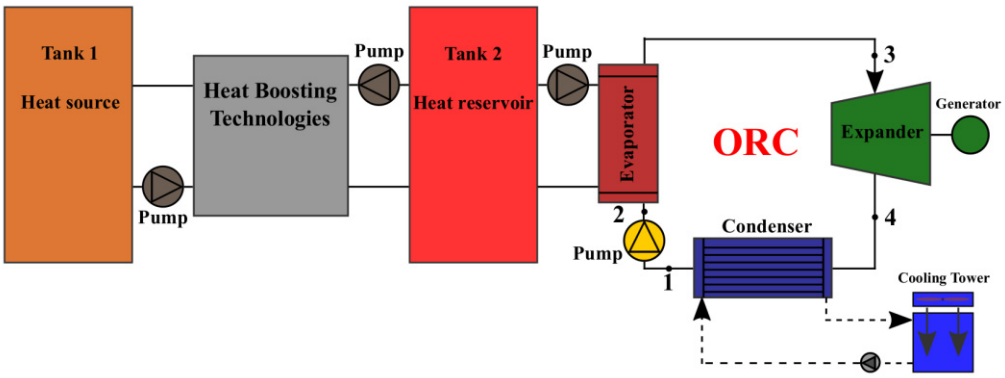

Figure 1-3 Schematic diagram of the ORC power generation from low-grade industrial waste heat (IWH) by using heat-boosting technologies as heating booster

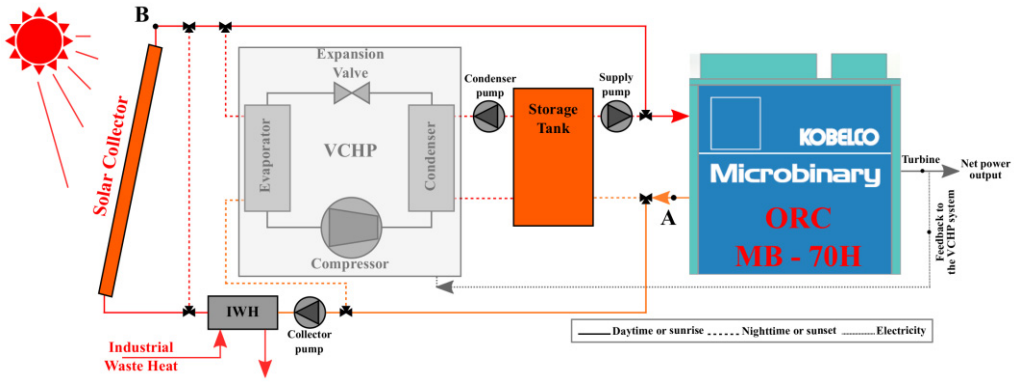

Figure 1-4 Schematic diagram of the VCHP-ORC power generation from low-grade industrial waste heat (IWH) combined with solar water heating system (SWHS)

Finally in Chapter 6, areas where the only heat source is a SWHS were considered, particularly the case which would make the use of heat boosters lose their effectiveness. The study in this part was done taking into account systems requiring only solar collectors, a situation more common in Thailand. This would be of interest to the DEDE who could do more to reduce implementation barriers relating to the use of such system. In this part, a mathematical model was developed, and the performance of a small-scale Solar Organic Rankine Cycle (SORC) power system with heat source temperature below 100 °C was simulated. The main components of the system (as shown in Figure 1-5) are solar collectors, ORC power generation, a cooling tower, and a collector pump. In the system operation, the

outlet hot water from the ORC system is pumped by the collector pump to the solar collector field for hot water production. In this step, the collector mass flow rate is adjusted to achieve the high-temperature hot water. After that, the high-temperature hot water is supplied to the ORC for power generation.

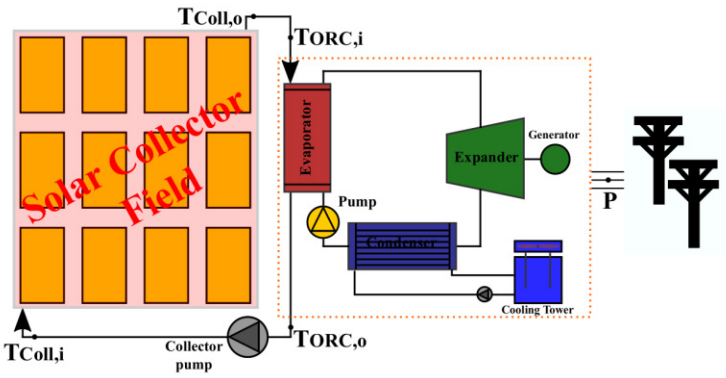

Figure 1-5 A small Solar Organic Rankine Cycle (SORC) power system

1.2 Objectives

1) Study the effect of working fluids in terms of types and evaporating temperature, with respect to the thermal efficiency of an ORC system for power generation and the coefficient of performance (COP) of the vapor compression heat pump (VCHP).
2) Develop a mathematical model and simulation to evaluate the ORC system for power generation from either low-grade industrial waste heat (IWH) and solar water heating systems (SWHS).
3) Evaluate the levelized cost of electricity (LCOE) and the environmental impact of the system.

1.3 Scope of the Thesis

1) Simulations on three types of heat boosting technologies: Vapor Compression Heat Pump (VCHP), Gas Engine-driven Heat Pump (GEHP), and Absorption Heat Transformer (AHT).
2) Use of H_2O-LiBr solutions as working fluid for the Absorption Heat Transformer.
3) Use of different types of solar collectors in the simulations: Flat-plate, heat pipe evacuated-tube, and compound parabolic concentrator (CPC).
4) Weather data taken from representatives cities of the north, central, west, south, north-east and east part of Thailand: Chiang Mai, Bangkok, Ratchaburi, Songkhla, Nakhon Ratchasima, and Chon Buri.
5) The industrial waste heat selected as source is hot water at temperatures that ranges between 60 to 70 °C.
6) In simulations the temperature, pressure, mass flow rate of the VCHP, GEHP, AHT systems and the mass flow rate of the heat source have been taken into account.
7) ORC power generation systems considered in the simulation are not larger than 60 kW_e.

1.4 Expected Benefits

1) A novel technical solution for ORC power generation from low-temperature heat source.
2) A system capable of reducing energy intensity, increase energy efficiency for industrial processes, as well as reduce pollutants in the industry sector.
3) A system capable of aiding the Ministry of Energy of Thailand in their goal to reduce energy intensity by 30 percent on 2036.

1.5 Outline of the Thesis

This thesis is divided in seven chapters. *Chapter 1* introduces the main concept and the scope of the thesis. *Chapter 2* covers the theoretical background behind each of the system components SWHS, VCHP, GEHP, AHT and ORC systems. *Chapter 3* covers the method used to find a suitable working fluid for the ORC and the VCHP systems, by testing over 19 refrigerants. In addition, this section was shown the step how to validate the mathematically modeled of the ORC and the heating booster.

Chapter 4 proposes an ORC power generation system capable of recovering industrial waste heat (IWH) with temperature below 70 °C, which applies three types of heat boosting technologies: VCHP, GEHP and AHT systems. The systems were mathematically modeled considering a thermal capacity of 250 kW for all three systems, with R-365mfc as working fluid for VCHP and GEHP, while the AHT uses H_2O-LiBr. For each combination, a 20 kW_e ORC power generator with R-245fa as working fluid was considered. The mathematical model was simulated to evaluate the power output, the environmental impact, and the levelized cost of electricity (LCOE) of the system.

Chapter 5 presents a system where some parts are fixed in order to explore the viability of using an ORC system that takes in low-grade heat by using a VCHP system. In this part, we introduce a similar system with a SWHS and a VCHP for heating boosting. A 400 kW thermal capacity VCHP with R-365mfc, is used to rise the heat and then supplying it to a 60 kW_e ORC power generator with R-245fa from KOBELCO Company. Flat-plate, heat pipe evacuated-tube and compound parabolic concentrator (CPC) solar collectors between 300 and 700 units connected in parallel connection, were used to generate heat. The weather from six industrial areas of Thailand were taken for simulations. A mathematical model of the system was simulated and its net power output, environmental impact, and the LCOE of the system were evaluated.

Chapter 6, we improve the system by trying to find the optimal configuration that will not require the heat pump. In this part, we describe a small-scale Solar Organic Rankine Cycle (SORC) for power generation for temperature below 100 °C. The system was analyzed with a combination of different capacities ORC systems that uses R-245fa as working fluid (20 and 60 kW_e from IHI Company, and KOBELCO Company, respectively) in combination with four different models of stationary solar collectors (SORC-I, SORC-II, SORC-III, and SORC-IV). Three types of solar collectors were employed to generate heat: flat-plate, evacuated-tube and CPC. The system was mathematically modeled and simulated to evaluate

the maximum power output, the CO_2 emission, and the LCOE. Bangkok, a representative city in the central part of Thailand, weather data was selected for simulations. The results were summarized in the form of a formula that takes the model, type and number of employed solar collectors and outputs its effects on the system in terms of power output and environmental impact. From the results the LCOE was calculated, and for the system with the lowest value it was determined the best ORC system for its type and number of solar collectors employed.

Chapter 7 shows the conclusions and future works of this study.

1.6 Key Words

Solar water heating system (SWHS); Levelized cost of electricity (LCOE); Low-grade industrial waste heat (IWH); Vapor compression heat pump (VCHP); Gas engine-driven heat pump (GEHP); Absorption heat transformer (AHT); Organic Rankine Cycle (ORC).

2

Theory

In this chapter we discussed in the theoretical of the main components of the system are solar water heating system (SWHS), vapor compression heat pump (VCHP), gas engine-driven heat pump (GEHP), absorption heat transformer (AHT), and Organic Rankine Cycle (ORC) systems.

2.1 Solar Thermal Energy

2.1.1 Mathematical Modeling of Solar Radiation on Tilted Surface [36]

The solar radiation at each hour of this day was calculated based on the "Hottle" model. One of the most well-know empirical models referring to clear sky conditions is the "Hottle" model, yielding numerical results close enough to true value [36].

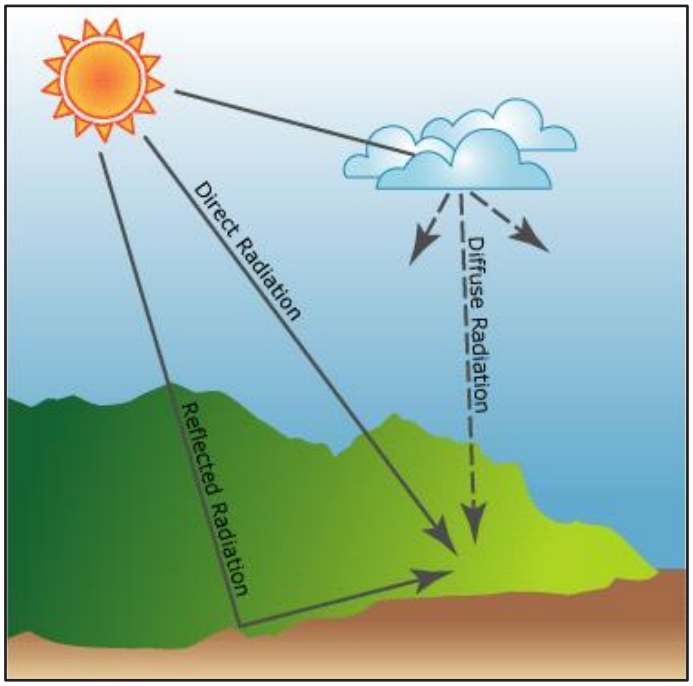

Figure 2-1 Types of the solar radiation [37]

- **Definitions**

Types of the solar radiation as shown in Figure 2-1 can be explained as follows:

Beam or Direct Radiation The solar radiation received from the sun without having been scattered by the atmosphere.

Diffuse Radiation	The solar radiation received from the sun after its direction has been changed by scattering by the atmosphere.
Total Solar Radiation	The sum of the beam and the diffuse radiation on a surface.
The solar constant	The energy from the sun per unit time. A value of 1367 W/m^2
Solar Time	Time based on the apparent angular motion of the sun across the sky with solar noon the time the sun crosses the meridian of the observer. Solar time is the time used in all of the sun-angle relationships.

The different in minutes between solar time and standard time is

$$Solar\ Time - Standard\ Time = 4(L_{st} - L_{loc}) + E \tag{2-1}$$

where L_{st} : The standard meridian for the local time zone
L_{loc} : The longitude of the location ($0° \leq L_{loc} \leq 360°$)
E : The equation of time (in minutes)

The equation of time (in minutes) is

$$E = 229.2(0.000075 + 0.001868cosB - 0.032077sinB - 0.014615cos2B - 0.04089sin2B) \tag{2-2}$$

when

$$B = (n-1)\frac{360}{365} \tag{2-3}$$

where n : The day of the year ($1 \leq n \leq 365$)

- **Beam or Direct Radiation**

The angle and a set of consistent sign convention are as follows:

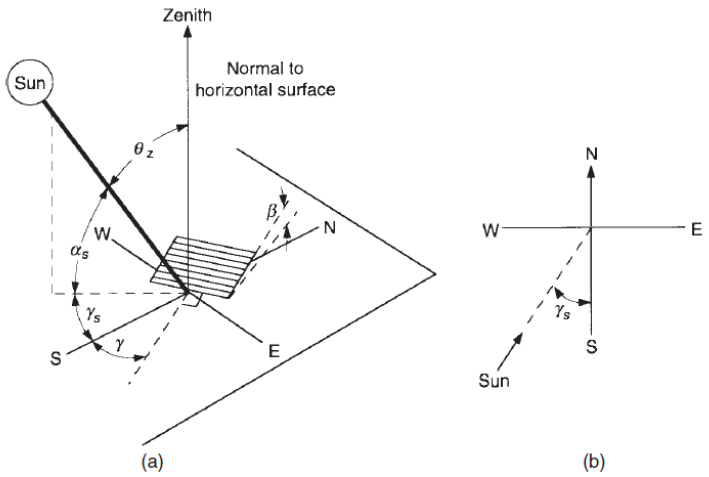

Figure 2-2 (a) Zenith angle (θ_z), slope (β), surface azimuth angle (γ), and solar azimuth angle (γ_s) for a tilted surface, and (b) Plan view showing solar azimuth angle (γ_s)

$\emptyset$: **Latitude**, the angular location north of south of the equator (north positive); $-90° \leq \emptyset \leq 90°$

δ : **Declination angle**, the angular position of the sun at solar noon with respect to the plane of the equator (north positive); $-23.45° \leq \delta \leq 23.45°$

β : **Slope**, the angle between the plan of the surface and the horizontal; $0° \leq \beta \leq 180°$ ($\beta > 90°$; mean that the surface has a downward-facing component)

γ : **Surface azimuth angle**, the deviation of the projection on a horizontal plane of the normal to the surface from the local meridian (with in zero the south, east negative, and west positive); $180° \leq \gamma \leq 180°$

ω : **Hour angle**, the angular displacement of the sun east or west of the local meridian due to rotation of the earth on it axis at 15° per hour (morning negative and afternoon positive); $-90° \leq \omega \leq 90°$

θ : **Angle of incidence**, the angle between the beam radiation on a surface and the normal to that surface.

θ_z : **Zenith angle**, the angle between the vertical and the line to the sun, which is the angle of incidence of beam radiation on a horizontal surface.

- **The Declination Angle (δ):**

$$\delta = 23.45 sin\left(360\frac{284+n}{365}\right) \tag{2-4}$$

Table 2-1 Recommended an average day for months and values of $\boldsymbol{n}$ by months

Month	Jan	Feb	Mar	Apr	May	Jun	Jul	Aug	Sep	Oct	Nov	Dec
Date	17	16	16	15	15	11	17	16	15	15	14	10
$\boldsymbol{n}$	17	47	75	105	135	162	198	228	258	288	318	344

- **The Angle of Incidence of Beam Radiation on Surface (θ):**

$$\begin{aligned} cos\theta = {} & sin\delta sin\emptyset cos\beta - sin\delta cos\emptyset sin\beta cos\gamma \\ & + cos\delta cos\emptyset cos\beta cos\omega \\ & + cos\delta sin\emptyset sin\beta cos\gamma cos\omega \\ & + cos\delta sin\beta sin\gamma sin\omega \end{aligned} \tag{2-5}$$

- **The Zenith Angle of the Sun (θ_z):**

For horizontal surface, its value must be between 0 and 90° when the sun is above the horizontal. For this situation, $\beta = 0$

$$cos\theta_z = cos\emptyset cos\delta cos\omega + sin\emptyset sin\delta \tag{2-6}$$

- **Sunset Hour Angle (ω_s):**

when $$\theta_z = 90°$$

$$cos\omega_s = -\frac{sin\emptyset sin\delta}{cos\emptyset cos\delta} = -tan\emptyset tan\delta \tag{2-7}$$

- **Ratio of Beam Radiation on Tilted Surface to that on Horizontal Surface (R_b)**

The ratio of beam radiation on the tilted surface to that on a horizontal surface at any time as shown in Figure 2-3, it can be calculated exactly by appropriate use indicates the angle of incidence of beam radiation on the horizontal and tilted surfaces. The ratio is given by:

$$R_b = \frac{G_{b,T}}{G_b} = \frac{G_{b,n}}{G_{b,n}}\frac{cos\theta}{cos\theta_z} = \frac{cos\theta}{cos\theta_z} \tag{2-8}$$

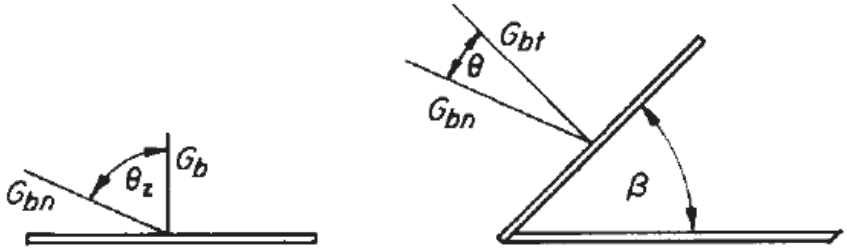

Figure 2-3 Beam radiation on horizontal and tilted surface

- **Radiation on a Horizontal Surface (H_o)**

Radiation on a horizontal surface in daily joules per square meter per day is:

$$H_o = \frac{24 \times 3600 \times G_{SC}}{\pi}\left[1 + 0.033cos\frac{360n}{365}\right]\left[cos\emptyset cos\delta sin\omega_s + \frac{\pi\omega_s}{180}sin\emptyset sin\delta\right] \tag{2-9}$$

where ω_s : The sunset hour angle (in degrees)

G_{SC} : Solar constant ($1367\ \frac{W}{m^2}\ or\ 433\frac{Btu}{ft^2hr}\ or\ 4.92\frac{MJ}{m^2hr}$)

- **The Ratio of Daily Total Diffuse (H_d) per Daily Total Radiation (H) as Given by:**

$$\frac{H_d}{H} = -4.6408 + 26.5495\left(\frac{H}{H_o}\right) - 28.3422\left(\frac{H}{H_o}\right)^2 - 31.4546\left(\frac{H}{H_o}\right)^3 + 46.442\left(\frac{H}{H_o}\right)^4 \tag{2-10}$$

where H_d : The daily total diffuse radiation (MJ/m^2-day)

H : The daily total radiation (MJ/m^2-day)

- **Estimation of Hourly Radiation (I) from Daily Data**

$$r_t = \frac{I}{H} = \frac{\pi}{24}(a + bcos\omega)\frac{cos\omega - cos\omega_s}{sin\omega_s - \frac{\pi\omega_s}{180}cos\omega_s} \tag{2-11}$$

The coefficients a and b are given by:

$$a = 0.4090 + 0.5016sin(\omega_s - 60) \quad (2\text{-}12)$$

$$b = 0.6609 + 0.4767sin(\omega_s - 60) \quad (2\text{-}13)$$

where r_t : The ratio of hourly total to daily total radiation

- **The Ratio of Hourly Diffuse (I_d) to Daily Total Diffuse (H_d) Radiation (r_d)**

$$r_d = \frac{I_d}{H_d} = \frac{\pi}{24}\left(\frac{cos\omega - cos\omega_s}{sin\omega_s - \frac{\pi\omega_s}{180}cos\omega_s}\right) \quad (2\text{-}14)$$

- **Radiation on Sloped Surface**

The total solar radiation (I_T) on the tilted surface for an hour:

$$I_T = I_b R_b + I_d\left(\frac{1 + cos\beta}{2}\right) + I\rho_g\left(\frac{1 - cos\beta}{2}\right) \quad (2\text{-}15)$$

$$I_b = I - I_d \quad (2\text{-}16)$$

where ρ_g : Ground reflectance normally of the order 0.2 and low collector slopes. However, with ground reflectance of 0.6 to 0.7 typical of snow and with high slope.

Calculation steps for evaluating the solar radiation on tilting plan are shown in Figure 2-4. Inputs of the simulation were the step time, day of year (n), latitude ($\emptyset$), slope (β), surface azimuth angle (γ), ground reflectance (ρ_g), solar constant (G_{sc}), and the daily total radiation (H). For the step of calculations, the mathematical model were evaluated to find out the total solar radiation (I_T) on the tilted surface for an hour.

2.1.2 Useful Heat Rate from Solar Collectors

There are basically two types of solar collectors: Non-concentrating and Concentrating solar collectors [38, 39].

- **Non-Concentrating or Stationary Solar Collectors**

These collectors are permanently fixed in position and do not track to the sun. Normally, it can be separate in three types: (i) Flat-plate, (ii) Evacuated-tube, and (iii) Compound parabolic concentrator (CPC) solar collectors. As shown in the following:

Flat-plate solar collectors

A typical of flat-plate solar collector is shown in Figure 2-5. When solar radiation passes through a transparent cover and impinges on the absorber surface, this energy is absorbed by the plate and then transferred to the heat transfer fluids (HTF) in the tubes to be carried away for storage or use. The underside of the absorber plate and the side of casing are well insulated to reduce heat losses. Flat-plate solar collectors are usually employed for low-temperature applications up to 100 ˚C.

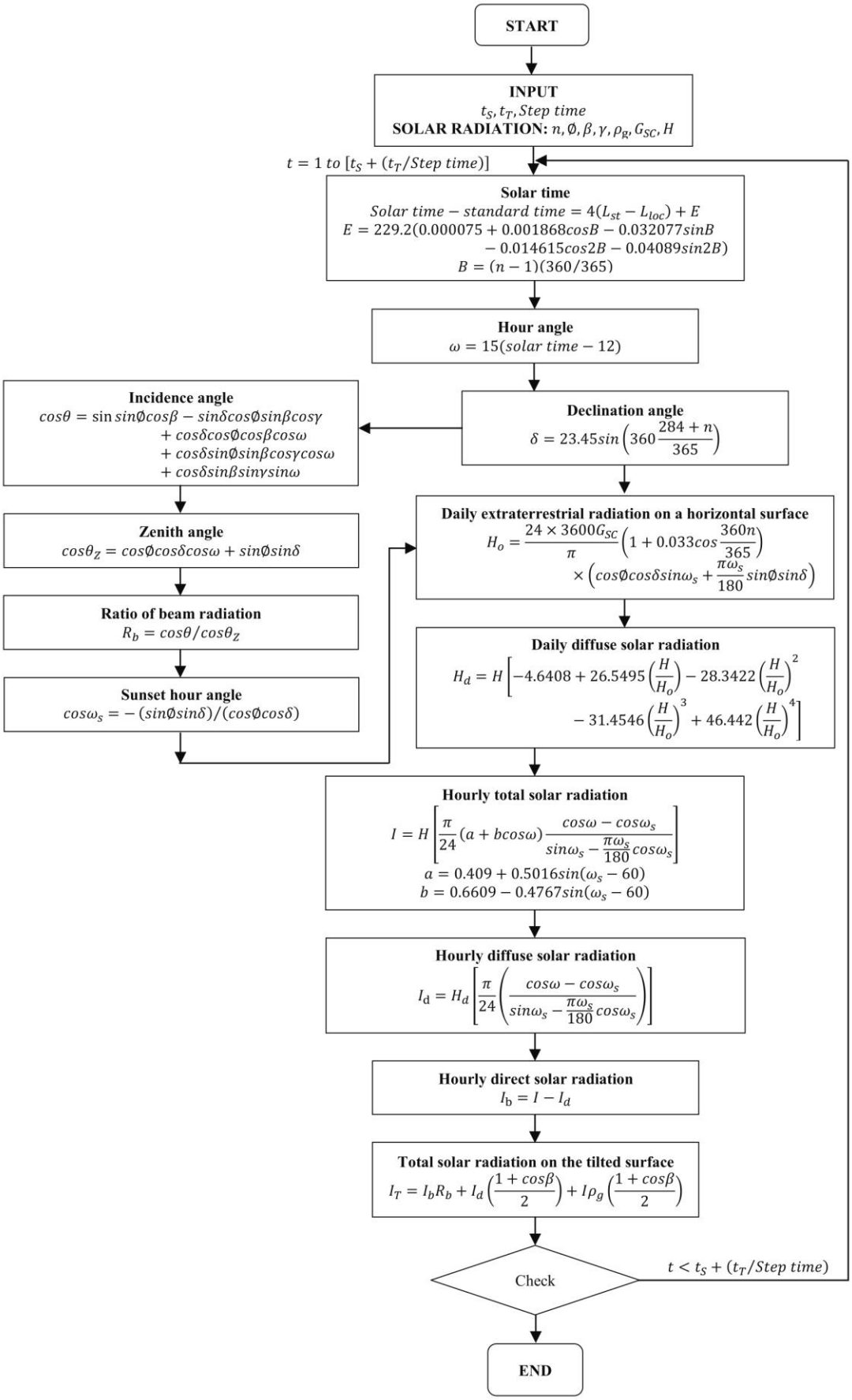

Figure 2-4 Calculation steps for evaluating the solar radiation on tilting plan

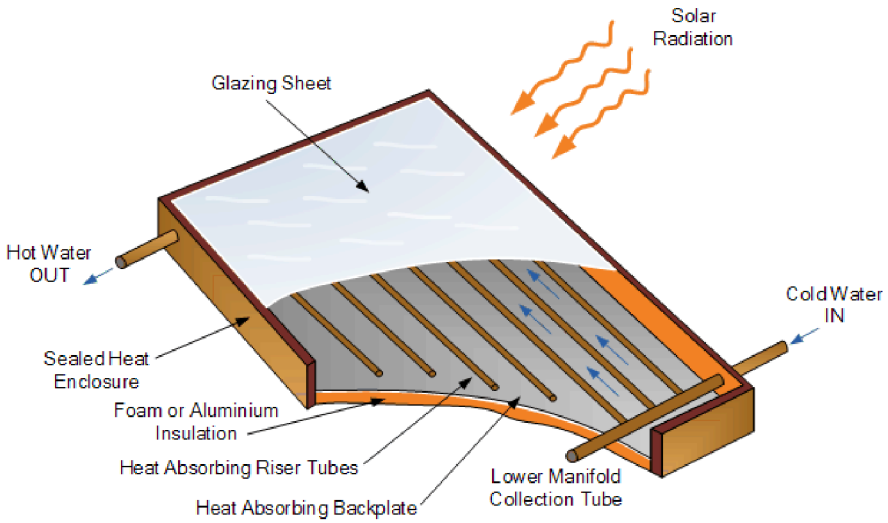

Figure 2-5 Flat-plate solar collectors [40]

Evacuated-tube solar collectors

Evacuated-tube solar collectors have demonstrated that the combination of a selective surface and effective connection suppressor can result in good performance at high-temperature. This is given the evacuated-tube solar collectors an advantage over flat-plate solar collectors in day-long performance. A typical evacuated-tube solar collectors is shown in Figure 2-6.

Figure 2-6 Evacuated-tube solar collectors [41]

Heat pipe evacuated-tube solar collectors, these collectors consist of a heat pipe inside a vacuum-sealed tube, as shown in Figure 2-7. Heat pipe is used liquid-vapor phase change materials to transfer heat at high efficiency. The heat pipe contains a small amount of fluid that undergoes and evaporating condensing cycle. In this cycle, solar heat evaporates the liquid, and the vapor travels to the heat sink region where it condenses and releases its at the latent heat. The condensed fluid return back to the solar collectors and the process is repeated.

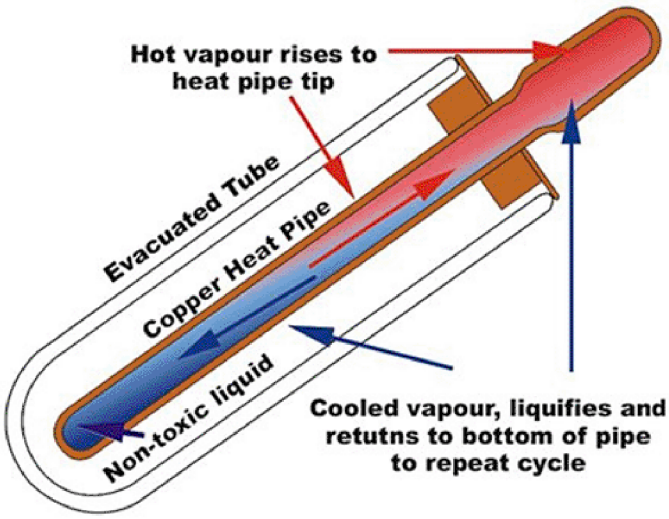

Figure 2-7 Heat pipe evacuated-tube solar collectors [42]

From Figure 2-7, medium fluid flows through the manifold and pick up the heat from the tubes. The heated liquid circulates through another heat exchanger and gives of its heat to the water that is stored in a storage tank.

Compound parabolic concentrator (CPC) solar collectors

Compound parabolic concentrator (CPC) solar collectors are non-imaging concentrators. These have the capability of reflecting to the absorber all of the incident radiation. CPC solar collectors can accept radiation over a relatively wide range of angle. By using multiple internal reflections, any radiation that is entering the aperture, within the collector acceptance angle, finds its way to the absorber surface located at the bottom of the collectors. A typical of the CPC solar collectors and schematic diagram is shown in Figure 2-8 and Figure 2-9, respectively.

Figure 2-8 Compound parabolic concentrator (CPC) solar collectors [43]

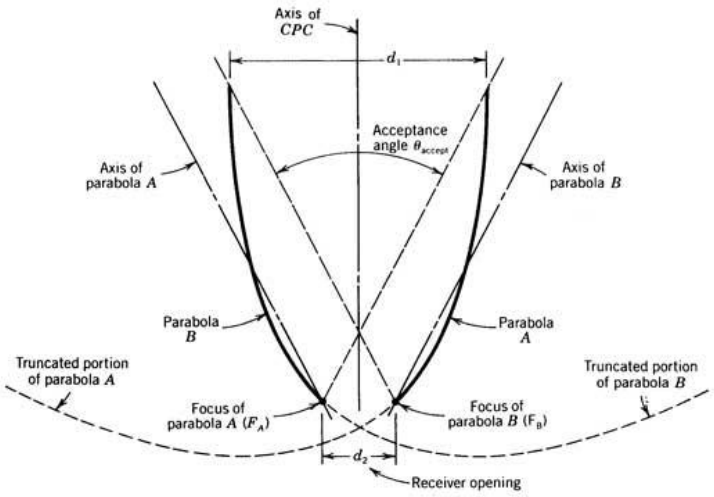

Figure 2-9 Schematic diagram of compound parabolic concentrator (CPC) solar collectors [44]

- **Concentrating Solar Collectors**

For the concentrating solar collectors, the solar energy is optically concentrated before being transferred into heat. Concentration can be obtained by reflection or refraction of solar radiation by use of the mirrors or lens. The reflected is concentrated in a focal zone, thus increasing the energy flux in the receiving target. The concentrating solar collectors can be separated in four types: (i) Parabolic trough collectors, (ii) Linear Fresnel reflectors, (iii) Parabolic dish collectors, and (iv) Central receiver concentrators, are shown in Figure 2-10.

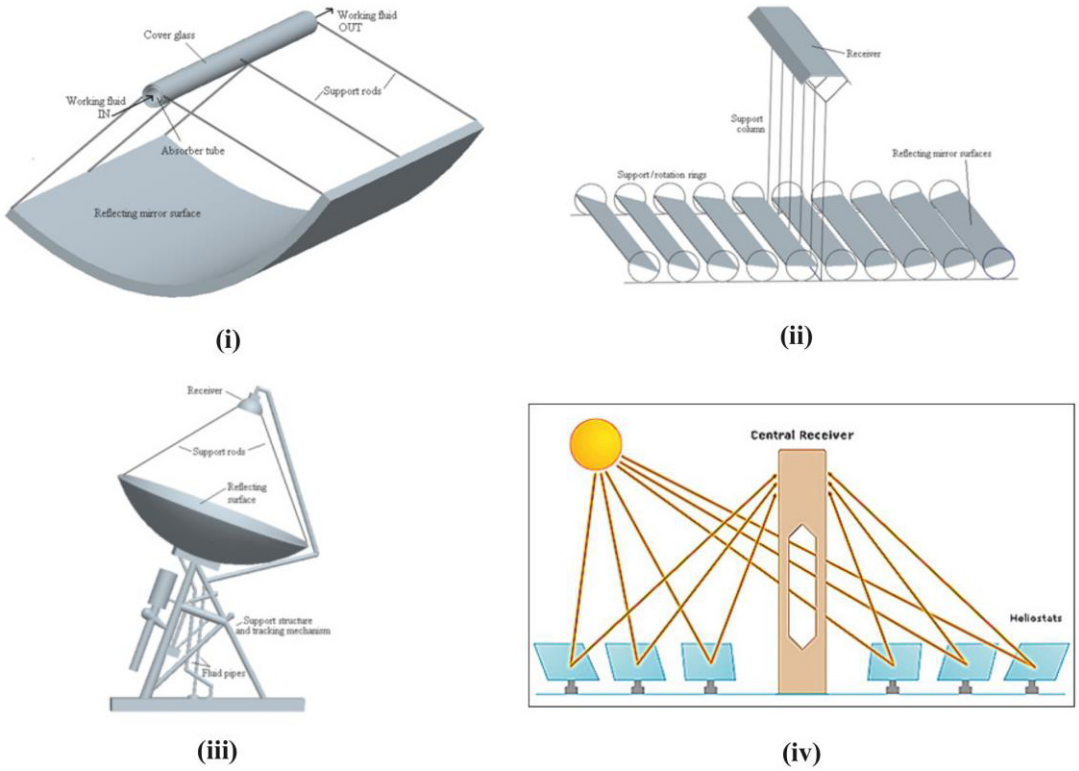

Figure 2-10 Concentrating solar collectors: (i) Parabolic trough collectors, (ii) Linear Fresnel reflectors, Parabolic dish collectors, and (iv) Central receiver concentrators [45, 46]

2.1.3 Solar Collectors Efficiency

- **Characteristics of Solar Collectors**

For simpler model, two parameters considered are the collector ability to absorb radiation and the collector heat loss. The simple model of the collector can be defined as instantaneous efficiency (η_{Coll}) as shown in Eq. (2-17).

$$\eta_{Coll} = \frac{Output}{Input} = \frac{\dot{Q}_{Coll}}{A_{Coll} I_T} = \frac{F_R\left[I_T(\tau\alpha)_e - U_L\left(T_{Coll,i} - T_{Amb}\right)\right]}{I_T} \tag{2-17}$$

when $F_R(\tau\alpha)_e$ and $F_R U_L$ are two parameters that describe how the collector works, where $F_R(\tau\alpha)_e$ is an indication of how energy is absorbed and $F_R U_L$ is an indication of how energy is lost. These two parameters constitute the simplest practical collector model.

- **Evaluation of Collector Efficiency and Collector Overall Heat Loss**

In order to evaluate $F_R(\tau\alpha)_e$ and $F_R U_L$, ASHRAE Standard testing is applied by exposing the operating collectors to solar radiation and measure the collector inlet and outlet hot water temperature ($T_{Coll,i}$ and $T_{Coll,o}$) and the water mass flow rate ($\dot{m}_w$). The collector useful heat gain ($\dot{Q}_{Coll}$) can be expressed as follows:

$$\dot{Q}_{Coll} = \dot{m}_w c_{p,w}\left(T_{Coll,o} - T_{Coll,i}\right) \tag{2-18}$$

The thermal performance of an operating collectors under steady conditions, in terms of the incident radiation can be expressed as:

$$\dot{Q}_{Coll} = A_{Coll} F_R\left[I_T(\tau\alpha)_e - U_L\left(T_{Coll,i} - T_{Amb}\right)\right] \tag{2-19}$$

where $(\tau\alpha)_{av}$: A transmittance – absorptance

Eq. (2-17) can be rearranged as:

$$\eta_{Coll} = \frac{\dot{Q}_{Coll}}{A_{Coll} I_T} = F_R(\tau\alpha)_e - \frac{F_R U_L\left(T_{Coll,i} - T_{Amb}\right)}{I_T} \tag{2-20}$$

And Eq. (2-18) can be used to define an instantaneous efficiency as based on the standard testing methods:

$$\eta_{Coll} = \frac{Output}{Input} = \frac{\dot{m}_w c_{p,w}\left(T_{Coll,o} - T_{Coll,i}\right)}{A_{Coll} I_T} \tag{2-21}$$

where
- $\dot{m}_w$: Water mass flow rate (kg/s)
- $c_{p,w}$: Specific heat of water (kJ/kg-K)
- A_{Coll} : Solar collector area (m^2)
- I_T : Total solar radiation (W/m^2)
- $T_{Coll,i}$: Collector inlet temperature of water (°C)
- $T_{Coll,o}$: Collector outlet temperature of water (°C)
- T_{Amb} : Ambient temperature (°C)
- $F_R(\tau\alpha)_e$: Optical efficiency

$F_R U_L$: Overall heat transfer coefficient (W/m^2-K)

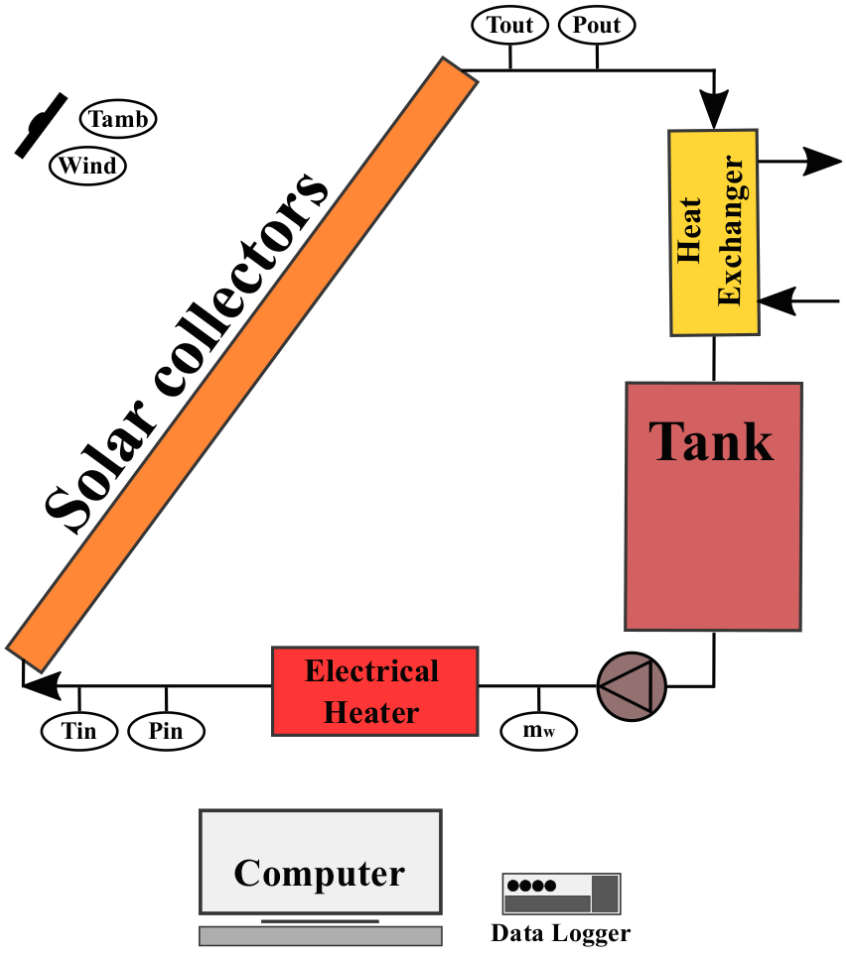

Figure 2-11 Schematic diagram of basic systems for solar collectors testing

From Figure 2-11 schematic diagram of basic systems for solar collectors testing, the procedures of ASHRAE 93 Standard testing can be summarized as follows:

1) Feeding the water into the solar collectors at a controlled inlet temperature.
2) Measuring the solar radiation on the plane of solar collectors (I_T).
3) Measuring the water flow rate ($\dot{m}_w$), the collector inlet and outlet hot water temperatures ($T_{Coll,i}$ and $T_{Coll,o}$), and ambient temperature (T_{Amb}).
4) Measuring the pressure (P) and pressure drop across the solar collectors (ΔP).

The general testing procedure is to operate the collectors in steady state conditions and, measure the parameters to determine the collector useful heat gain ($\dot{Q}_{Coll}$) from Eq. (2-18) and measure the total solar radiation on the plan of solar collectors (I_T), the collector inlet and outlet temperature of water ($T_{Coll,i}$ and $T_{Coll,o}$), and the ambient temperature (T_{Amb}), which are needed to analyze based on Eq. (2-20). Thus the transmittance-absorptance $(\tau\alpha)_n$ product for these test conditions is approximately equal to the normal-incidence value and is written as Figure 2-12

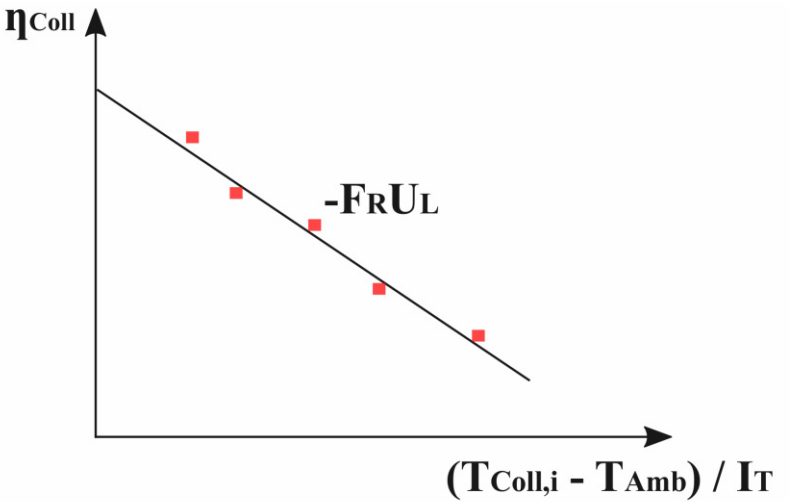

Figure 2-12 Experimental solar collectors efficiency data

Instantaneous efficiency is determined by $\eta_{Coll} = \dot{m}_w c_{p,w}(T_{Coll,o} - T_{Coll,i})/A_{Coll} I_T$ and is plotted as a function of $(T_{Coll,i} - T_{Amb})/I_T$. A simple plot of experimental data at under conditions of ASHRAE 93 Standard testing is shown in Figure 2-12. The plot between η_{Coll} and $(T_{Coll,i} - T_{Amb})/I_T$ are straight line with intercept $F_R(\tau\alpha)_e$ and slope $-F_R U_L$ (In testing, there are many data points and the least-squares fit is applied to find the best constants of the line equation).

2.1.4 Solar Water Heating System (SWHS) and Mathematical Modeling

- **Solar Water Heating System (SWHS)**

The solar water heating system (SWHS) as shown in Figure 2-13 usually mainly consists of solar collectors, thermal storage tank, and collector pump. For this SWHS, the solar collectors absorb solar radiation and convert it into heat. This heat is then absorbed by a HTF (e.g. water, molten salts, oil, etc.) and then stored in a thermal storage tank or directly used [47].

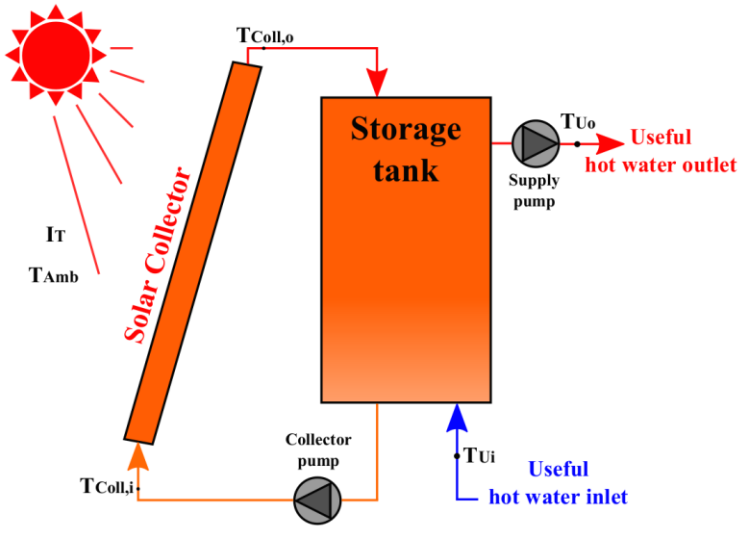

Figure 2-13 Schematic diagram of solar water heating system (SWHS)

- **Mathematical Modeling of Solar Collectors**

The collector useful heat gain or the heat transfer rate from the solar collectors ($\dot{Q}_{Coll}$) is calculated by the Eq. (2-18) or (2-19). If each collectors is connected in series connection as shows in Figure 2-14. The characteristics of the total unit in terms of $F_R(\tau\alpha)_e$ and $F_R U_L$ can be evaluated from [48].

$$(F_R(\tau\alpha)_e)_{Total} = (F_R(\tau\alpha)_e)_{Single\ unit}\left[\frac{1-(1-K)^{N_{Series}}}{N_{Series}K}\right] \tag{2-22}$$

$$(F_R U_L)_{Total} = (F_R U_L)_{Single\ unit}\left[\frac{1-(1-K)^{N_{Series}}}{N_{Series}K}\right] \tag{2-23}$$

where $K = \frac{A_{Coll}(F_R U_L)_{Single\ unit}}{\dot{m}_w c_{p,w}}$

N_{Series} : Number of collectors in series connection

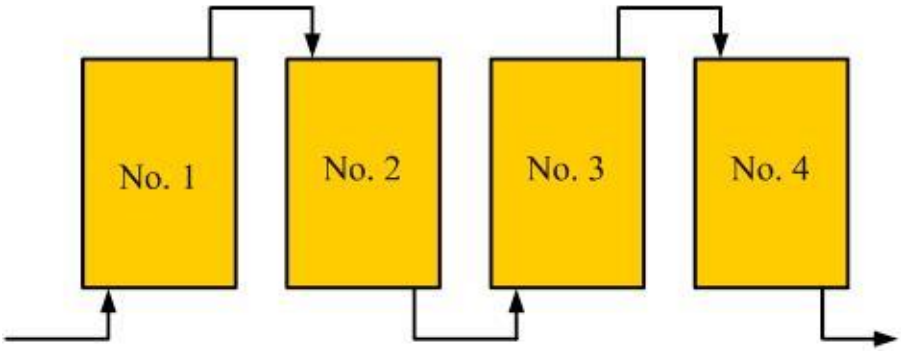

Figure 2-14 An example of solar collectors is connected in series connection

If the collectors is to be used at a flow rate other than that of the test conditions (For ASHRAE 93 Standard testing: $\dot{m}_{STD}$ = 75 kg/m^2-hr), an approximate analytical correction to $F_R(\tau\alpha)_e$ and $F_R U_L$ can be obtained from the ratios of values of r. The ratio r by which $F_R(\tau\alpha)_e$ and $F_R U_L$ are to be corrected is then given by

$$r = \frac{\frac{\dot{m}_w c_{p,w}}{A_{Coll}F'U_L}\left[1-exp\left(-A_{Coll}F'U_L/\dot{m}_w c_{p,w}\right)\right]\Big|_{use}}{\frac{\dot{m}_{STD} c_{p,w}}{A_{Coll}F'U_L}\left[1-exp\left(-A_{Coll}F'U_L/\dot{m}_{STD} c_{p,w}\right)\right]\Big|_{test}} \tag{2-24}$$

when $$F'U_L = -\frac{\dot{m}_w c_{p,w}}{A_c} ln\left[1-\frac{(F_R U_L)A_c}{\dot{m}_w c_{p,w}}\right] \tag{2-25}$$

Then characteristics of the new water flow rate in terms of $F_R(\tau\alpha)_e$ and $F_R U_L$ can be evaluated from

$$\left(F_R(\tau\alpha)\right)_{new} = \left(F_R(\tau\alpha)\right)_{test} \times r \tag{2-26}$$

$$(F_R U_L)_{new} = (F_R U_L)_{test} \times r \tag{2-27}$$

2.1.5 Mathematical Modeling of the Thermal Energy Storage Tank

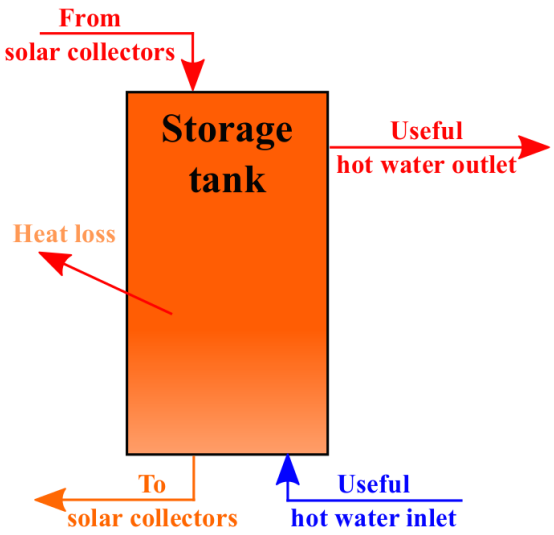

Figure 2-15 Energy balance of the thermal energy storage tank

Figure 2-15 shows an energy balance for calculation of the thermal energy storage tank. The energy storage capacity of a water storage unit at uniform temperature (fully mixed or non-stratified) operating over a finite temperature difference is given by

$$\dot{Q}_{ST} = \left(Mc_{p,w}\right)_{ST} \Delta T_{ST} \tag{2-28}$$

where $\dot{Q}_{ST}$: The total heat capacity for a cycle operating through to the temperature range ΔT_{ST}

M : Mass or volume of water in the unit (kg or m^3)

An energy balance on the non-stratified tank is given by

$$\left(Mc_{p,w}\right)_{ST} \frac{dT_{ST}}{dt} = Energy\ input - Energy\ output - Energy\ loss \tag{2-29}$$

where $Energy\ input$: Rate of energy input (kW_{th})

$Energy\ output$: Rate of energy output (kW_{th})

$Energy\ loss$: Rate of energy loss to the environment (kW_{th})

From Eq. (2-29), using the numerical method, the water temperature can be calculated from

$$T_{ST}^{t+\Delta t} = T_{ST}^{t} + \frac{\Delta t}{\left(Mc_{p,w}\right)_{ST}} [Energy\ input - Energy\ output - Energy\ loss] \tag{2-30}$$

where $T_{ST}^{t+\Delta t}$: The temperature of water at time equal to $t + \Delta t$

T_{ST}^{t} : The temperature of water at time t

t : Time

Δt : Time step

2.1.6 Mathematical Modeling of an Ambient Temperature

The ambient temperature is modeled by a sinusoidal function, taking into account the daily maximum and minimum ambient temperature. The ambient temperature at any time can be calculated as follows [49]:

$$T_{Amb}(t) = \frac{1}{2}\left[(T_{max} + T_{min}) + (T_{max} + T_{min})sin\left(\frac{2\pi(t - t_p)}{24}\right)\right] \quad (2\text{-}31)$$

where $T_{Amb}(t)$: The ambient temperature at time t
T_{max} : The maximum ambient temperature of the day (˚C)
T_{min} : The minimum ambient temperature of the day (˚C)
t_p : 9 hr
t : The time in hours of interest

Calculation steps for evaluating the SWHS are shown in Figure 2-16. Inputs of the simulation were the hourly total solar radiation on the sloped surface (I_T), step time, mass or volume of water in the storage tank (M), total number of collectors (N_{Coll}), number of collectors in series connection (N_{Series}), collector hot water flow rate ($\dot{m}_w$), useful hot water flow rate or demand of hot water ($\dot{m}_L$), initial hot water temperature in the tank ($T_{ST,i}$), demand of hot water temperature (T_{Set}) and ambient temperature (T_{Amb}). For the step of calculations, the system were evaluated to find out energy input from solar collectors and auxiliary heater, energy output to the user (demand of hot water), energy loss (heat loss), and hot water temperature in the tank.

2.2 Industrial Waste Heat (IWH)

Industrial waste heat (IWH) is the unusable heat generated from hot combustion gases discharged to the atmosphere, heated products exiting industrial processes, and heat transfer from hot equipment surfaces [9]. From the research publication of BSC Incorporated [9], it was reported that the quantity of IWH was as much as 20 to 50% of industrial energy consumption. Moreover, exhausted gases are mostly at relatively high temperature while water streams are mostly liquids at low-temperature [50].

Waste heat sources from industries can be classified in three different temperature levels as low-temperature (< 230 ºC), medium-temperature (230 – 650 ºC), and high-temperature (> 650 ºC). This temperature classification of IWH sources with typical recovery method is listed in Table 2-2. From the list, none of available technologies can produce electricity from the heat with temperature below 70 ºC. Therefore, if there is a technology applicable for power generation with below 70 ºC heat source, this heat will become more beneficial and interesting energy source for industrial sectors.

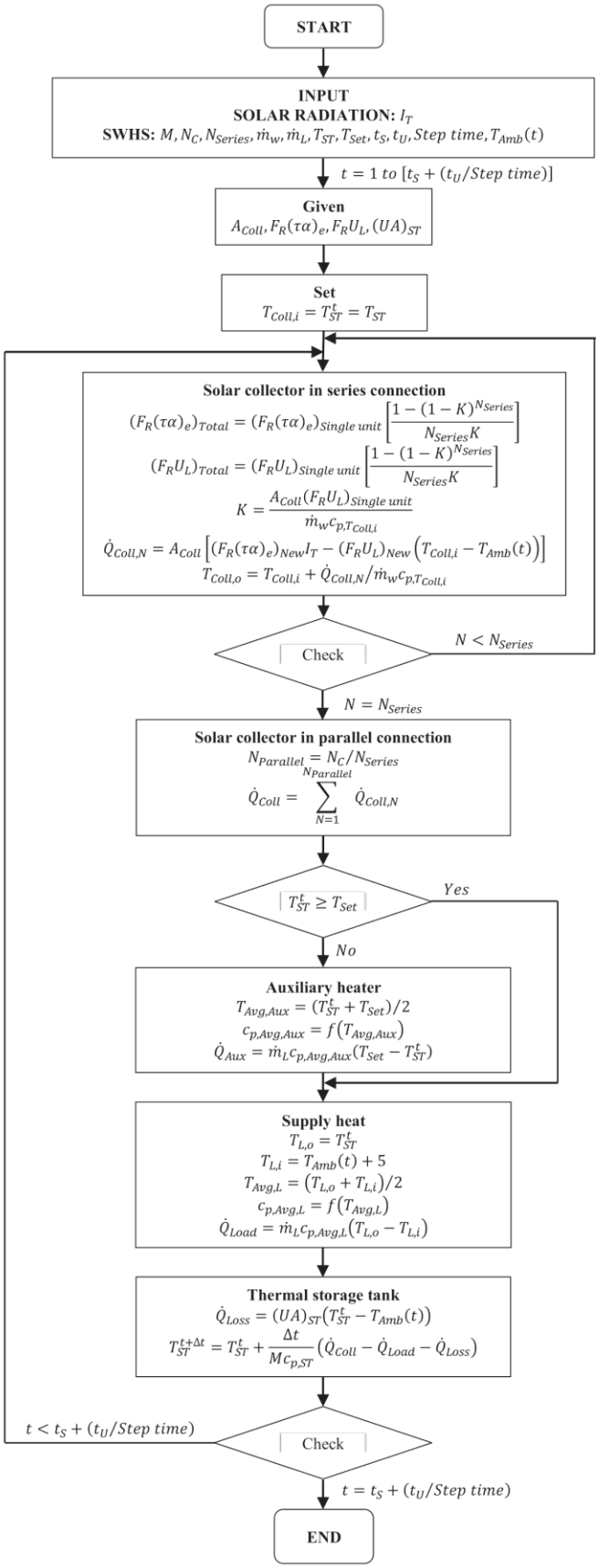

Figure 2-16 Calculation step of the solar water heating system (SWHS)

Table 2-2 Temperature classification of industrial waste heat (IWH) sources with typical recovery method [9]

Categories	Example sources	Temperature (°C)	Typical Recovery Methods / Technologies
High	Nickel refining furnace	1370 – 1650	Combustion air preheater
(> 650 °C)	Steel electric arc furnace	1370 – 1650	
	Basic oxygen furnace	1200	Steam generation for process
	Aluminum reverberatory furnace	1100 – 1200	heating or for mechanical /
	Copper refining furnace	760 – 820	electrical work
	Steel heating furnace	930 – 1040	
	Copper reverberatory furnace	900 – 1090	Transfer to medium-low
	Hydrogen plants	650 – 1430	temperature processes
	Fume incinerators	1300 – 1540	
	Coke oven	650 – 1000	
	Iron cupola	820 – 980	
Medium	Steam boiler exhaust	230 – 480	Combustion air preheat
(230 - 650 °C)	Gas turbine exhaust	370 – 540	Steam / power generation
	Reciprocating engine exhaust	320 – 590	Organic Rankine Cycle for
	Heat treating furnace	430 – 650	power generation
	Drying & baking ovens	230 – 590	Furnace load preheating,
	Cement kilin	450 – 620	Feed water preheating,
			Transfer to low-temperature processes
Low	Exhaust gases exiting recovery	70 – 230	Space heating
(< 230 °C)	Devices in gas-fired boilers,		
	Ethylene furnaces, etc.		Domestic water heating
	Process steam condensate	50 – 90	
	Cooling water from:		Upgrading via a heat pump to
	Furnace doors	30 – 50	increase temperature for end use
	Annealing furnaces	70 – 230	Organic Rankine Cycle
	Air compressors	30 – 50	
	Internal combustion engines	70 – 120	
	Air conditioning and	30 – 40	
	Refrigeration condensers		
	Drying, baking, and curing ovens		
	Hot processed liquids/solids		

2.3 Organic Rankine Cycle (ORC)

An Organic Rankine Cycle (ORC) power generation has the favorable characteristics of simple structure, high reliability, low cost and easy maintenance. Its proved to be one of the most reliable and an efficient solution that utilizes the low-temperature heat such as industrial and household waste heat, gas, steam turbines, and internal combustion engines exhaust heat, solar, geothermal, biomass, etc.

2.3.1 System Description

A schematic diagram of the ORC system and the corresponding T-s diagram are shown in Figure 2-17 and Figure 2-18, respectively. The system mainly consists of condenser, pump, evaporator, turbine and generator. For the system operations; at state 2, low-temperature HTF of the ORC system is heated by the heat source via a heat exchanger to state 3 at which the HTF is at saturated vapor state with high pressure through an evaporator. From state 3 to 4, the vapor is expanded through a turbine expander to generate power. Finally, it is condensed to a saturated liquid in the condenser at state 1 to complete the cycle.

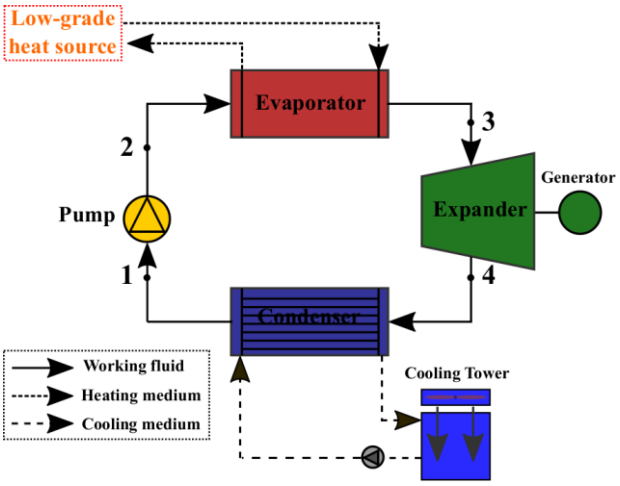

Figure 2-17 Schematic diagram of the ORC system

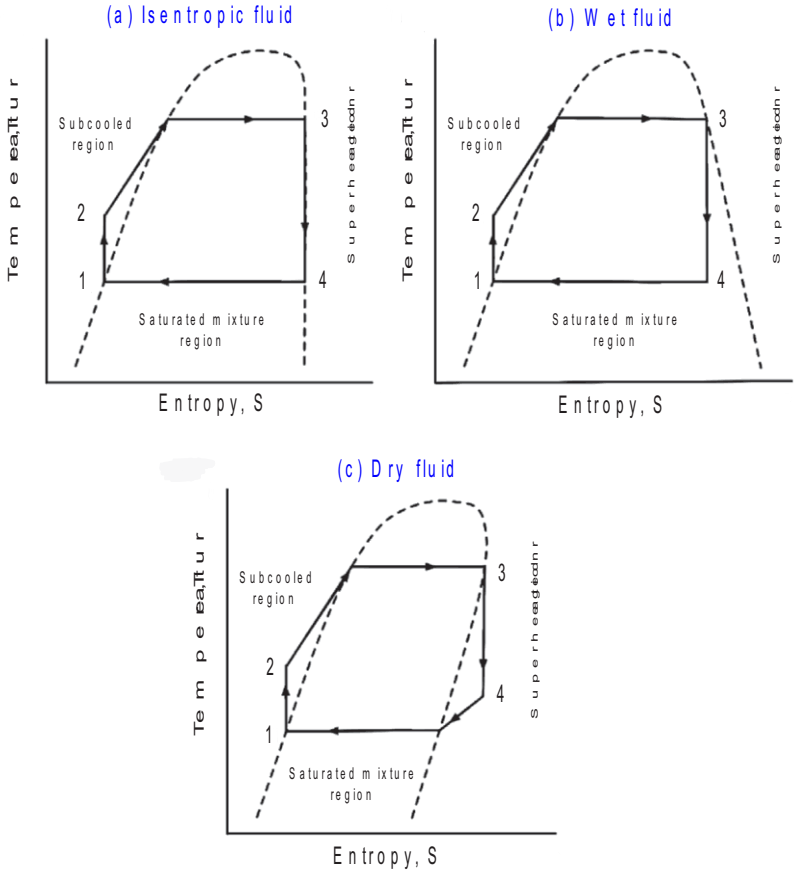

Figure 2-18 T-s diagram of the ideal ORC system [15, 51]

From Figure 2-18, the process 1 to 2 is isentropic compression for liquid pumping and the process 3 to 4 is isentropic expansion in a turbine. In practice, there are effects of heat loss and friction on the cycle performance therefore, the actual exit state of the pump and the turbine are states 2a and 4a, respectively as shown in Figure 2-19.

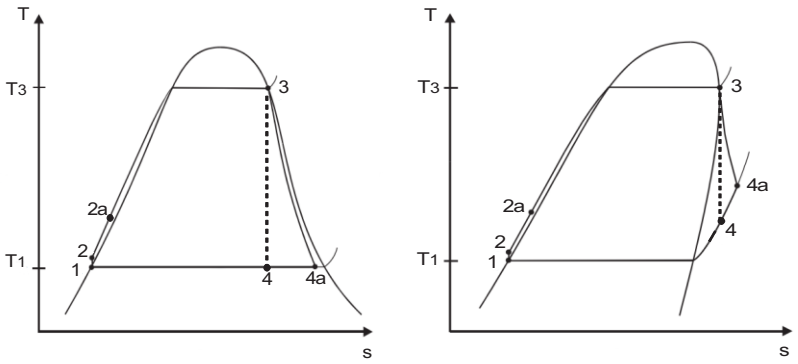

(a) Wet fluid (b) Dry fluid

Figure 2-19 T-s diagram of the actual ORC system [52]

From Figure 2-19 (b), the turbine outlet temperature (T_{4a}) is higher than the pump outlet temperature (T_{2a}). It means that, the system can be rewarding to implement an internal heat exchanger (IHE) into the cycle as shown in Figure 2-20. The turbine exhaust flows into the IHE and cools in the process 4a to 4IHE by transferring heat to the compressed liquid that is heated in the process 2a to 2IHE as shown in Figure 2-21. Therefore, the heat input rate to the evaporator is lower than that without IHE. From the above results, it could be seen that adding the IHE into the ORC system, the thermal efficiency of the cycle could be improved.

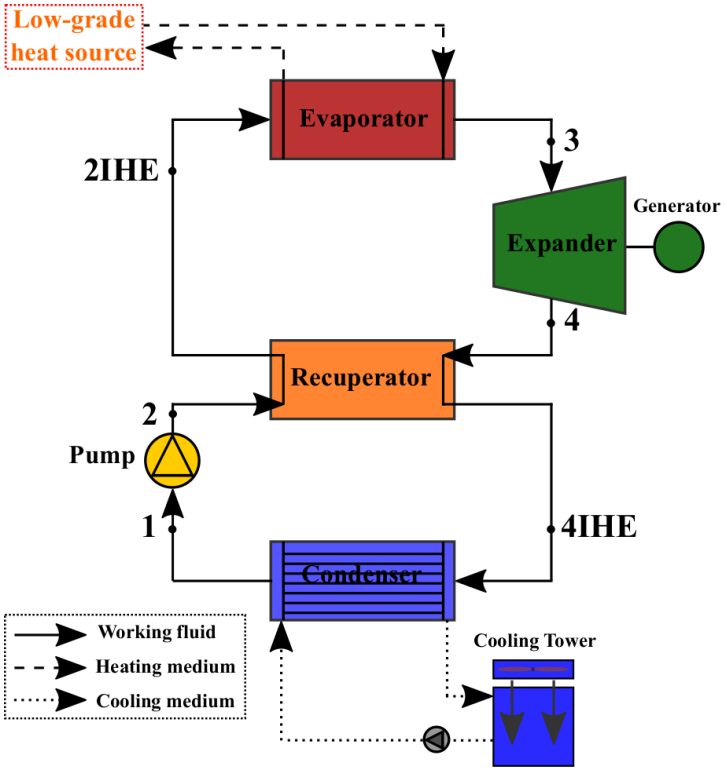

Figure 2-20 Schematic diagram of the ORC with internal heat exchanger (IHE)

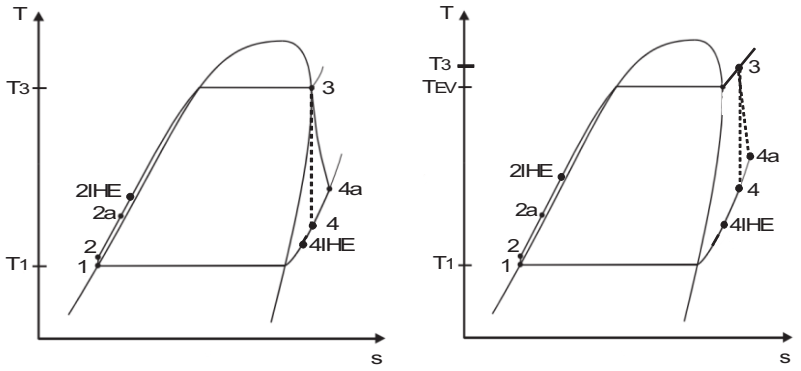

(a) Saturated vapor (b) Super heating

Figure 2-21 T-s diagram of the ORC with internal heat exchanger (IHE)

2.3.2 Mathematical Model of the Organic Rankine Cycle (ORC) System

The equation used to calculate the performances of the ORC system with and without IHE are summarized as follows [28, 53]:

For the ORC without IHE

Pump

$$\dot{W}_{Pump,ORC} = \frac{\dot{m}_{r,ORC} v_1 (P_2 - P_1)}{\eta_{Pump,ORC}} \tag{2-32}$$

$$\dot{W}_{Pump,ORC} = \dot{m}_{r,ORC} (h_{2a} - h_1) \tag{2-33}$$

$$h_{2a} = \frac{v_1 (P_2 - P_1)}{\eta_{Pump,ORC}} + h_1 \tag{2-34}$$

Pump efficiency

$$\eta_{Pump,ORC} = \frac{P_2 - P_1}{h_{2a} - h_1} \tag{2-35}$$

Evaporator

$$\dot{Q}_{Evap,ORC} = \dot{m}_{r,ORC} (h_3 - h_{2a}) \tag{2-36}$$

Turbine

$$\dot{W}_{Tur} = \dot{m}_{r,ORC} (h_3 - h_4) \eta_{Tur} \tag{2-37}$$

Turbine efficiency

$$\eta_{Tur} = \frac{h_3 - h_{4a}}{h_3 - h_4} \tag{2-38}$$

Condenser

$$\dot{Q}_{Cond,ORC} = \dot{m}_{r,ORC} (h_{4a} - h_1) \tag{2-39}$$

Thermal efficiency

$$\eta_{th,ORC} = \frac{\dot{W}_{Tur} - \dot{W}_{Pump,ORC}}{\dot{Q}_{Evap,ORC}} \tag{2-40}$$

For the ORC with IHE

Evaporator

$$\dot{Q}_{Evap,ORC} = \dot{m}_{r,ORC}\left(h_3 - h_{2,IHE}\right) \tag{2-41}$$

Condenser

$$\dot{Q}_{Cond,ORC} = \dot{m}_{r,ORC}\left(h_{4,IHE} - h_1\right) \tag{2-42}$$

Internal Heat Exchanger (IHE)

$$\dot{Q}_{IHE} = \dot{m}_{r,ORC} c_{p,4a}\left(T_{4a} - T_{4,IHE}\right) \tag{2-43}$$

$$\dot{Q}_{IHE} = \dot{m}_{r,ORC} c_{p,2a}\left(T_{2,IHE} - T_{2a}\right) \tag{2-44}$$

$$\dot{Q}_{IHE} = \varepsilon_{IHE}\left(\dot{m}_{r,ORC} c_p\right)_{min}\left(T_{4a} - T_{2a}\right) \tag{2-45}$$

2.4 Heat Boosting Technologies

Heat boosting technologies, as an efficient and energy conservation technology, present unique advantages for environmental protection and energy usage [35]. In addition, these technologies are more efficient than the electrical heating system [54-57]. Generally, heat boosters use the external energy input to drive a cycle that extracts heat from the low-temperature heat source to the high-temperature heat sink/heat reservoir.

2.4.1 Vapor Compression Heat Pump (VCHP) System

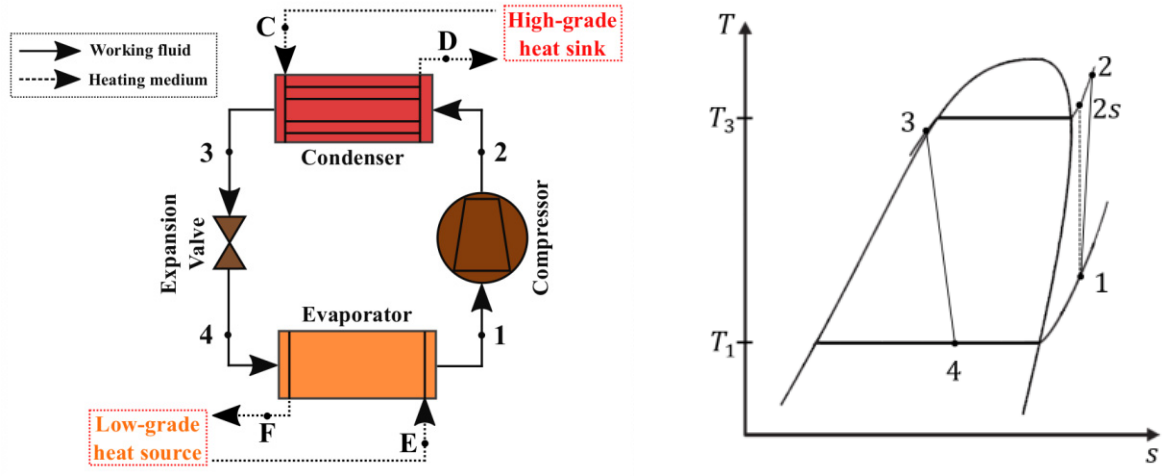

(a) (b)

Figure 2-22 (a) Schematic diagram and (b) T-s diagram of the VCHP system

- **System Description**

The vapor compression heat pump (VCHP) system is a thermal upgrading device driven by electrical power. In general, it consists of compressor, condenser, expansion valve, and evaporator. A schematic diagram of the VCHP system and corresponding T-s diagram are shown in Figure 2-22. For the system operations; at state 4, a low-temperature HTF of the

VCHP system is heated by the heat source via a heat exchanger. From state 1 to 2, the HTF is compressed in the compressor to increase its temperature and pressure, and state 2s is the corresponding states for the isentropic case. From state 2 to 3, the high-temperature HTF is condensed by releasing the heat at the condenser via a heat exchanger and its pressure due to throttling effect. At state 4, the low-temperature HTF is entering the evaporator to restart next cycle.

- **Mathematical Model of the VCHP System**

The energy equations of the VCHP system are summarized as follows:

The rate of heat transfer to the VCHP evaporator ($\dot{Q}_{Evap,VCHP,th}$):

$$\dot{Q}_{Evap,VCHP,th} = \dot{m}_{r,VCHP}(h_1 - h_4) = \left(\dot{m}c_p\right)_{w1}(T_E - T_F) \tag{2-46}$$

The rate of heat transfer from the VCHP condenser ($\dot{Q}_{Cond,VCHP}$):

$$\dot{Q}_{Cond,VCHP,th} = \dot{m}_{r,VCHP}(h_2 - h_3) = \left(\dot{m}c_p\right)_{w2}(T_D - T_C) \tag{2-47}$$

The work input to the VCHP system ($\dot{W}_{Comp,VCHP}$):

$$\dot{W}_{Comp,VCHP,th} = \dot{Q}_{Cond,VCHP,th} - \dot{Q}_{Evap,VCHP,th} = \dot{m}_{r,VCHP}(h_2 - h_1) \tag{2-48}$$

$$\dot{W}_{Comp,VCHP,el} = \frac{\dot{W}_{Comp,VCHP,th}}{\eta_{Comp,ME}\eta_{Comp,MO}} \tag{2-49}$$

$$\eta_{Comp,VCHP,isen} = \frac{h_{2,isen} - h_1}{h_2 - h_1} \tag{2-50}$$

Coefficient of performance of the VCHP system (COP_{VCHP}):

$$COP_{VCHP} = \frac{\dot{Q}_{Cond,VCHP,th}}{\dot{W}_{Comp,VCHP,th}} = \frac{h_2 - h_3}{h_2 - h_1} \tag{2-51}$$

Calculation step of the VCHP system as shown in Figure 2-23. Inputs of the simulation were the heat source and heat sink/reservoir temperature (T_E and T_D), mass flow rate of heat source and heat sink/reservoir ($\dot{m}_{w1}$ and $\dot{m}_{w2}$), working fluid or refrigerant, isentropic compressor efficiency ($\eta_{Comp,VCHP,isen}$), mechanical and motor compressor efficiency ($\eta_{Comp,ME}$ and $\eta_{Comp,MO}$), degree of superheating (SH) and sub-cooling (SC), heat exchanger effectiveness (ε_{HX}), temperature different (ΔT_{HX}), and pinch point temperature (PT). For the step of calculations, the system were evaluated to find out the energy balance of the system consists of rate of heat transfer to the VCHP evaporator ($\dot{Q}_{Evap,VCHP}$), rate of heat transfer from the VCHP condenser ($\dot{Q}_{Cond,VCHP}$), power input to the VCHP compressor ($\dot{W}_{Comp,VCHP,el}$), and coefficient of performance of the VCHP system (COP_{VCHP}).

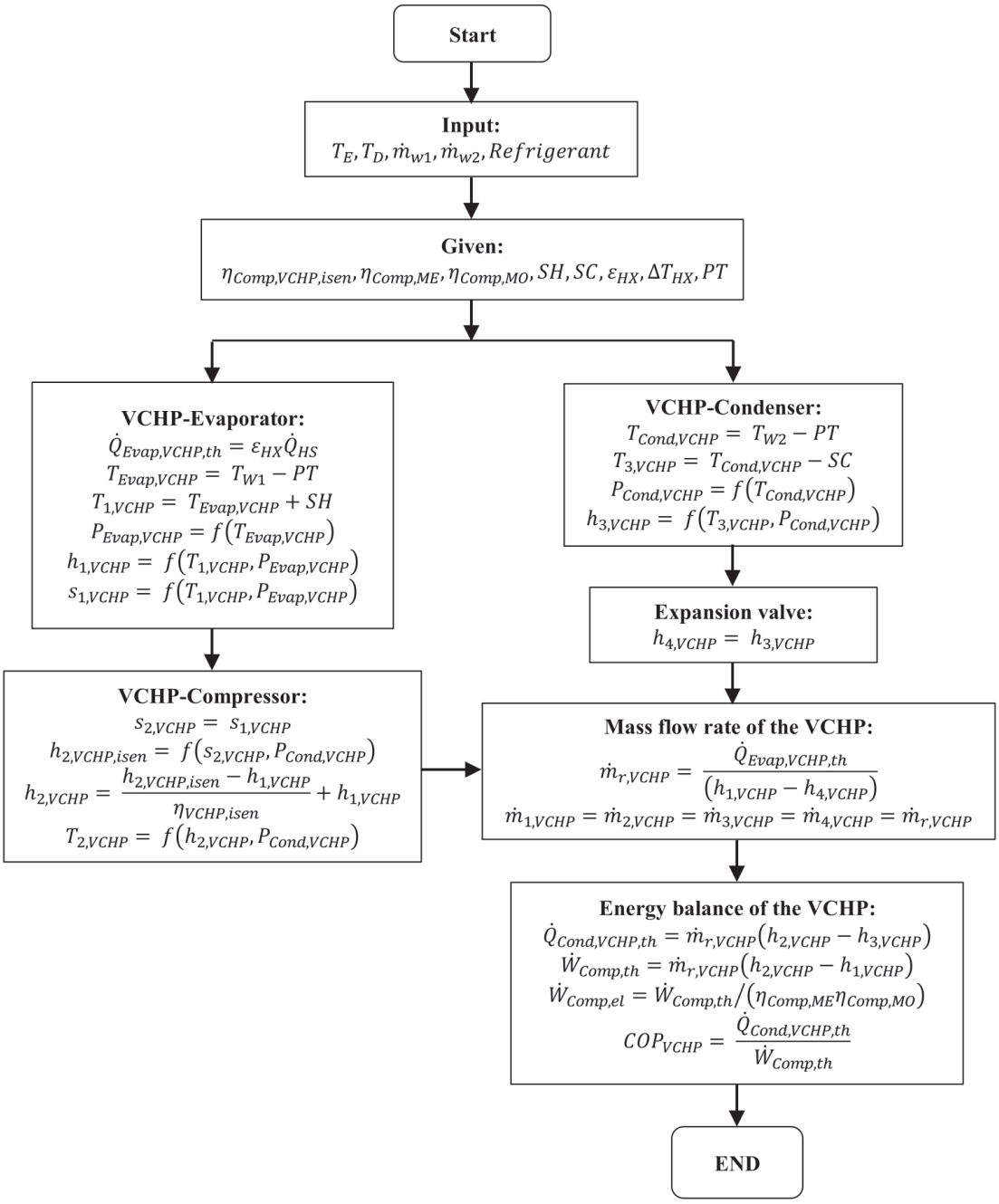

Figure 2-23 Calculation step of the VCHP system [58]

2.4.2 Gas Engine-driven Heat Pump (GEHP) System

- **System Description**

The gas engine-driven heat pump (GEHP) system is a vapor compression refrigeration type with an open compressor. It is driven by gas-fuel (i.e. Natural Gas (NG), Liquid Petroleum Gas (LPG)) internal combustion engine instead of an electrical motor. A schematic diagram of the GEHP system is shown in Figure 2-24. The GEHP system mainly consists of two parts: (i) heat pump consisting of compressor, condenser, expansion valve, and evaporator, and (ii) gas engine system to drive the compressor. Normally the efficiency of a gas engine is not very high (about 30 – 40%). However, the waste heat of fuel combustion

can be utilized from the exhaust gas and the heat released by engine cylinder jacket approximately 80% [59].

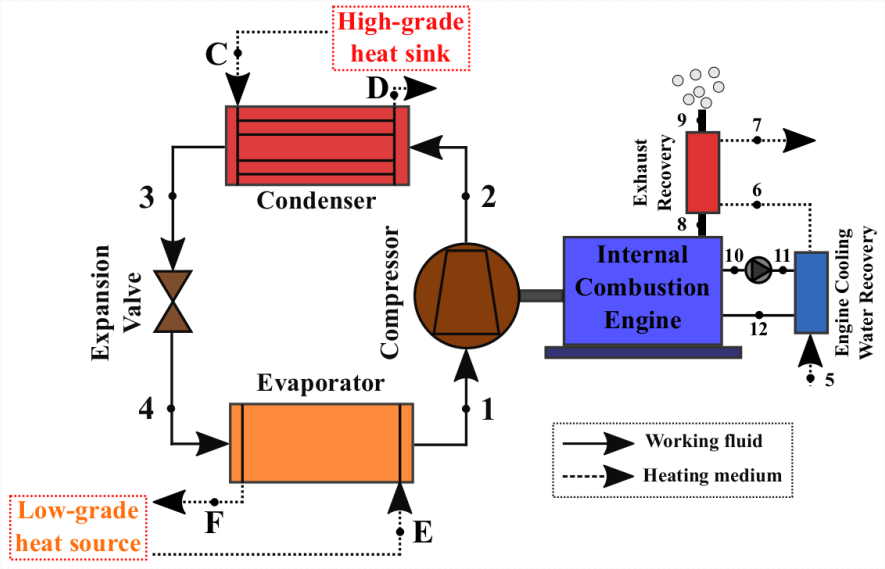

Figure 2-24 Schematic diagram of the GEHP system

- **Mathematical Model of the GEHP System**

The energy equations of the GEHP system are summarized as follows [59]:

Gas engine power consumption ($\dot{W}_{Comp,GEHP}$):

$$\dot{W}_{Comp,GEHP} = \dot{W}_{ge,i} \cdot \eta_{GEHP,ME} \cdot \eta_{belt} \tag{2-52}$$

Gas engine thermal efficiency ($\eta_{ge,th}$):

$$\eta_{ge,th} = \frac{\dot{W}_{ge,i}}{\dot{Q}_{i,GEHP}} = \frac{\dot{W}_{ge,i}}{\dot{m}_{fuel} \cdot q_{LHV} \cdot \eta_{Comb}} \tag{2-53}$$

Fuel mass flow rate ($\dot{m}_{fuel}$):

$$\dot{m}_{fuel} = \frac{\dot{W}_{ge,i}}{\eta_{Comb} \cdot \eta_{ge,th} \cdot q_{LHV}} = \frac{\dot{W}_{Comp,GEHP}}{\eta_{Comb} \cdot \eta_{GEHP,ME} \cdot \eta_{belt} \cdot \eta_{ge,th} \cdot q_{LHV}} \tag{2-54}$$

Coefficient of performance of the GEHP system (COP_{GEHP}):

$$COP_{GEHP} = \frac{\dot{Q}_{Cond,GEHP}}{\dot{Q}_{i,GEHP}} = \frac{\dot{Q}_{Cond,GEHP}}{\dot{m}_{fuel} \cdot q_{LHV} \cdot \eta_{comb}} = \frac{\dot{Q}_{Cond,GEHP}}{\dot{W}_{Comp,GEHP}} \cdot \eta_{GEHP,MO} \cdot \eta_{belt} \cdot \eta_{ge,th} \tag{2-55}$$

Calculation step of the GEHP system as shown in Figure 2-25. Input of the simulation were the heat source and heat sink/reservoir temperature (T_E and T_D), mass flow rate of heat source and heat sink/reservoir ($\dot{m}_{w1}$ and $\dot{m}_{w2}$), isentropic compressor efficiency ($\eta_{GEHP,isen}$), mechanical ($\eta_{GEHP,ME}$), gas engine ($\eta_{ge,th}$), gas engine combustion (η_{Comb}) and power transmission (η_{belt}) efficiency, and fuel lower heating value (q_{LHV}). For the step of calculations, the system were evaluated to find out the energy balance of the system consists of rate of heat transfer from the GEHP condenser ($\dot{Q}_{Cond,GEHP}$), fuel consumption ($\dot{m}_{fuel}$), and coefficient of performance of the GEHP system (COP_{GEHP}).

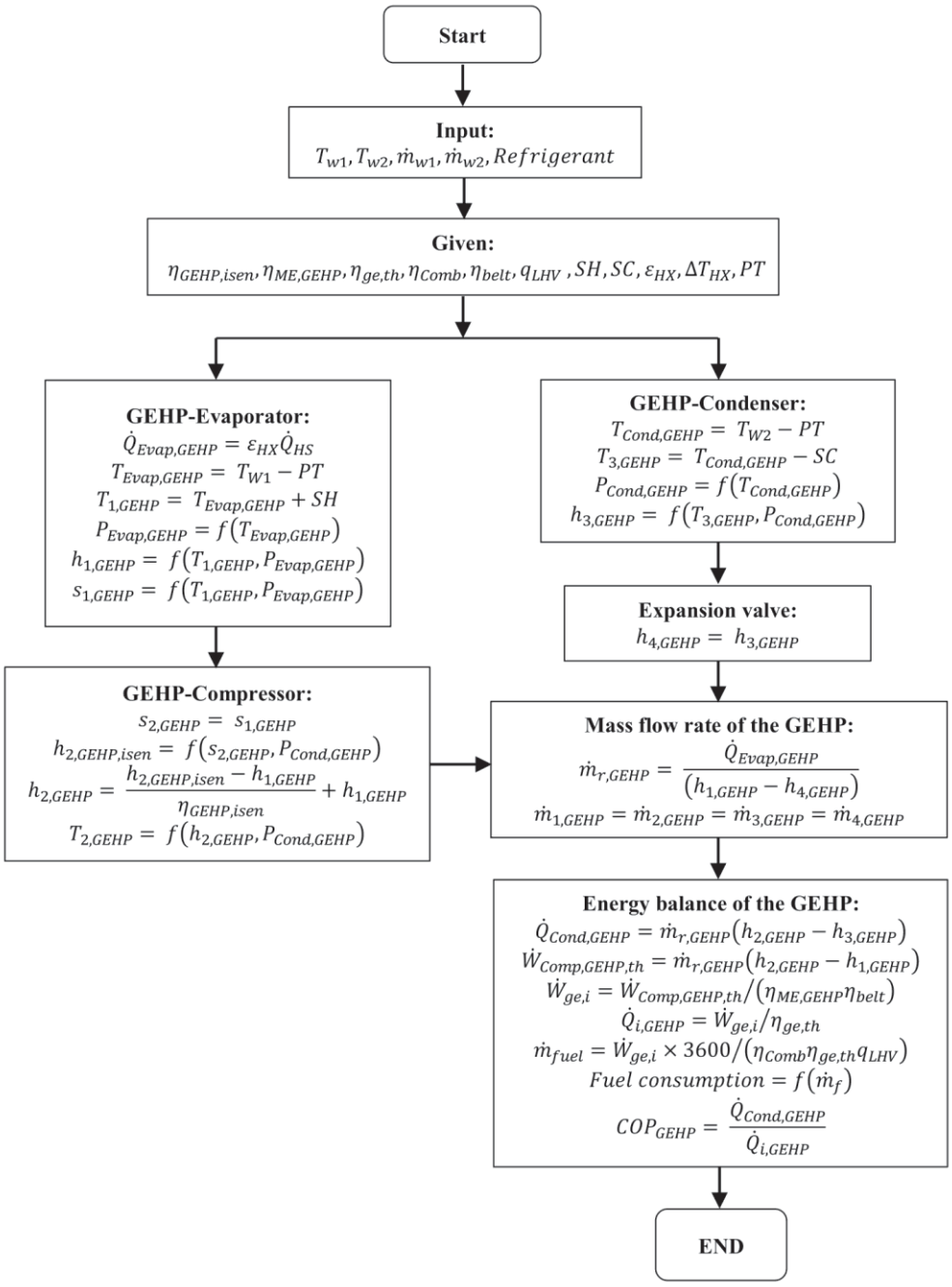

Figure 2-25 Calculation step of the GEHP system

2.4.3 Absorption Heat Transformer (AHT) System

- **System Description**

The absorption heat transformer (AHT) system is one of heat pump technologies; it used for the heating process produce the water at high-temperature from a low-to-medium temperature heat source. The system usually consists of generator, water pump, solution pump, evaporator, absorber, condenser, and cooling tower. A schematic diagram of the AHT system is shown in Figure 2-26. For the system operations; at the generator, a binary liquid mixture consisting of a volatile component (absorbent) is heated by the low-grade heat source via a heat exchanger. At state 1, some part of the absorbent is boiled at a low-pressure

($P_{AHT,Cond}$) and a generator temperature ($T_{AHT,Gend}$). It is then condensed from vapor to liquid state in the condenser at a condenser temperature ($T_{AHT,Cond}$) at state 2. After that, the absorbent in a liquid phase is pumped to the evaporator at state 3, of which the pressure ($P_{AHT,Evap}$) is higher than that of the condenser. At the evaporator, the absorbent of the AHT system is heated by the low-grade heat source via a heat exchanger. At state 4, then a part of the absorbent in a form of vapor enters to the absorber at the same pressure as the evaporator. Meanwhile, the pressure of a liquid mixture from the absorber is increased at state 7. In the absorber, the strong solution absorbs the absorbent vapor, and the weak solution leaves the absorber at state 8. During absorption process, heat is released at a high temperature ($T_{AHT,Abs}$) which is greater than those at the generator and the evaporator. After that, the weak solution at state 8, from the absorber is then throttled to a low-pressure through the IHE at state 9, into the generator again at state 10, and new cycle restarts [58].

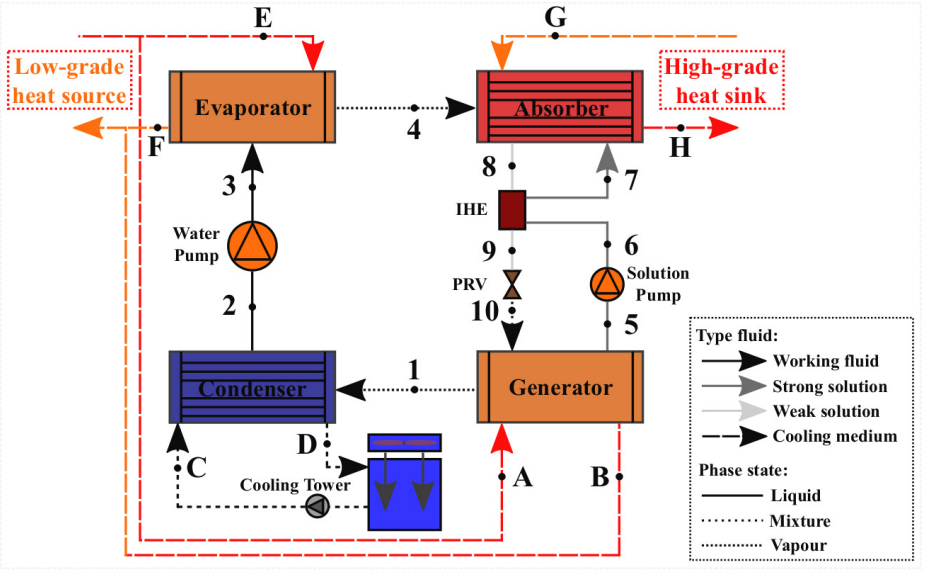

Figure 2-26 Schematic diagram of the AHT system

- **Mathematical Model of the VCHP System**

The energy equations of the AHT system are summarized as follows [58]:

The rate of heat transfer to the Generator ($\dot{Q}_{Gen}$):

$$\dot{Q}_{Gen} = \dot{m}_1 h_1 + \dot{m}_5 h_5 - \dot{m}_{10} h_{10} \tag{2-56}$$

$$\dot{m}_{10} = \dot{m}_1 + \dot{m}_5 \tag{2-57}$$

$$\dot{m}_{10} X_{10} = \dot{m}_5 X_5, (X_1 = 0) \tag{2-58}$$

From Eq. (2-57) and Eq. (2-58)

$$\dot{m}_5 = \frac{\dot{m}_1 X_{10}}{X_5 - X_{10}} \tag{2-59}$$

and $$\dot{m}_{10} = \frac{\dot{m}_1 X_5}{X_5 - X_{10}} \quad (2\text{-}60)$$

The rate of heat transfer to the AHT condenser ($\dot{Q}_{Cond,AHT}$):

$$\dot{Q}_{Cond,AHT} = \dot{m}_{ref}(h_1 - h_2) \quad (2\text{-}61)$$

$$\dot{m}_{ref} = \dot{m}_1 = \dot{m}_2 = \dot{m}_3 = \dot{m}_4 \quad (2\text{-}62)$$

The work input to the AHT pump and the AHT solution pump:

$$W_{P,AHT,th} = \left(P_{Evap,AHT} - P_{Cond,AHT}\right)\left(\frac{v_2 \dot{m}_2}{\eta_P}\right) \quad (2\text{-}63)$$

$$W_{P,AHT,el} = W_{P,AHT,th}/\left(\eta_{P,ME}\eta_{P,MO}\right) \quad (2\text{-}64)$$

$$W_{SP,AHT,th} = \left(P_{Evap,AHT} - P_{Cond,AHT}\right)\left(\frac{v_5 \dot{m}_5}{\eta_{SP}}\right) \quad (2\text{-}65)$$

$$W_{SP,AHT,el} = W_{SP,AHT,th}/\left(\eta_{P,ME}\eta_{P,MO}\right) \quad (2\text{-}66)$$

$$h_2 \approx h_3 \quad (2\text{-}67)$$

$$h_5 \approx h_6 \quad (2\text{-}68)$$

The rate of heat transfer to the AHT evaporator ($\dot{Q}_{Evap,AHT}$):

$$\dot{Q}_{Evap,AHT} = \dot{m}_{ref}(h_4 - h_3) \quad (2\text{-}69)$$

The rate of heat transfer to the absorber ($\dot{Q}_{Abs,AHT}$):

$$\dot{Q}_{Abs} = \dot{m}_4 h_4 + \dot{m}_7 h_7 - \dot{m}_8 h_8 \quad (2\text{-}70)$$

$$\dot{m}_8 = \dot{m}_4 + \dot{m}_7 \quad (2\text{-}71)$$

$$\dot{m}_8 X_8 = \dot{m}_7 X_7 \quad (2\text{-}72)$$

The AHT Internal Heat Exchanger (IHE)

$$\dot{Q}_{IHE} = \dot{m}_8 c_{p8}(T_8 - T_9) = \dot{m}_6 c_{p6}(T_7 - T_6) = \varepsilon_{HX}\left(\dot{m}c_p\right)_{min}(T_8 - T_6) \quad (2\text{-}73)$$

$$\dot{m}_8 = \dot{m}_9 \quad (2\text{-}74)$$

$$\dot{m}_6 = \dot{m}_7 \quad (2\text{-}75)$$

AHT Expansion valve (Throttling process)

$$h_9 = h_{10} \tag{2-76}$$

Coefficient of performance of the AHT system (COP_{AHT}):

$$COP_{AHT} = \frac{\dot{Q}_{Abs,AHT}}{\dot{Q}_{Evap,AHT} + \dot{Q}_{Gen} + W_{P,AHT,th} + W_{SP,AHT,th}} \tag{2-77}$$

Calculation step of the AHT system as shown in Figure 2-27. Input of the simulation were the heat source temperature ($T_A \; and \; T_E$), mass flow rate of heat source ($\dot{m}_w$), ambient temperature (T_{Amb}), minimum concentration of weak H_2O-LiBr solution (X_{min}), and difference of strong and weak H_2O-LiBr solution ($\Delta X_{s,min}$), isentropic water pump and solution pump efficiency ($\eta_{AHT,P,isen}$ and $\eta_{AHT,SP,isen}$). For the step of calculations, the system were evaluated to find out the energy balance of the system consists of rate of heat transfer to the AHT evaporator and the AHT generator ($\dot{Q}_{Evap,AHT}$ and $\dot{Q}_{Gen}$), rate of heat transfer from the AHT condenser and the AHT absorber ($\dot{Q}_{Cond,AHT}$ and $\dot{Q}_{Abs,AHT}$), power input to the AHT pump and the AHT solution pump ($W_{P,AHT,el}$ and $W_{SP,AHT,el}$), and coefficient of performance of the AHT system (COP_{AHT}).

2.5 Economic Analysis

The economic analysis of the integrated system was carried out in term of the levelized cost of electricity (LCOE) as presented in the studies of [60-62], which could be calculated by:

$$LCOE = \frac{(c)(C_{Invest}) + \dot{C}_{O\&M}}{E_{Annual\ Net\ Power}} \tag{2-78}$$

$$c = \frac{i_d(1+i_d)^Y}{(1+i_d)^Y - 1} + k_{insurance} \tag{2-79}$$

where $LCOE$: The levelized cost of electricity (USD/kWh)

c : The capital recovery factor (crf) is a ratio used to calculate the present value of an annuity (a series of equal annual cash flows)

C_{Invest} : The total investment cost of the system (USD)

$\dot{C}_{O\&M}$: The operation and maintenance cost of the system (USD/Year)

$E_{Annual\ Net\ Power}$: The annual net power (kWh/Year)

i_d : The real debt interest rate (%)

Y : The depreciation period in year (Year)

k : The annual insurance rate (%/Year)

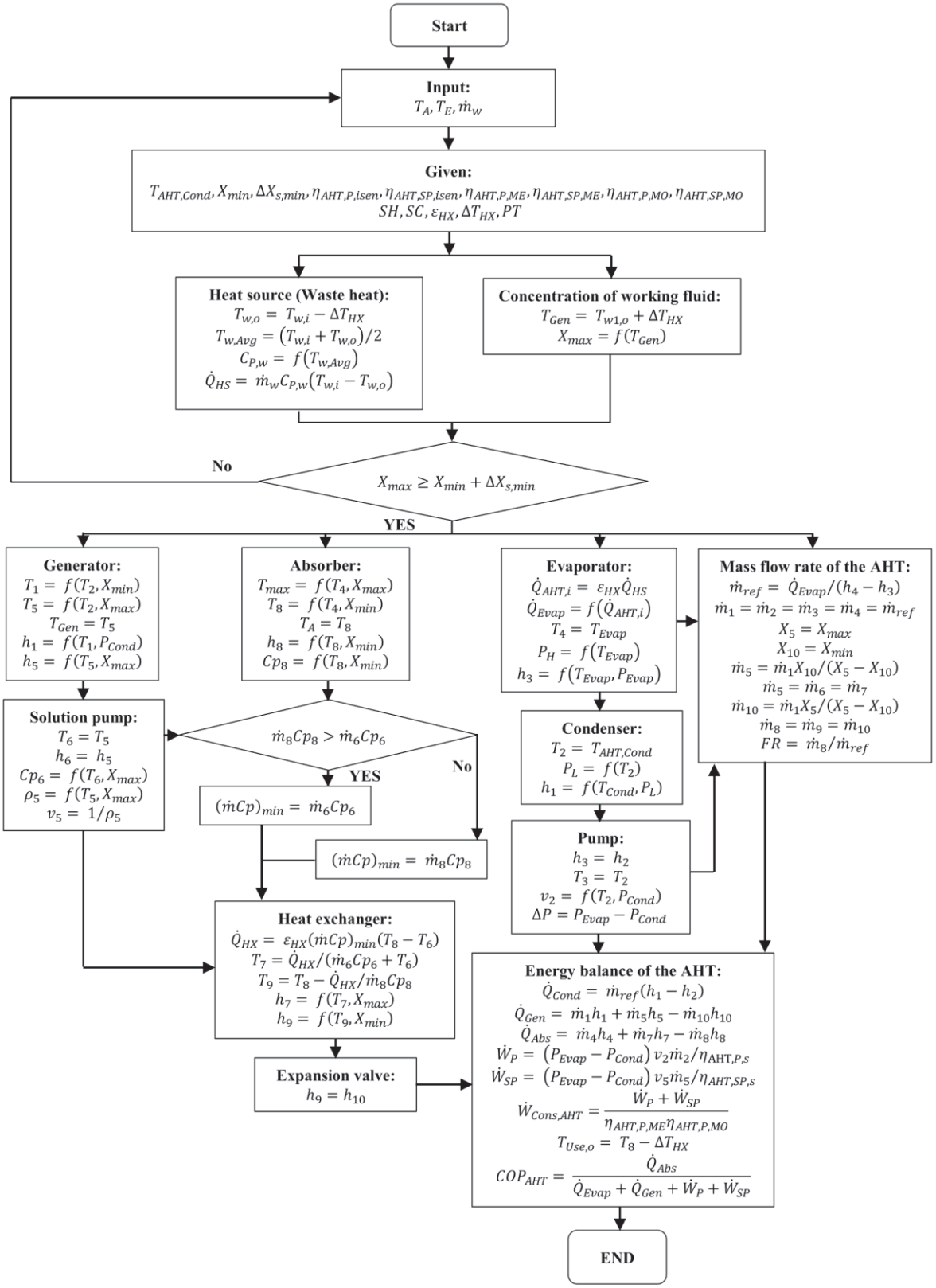

Figure 2-27 Calculation step of the AHT system [63]

3

Working Fluid Selection

This chapter presents a process of working fluids selection that is suitable for Organic Rankine Cycle (ORC) and Vapor Compression Heat Pump (VCHP) systems.

3.1 Introduction

The selection of working fluids is very important for both the ORC and the VCHP systems performance and economy since working fluids can affect the efficiency of systems, the size of the system components, the system stability and safety and environmental concerns [64]. Recently, many researchers have focused their work studying on working fluid selections. For ORC system, Junjiang and Li, [64] presented a comprehensive review of working fluid selection (including pure fluids and mixtures) in the ORC system. Based on their review, the types of working fluids (mainly dry or wet) affect the operation and layout of a system. They noted that thermal physical properties of working fluids can be used as a performance index in comparing different fluids, in which the ratio of vaporization latent heat and sensible heat, critical parameters and molecular complexity are more important. The selection of working fluid is a tedious process, influenced by heat source types, temperature level and the performance indexes, and thus they should be included in every design process of ORC plants.

In Liu et al. [65] analysis of the performance of ORC subjected to the influence of working fluids, findings showed that the presence of hydrogen bond in certain molecules such as water, ammonia, and ethanol may result in wet fluid conditions due to larger vaporizing enthalpy, and is regarded as inappropriate for ORC systems. The concepts of series and parallel circuits of ORC and heat production for geothermal resources with temperatures below 177 °C (450 K) have also been studied, i.e. Heberle and Brüggemann [66]. The working fluids consisting of isopentane, isobutene, R-245fa, and R-227ea were investigated for their use in ORC. Their results showed that, in case of series circuit, working fluids with high critical temperatures like isopentane are suitable. In parallel circuits, fluids with low critical temperatures, such as isobutene and R-227ea should be favored. Tchanche et al. [67] comparatively assessed thermal performance of 20 fluids for their use in low-temperature Solar Organic Rankine Cycle (SORC) systems. Their findings pointed out that it is difficult to find an ideal working fluid which exhibits high efficiencies, low turbine outlet volume flow rate, reasonable pressures, low ozone depletion potential (ODP), low global warming potential (GWP) and is non-flammable, non-toxic and non-corrosive. Moreover, R-134a followed by R-152a, R-290, R-600 and R-600a emerged as most suitable fluids for low-temperature applications with heat source temperature below 90 °C. Wang et al. [68-70]

studied the performance of the SORC system on R-245fa and zeotropic mixtures. The results showed that the SORC system with R-245fa as working fluid is suitable and performance is acceptable. Wang et al. [71] investigated on different organic working fluids for the flat-plate solar collectors driven regenerative ORC. The results found that R-245fa and R-123 were suitable for the system due to their low operating pressure and high system performance.

On VCHP system, Filippo et al. [72] studied parameters which are important in selecting working fluids consisting of high coefficient of performance (COP), small suction compressor displacement and compressor ratio, not too high a condensing pressure and not too low an evaporating pressure. Besides these strict thermodynamic criteria, a good working fluid must have good stability at high temperatures, low flammability and no chemical reaction when it comes in contact with metals, polymers and lubricant oils. Moreover, it must not be toxic and must be neither an 'ozone killer' nor a greenhouse gas. Chaichana et al., [73] presented a comparative assessment of natural working fluids with R-22 in terms of their characteristics and thermo-physical properties, and thermal performance. In their assessment, R-744 is not suitable for solar-boosted heat pumps because of its low critical temperature and high operational pressures. On the other hand, Ammonia (R-717) seems to be a more appropriate substitute in terms of operational parameters and overall performance. R-290 and R-1270 are identified as candidates for direct drop-in substitutes for R-22.

Considering the above mentioned literature, selection of working fluids for both the ORC and VCHP systems is critical to achieve high cycle thermal efficiencies as well as maximizing the heat extraction from the heat source. In this Chapter, steps for working fluid selection that is appropriate for the ORC and the VCHP systems are presented.

3.2 Working Fluid

Selecting a working fluid is a preliminary important step in order to utilize low to medium to low-grade energy or low-grade heat source to generate high-grade energy. The choice of working fluid is a crucial factor in the systems. Thermo-physical properties of working fluids have major impacts on system efficiency, economic viability, components' size, system stability, safety and environmental issues [64, 74, 75]. Moreover, other important thermos-physical properties that should be considered in the selection of working fluids are discussed below [15]:

- ***Latent heat of vaporization:*** An example of low-grade waste heat sources used in ORC systems, organic fluids with lower latent heat of vaporization are preferable as they allow the heat transfer process in the evaporator to occur mostly at variable temperature [64].
- ***Specific volume:*** Having low specific volume (large vapor density) is perhaps one of the most important advantages of working fluids. Fluids with low specific volume yield smaller volume flow rates and consequently results in smaller heat exchanger and expander sizes and hence reduce the size, and cost remarkably.

- ***Critical temperature:*** A cycle configuration of good efficiency is obtained only from fluids with a critical temperature close to the maximum temperature of the heat source [76].
- ***Thermal stability:*** Under high working temperature and pressure, there is a possibility for organic fluids to decompose leading to corrosion and ignition. Therefore, it is necessary that their thermal stability is maintained under elevated temperatures.
- ***Environmental impacts:*** The selection of working fluid should follow the current and possibly future environment protection standards and regulations by having zero ODP, minimal GWP, and low atmospheric lifetime (ALT).
- ***Safety:*** For operators' health and safety issues, it is preferable to use non-toxic and non-flammable organic fluids to protect personnel in case of fluid leakage from the system.
- ***Molecular weight:*** It is inversely proportional to the specific enthalpy drop across the turbine. So the larger the molecular weight, the smaller the specific enthalpy drop, and consequently the lower the number of stages required for the turbine which reduces the cost and complexity.
- ***Material compatibility:*** Working fluids should have non-corrosive and non-eroding characteristics to most common engineering materials that are used for manufacturing VCHP and ORC components such as heat exchangers, turbine, seals and gaskets and connecting pipes.
- ***Viscosity:*** A low viscosity both in liquid and vapor phases is beneficial in order to reduce the size of heat exchangers and pipes frictional losses.
- ***Cost and availability:*** Due to the international protocol obligating the phase-out of some common working fluids and also newly proposed legislations such as F-gas regulation, a market search is necessary to respond to the availability and cost effectiveness of candidate fluid prior to its selection.

Table 3-1 Physical properties of working fluids [77-80]

Working Fluid	Chemical Formular	Molar Mass (g/mol)	Critical Temperature (°C)	Critical Pressure (MPa)	ODP	GWP	Toxicity	Flammability
Ammonia (R-717)	NH_3	17.03	132.25	11.33	0.00	0.0	High	High
Butane	C_4H_{10}	58.12	151.98	3.80	0.00	4.0	Low	Extremely
Cis-butene	C_4H_8	56.11	162.60	4.23	-	-	Non	Extremely
Isobutane	C_4H_{10}	58.12	134.66	3.63	0.00	3.0	Low	Extremely
Propane	C_3H_8	44.10	96.68	4.25	0.00	0.0	Low	Extremely
R-22	$CHClF_2$	86.47	96.14	4.99	0.03	1780.0	Non	Non
R-113	$C_2F_3Cl_3$	187.40	214.06	3.39	1.00	6130.0	Low	Non
R-123	$CHCl_2CF_3$	152.93	183.68	3.66	0.02	77.0	High	Non
R-134a	CH_2FCF_3	102.03	101.06	4.06	0.00	1430.0	Non	Non
R-227ea	C_3HF_7	170.03	101.75	2.93	0.00	3220.0	Low	Non
R-236fa	$C_3H_2F_6$	152.04	124.92	3.20	0.00	9810.0	Low	Non
R-245ca	$C_3F_5H_3$	134.05	174.42	3.93	0.00	693.0	-	-
R-245fa	$C_3H_3F_5$	134.05	154.01	3.65	0.00	820.0	Low	Non
R-365mfc	$C_4F_5H_5$	148.08	186.85	3.27	0.00	890.0	Non	Non
R-1234yf	$C_3F_4H_2$	114.04	94.70	3.38	0.00	4.0	Non	Mildly
R-1234ze	$C_3F_4H_2$	114.04	109.37	3.64	0.00	< 1.0	Non	Non
R-1234zez	$C_3F_4H_2$	114.04	150.12	3.53	0.00	< 10.0	-	-
R-C318	C_4F_8	200.03	115.23	2.78	0.00	10300.0	Low	Non
Trans-butene	C_4H_8	56.11	101.75	2.93	-	-	-	Extremely

In this study, 19 working fluids were compared: Ammonia (R-717), Butane, Cis-butene, Isobutane, Propane, R-22 (Chlorodifluoromethan), R-113 (Trichlorotrifluoroethane), R-123 (2,2-Dichloro-1,1,1-trifluoroethane), R-134a (1,1,1,2-Tetrafluoroethane), R-227ea (1,1,1,2,3,3,3-Heptafluoropropane), R-236fa (1,1,1,3,3,3-Hexafluoropropane), R-245ca (1,1,2,2,3-Pentafluoropropane), R-245fa (1,1,1,3,3-Pentafluoropropane), R-365mfc (1,1,1,3,3-Pentafluorobutane), R-1234yf (2,3,3,3-Tetrafluoropropene), R-1234ze (1,3,3,3-Tetrafluoropropene), R-1234zez (trans-1,3,3,3-tetrafluoroprop-1-ene), R-C318 (Octafluorocyclobutane), and Trans-butene (2-Butene). The physical properties of the working fluids are shown in Table 3-1, and their T-s diagrams of saturated vapor line are shown in Figure 3-1.

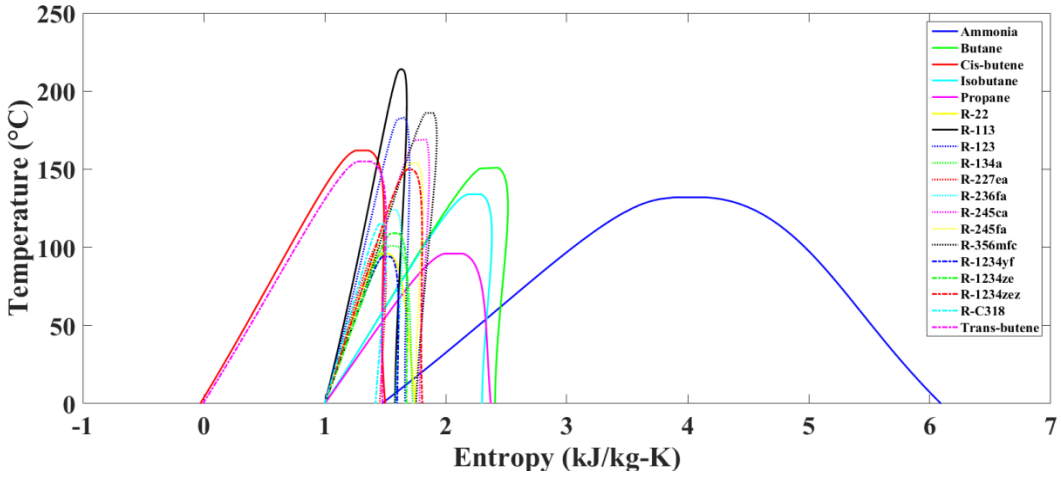

Figure 3-1 T – s diagram of saturated vapor line of the considered working fluids

3.3 Organic Rankine Cycle (ORC)

In this part a suitable working fluid of the ORC system has been selected. The schematic diagram of the ORC without and with internal heat exchanger (IHE) is shown in Figure 3-2 and Figure 3-3, respectively. The indicator considered in this study consisted of thermal efficiency, maximum pressure in the cycle, steam quality (x), mass flow rate, and heat input to the system [53].

3.3.1 Operating Conditions and Assumptions

The assumption of a suitable working fluid of the ORC system is as follows: the pressure drops in the components other than the ORC pump and the turbine, such as the ORC evaporator, the ORC condenser, the IHE, and the piping system, were neglected. The working conditions for the evaluation are stated below:

1. The ORC condenser temperature ($T_{ORC,Cond}$) was 35 ºC.
2. The ORC evaporator temperature ($T_{ORC,Evap}$) varied from 60 to 100 ºC.
3. Isentropic efficiencies of pump ($\eta_{Pump,isen}$) and turbine ($\eta_{Tur,isen}$) were 80 and 85%, respectively [53].
4. IHE effectiveness (ε_{IHE}) was 85% [53].
5. Power output of the ORC system ($\dot{W}_{Tur}$) was 60 kW_{th}.
6. Properties of working fluid were based upon REFPROP NIST7.0 [81].

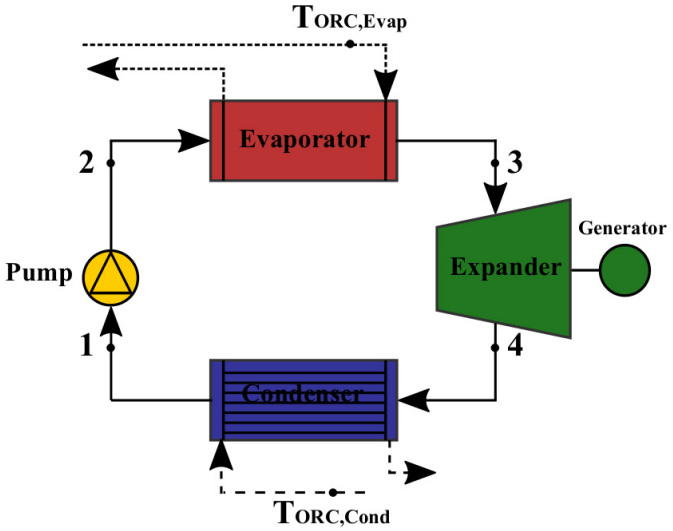

Figure 3-2 Schematic diagram of the ORC system without internal heat exchanger (IHE)

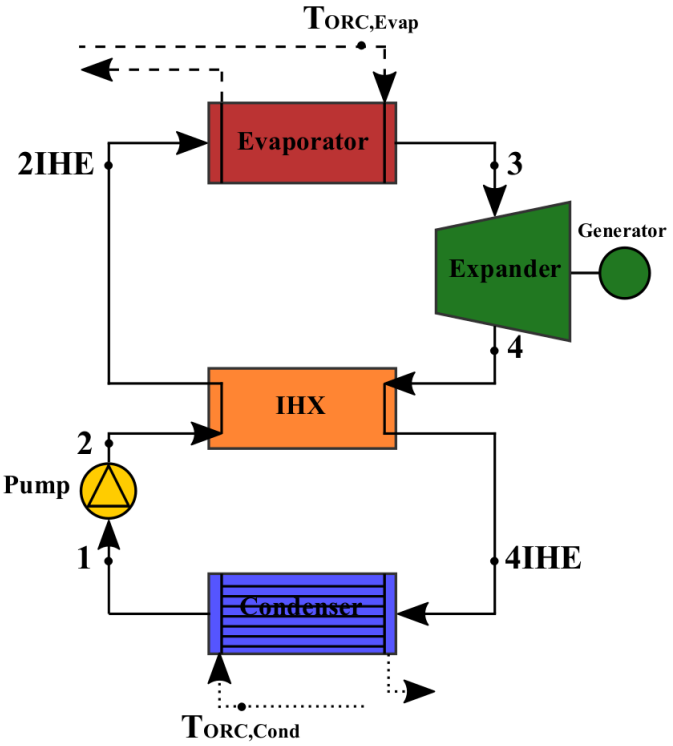

Figure 3-3 Schematic diagram of the ORC system with internal heat exchanger (IHE)

The calculation steps for evaluating the cycle performances of the ORC system with wet, isentropic and dry fluids, with and without IHE are shown in Figure 3-4 to Figure 3-6. Inputs of the simulation were the ORC condenser temperature ($T_{ORC,Cond}$), the ORC evaporator temperature ($T_{ORC,Evap}$), isentropic efficiency of pump ($\eta_{Pump,isen}$) and turbine ($\eta_{Turbine,isen}$), IHE effectiveness (ε_{IHE}), and ORC capacity. For the step of calculations, the properties of working fluid of each component were evaluated to find out the thermal efficiency (η_{th}), maximum pressure in the cycle, steam quality (x), mass flow rate ($\dot{m}_{ORC}$), and heat input to the system ($\dot{Q}_{ORC,Evap}$).

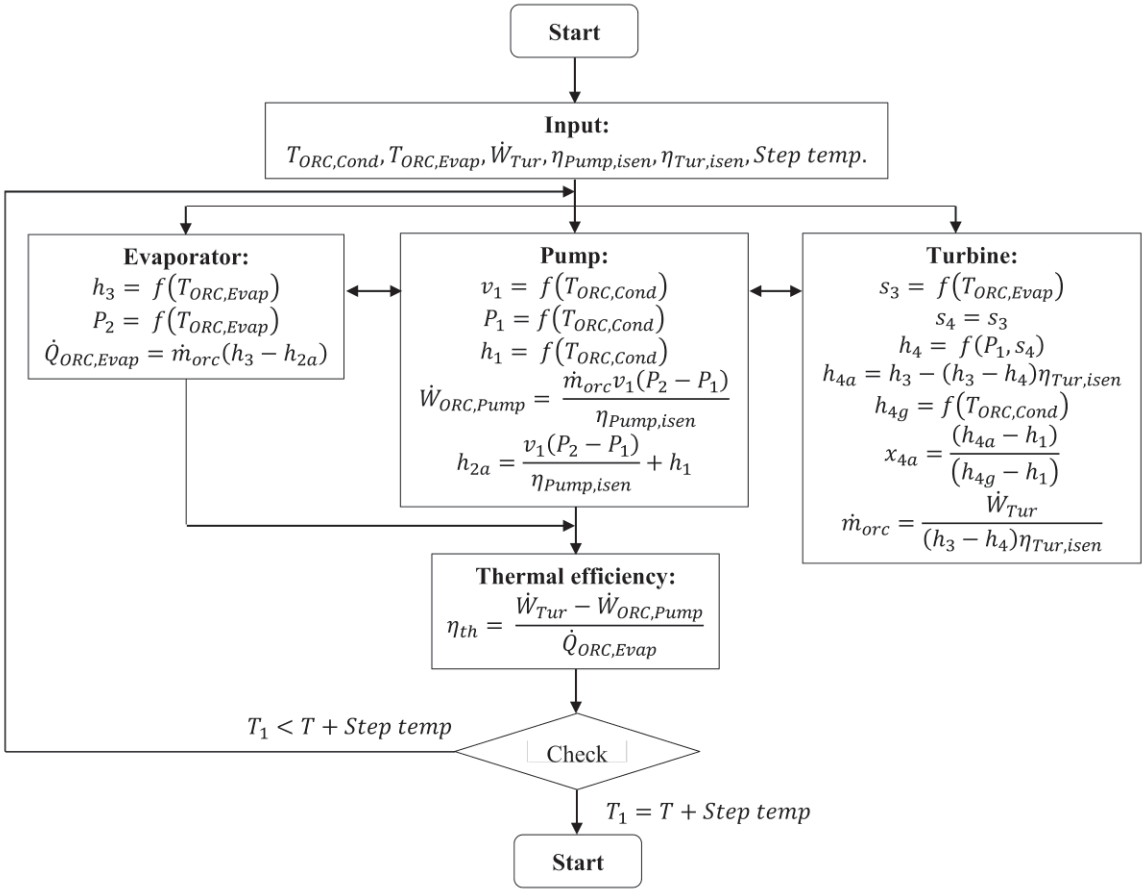

Figure 3-4 Calculation steps of the ORC power generation without internal heat exchanger (IHE) using wet and isentropic fluid as a working fluid and saturated vapor state at the turbine inlet [53]

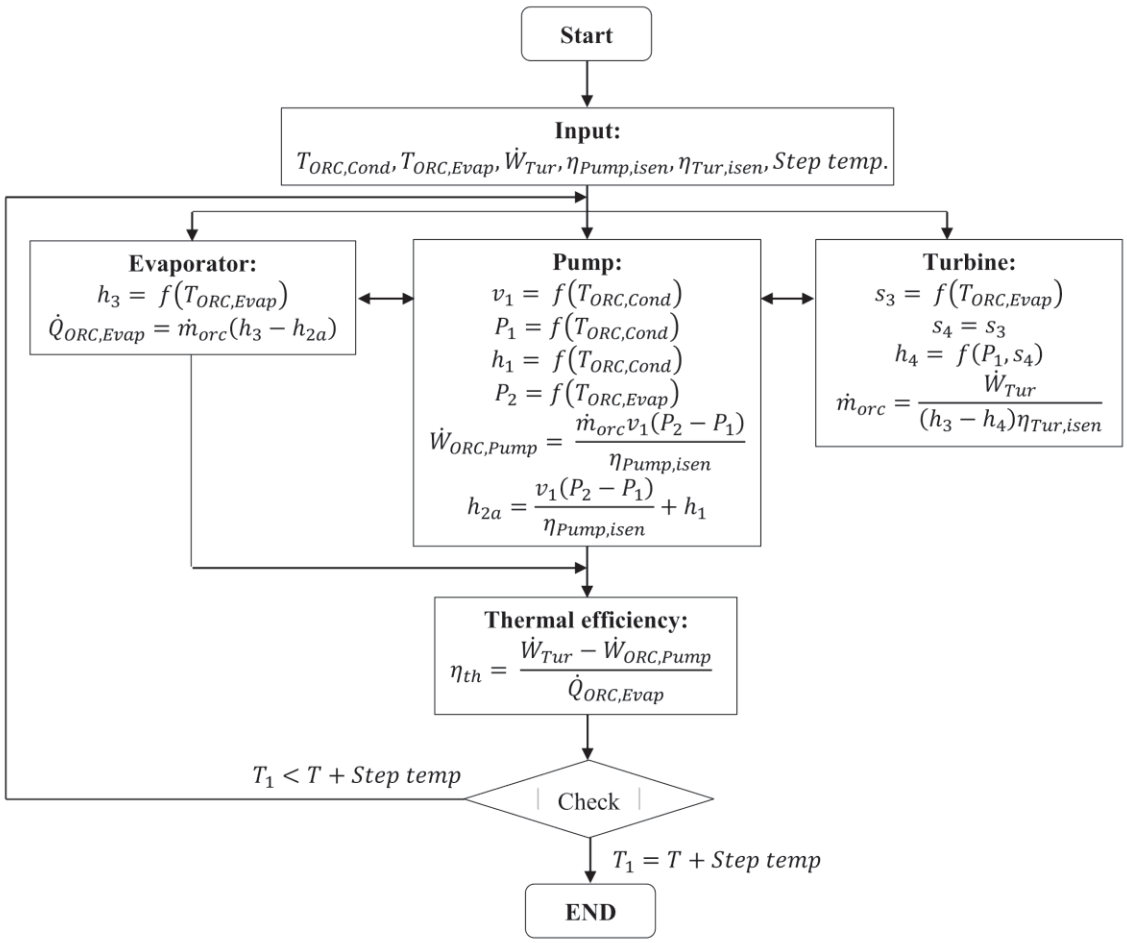

Figure 3-5 Calculation steps of the ORC power generation without internal heat exchanger (IHE) using dry fluid as a working fluid and saturated vapor state at the turbine inlet [53]

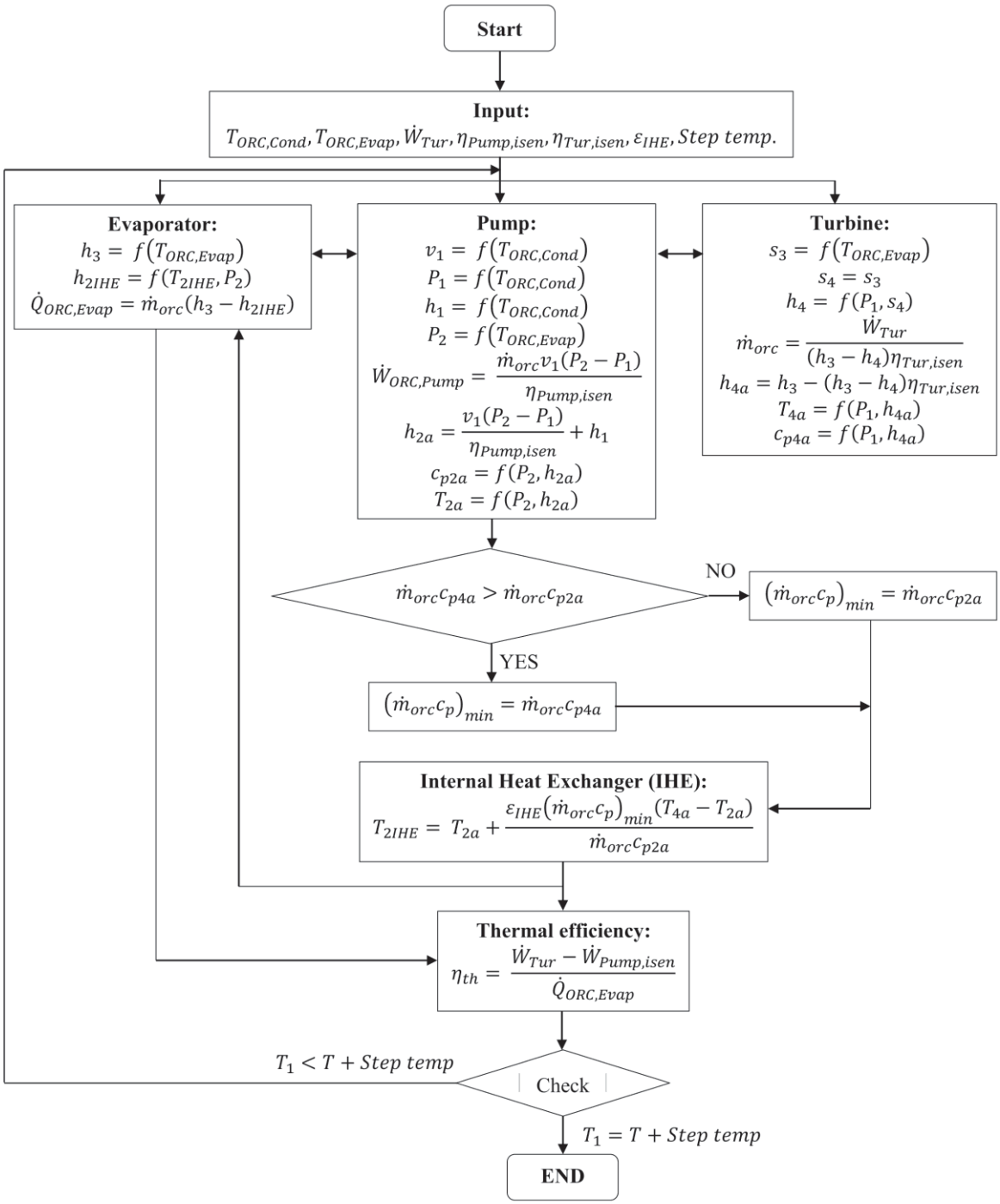

Figure 3-6 Calculation steps of the ORC power generation with internal heat exchanger (IHE) using dry fluid as a working fluid and saturated vapor state at the turbine inlet [53]

3.3.2 Results and Discussion

- **Validation of Mathematical Model of the ORC Power Generation**

The mathematical or theoretical modeling of the ORC power generation was validated using the previously published data under the same operating conditions of Saleh et al., [52] and Tchanche et al., [67], as shown by the working conditions in Table 3-2. The calculation steps of the ORC power generation are shown in Figure 3-4 to Figure 3-6. These steps were used to find out mass flow rate ($\dot{m}_{ORC}$), rate of heat transfer to the ORC evaporator ($\dot{Q}_{ORC,Evap}$), ORC thermal efficiency (η_{th}), and quality (x) of the system. The comparison of results between the mathematical modeling (present study) and the published data are shown in Figure 3-7, Figure 3-8, Table 3-3, and Table 3-4. The results obtained from the present study suggest that the variable value of the mathematical modeling was not significantly different in comparison to the published data. It means that the mathematical modeling of the ORC power generation developed in this study can be applied to estimate the power output of the ORC system.

Table 3-2 Operating conditions for validation of saturated vapor state at the turbine inlet temperature of Saleh et al., [52] and Tchanche et al., [67]

Published data	Refrigerants	$\eta_{Pump,ORC}$ (%)	$\eta_{Tur,th}$ (%)	$T_{Tur,i}$ (°C)	T_{Amb} (°C)
Saleh et al., [52]	R-134a, and R-245fa	65.0	85.0	68.0 – 100.0	30.0
Tchanche et al., [67][1]	R-123, and R-134a	80.0	44.1	81.0 – 160.0	35.0
Tchanche et al., [67][2]	R-123, R-134a, and R-717	80.0	44.1	75.0	35.0

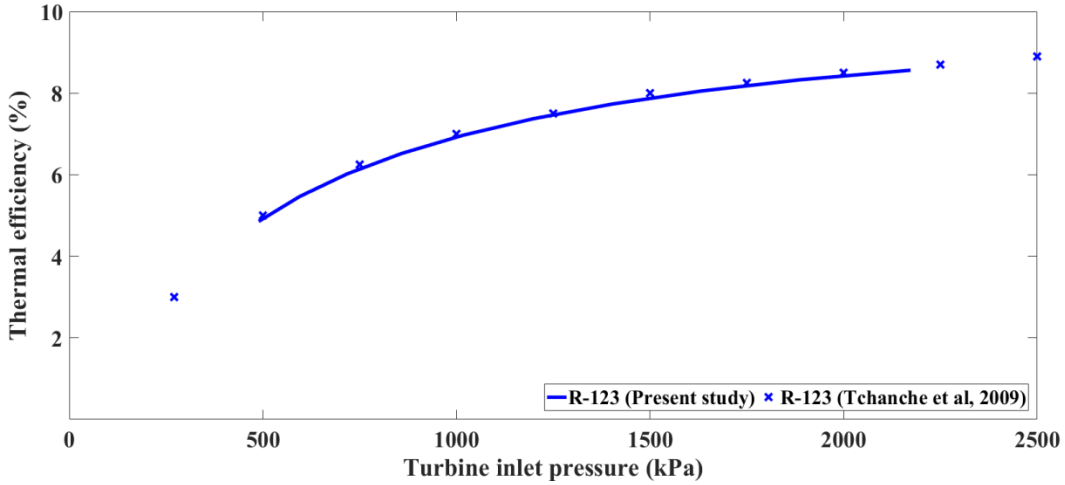

Figure 3-7 ORC thermal efficiency (%) comparison between the mathematical modeling (present study) and the published data of Tchanche et al., [67][1] *(R-123 as working fluids)*

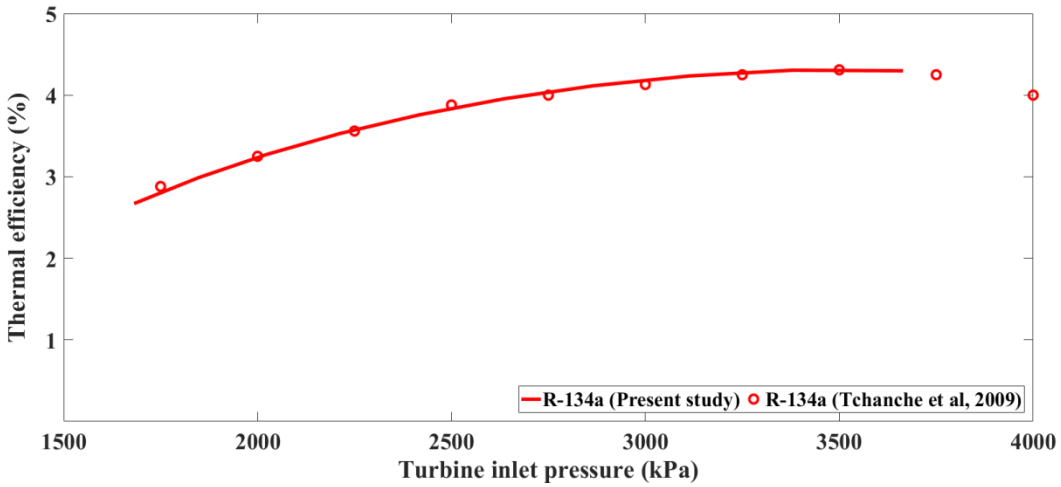

Figure 3-8 ORC thermal efficiency (%) comparison between the mathematical modeling (present study) and the published data of Tchanche et al., [67][1] *(R-134a as working fluids)*

Table 3-3 Comparison results between the mathematical modeling (present study) and the published data of Saleh et al., [52]

Refrigerants	Variable	Published data	Present study	Difference (%)
R-134a	$\eta_{Tur,th}$ (%), without IHE	7.74	7.72	0.26
R-245fa	$\eta_{Tur,th}$ (%), without IHE	12.52	12.57	0.40
	$\eta_{Tur,th}$ (%), with IHE	13.07	13.06	0.08

Table 3-4 Comparison results between the mathematical modeling (present study) and the published data of Tchanche et al., [67][2]

Refrigerants	Variable	Published data	Present study	Difference (%)
R-123	$\dot{m}_{ORC}$ (kg/s)	0.23	0.23	0.00
	$\dot{Q}_{ORC,Evap}$ (kW_{th})	43.54	43.70	0.37
	$\eta_{Tur,th}$ (%)	4.46	4.44	0.45
	x	1.00	1.00	0.00
R-134a	$\dot{m}_{ORC}$ (kg/s)	0.24	0.24	0.00
	$\dot{Q}_{ORC,Evap}$ (kW_{th})	43.57	43.58	0.02
	$\eta_{Tur,th}$ (%)	3.70	3.70	0.03
	x	0.99	1.02	3.03
R-717	$\dot{m}_{ORC}$ (kg/s)	0.04	0.04	0.00
	$\dot{Q}_{ORC,Evap}$ (kW_{th})	41.63	41.61	0.05
	$\eta_{Tur,th}$ (%)	4.35	4.35	0.00
	x	0.92	0.95	3.26

Effect of Pump and Turbine Efficiency

Pump ($\eta_{Pump,ORC}$) and turbine (η_{Tur}) efficiency are the most critical parameters in evaluating ORC power generation. Using Eq. (2-23), it was found that when the value of the pump efficiency is low, the amount of power input to the ORC pump needed is high. And using Eq. (2-27), it was observed that when the value of the turbine efficiency is high, the system (or the turbine) can generate a high power output. These effects were then considered. The working conditions for evaluating the thermal efficiency of the ORC system were set at temperature of 35 ºC for the ORC condenser and 70 to 95 ºC for the ORC evaporator. The turbine and pump efficiency changed from 20 to 100% and 50 to 100% (with 10% increment), respectively.

The thermal efficiency of the ORC system when the turbine efficiency was set at 44% (*Tchanche et al., [67]*) and the pump efficiency varied from 50 to 100% is shown in Figure 3-9. It was found that the pump efficiency was not a significant factor affecting thermal efficiency because a few amount of power input is required for the ORC pump as compared with that of the power output from the turbine. However, when the pump efficiency was set at 80% (*Tchanche et al., [67]*) and the turbine efficiency varied from 20 to 100%, the results found that the turbine efficiency was the most significant parameter regarding thermal efficiency (as shown in Figure 3-10). The thermal efficiency of the system increased when the turbine efficiency increased. From the above results, it can be assumed that the turbine efficiency is a critical parameter for evaluating ORC power generation.

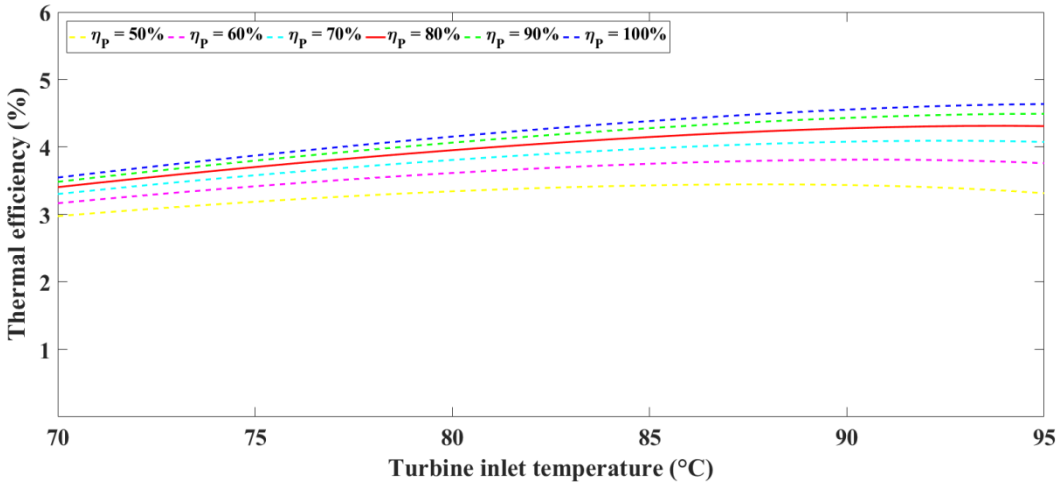

Figure 3-9 Thermal efficiency (%) of the ORC system when the turbine inlet temperature increases from 70 to 95 °C and the pump efficiency from 50 to 100%, with the turbine efficiency set at 44%

- **Evaporating Temperature or Turbine Inlet Temperature**

Evaporating or turbine inlet temperature is the maximum temperature of a working fluid or refrigerant in the ORC system. When the working fluid entered the turbines as a saturated vapor, based on results of thermal efficiency of the ORC system as shown in Figure 3-11, it was found that the thermal efficiency of the system increased as the turbine inlet temperature increased. The turbine inlet temperature was at around 95 ºC, and Ammonia (R-717) was the

working fluid that gave the highest thermal efficiency followed by R-123, R-113, Cis-butene, Trans-butene, R-1234zez, R-245ca, R-365mfc, Butane, R-245fa, Isobutane, R-236fa, R-1234ze, R-134a, R-C318, R-227ea, and R-22 respectively. Moreover, at the same turbine inlet temperature, R-1234yf and Propane were inappropriate because the ORC system was not working. For more information, Figure 3-12 shown comparison of the thermal efficiency of the ORC system when the turbine inlet temperature was at around 95 °C.

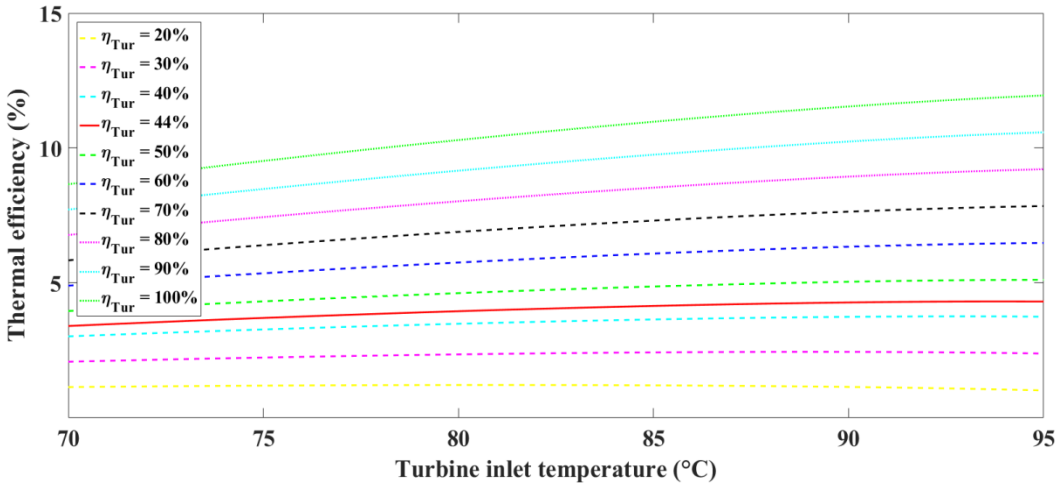

Figure 3-10 Thermal efficiency (%) of the ORC system when the turbine inlet temperature increases from 70 to 95 °C and the turbine efficiency from 20 to 100%, with the pump efficiency set at 80%

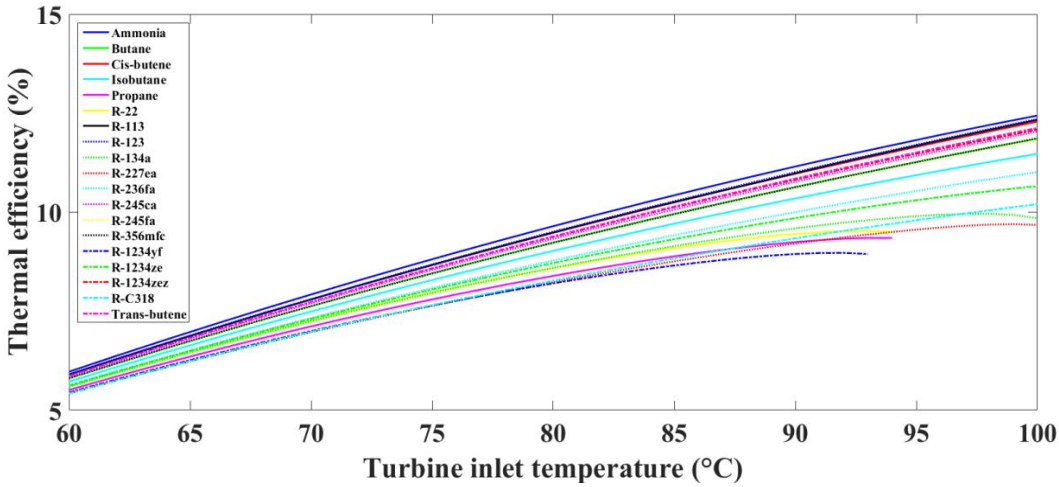

Figure 3-11 Thermal efficiency (%) of the ORC system when the turbine inlet temperature increases from 60 to 100 °C

- **Maximum Cycle Pressure**

Evaporating pressure is the maximum cycle pressure of a working fluid in the ORC system. It depends on the turbine inlet temperature. If the evaporating pressure is high, the evaporator coil must be thick to withstand the high pressure. It means that the cost of the evaporator coil will be expensive [53]. Figure 3-13 shows the thermal efficiency (%) of the ORC system, when the turbine inlet pressure increases. The results showed that R-113 was the working fluid that gave the highest thermal efficiency in the lowest of turbine inlet

pressure, followed by R-365mfc, R-123, R-245ca, R-245fa, R-1234zez, Cis-butene, Trans-butene, Butane, R-236fa, Isobutane, R-C318, R-1234ze, R-227ea, R-134a, R-1234yf, Propane, Ammonia (R-717), and R-22, respectively. In Figure 3-14 and Figure 3-15 shown the comparison of evaporating pressure of the system when the thermal efficiency of 8.0%, and when the turbine inlet temperature was at around 95 °C, respectively.

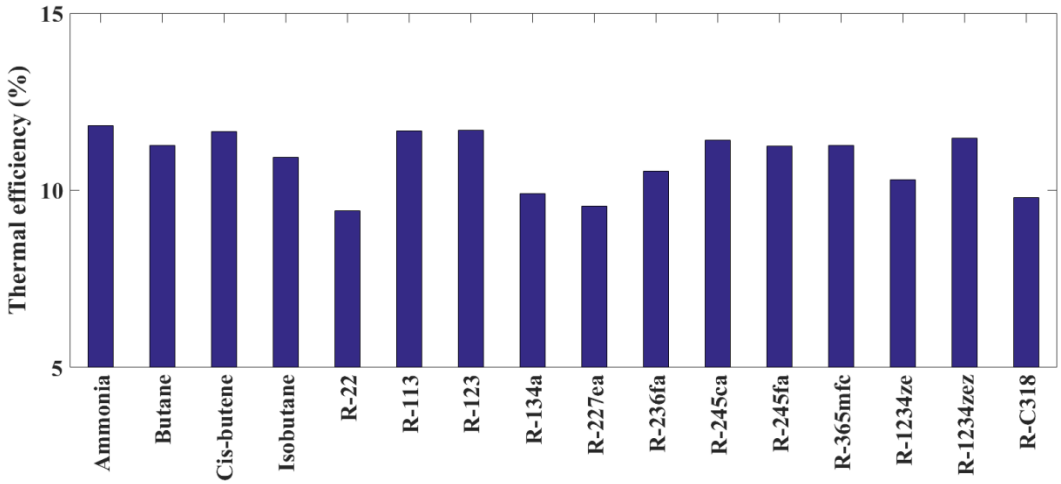

Figure 3-12 Comparison of the thermal efficiency (%) of the ORC system when the turbine inlet temperature set at 95 °C

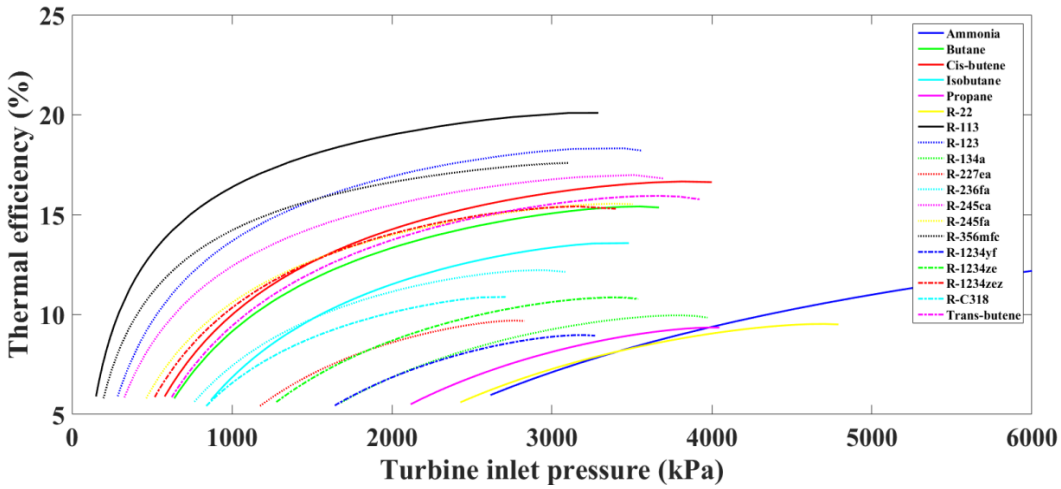

Figure 3-13 Thermal efficiency (%) of the ORC system when the turbine inlet pressure increases

- **Steam Quality (x)**

The quality of working fluids is observed in the fraction of vapor in the mixture. If the quality from the turbine exit becomes lower, the working fluid that passes through the turbine can erode the turbine blades. It means that there is a need for maintenance [53]. The quality of wet and some isentropic fluids as the turbine inlet temperature increases from 60 to 100 °C is shown in Figure 3-16. It was found that the quality of wet and some isentropic fluids decreased as the turbine inlet temperature increased. Considering the turbine inlet

temperature at around 95 °C, the quality for R-22 was the lowest, followed by ammonia (R-717), Propane, and R-134a, respectively.

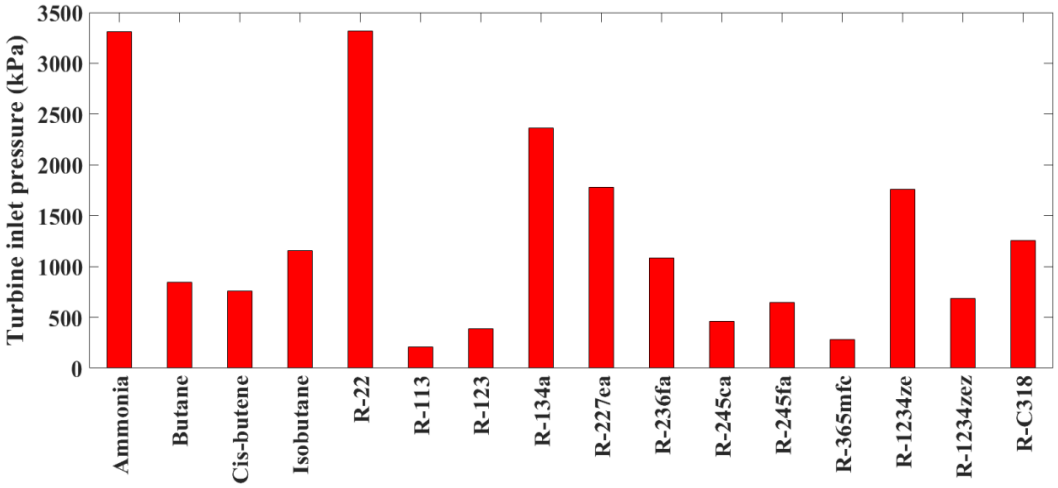

Figure 3-14 Comparison of evaporating pressure (kPa) of the ORC system when the thermal efficiency (%) of 8.0%

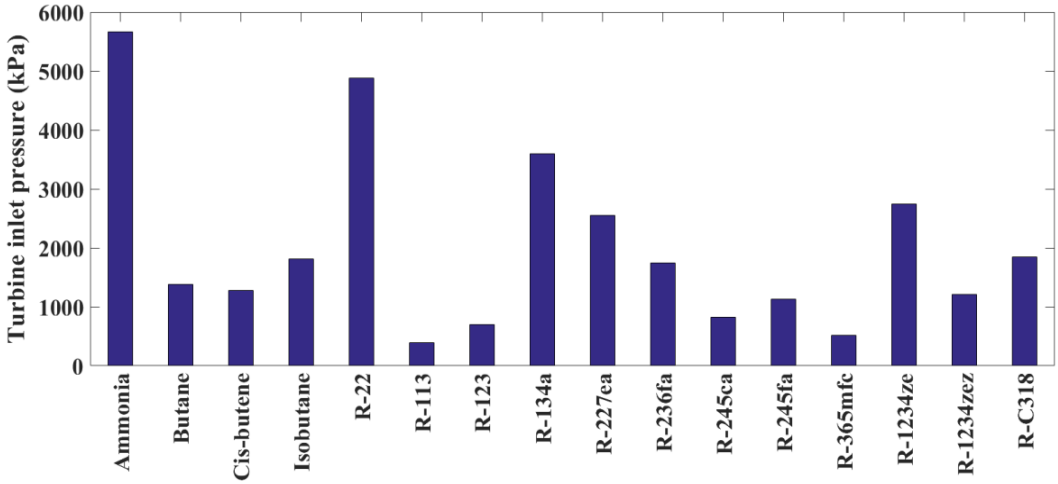

Figure 3-15 Comparison of evaporating pressure (kPa) of the ORC system when the turbine inlet temperature set at 95 °C

- **Mass Flow Rate of Working Fluid**

The amount of working fluid flow rate has an effect to the system component. If there is a large amount of working fluid flow rate, large sizing of the system components is needed. Also the investment of the system components increases [53]. Mass flow rate (kg/s) of the ORC system when the turbine inlet temperature increases from 60 to 100 °C is shown in Figure 3-17. The results showed that the amount of working fluid flow rate slightly decreased as the turbine inlet temperature increased. Considering the turbine inlet temperature was at around 95 °C, Ammonia (R-717) was the working fluid that gave the lowest mass flow rate followed by Cis-butene, Trans-butene, Butane, Isobutane, R-245ca, R-365mfc, R-1234zez, R-245fa, R-123, R-113, R-1234ze, R-134a, R-236fa, R-22, R-C318, and R-227ea, respectively. Moreover, at the same turbine inlet temperature R-1234yf and Propane were

inappropriate because the ORC system was not working. For more understanding, Figure 3-18 shown comparison of the mass flow rate of the ORC system when the turbine inlet temperature was at around 95 °C.

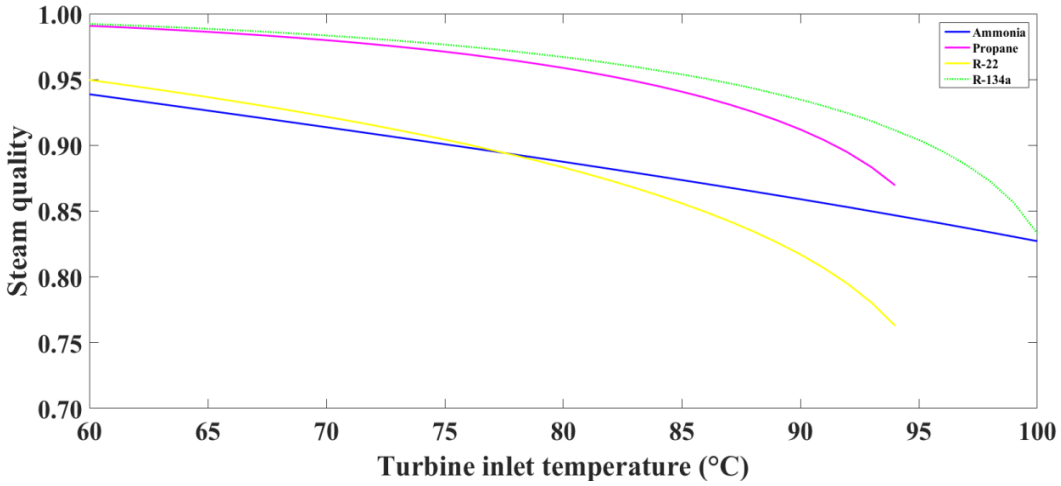

Figure 3-16 Steam quality (x) of wet and some isentropic working fluid when the turbine inlet temperature increases from 60 to 100 °C

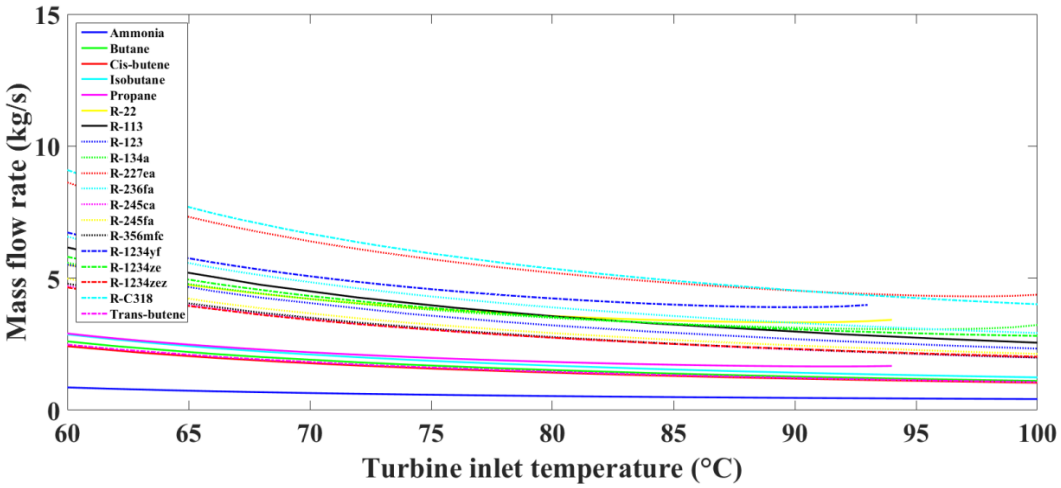

Figure 3-17 Mass flow rate (kg/s) of the ORC system when the turbine inlet temperature increases from 60 to 100 °C

- **Heat Input Rate to the Evaporator**

Figure 3-19 shows the heat input rate (kW) of the ORC system when the turbine inlet temperature increases from 60 to 100 °C. It was found that the heat input rate to the evaporator decreased as the turbine inlet temperature increased. Considering the turbine inlet temperature was at around 95 °C, Ammonia (R-717) was the working fluid that gave the lowest heat input rate followed by R-22, Cis-butene, Trans-butene, R-123, R-1234zez, R-113, Butane, Isobutane, R-245ca, R-245fa, R-134a, R-1234ze, R-365mfc, R-236fa, R-227ea, and R-C318, respectively. Moreover, at the same turbine inlet temperature R-1234yf and Propane were inappropriate, because the ORC system was not working. For more information, Figure

3-20 shown comparison of the heat input rate of the ORC system when the turbine inlet temperature was at around 95 °C.

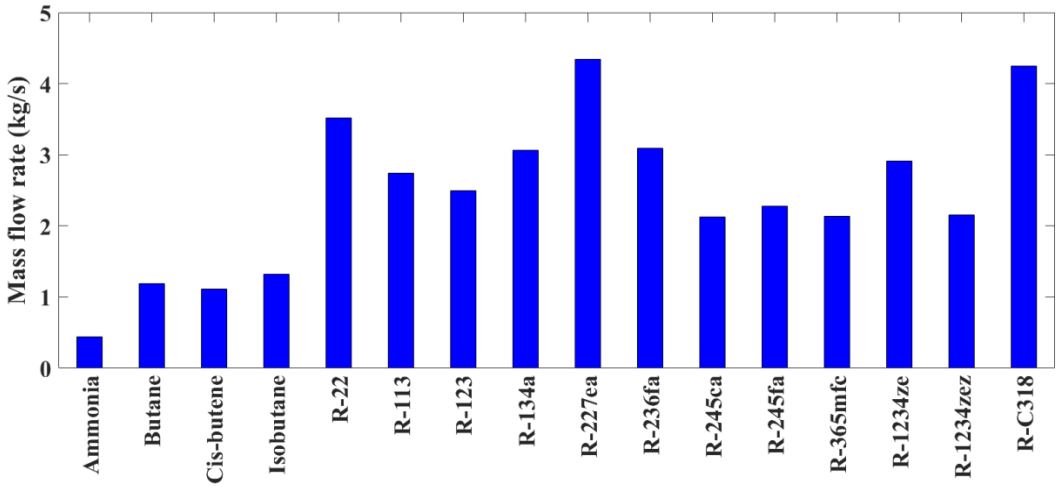

Figure 3-18 Comparison of the mass flow rate (kg/s) of the ORC system when the turbine inlet temperature set at 95 °C

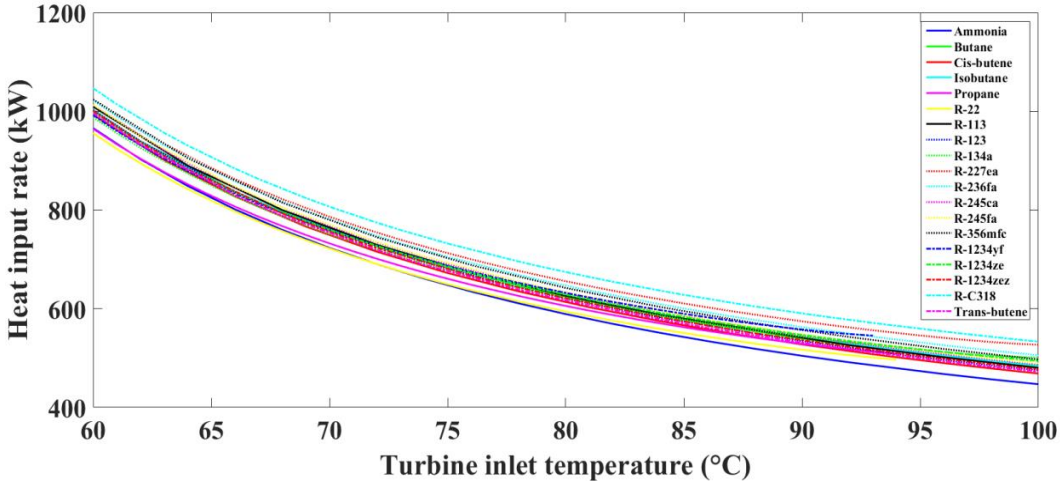

Figure 3-19 Heat input rate (kW) to the ORC evaporator when the turbine inlet temperature increases from 60 to 100 °C

- **Internal Heat Exchanger (IHE)**

In case of the turbine outlet temperature (state 4), as shown in Figure 3-3, it was higher than the pump outlet temperature (state 2). The ORC system can improve the thermal efficiency (%) of the system by implementing an IHE into the ORC cycle. Figure 3-21 shows the thermal efficiency of the ORC system with IHE when the turbine inlet temperature increases from 60 to 100 °C. The results showed that the thermal efficiency of the ORC system with IHE was higher than that of the ORC system without IHE due to the low heat input rate of the system (as shown in Figure 3-22).

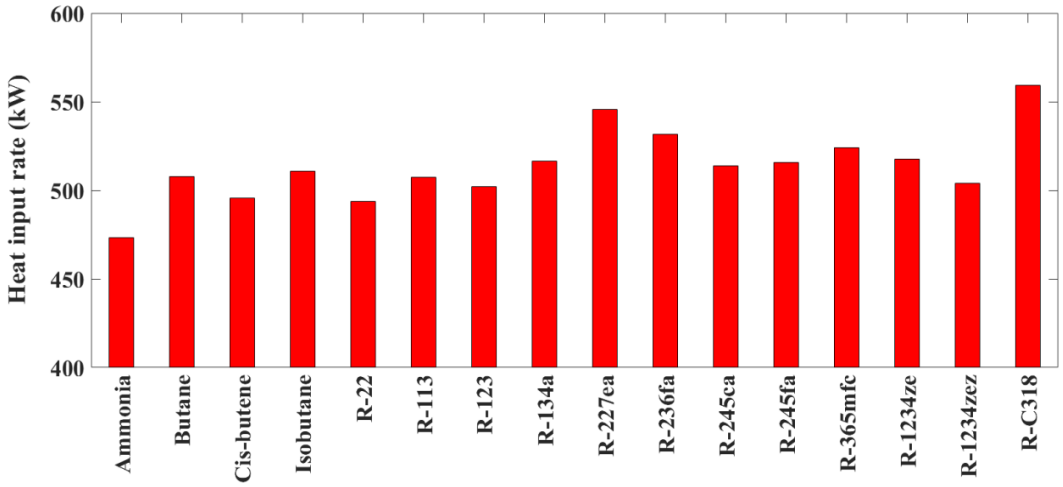

Figure 3-20 Comparison of the heat input rate (kW) of the ORC system when the turbine inlet temperature set at 95 °C

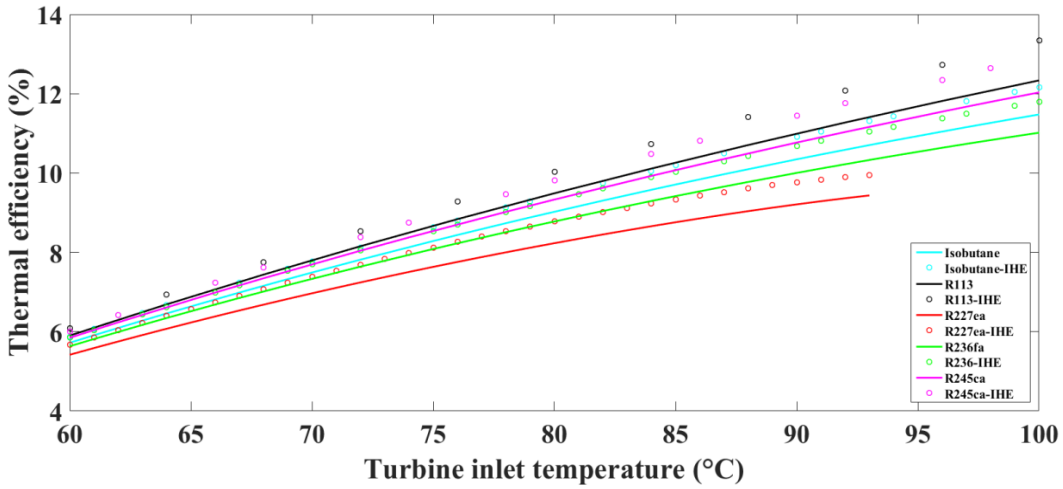

Figure 3-21 Thermal efficiency (%) of the ORC system with and without internal heat exchanger (IHE) when the turbine inlet temperature increases from 60 to 100 °C

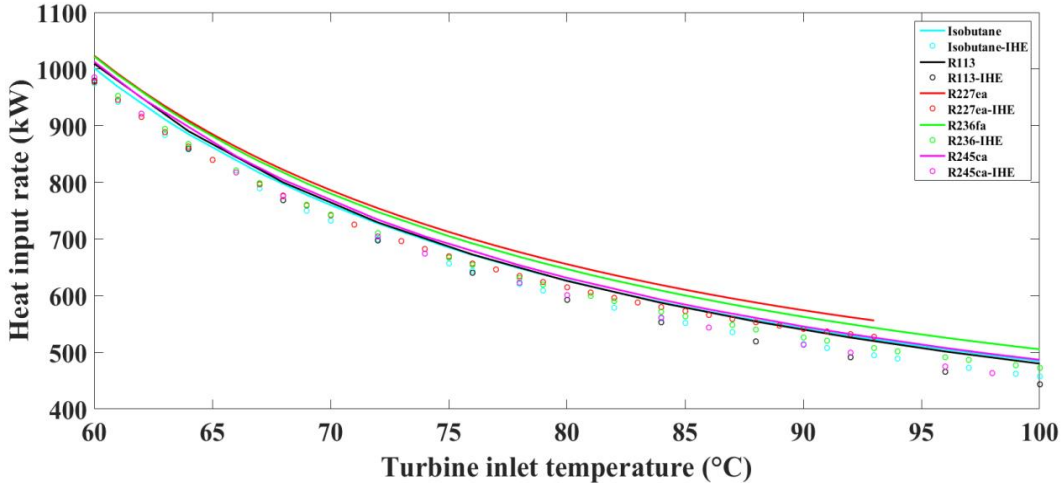

Figure 3-22 Heat input rate (kW) of the ORC system with and without internal heat exchanger (IHE) when the turbine inlet temperature increases from 60 to 100 °C

3.3.3 Conclusion

From the abovementioned results, important findings are summarized as follows:

1. R-1234yf and Propane were not suitable because the ORC system was not working as the turbine inlet temperature was at around 95 °C.
2. Ammonia (R-717), Propane, R-22 and R-134a were not suitable working fluid due to their low steam quality.
3. R-365mfc, Cis-butene, R-245ca, Trans-butene, R-113, R-123, Butane, R-245fa, R-1234zez and Isobutane, seemed appropriate to be used because they gave low mass flow rate, low evaporating pressure, and high thermal efficiency.
4. As considered in terms of low-GWP, low-toxicity, and non-flammable; R-245ca, R-365mfc, R-245fa, and R-1234zez were suitable in this study (as shown in Figure 3-23).

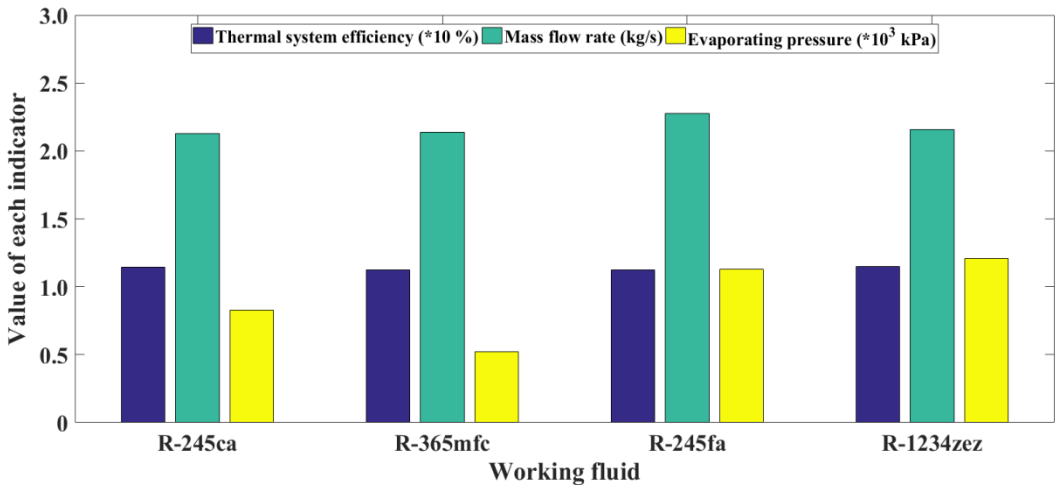

Figure 3-23 Thermal system efficiency (×10, %), Mass flow rate (kg/s), and Evaporating pressure ($\times 10^3$, kPa) of the ORC system when R-245ca, R-365mfc, R-245fa, and R-1234zez as working fluids

3.4 Heat Boosting Technologies

In this study, the assumption of the efficiency of the compressor, the gas engine mechanical, the gas engine combustion, the gas engine thermal, the power transmission, the water pump, and the solution pump were made in the previous studies [55, 56, 58, 82]. A reasonable value for mathematical or theoretical modeling of the VCHP, the GEHP, and the AHT system, which was not too high-value for the evaluation of the systems, was obtained. This method (theoretical modeling) is the most popular technique (used not only in this study) for evaluating the systems. The mathematical modeling (developed in this study) of each heating booster can be applied for estimating heat input rate, heat output rate, power input, and coefficient of performance (COP) of the systems.

3.4.1 Vapor Compression Heat Pump (VCHP)

In this part the suitable working fluid of the VCHP system (as shown in Figure 3-24) has been selected. To identify the suitable working fluid of the VCHP system, seven indicators were considered in this study [63], and they consist of mass of refrigerant per unit heat output (MPH), volume flow rate of refrigerant, displacement volume, high-side pressure, refrigerant temperature at the compressor outlet, pressure ratio, and coefficient of performance of the VCHP system (COP_{VCHP}).

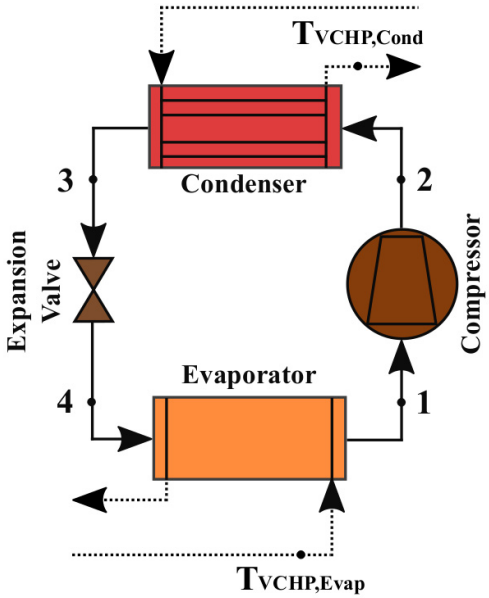

Figure 3-24 The schematic diagram of the VCHP system

- **Operating Conditions and Assumptions for the VCHP System**

The working conditions for the evaluation were:

1. The VCHP evaporator temperature ($T_{VCHP,Evap}$) was 60 ºC.
2. Total cooling capacity ($\dot{Q}_{VCHP,Evap}$) was 10 kW.
3. Required hot water temperature ($T_{VCHP,Cond}$) varied from 70 to 90 ºC.
4. The pressure drops at the VCHP condenser and the evaporator was neglected.
5. Isentropic compressor efficiency ($\eta_{Comp,isen}$) was 80% [63].
6. Degree of sub-cooling (SC) and superheating (SH) was 5.0 ºC.
7. Properties of working fluids were based upon REFPROP NIST7.0 [81].

The step for calculating the selection of working fluid of the VCHP system is shown in Figure 3-25. Inputs of the simulation were the VCHP evaporator temperature ($T_{VCHP,Evap}$), the VCHP condenser temperature ($T_{VCHP,Cond}$), type of working fluid and cooling capacity ($\dot{Q}_{VCHP,Evap}$) of the VCHP system, isentropic efficiency of compressor ($\eta_{Comp,isen}$), and degree of sub-cooling (SC) and superheating (SH). For the step of calculations, the properties of working fluid of each component were evaluated to find out the mass of refrigerant per unit heat output (MPH), volume flow rate of refrigerant, displacement volume, high-side pressure, refrigerant temperature at the compressor outlet, pressure ratio, and coefficient of

performance of the VCHP system (COP_{VCHP}) in the VCHP system for generating hot water temperature at around 70 to 90 ºC.

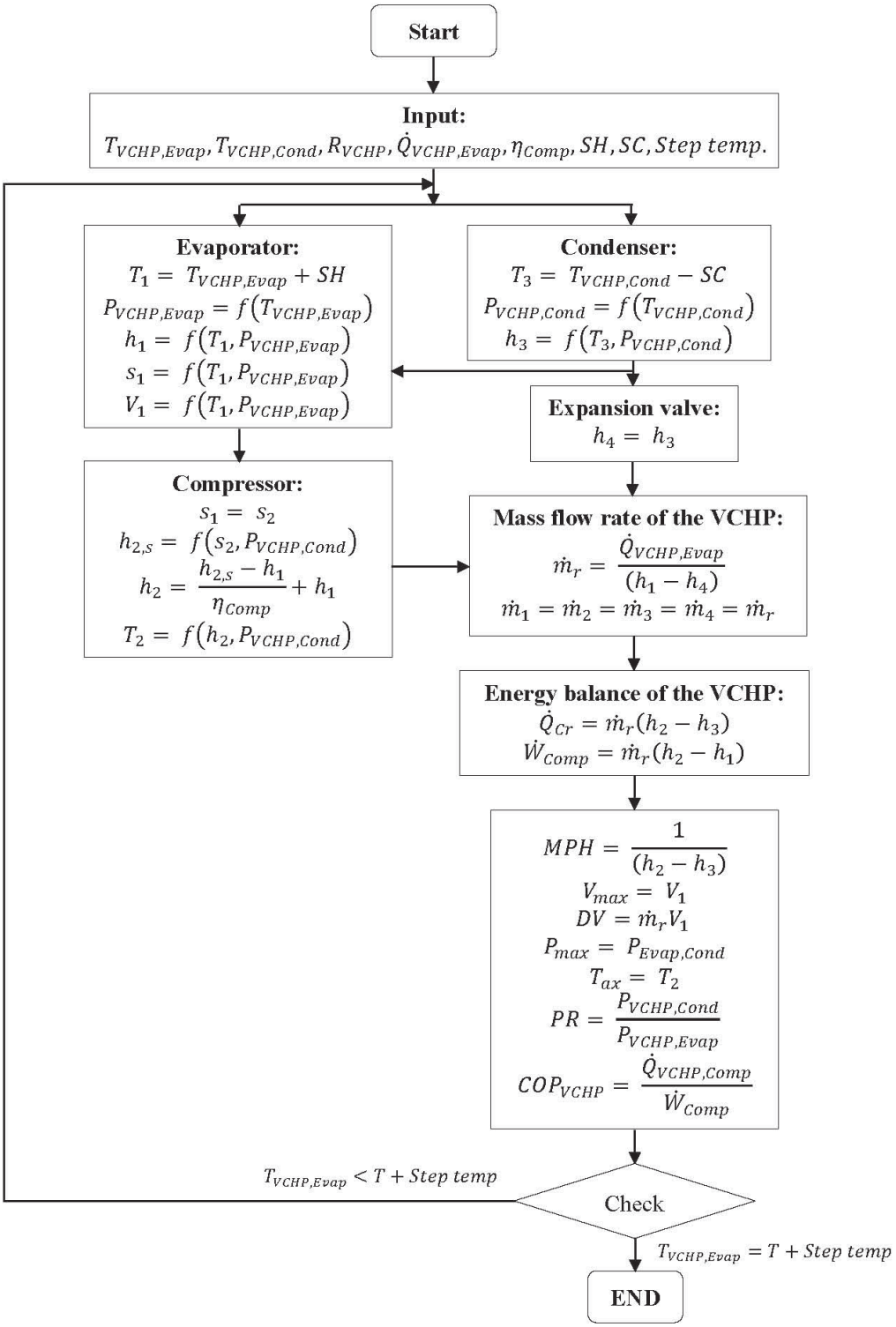

Figure 3-25 Calculation steps for selecting working fluids of the VCHP system [63]

- **Results and Discussion**

Effect of Compressor Efficiency for the VCHP System

The compressor efficiency ($\eta_{Comp,isen}$) was the most critical parameter for the evaluation of the VCHP system in this study. Using Eq. (2-50), it was found that when the value of the compressor efficiency is low, the amount of the power input to the compressor needed is high. In this part, the effect of this parameter was considered. The working conditions for the evaluation of coefficient of performance of the VCHP system (COP_{VCHP}) are the following: the compressor efficiency varied from 50 to 100% (with 10% increment) and the degree of sub-cooling (T_{SC}) and superheating (T_{SH}) changed from 5 to 15 ºC (with 5 ºC increments).

The COP_{VCHP} of the system when the compressor efficiency and the degree of superheating was set at 85% and 5 ºC, respectively, and the degree of sub-cooling varied from 5 to 15 ºC is shown in Figure 3-26. It was found that the degree of sub-cooling had minimal effects in terms of COP_{VCHP}. The same can be said to the condenser temperature. The COP_{VCHP} of the system slightly increased when the degree of sub-cooling increased.

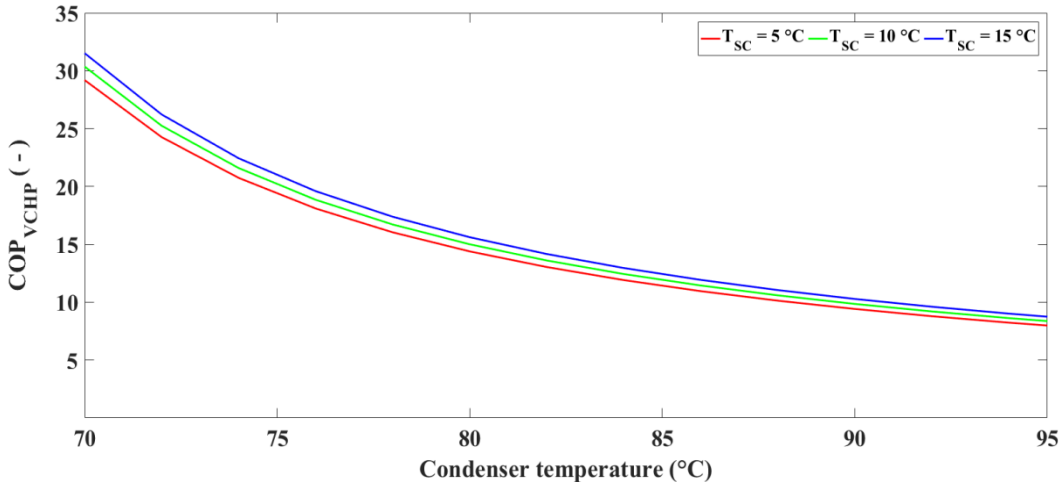

Figure 3-26 COP_{VCHP} (-) of the VCHP system when the condenser temperature increases from 70 to 95 °C and the degree of sub-cooling from 5 to 15 °C, with the degree of superheating of 5 °C

Furthermore, when the compressor efficiency was set at 85%, the degree of sub-cooling at 5 ºC, and the degree of superheating varied from 5 to 15 ºC, the results showed that the degree of superheating was not a significant factor of COP_{VCHP} (as shown in Figure 3-27). However, when the compressor efficiency varied from 50 to 100%, and the degree of sub-cooling and superheating was set at 5 ºC based on results of COP_{VCHP} and work input to the compressor (as shown in Figure 3-28 and Figure 3-29, respectively), it was found that the compressor efficiency was the most significant factor of the COP_{VCHP} and work input to the compressor (W_{Comp}). It can then be assumed that the compressor efficiency is a critical parameter for evaluating the VCHP system.

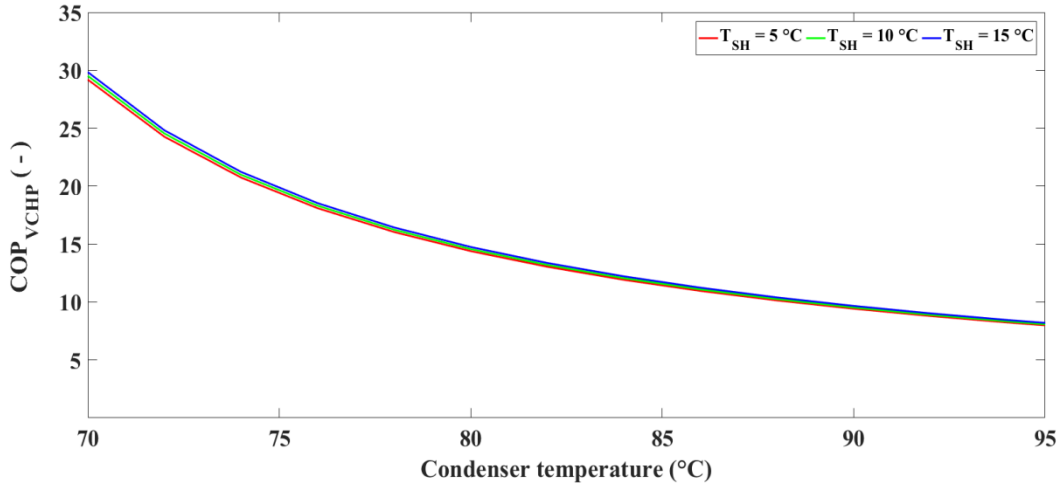

Figure 3-27 COP (-) of the VCHP system when the condenser temperature increases from 70 to 95 °C and the degree of sub-cooling from 5 to 15 °C, with the degree of superheating of 5 °C

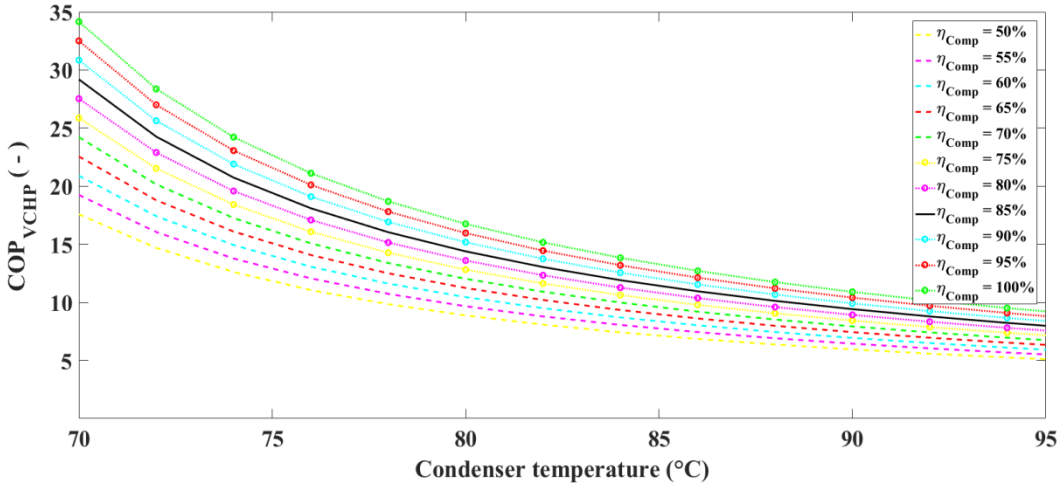

Figure 3-28 COP (-) of the VCHP system when the condenser temperature increases from 70 to 95 °C and the compressor efficiency from 50 to 100%, with the degree of sub-cooling and superheating of 5 °C

Mass of Refrigerant per Unit Heat Output (MPH)

The mas of refrigerant per unit heat output (MPH) was utilized to find out the amount of refrigerant used in the VCHP system which was compared with the amount of the heat generated from the system. Based on the same amount of the heat generated by the system, if the value of MPH is higher, the amount of refrigerant needed is higher. Also high compression work and a large scale of system components are needed [63]. Figure 3-30 shows the MPH of 19 refrigerants when the condenser temperature increases from 70 to 90 °C. It was found that the MPH of the system increased as the temperature of the condenser increased. Moreover, Ammonia (R-717) had the lowest values of MPH, followed by Cis-butene, Trans-butene, Butane, Isobutane, Propane, R-1234zez, R-365mfc, R-245ca, R-245fa, R-123, R-113, R-22, R-134a, R-1234ze, R-236fa, R-1234yf, R-227ea, and R-C318, respectively. However, Ammonia (R-717), Cis-butene, Trans-butene, Butane, Isobutane,

Propane, R-245fa, R-123, R-113, R-236fa, R-1234yf, R-227ea, and R-C318 were inappropriate since these refrigerants are flammable and toxic as shown in Table 3-1. Thus, the refrigerants suitable in this indicator were R-1234zez, R-365mfc, R-245ca, R-22, R-134a, and R-1234ze. Figure 3-31 shown the comparison of MPH when the VCHP system used R-1234zez, R-365mfc, R-245ca, R-22, R-134a, and R-1234ze as working fluids, and the condenser temperature was around at 70 °C.

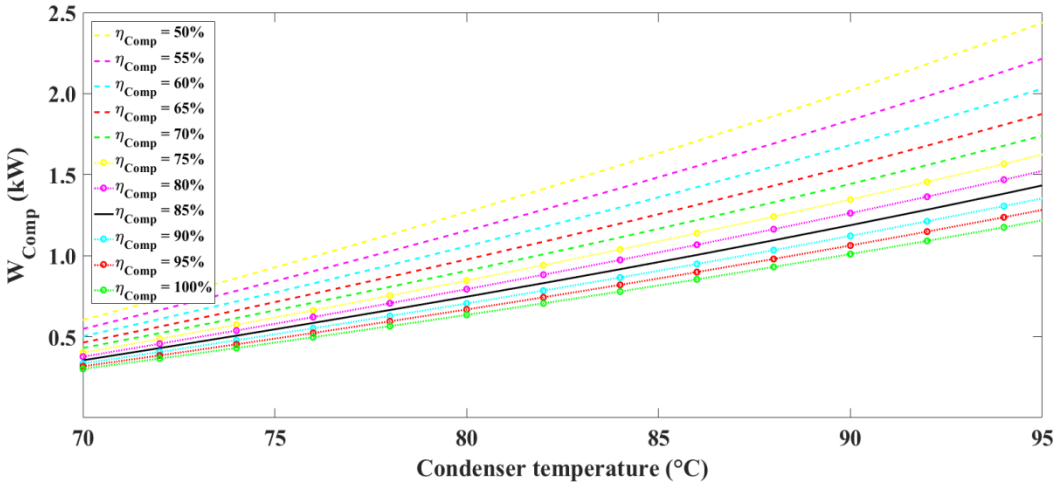

Figure 3-29 Work input to the VCHP compressor (W_{Comp}) when the condenser temperature increases from 70 to 95 °C and the compressor efficiency from 50 to 100%, with the degree of sub-cooling and superheating of 5 °C

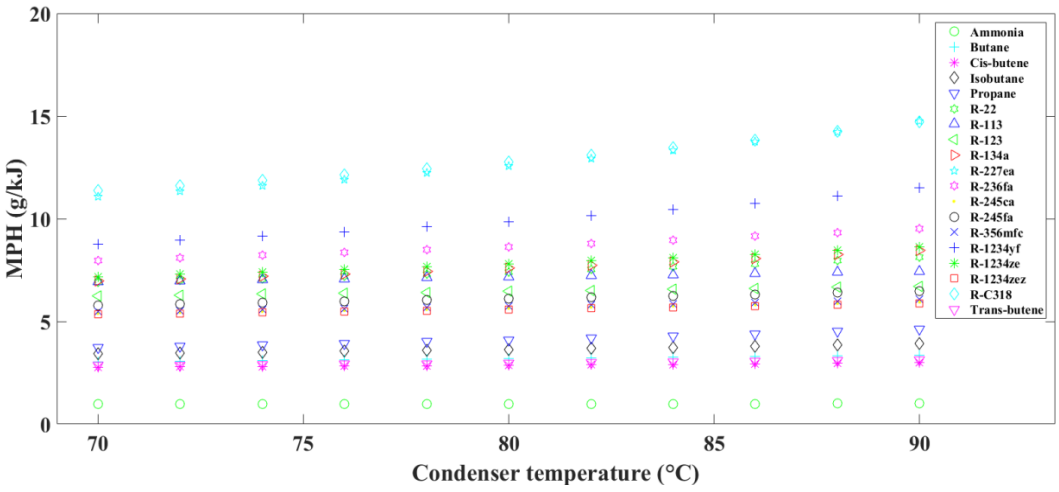

Figure 3-30 MPH (g/kJ) of the VCHP system when the condenser temperature increases from 70 to 90 °C

Vapor Volume Flow Rate and Displacement Volume

The vapor volume flow rate of refrigerant at the compressor inlet should be selected to match with the displacement volume of compressor [63], vapor volume flow rate and displacement volume as shown in Figure 3-32 and Figure 3-33, respectively. If the value of displacement volume is high, a big size of the compressor is required [63]. From Figure 3-33, it should be noted that the displacement volume of the compressor increased as the

temperature of condenser increased. According to six refrigerants that were appropriated in terms of the MPH indicator, non-flammable, and non-toxic, it found that R-22 had the lowest value of displacement volume followed by R-134a, R-1234ze, R-1234zez, R-245ca, and R-365mfc, respectively. In addition, when a comparison was made between R-22 and R-365mfc, it was found that R-365mfc gave a higher value which was around 600% of that from R-22, which means that the displacement volume of the R-365mfc compressor is approximately 6 times of the R-22 compressor. For more clarification, when the VCHP system used R-1234zez, R-365mfc, R-245ca, R-22, R-134a, and R-1234ze as working fluids and the condenser temperature was around at 70 °C, the vapor volume flow rate and the displacement volume as shown in Figure 3-34 and Figure 3-35, respectively.

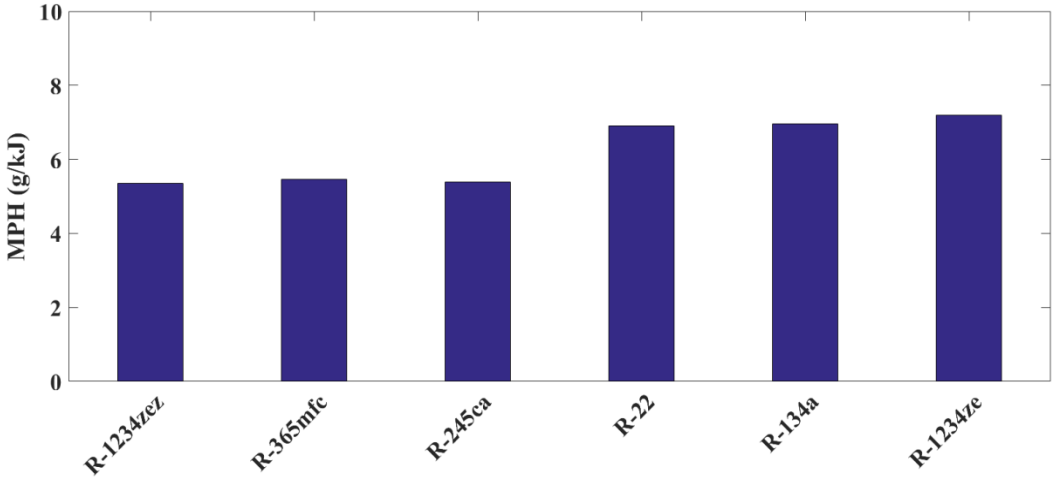

Figure 3-31 MPH (g/kJ) of the VCHP system when R-1234zez, R-365mfc, R-245ca, R-22, R-134a, and R-1234ze as working fluids with the condenser temperature of 70 °C

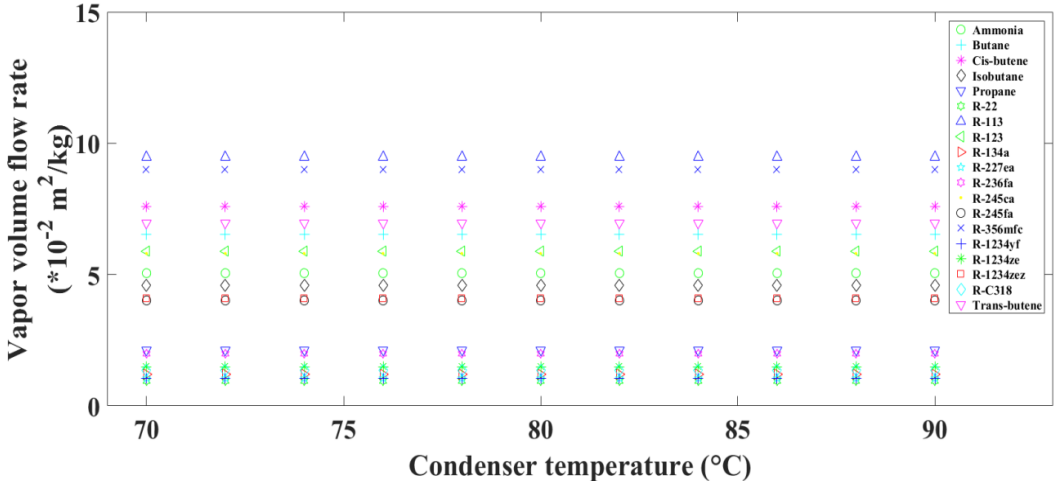

Figure 3-32 Vapor volume flow rate ($\times 10^{-2}$ m^2/kg) of the VCHP system when the condenser temperature increases from 70 to 90 °C

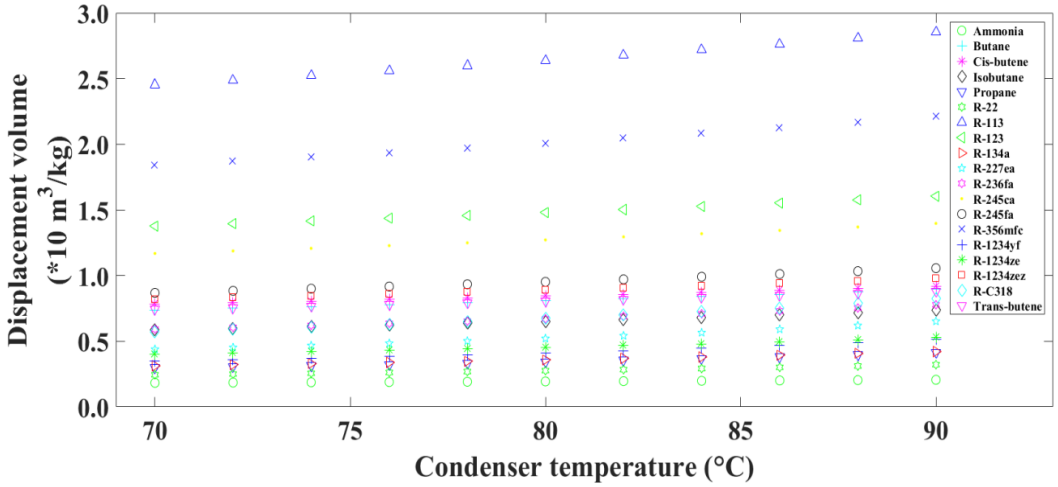

Figure 3-33 Displacement volume (×10 m^3/kg) of the VCHP system when the condenser temperature increases from 70 to 90 °C

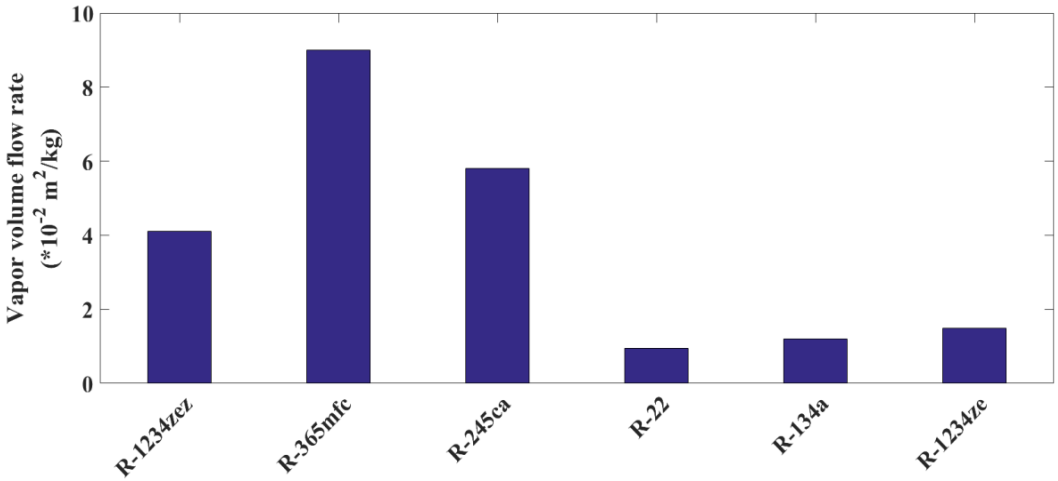

Figure 3-34 Vapor volume flow rate (×10^{-2} m^2/kg) of the VCHP system when R-1234zez, R-365mfc, R-245ca, R-22, R-134a, and R-1234ze as working fluid with the condenser temperature of 70 °C

Discharge Pressure and Discharge Temperature

Discharge pressure is the maximum pressure of refrigerant in the VCHP system as shown in Figure 3-36. If the value is high, the thickness of coil and the fittings should have a special design which results in high initial investment, and high compression work is consumed [63]. From Figure 3-36, it should be noted that discharge pressure in the system increased as the temperature of condenser increased. Of the six refrigerants that were appropriated in terms of the MPH indicator, non-flammable, and non-toxic, it was found that R-365mfc had the lowest value of discharge pressure followed by R-245ca, R1234zez, R-1234ze, R-134a, and R-22, respectively (as shown in Figure 3-37). For discharge temperature, it is also the maximum temperature of refrigerant in the VCHP system as shown in Figure 3-38. If the value is high, the lubricant used in the system will not be stable [63]. It was found that R-365mfc had the lowest value of discharge temperature followed by R-245ca, R-1234ze, R-1234zez, R-134a, and R-22, respectively (as shown in Figure 3-39).

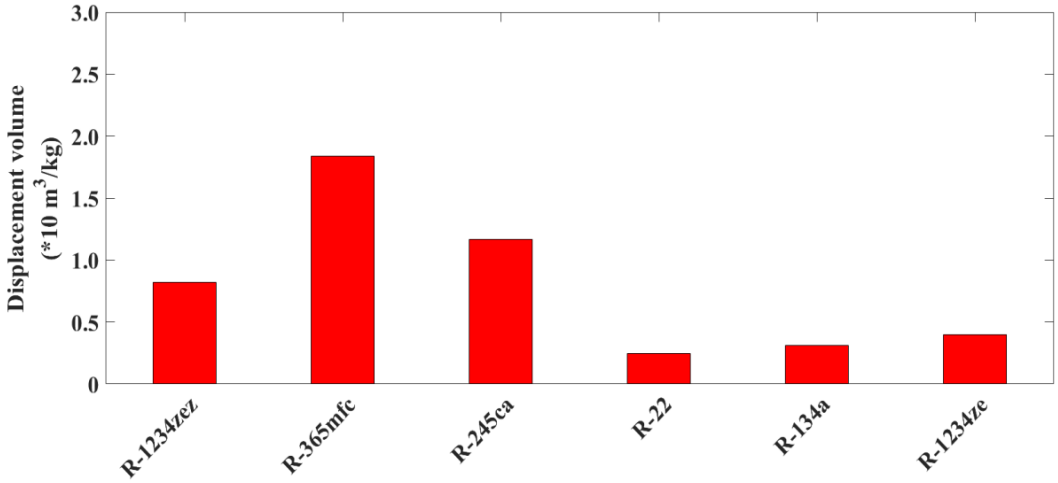

Figure 3-35 Displacement volume (×10 m^3/kg) of the VCHP system when R-1234zez, R-365mfc, R-245ca, R-22, R-134a, and R-1234ze as working fluids with the condenser temperature of 70 °C

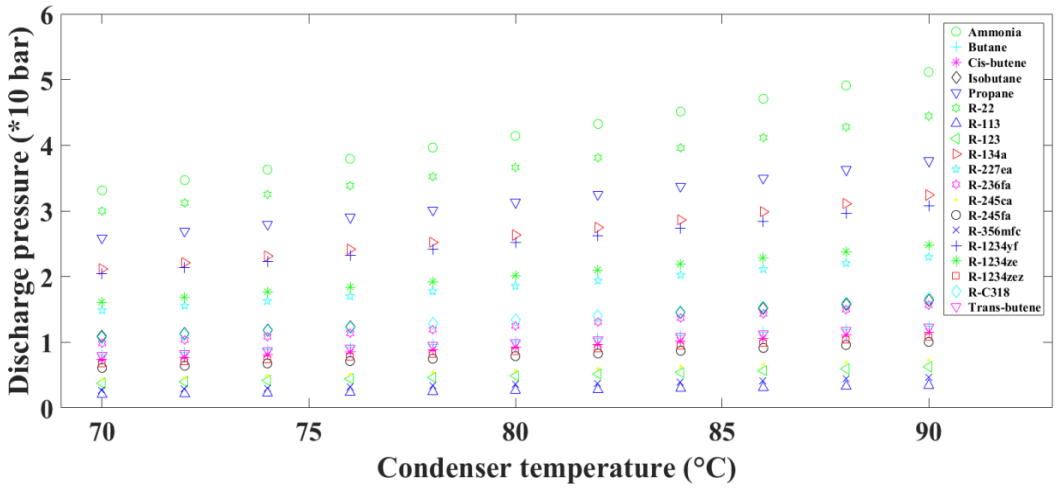

Figure 3-36 Discharge pressure (×10 bar) of the VCHP system when the condenser temperature increases from 70 to 90 °C

Pressure Ratio

Pressure ratio is the ratio of the condenser pressure to the evaporator pressure. If its value is high the compressor work will consume high power input [63], as shown in Figure 3-40. The results showed that pressure ratio of the VCHP system increased as the temperature of condenser increased. According to six refrigerants that were appropriated in terms of the MPH indicator, non-flammable, and non-toxic, it was found that R-22 had the lowest value of pressure ratio followed by R-134a, R-1234ze, R-1234zez, R-245ca, and R-365mfc, respectively (as shown in Figure 3-41).

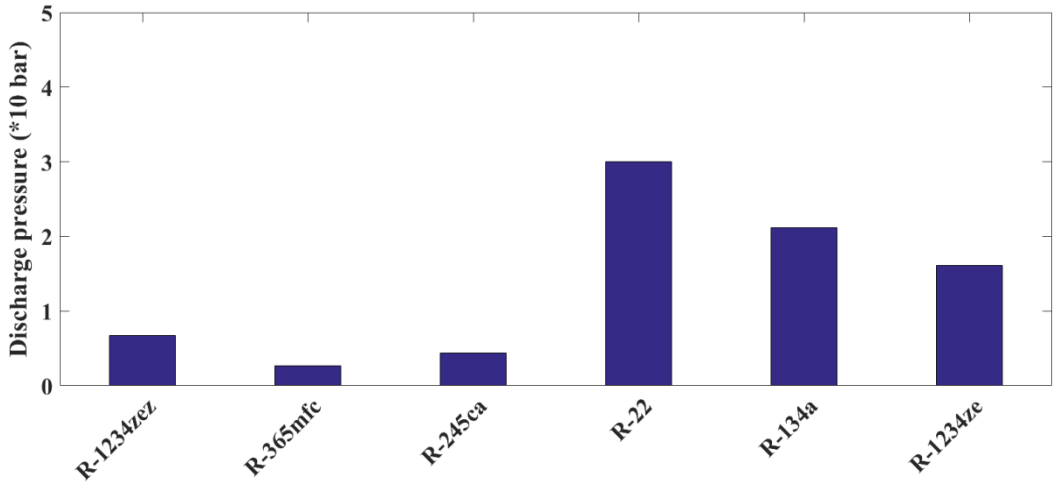

Figure 3-37 Discharge pressure (×10 bar) of the VCHP system when R-1234zez, R-365mfc, R-245ca, R-22, R-134a, and R-1234ze as working fluids with the condenser temperature of 70 °C

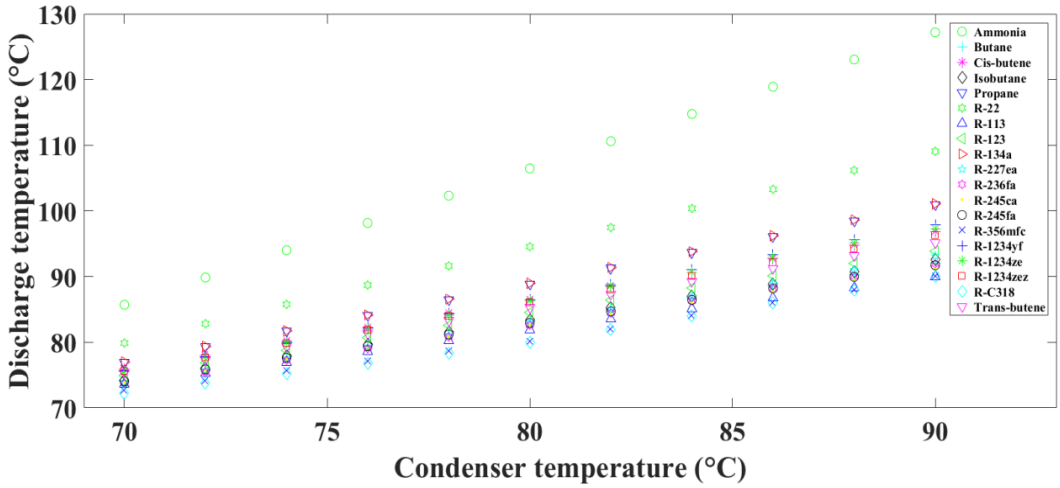

Figure 3-38 Discharge temperature (°C) of the VCHP system when the condenser temperature increases from 70 to 90 °C

COP_{VCHP}

Figure 3-42 shows the ideal heating COP of the VCHP system with different types of refrigerant. Based on the results, the COP of the system decreased as the temperature of condenser increased. According to six refrigerants that were appropriated in terms of the MPH indicator, non-flammability, and non-toxicity, R-365mfc had the highest value of COP followed by R-245ca, R-1234zez, R-1234ze, R-134a, and R-22, respectively (as shown in Figure 3-43).

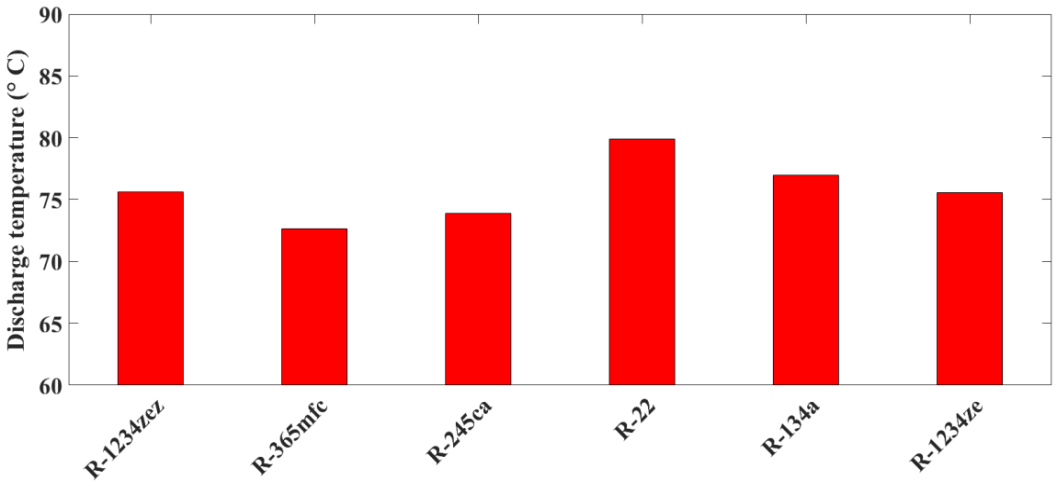

Figure 3-39 Discharge temperature (°C) of the VCHP system when R-1234zez, R-365mfc, R-245ca, R-22, R-134a, and R-1234ze as working fluids, and the condenser temperature of 70 °C

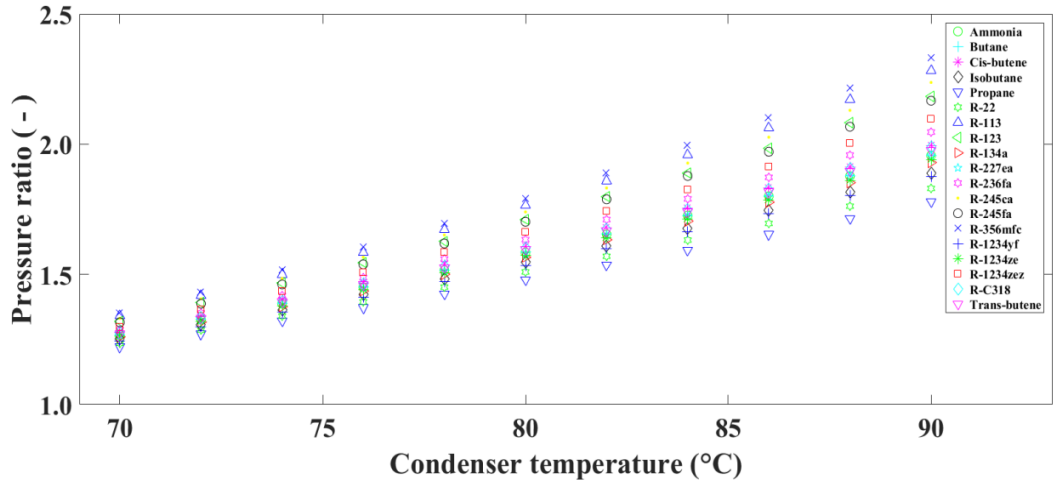

Figure 3-40 Pressure ratio (-) of the VCHP system when the condenser temperature increases from 70 to 90 °C

Conclusion

From the above mentioned, as considered in terms of non-flammability and non-toxicity, the six refrigerants appropriated were R-1234zez, R-365mfc, R-245ca, R-22, R-134a, and R-1234ze. However, it can be concluded that the suitable working fluid of the VCHP system is R-365mfc, due to its lower maximum temperature and pressure for the VCHP compressor. Additionally, it gives the highest value of COP of the VCHP system for supplying heat at around 70 to 90 ºC (as shown in Figure 3-44). In this study, R-365mfc was selected for the VCHP system. Nevertheless, as consider in terms of environmental impact, it was found that R-1234ze had the lowest value of ODP and GWP followed by R-1234zez, R-245ca, R-365mfc, R-134a, and R-22, respectively (as shown in Table 3-1).

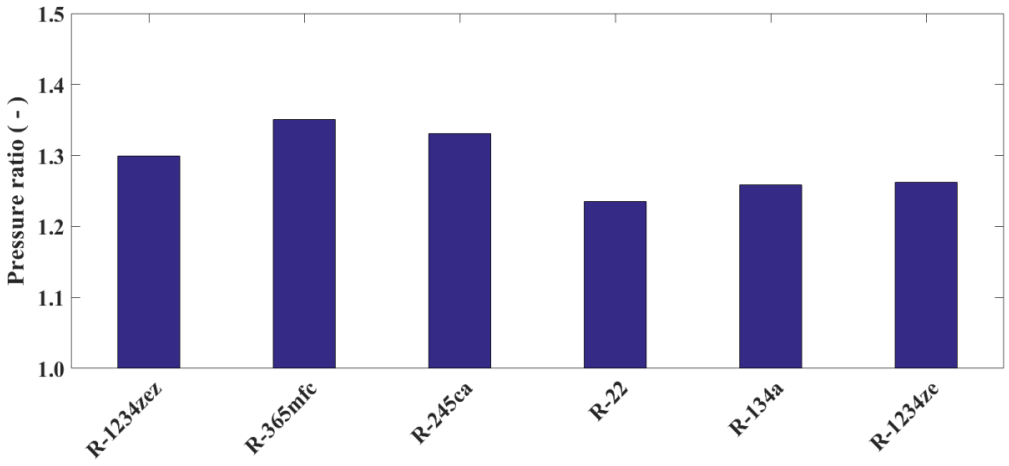

Figure 3-41 Pressure ratio (-) of the VCHP system when R-1234zez, R-365mfc, R-245ca, R-22, R-134a, and R-1234ze as working fluids with the condenser temperature of 70 °C

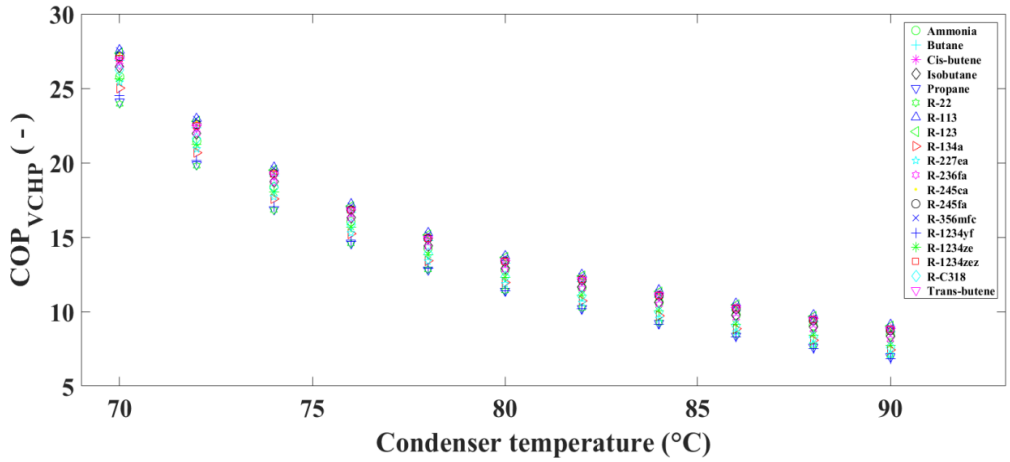

Figure 3-42 COP (-) of the VCHP system when the condenser temperature increases from 70 to 90 °C

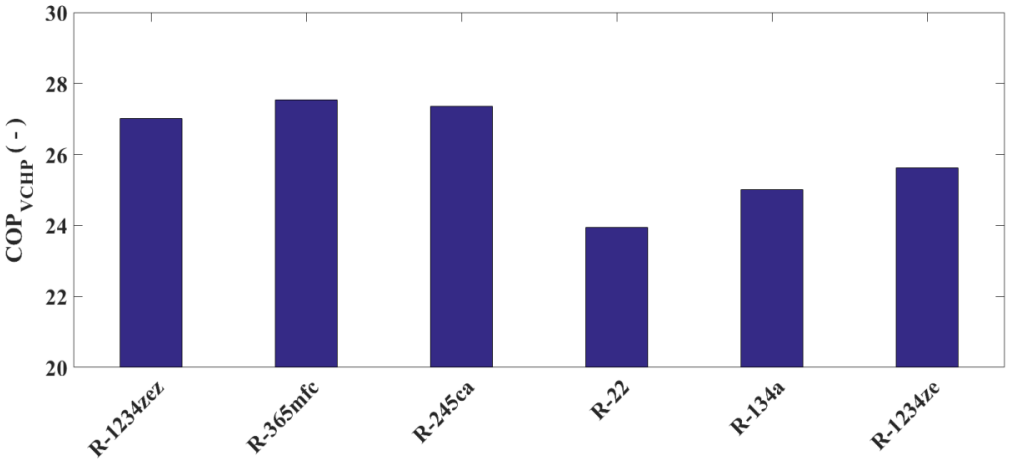

Figure 3-43 COP_{VCHP} (-) of the VCHP system when R-1234zez, R-365mfc, R-245ca, R-22, R-134a, and R-1234ze as working fluids with the condenser temperature of 70 °C

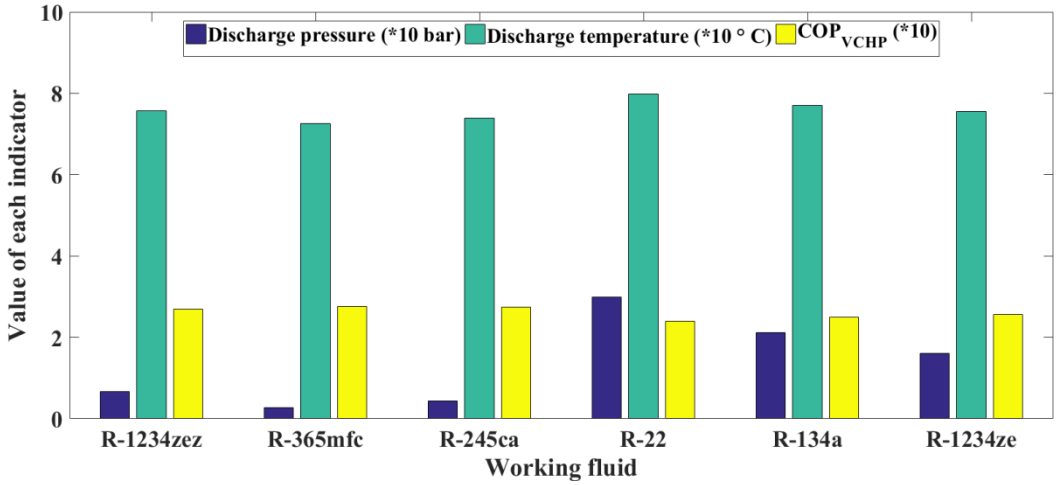

Figure 3-44 Discharge pressure (×10, bar), Discharge temperature (×10, °C), and COP_{VCHP} (×10) of the VCHP system when R-1234zez, R-365mfc, R-245ca, R-22, R-134a, and R-1234ze as working fluids with the condenser temperature of 70 °C

3.4.2 Gas Engine-driven Heat Pump (GEHP)

Effect of Engine Mechanical and Gas Engine Thermal Efficiency for the GEHP System

The schematic diagram of the GEHP system is shown in Figure 2-24. The engine mechanical ($\eta_{ME,GEHP}$) and gas engine thermal ($\eta_{ge,th}$) efficiency were the most critical parameters for evaluating the GEHP system. Based on the Eq. (2-54), the assumption of gas engine combustion (η_{comb}), power transmission (η_{belt}) efficiency, and fuel lower heating value (q_{LHV}) were omitted. It was found that when the values of engine mechanical and gas engine thermal efficiency are low, the amount of the fuel energy input to the gas engine needed is high. In this part, these two parameters were considered. The working conditions for the evaluation of coefficient of performance of the GEHP system (COP_{GEHP}) and the fuel energy were the engine mechanical and the engine thermal efficiency varying from 50 to 100% (with 5% increment). The combustion and the power transmission efficiency was 95%. The results of the COP_{GEHP} when the engine mechanical efficiency changed from 50 to 100% and the gas engine thermal efficiency was set at 45% are shown in Figure 3-45. Additionally, the results of the COP_{GEHP} when the gas engine thermal efficiency varied from 40 to 100% and the engine mechanical efficiency was set at 80% are shown in Figure 3-46.

It was found that the engine mechanical and the gas engine thermal efficiency were significant factors in terms of COP_{GEHP}. The COP_{GEHP} of the system increased when these two parameters increased. The fuel energy of the system when the engine mechanical efficiency varied from 50 to 100% and the gas engine thermal efficiency was set around at 45% is shown in Figure 3-47, while Figure 3-48 shows the case when the gas engine thermal efficiency changed from 40 to 100% and the engine mechanical efficiency was set at 80%. The results showed that the fuel energy of the system decreased when the engine mechanical and the gas engine thermal efficiency increased. It can then be assumed that these two parameters are critical for evaluating the GEHP system.

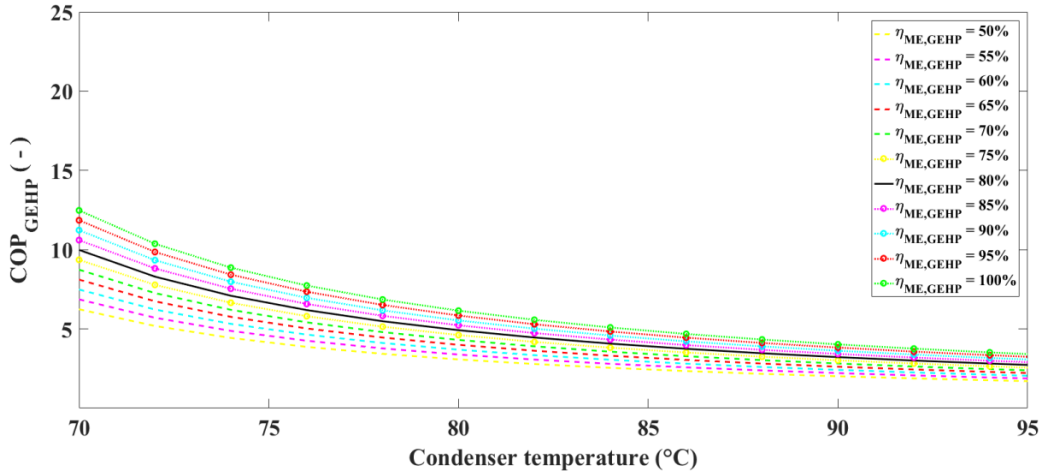

Figure 3-45 COP (-) of the GEHP system when the engine mechanical efficiency increases from 50 to 100% with the gas engine thermal efficiency of 45%

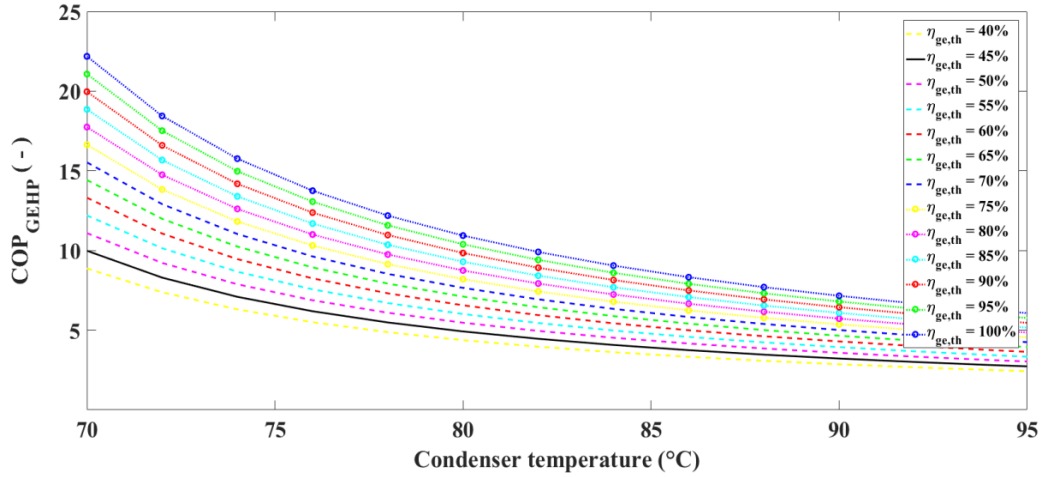

Figure 3-46 COP (-) of the GEHP system when the gas engine thermal efficiency increases from 40 to 100% with the engine mechanical efficiency of 80%

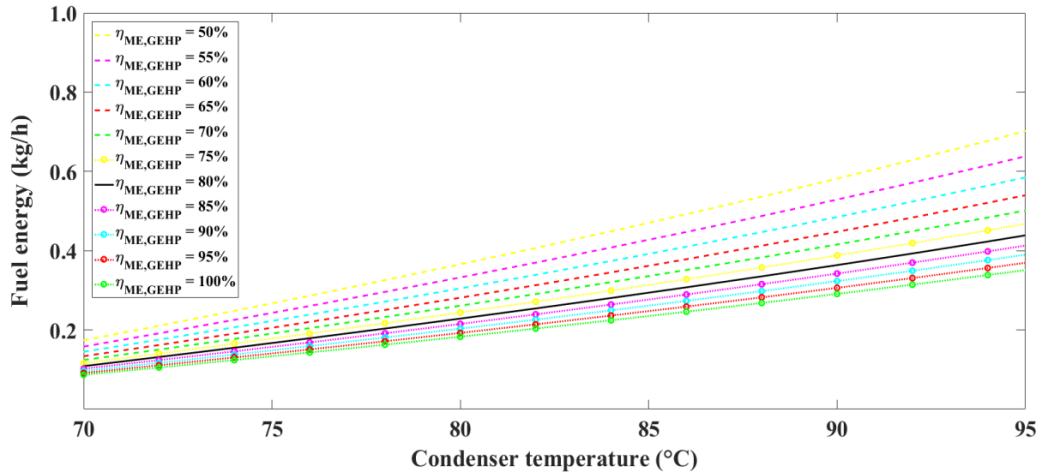

Figure 3-47 Fuel energy of the GEHP system when the engine mechanical efficiency increases from 50 to 100% with the gas engine thermal efficiency of 45%

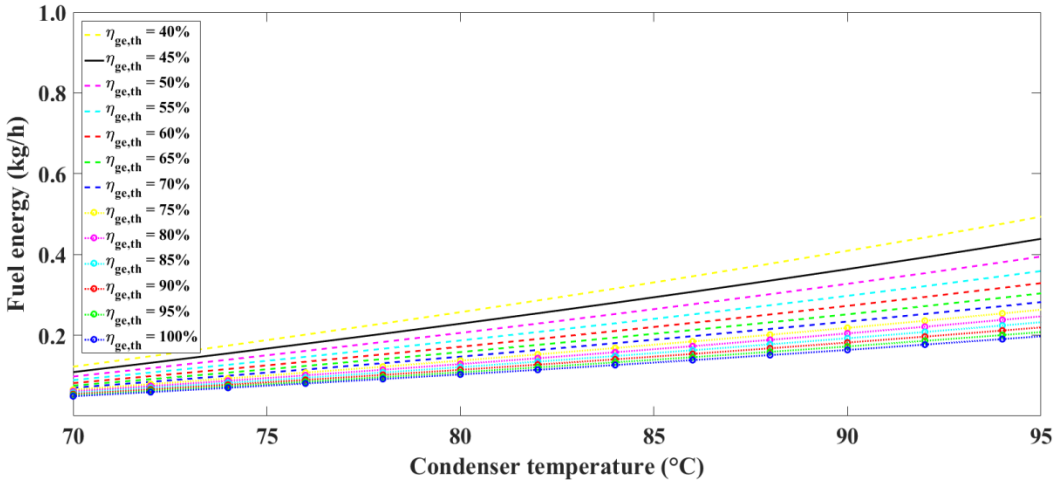

Figure 3-48 Fuel energy of the GEHP system when the gas engine thermal efficiency increases from 40 to 100% with the engine mechanical efficiency of 80%

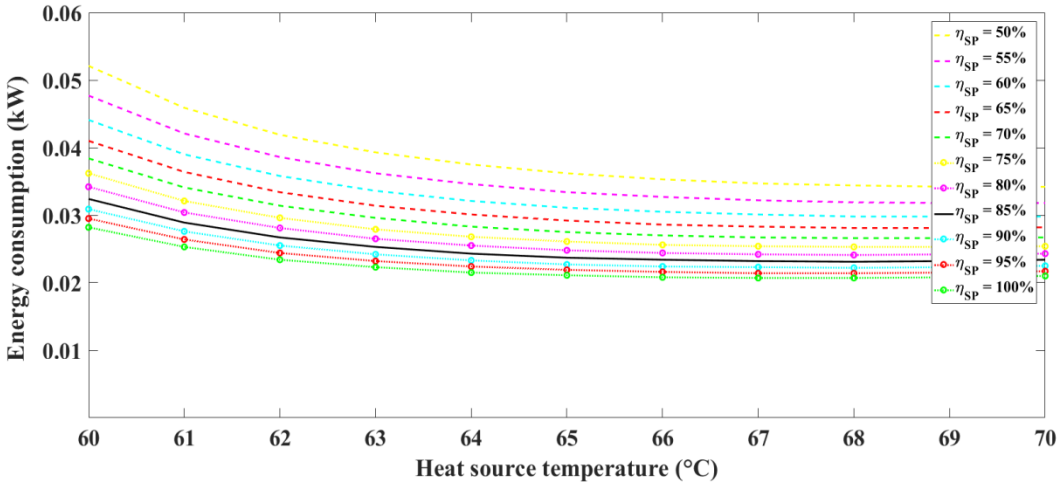

Figure 3-49 Energy consumption of the AHT system when the solution pump efficiency increases from 50 to 100% with the water pump efficiency of 50%

3.4.3 Absorption Heat Transformer (AHT)

Effect of Water Pump and Solution Pump Efficiency for the AHT System

The schematic diagram of the AHT system is shown in Figure 2-26. The water pump (η_P) and solution pump (η_{SP}) efficiency were the most critical parameters for evaluating the AHT system. Using Eq. (2-63) and (2-65), it was found that when the value of the water pump and solution pump efficiency is low the high power input for the system needed is high. In this part, the effects of these two parameters were considered. The working conditions for the evaluation of coefficient of performance of the AHT system (COP_{AHT}) were the water pump, and solution pump efficiency varying from 50 to 100% (with 5% increment). The minimum concentration of a weak H_2O-LiBr solution was 45% LiBr, and the minimum concentration difference of strong and weak H_2O-LiBr solution was 2% LiBr. The evaluation results in terms of the energy consumption from the summation of the water pump and the solution pump are shown in Figure 3-49 and Figure 3-50. The results showed that the power consumption decreased when the water pump and solution pump efficiency increased.

In addition, the efficiency of the solution pump was a significant factor in relation to the power consumption of the AHT system.

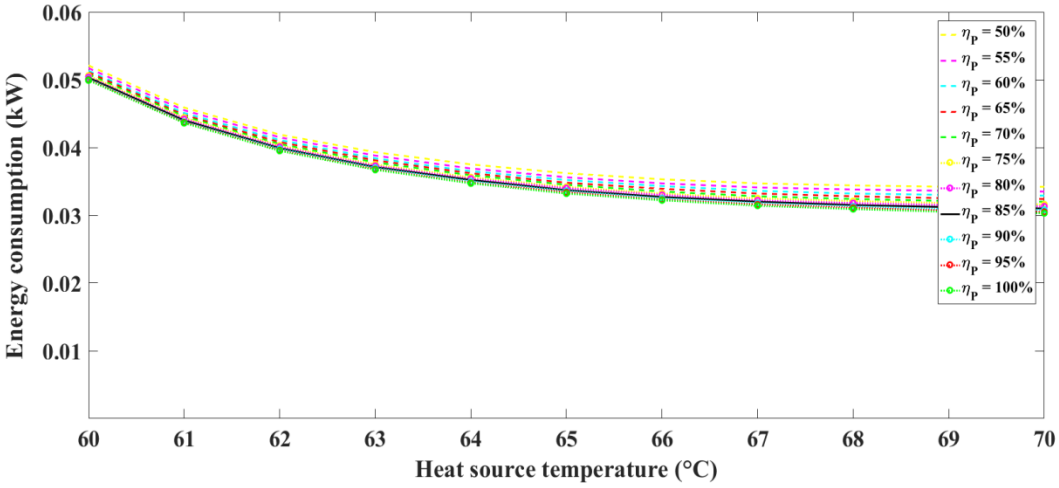

Figure 3-50 Energy consumption of the AHT system when the water pump efficiency increases from 50 to 100% with the solution pump efficiency of 50%

In terms of the COP_{AHT}, the evaluation results when the solution pump efficiency varied from 50 to 100% and the water pump efficiency was set at 50% are shown in Figure 3-51, while Figure 3-52 shows results when the water pump efficiency changed from 50 to 100%, and the solution pump was set at 50%. It was found that the water pump and solution pump efficiency were not significant factors affecting COP_{AHT} since the energy input to these two devices was very low, as shown in Figure 3-49 and Figure 3-50.

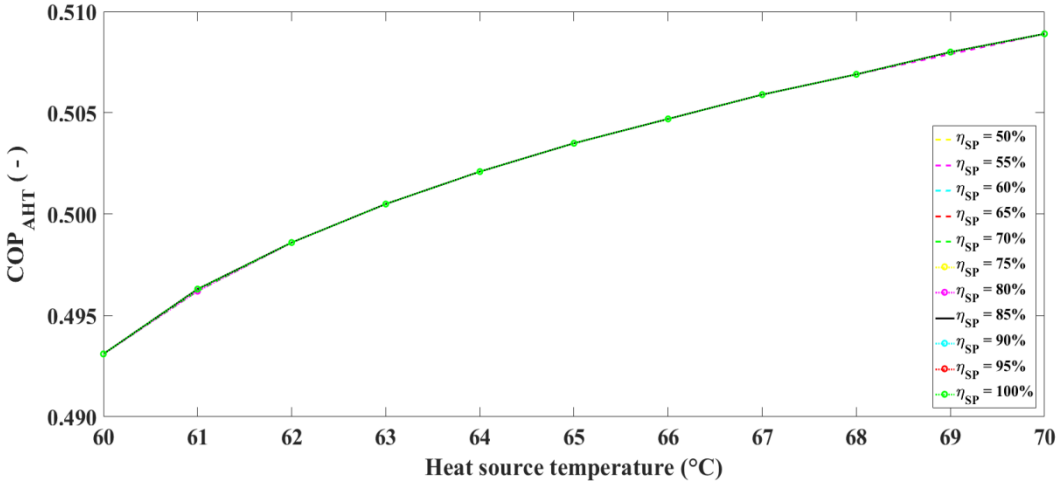

Figure 3-51 COP (-) of the AHT system when the solution pump efficiency increases from 50 to 100% with the water pump efficiency of 50%

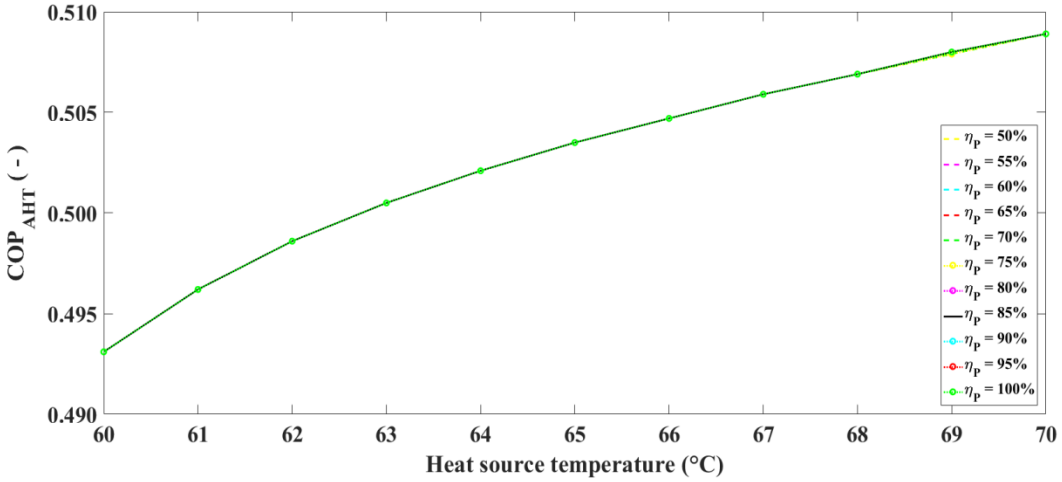

Figure 3-52 COP (-) of the AHT system when the water pump efficiency increases from 50 to 100% with the solution pump efficiency of 50%

3.5 Validate the Model Used in the Study

According to the results mentioned in 3.3 Organic Rankine Cycle (ORC), the mathematical or theoretical modeling of the ORC system was validated with the use of previously published data. The results suggest that the variable value of the mathematical modeling (present study) was not significantly different when compared with the published data. It can be said that the modeling of the ORC power generation can be applied to estimate the power output from the ORC system. And in 3.4 Heat Boosting Technologies, the assumption of the efficiency of the compressor, the gas engine mechanical, the gas engine combustion, the gas engine thermal, the power transmission, the water pump, and the solution pump were made in previous studies [55, 56, 58, 82]. A reasonable value for the modeling of the heating booster was obtained, which was not too high-value for evaluating the system. Moreover, in Chapters 5 and 6, the performance characteristic of ORC power generation and the characteristic of solar collectors were obtained from a company. It means that these values were experimental or that the devices were already validated. Therefore, in Chapters 4, 5, and 6, even if the combinations proposed in the present study were not experimentally tested, the results still hold since the assumptions made for each component working on its own (considering its operation parameters) were also taken when the system functioned as a whole.

4

Low Temperature Upgrading Technologies for an ORC Power Generation

This Chapter is presents a simulation results of the different heat boosting technologies that use to rise the low-temperature heat source, from the low-grade industrial waste heat (IWH), to the high-temperature heat sink/heat reservoir for ORC power generation. These heat boosters that available in the market studied are (i) Vapor compression heat pump (VCHP), (ii) Gas engine-driven heat pump (GEHP), and (iii) Absorption heat transformer (AHT) systems.

4.1 Introduction

In industry processes, approximately 50 percent of the total energy introduced to the system is released to the environment and wasted. About 60 percent of the heat disposed has temperatures lower than 230 °C, which presents a large opportunity for heat recovery [7, 8]. Unfortunately, it is only marginally profitable to recover energy from heat source below 340 °C [9] to convert such low-temperature heat into electricity using steam-operated Rankine cycle. Nevertheless it is viable for power generation if ORC, which uses an organic compound as working fluid instead of water, is deployed [11, 13].

Recently, many researchers had been working on the design, analysis, and development of ORC systems for low-temperature waste heat conversion. Tchanche et al., [83] showed that the market of ORC in waste heat recovery applications are growing faster among all other ORC solutions, with an enormous potential in industry and combined cycle power plants. Campana et al., [19] evaluated the energy savings and CO_2 emission of ORC units based on real operating data of cement, steel, glass, and oil & gas industries. Liu et al., [20] designed and modified a hybrid energy supply system, including GEHP systems and ORC using gas engine waste heat as a low-grade heat source in order to transfer the low-grade gas engine waste heat into electricity through ORC. Bor et al., [84] investigated the potential of several alternative technologies for upgrading low-temperature waste heat such as compression-resorption, vapor compression and trans-critical heat pumps, or for the conversion using organic Rankine, Kalina and trilateral cycle engines. The waste heat has a temperature level of 46 to 60 °C with large amounts of heat released to the environment. Chaiyat, [21] proposed a concept to generate electricity from low-temperature heat using an AHT coupled with ORC. Sonsaree et al., [22] presented power generation using an ORC system combined with a gas engine-driven heat pump (GEHP) by utilizing the low-grade

IWH. Their results suggest that GEHP-ORC system is feasible for industries that have low-temperature heat sources available.

From current literature, it is evident that ORC is a well-developed waste heat recovery technology that is capable of generating mechanical or electrical work. Nevertheless, for heat source temperature below 70 ºC, it is less attractive due to a combination of market and technical barriers [18, 23], resulting in a large amount of heat from industrial processes is disposed into environment. If an ORC system could be applied for power generation at heat source temperature below 70 ºC, the industrial sector could benefit from the utilization of such energy source and save costs in energy consumption [85], as well as in the reduction in operation cost, increased energy efficiency of the industrial processes [34], and reduce emission of pollutants. Considering the above mentioned, by augmenting the temperature of low-temperature heat source, to achieve a higher temperature difference between the heat reservoir to the heat sink, is an attractive approach for ORC power generation. In this Chapter, the objective is to mathematically model and analyze three different heat boosting technologies (VCHP, GEHP, and AHT systems) to rise a low-temperature heat sufficiently for effective power generation using an ORC system in the interest of economic and environmental impact.

4.2 System Descriptions

The schematic diagram of an ORC power generation system combined with different heat boosting technologies, is shown in Figure 4-1. Moreover, the combination of the VCHP-ORC, the GEHP-ORC, and the AHT-ORC power generations is shown in Figure 4-2 to Figure 4-4, respectively. The main components of the system are: heat boosting technology (VCHP, GEHP, and AHT systems), ORC system, and storage tank. Waste heat from an industry process, with prescribed quantity and quality, is stored in thermal storage tank one. The heat grade is then augmented by any one of the proposed heat boosters to an equal-to or higher temperature heat and then is stored in the heat reservoir/thermal storage tank two. Finally, the heat from the thermal storage tank two is supplied to the ORC system to generate electricity.

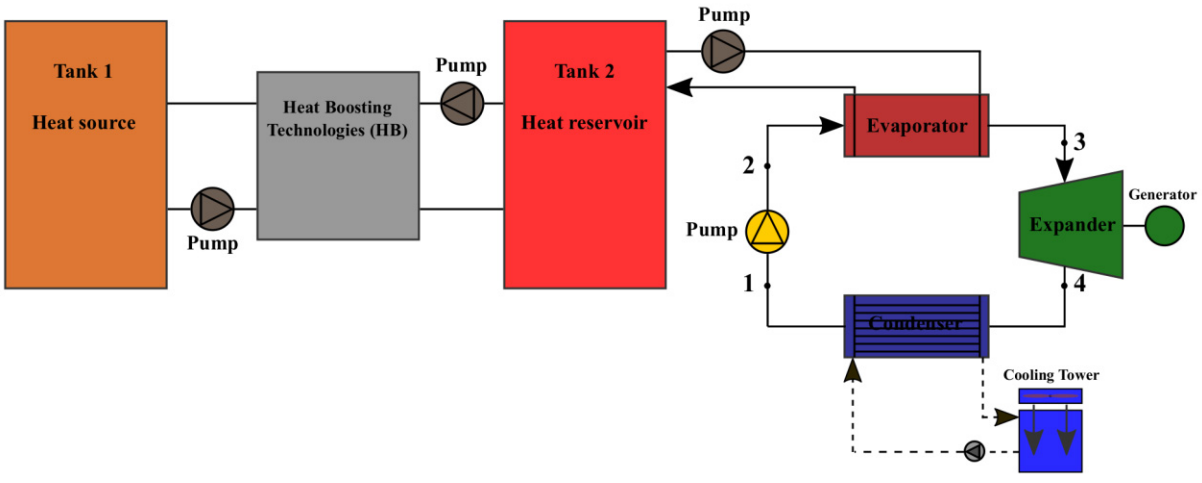

Figure 4-1 Schematic diagram of the proposed systems

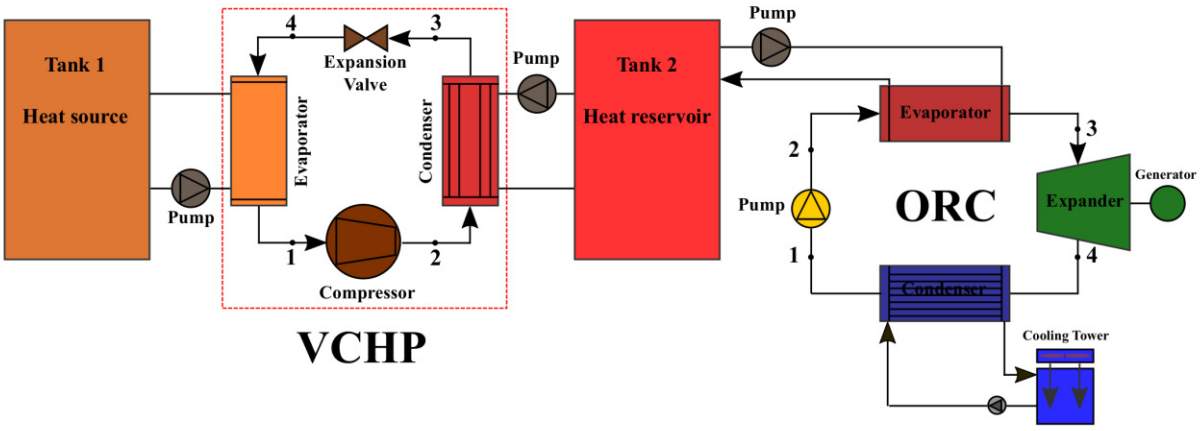

Figure 4-2 The VCHP-ORC power generation system

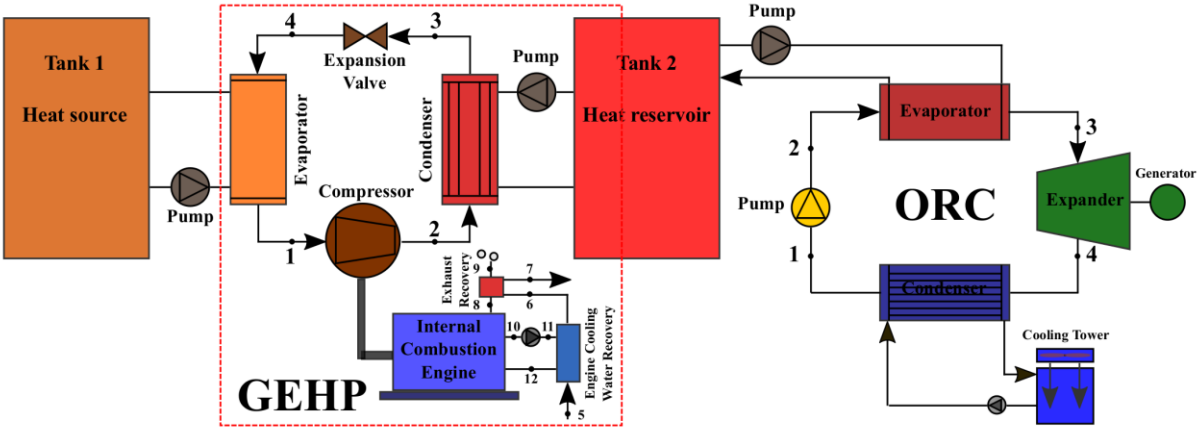

Figure 4-3 The GEHP-ORC power generation system

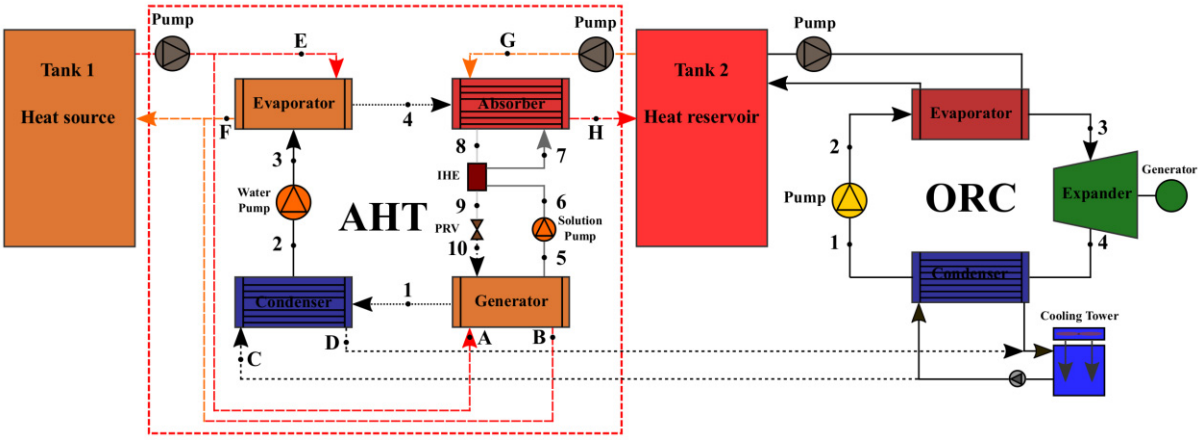

Figure 4-4 The AHT-ORC power generation system

4.3 Simulation Conditions

In the modeling of the three systems, the VCHP-ORC, the GEHP-ORC, and the AHT-ORC systems, it is assumed that steady state conditions are maintained and pressure drop in the overall system is neglected, with the exception of the turbine and pump from the ORC system. Heat loss to the environment from the evaporator, condenser, generator, and the piping system are also neglected. The temperature in the thermal storage tank is assumed to be uniform and non-stratified. The operation conditions of the systems are shown in Table 4-1 to Table 4-3. In the system, the degree of superheating (SH), sub-cooling (SC) and the pinch-point temperature difference (PT) are set at 5.0 °C. In addition, heat exchanger effectiveness (ε_{HX}) is assumed to be 90%. The thermodynamic properties of the VCHP, the GEHP and the ORC systems are calculated using REFPROP NIST7.0 [81]. The properties of H_2O-LiBr solution, in accordance to ASHRAE Handbook [86], Khairulin et al. [87], and Kaita [88], as shown in APPENDIX A Properties of Lithium Bromide-Water (LiBr-H_2O) Solutions are adopted. The cycle of the three systems were simulated in MATLAB.

Table 4-1 Initial condition of a 20 kW_e ORC system with R-245fa

Descriptions	Data
Organic Rankine Cycle (ORC) system:	
Cycle power (W_{ORC}), kW_e	20
Isentropic turbine efficiency ($\eta_{Tur,isen}$), %	85
Mechanical turbine efficiency ($\eta_{Tur,ME}$), %	90
Isentropic pump efficiency ($\eta_{ORC,P,isen}$), %	85
Mechanical pump efficiency ($\eta_{ORC,P,ME}$), %	95
Motor pump efficiency ($\eta_{ORC,P,MO}$), %	95
ORC condenser temperature ($T_{ORC,Cond}$), °C	30
Working fluid	R-245fa

Table 4-2 Initial condition of a 250 kW_{th} for the VCHP and the GEHP systems with R-365fmc

Descriptions	Data
Vapor compression heat pump (VCHP) system:	
Isentropic compressor efficiency ($\eta_{VCHP,isen}$), %	90
Mechanical compressor efficiency ($\eta_{Comp,ME}$), %	95
Motor compressor efficiency ($\eta_{Comp,MO}$), %	95
Gas engine-driven heat pump (GEHP) system:	
Isentropic compressor efficiency ($\eta_{GEHP,isen}$), %	90
Gas engine mechanical efficiency ($\eta_{ge,ME}$), %	82
Gas engine combustion efficiency ($\eta_{ge,comb}$), %	95
Efficiency of power transmission (η_{belt}), %	95
Gas engine thermal efficiency ($\eta_{ge,th}$), %	35
Fuel lower heating value (q_{LHV}) of Natural Gas (NG), kJ/kg [82]	44000
Chemical exergy content of Natural Gas (NG), kJ/kg [82]	45760
Capacity, kW_{th}	250
Working fluid [89]	R-365mfc

Table 4-3 Initial condition of a 250 kW_{th} AHT system with LiBr-H_2O

Descriptions	Data
Absorption Heat Transformer (AHT) system:	
Minimum concentration of weak H_2O-LiBr solution (X_{min}), %LiBr	45
Minimum concentration difference of strong and weak H_2O-LiBr solution ($\Delta X_{s,min}$), %LiBr	2
Isentropic efficiency of the water pump ($\eta_{AHT,P,isen}$) and the solution pump ($\eta_{AHT,SP,isen}$), %	85
Mechanical efficiency of the water pump ($\eta_{AHT,P,ME}$) and the solution pump ($\eta_{AHT,SP,ME}$), %	95
Motor efficiency of the water pump ($\eta_{AHT,P,MO}$) and the solution pump ($\eta_{AHT,SP,MO}$), %	95
AHT condenser temperature ($T_{AHT,Cond}$), °C	30
Capacity, kW_{th}	250

The calculation steps for evaluating the net power output of the VCHP-ORC and the GEHP-ORC systems are shown in Figure 4-5 and Figure 4-6, respectively. Inputs of the simulation were the low-grade IWH as a heat source/thermal storage tank one ($T_{w1,i}$) is varied from 60 to 68 °C, the heat reservoir/thermal storage tank two ($T_{w2,i}$) at 70 °C, and water flow rate ($\dot{m}_{HS}$). The working fluid of the VCHP and the GEHP systems is R-365mfc, and the ORC system is R-245fa. The given data is the fixed value of the calculation such as heat exchanger effectiveness (ε_{HX}), degree of sub-cooling (SC) and superheating (SH), isentropic VCHP compressor ($\eta_{VCHP,isen}$), gas engine mechanical ($\eta_{ge,ME}$), gas engine combustion ($\eta_{ge,comb}$), isentropic turbine ($\eta_{Tur,isen}$) and isentropic pump ($\eta_{ORC,P,isen}$) efficiency, efficiency of power transmission (η_{belt}), fuel lower heating value (q_{LHV}) of Natural Gas (NG), and ORC condenser temperature ($T_{ORC,Cond}$). For the step of calculations, the properties of working fluid of the VCHP system combined with the ORC system, and the GEHP system combined with the ORC system were evaluated to find out the net power output of the VCHP-ORC, and the GEHP-ORC systems, and fuel consumption of the GEHP-ORC system.

Moreover, Figure 4-7 shows the calculation steps for evaluating the net power output of the AHT-ORC system. The given data is the fixed value of the calculation such as minimum concentration of weak H_2O-LiBr solution (X_{min}), minimum concentration difference of strong and weak H_2O-LiBr solution ($\Delta X_{s,min}$), isentropic water pump ($\eta_{AHT,P,isen}$) and isentropic solution pump ($\eta_{AHT,SP,isen}$) efficiency. For the process of calculations, the properties of working fluid of the AHT combined with the ORC system are evaluated to find out the net power output of the AHT-ORC system.

4.4 Economic Analysis

Economic analysis of the integrated system are carried out in respect of the levelized cost of electricity (LCOE) as presented in the studies of Chaiyat and Kiatsiriroat [60] and Chaiyat [61]. In the economic assessment, the initial condition and the commercial cost of the three heat boosting technologies used to evaluate the capital cost of the system are shown in Table 4-4. Capital costs of the ORC power plant varies between 2000 to 3400 USD/kW_e [90-92] as given in Table 4-5. As shown, a small-scale ORC power plant for this study at around 2500 USD/kW_e was selected for the study.

Table 4-4 Initial condition, and cost data used for the economic evaluation of the system, when the heat pump capacity of 250 kW_{th}

Descriptions	Data
Condition	
Operation time, hour/day	24
Operation day, day/year	350
Investment cost	
Vapor Compression Heat Pump (VCHP) system [9, 93], USD/kW_{th}	261
Gas Engine-dirven Heat Pump (GEHP) system [9, 93], USD/kW_{th}	326
Absorption Heat Transformer (AHT) system [9, 93], USD/kW_{th}	641
Cost of the NGV [94], USD/kg	0.37
Surcharge for construction and engineering, %	10
Operation & maintenance (O&M) cost	
Operation & maintenance cost (% of investment cost per year)	1
Life time of plant, year	25

Table 4-5 Commercial cost of the ORC power system

Company	ORC capacity (kW_e)	Cost (USD/kW_e)
Ormat [91]	250 – 20000	2000
Infinity turbine [90]	2 – 3000	2500
Electratherm [91]	50	2530
Turboden [89]	200 – 15000	3400

4.5 Results and Discussion

Three different heat boosting technologies were mathematically applied to elevate the temperature of the heat source, from the low-grade IWH at temperatures below 70 °C, to the high-temperature of the heat sink/heat reservoir before supplying the heat to the ORC power generation system, were simulated. The VCHP-ORC, the GEHP-ORC, and the AHT-ORC systems are compared based on net power output, energy consumption, thermal efficiency, life-time cost, the LCOE, CO_2 reduction, foot print of the heat boosting technologies, and effect of the heat source temperature on the systems are detailed as following:

4.5.1 Net Power Output and Energy Consumption of the System

Comparison of the net power output of the systems is shown in Figure 4-8, suggests that the GEHP-ORC and the AHT-ORC systems output are higher than that of the VCHP-ORC system, as electrical consumption of these two heat boosting technologies is low since the GEHP system uses fuel for energy while the AHT system deploys thermal energy as their main source to operate, instead of electrical energy. For instance, when the temperature of the heat source is 60 °C, the net power output and electrical consumption of the VCHP-ORC, the GEHP-ORC, and the AHT-ORC systems are 79.2 and 88.7 MWh/Year, 163.7 and 4.1 MWh/Year, and 159.0 and 4.7 MWh/Year, respectively.

It should be noted that the net power output of the VCHP-ORC system has decreasing electrical consumption as the temperature of the heat source increases, due to the reduction in power requirement of the VCHP system to augment the temperature of the heat source. For

example, when the temperature of the heat source is 64 °C, the net power output and electrical consumption of the system are 112.3 and 53.3 MWh/Year, respectively. Figure 4-9 shows the net power output (MWh/Year) and energy consumption (MWh/Year) of the VCHP-ORC system, when the heat source temperature increases (°C).

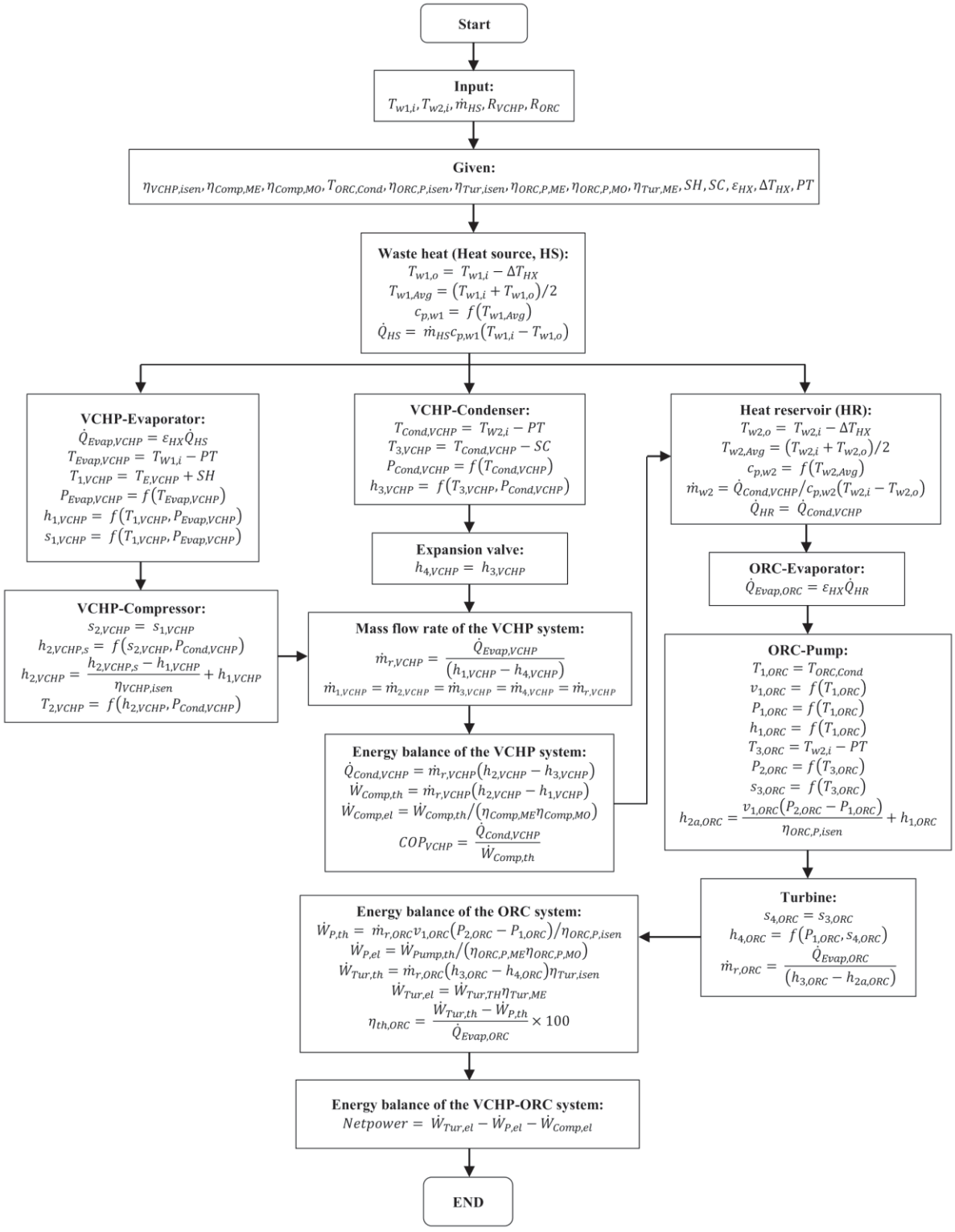

Figure 4-5 Calculation steps of the simulation program for evaluating the net power output of the VCHP-ORC power generation system

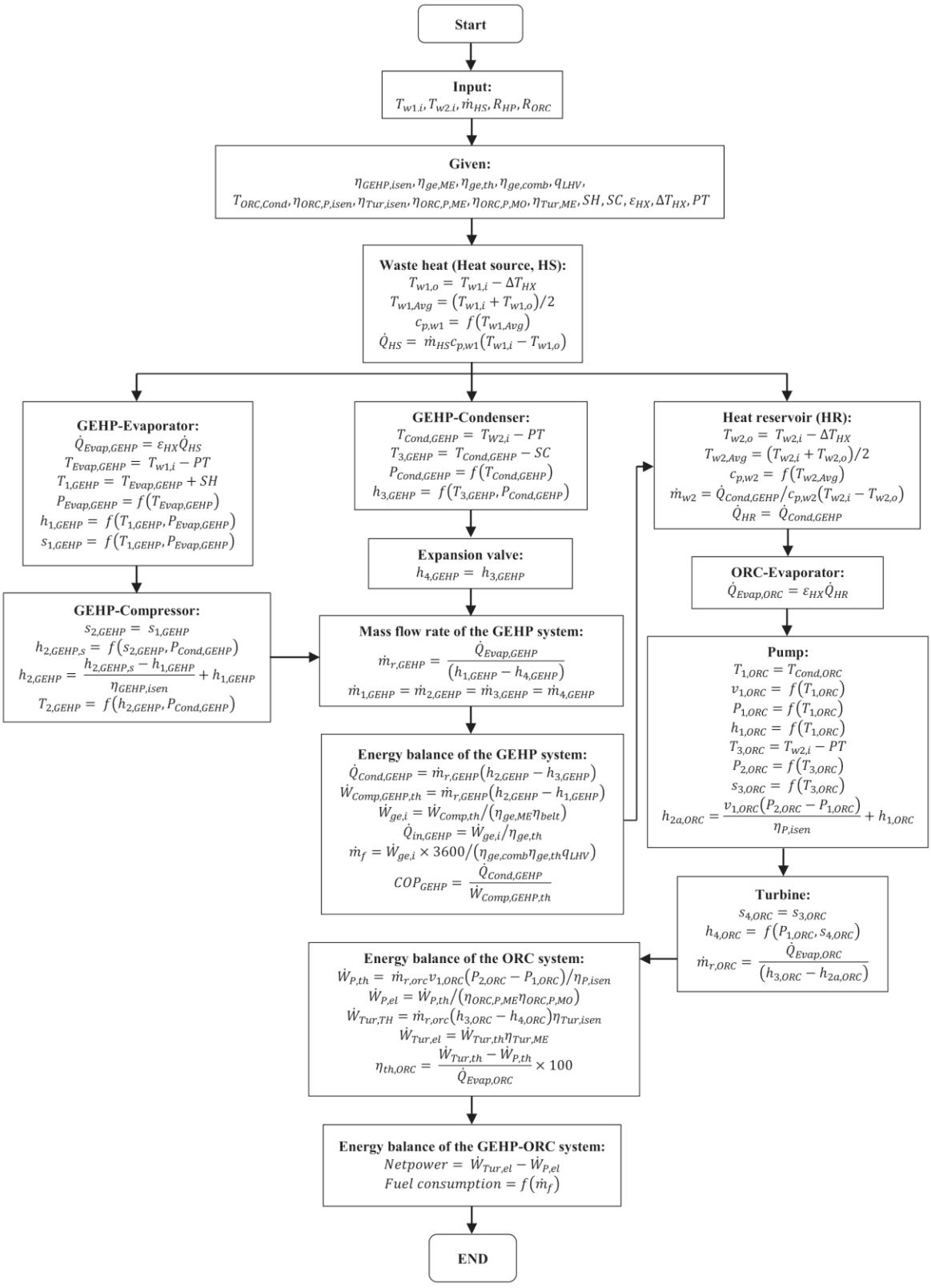

Figure 4-6 Calculation steps of the simulation program for evaluating the net power output of the GEHP-ORC power generation system

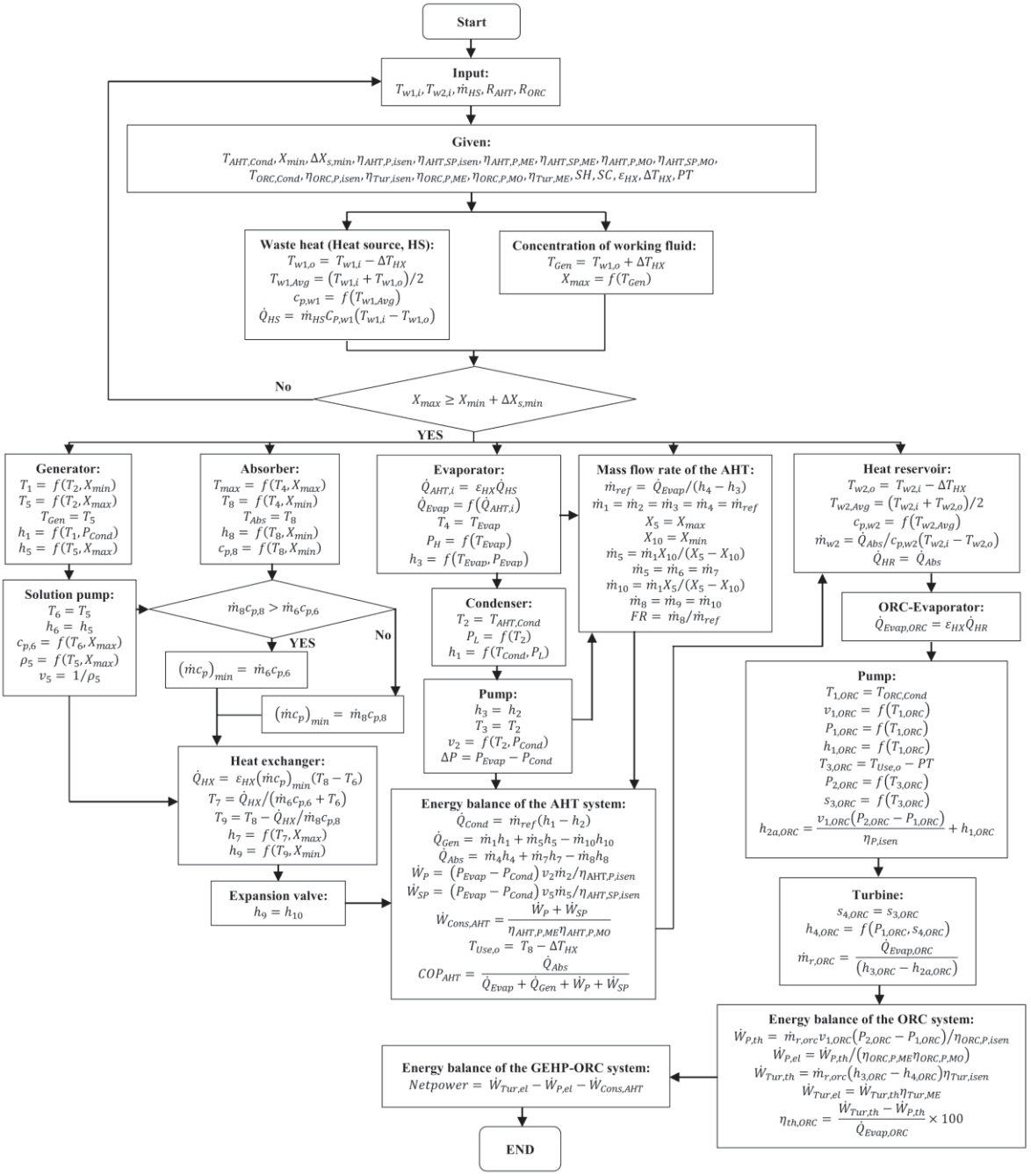

Figure 4-7 Calculation steps of the simulation program for evaluating the net power output of the AHT-ORC power generation system

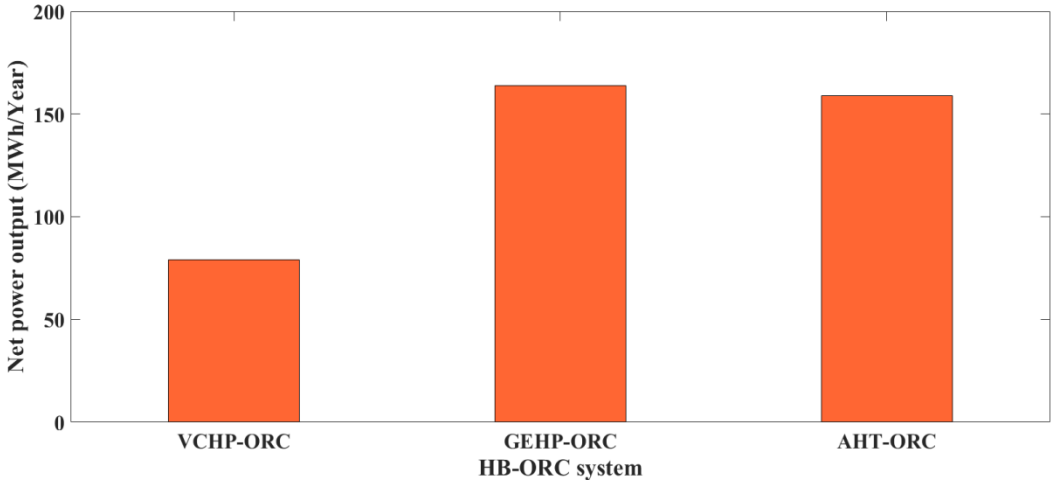

Figure 4-8 Comparisons of net power output of three systems when temperature of the heat source set at 60 °C

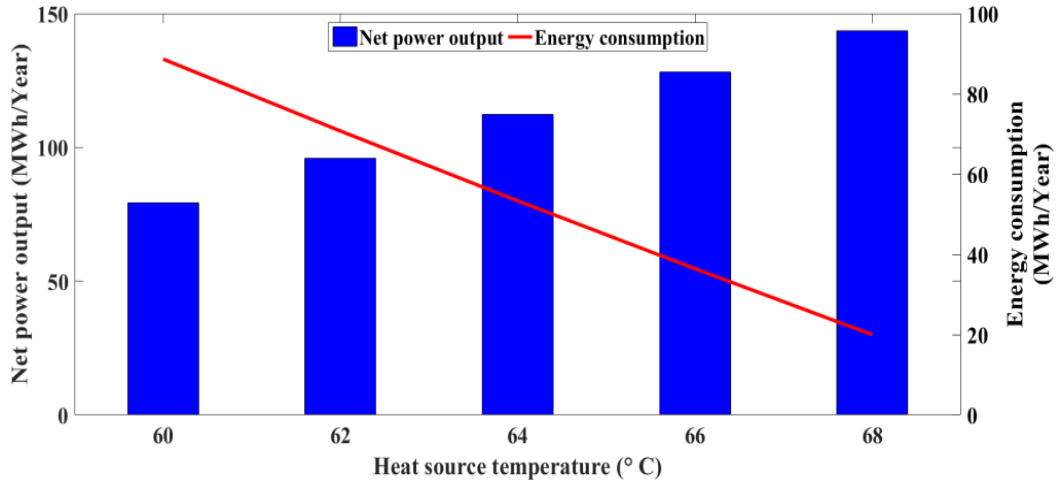

Figure 4-9 Net power output (MWh/Year) and energy consumption (MWh/Year) of the VCHP-ORC power generation system, when the heat source temperature increases (°C)

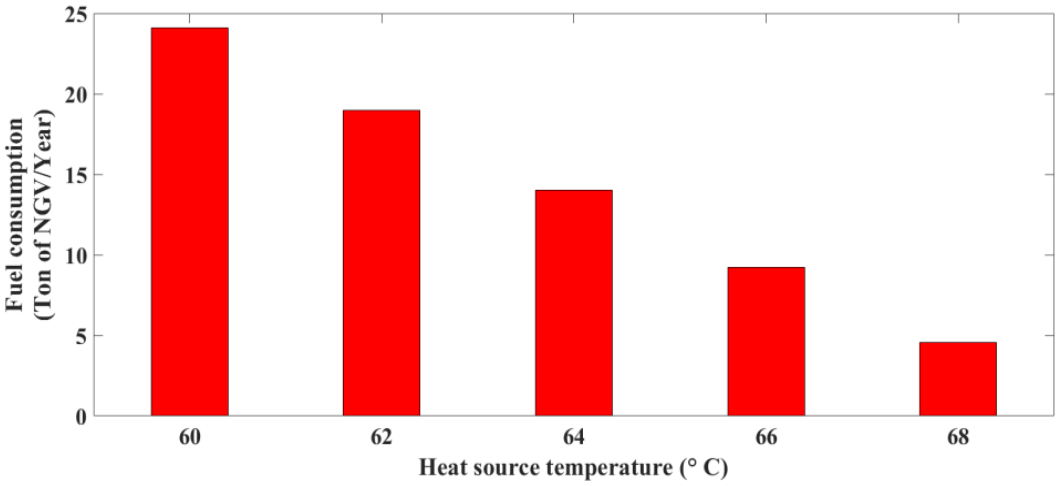

Figure 4-10 Effect of the heat source temperature (°C) on the fuel consumption (Ton of NGV/Year)

Also, it is pointed out that the fuel consumption of the GEHP-ORC system had the downward trend when the temperature of heat source increases due to reduced fuel energy requirements of the GEHP system to raise the low-temperature of the heat source. Figure 4-10 shows the effect of the heat source temperature (°C) on the fuel consumption (Ton of NGV/Year) of the GEHP-ORC system. When the temperature of heat source is 60 °C, the fuel consumption of the system is 24.1 Ton of NGV/Year, is higher when compared to the fuel consumption of system of 14.0 Ton of NGV/Year with heat source temperature at 64 °C.

4.5.2 Thermal Efficiency of the Systems

When the temperature of heat source varies from 60 to 68 °C, the thermal efficiency of the GEHP-ORC system is the highest followed by that of the VCHP-ORC system and AHT-ORC system, since the total energy output from the GEHP system is the highest among the three. Moreover, the results indicate that the thermal efficiency of the GEHP and the AHT systems combined with an ORC for power generation suffers insignificant change from variations in the heat source temperature. For instance, when the temperature of heat source is 60 °C, the thermal performance of the VCHP-ORC, the GEHP-ORC, and the AHT-ORC systems is 4.2, 6.5, and 4.1% respectively. Whereas, when the temperature of heat source is 64 °C, the thermal performance of the systems is 5.4, 6.7, and 4.4% respectively. The thermal efficiency of the system (%) is shown in Figure 4-11.

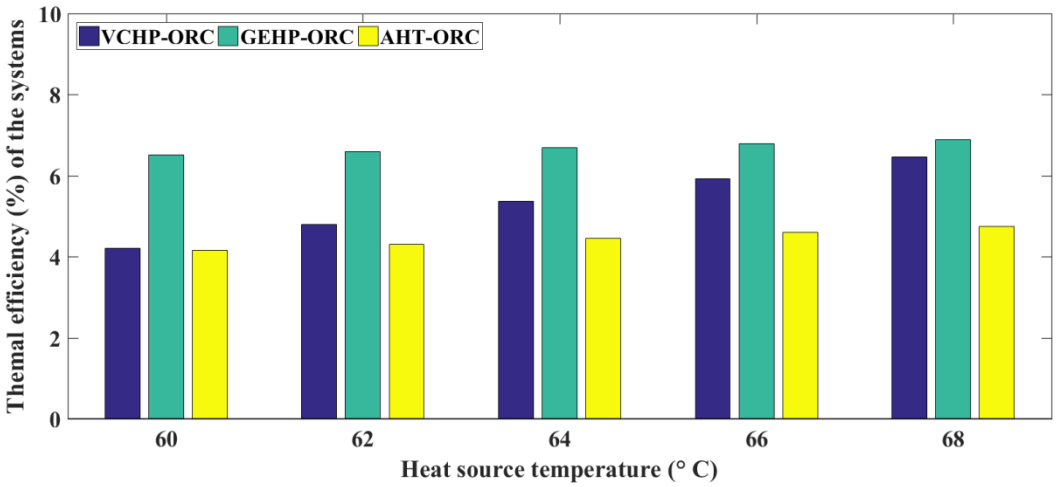

Figure 4-11 Thermal efficiency (%) of three systems

- **Comparisons of Energy and Exergy Balance of Three Systems**

In this part, energy and exergy balance of three systems: the VCHP-ORC, the GEHP-ORC, and the AHT-ORC systems are compared as shown in Figure 4-12. These figures offer a more detailed explanation on how the results were calculated for thermal efficiency of the systems. An exergy rate from heat transfer is calculated from $\mathrm{Ex} = \dot{Q}_{HS}(1 - T_{Amb}/T_H)$. For the calculation, we know the exergy of electrical energy, because it can be completely converted into work. In addition, the exergy of thermal energy can be calculated given the temperature of heat source and heat sink/heat reservoir, units in Kelvin (K). Finally, the exergy loss can be estimated because the energy input and output are the same.

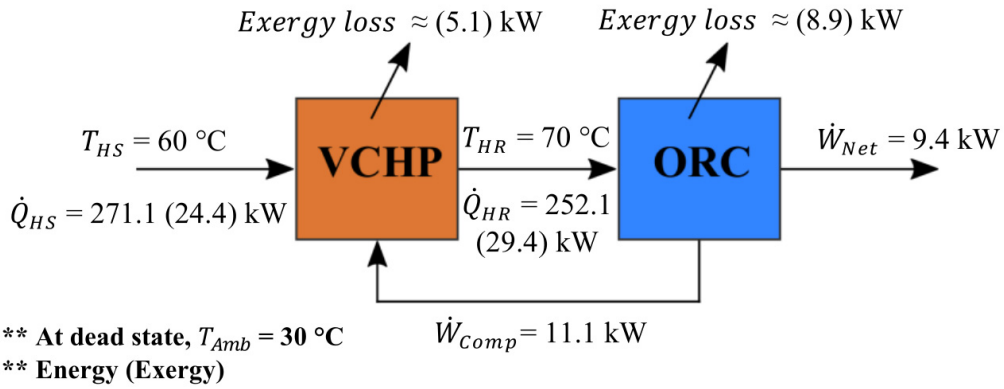

(i) VCHP-ORC power generation system

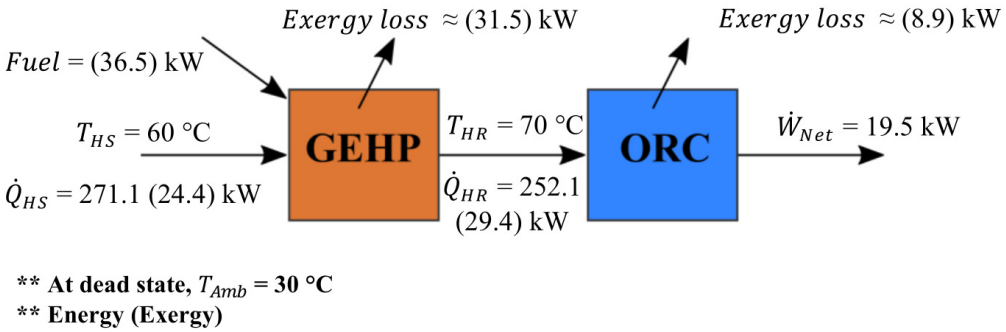

(ii) GEHP-ORC power generation system

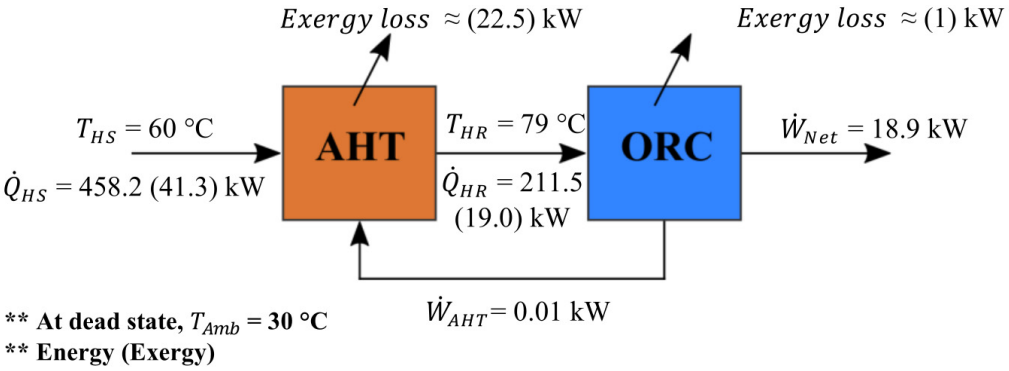

(iii) AHT-ORC power generation system

Figure 4-12 Energy and exergy balance of (i) the VCHP-ORC, (ii) the GEHP-ORC, and (iii) the AHT-ORC power generation systems

4.5.3 Economic Analysis

- **Lifetime Cost of the Systems**

The cost incurred throughout the lifetime of the system can be calculated from the summation of the investment cost, the operation & maintenance cost, and the fuel cost of the systems. In terms of the investment cost of heat boosting technologies per capacity, the AHT system has the highest at 641 USD/kW_{th}, whereas the GEHP and the VCHP systems have 326, and 261 USD/kW_{th}, respectively [9, 93], as shown in Table 4-4. In terms of the operation & maintenance cost, the same trend repeats with the AHT system incurring the highest cost followed by the GEHP and the VCHP systems. Finally, in terms of the fuel cost,

only the GEHP system is considered since it is driven by gas-fuel (Natural Gas (NG)) and uses an internal combustion engine.

From the above mentioned, when the temperature of heat source is 60 °C, the cost throughout the lifetime of these three systems are illustrated in Figure 4-13. The lifetime cost of the GEHP-ORC system is the highest at around at 413×10^3 USD due to the high fuel cost of the GEHP system, followed by the AHT-ORC and the VCHP-ORC systems with 270×10^3, and 166×10^3 USD of expenses respectively. It may be noted that the lifetime cost of the GEHP-ORC system is 1.5 and 2.5 times higher than that of the AHT-ORC and the VCHP-ORC systems, respectively. Moreover, the lifetime cost of the AHT-ORC system was 1.6 times higher than that of the VCHP-ORC system. According to these results, it is conclusive that the VCHP-ORC system stands out as the best candidate in terms of cost throughout the lifetime of the systems.

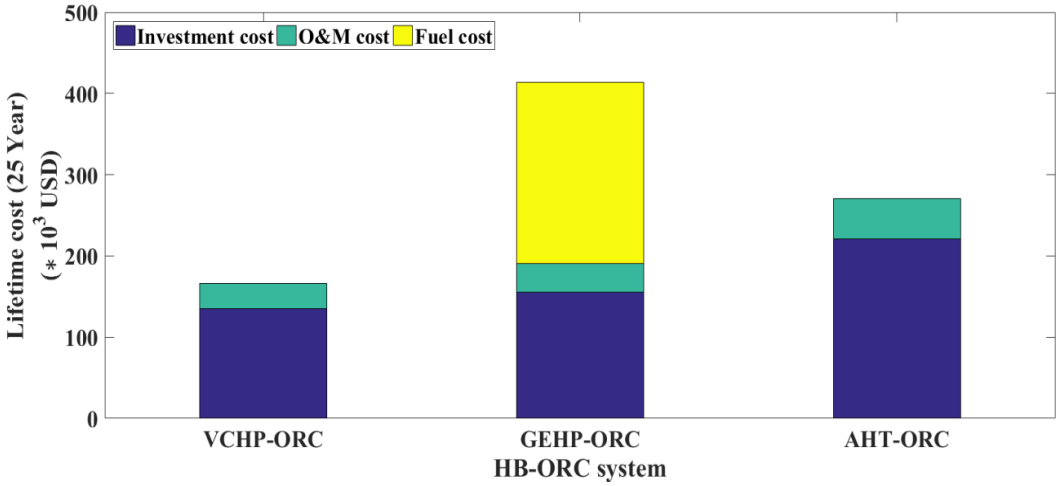

Figure 4-13 Costs throughout the lifetime of three systems

- **The Levelized Cost of Electricity (LCOE) of the System**

The LCOE was selected to represent the economic results of the ORC power generation combined with three different heat boosters. Table 4-6 illustrates the LCOE of three systems, when the heat source temperature increases. The analysis revealed that when the temperature of the heat source is 60 °C, the LCOE of the AHT-ORC system is the lowest at 0.068 USD/kWh, due to the high net power output and moderate cost throughout the lifetime of the system. On the other hand, the VCHP-ORC and GEHP-ORC systems, LCOE are 0.084, and 0.101 USD/kWh, respectively. Although the net power output of the GEHP-ORC system is higher than that of the VCHP-ORC system, the lifetime operation cost of the GEHP-ORC system is still very high which in turn impacts the LCOE.

Considering the effect of the cost of the ORC power plant, if the cost were in the order of 1500 USD/kW_e for a 20 kW_e while keeping the other costs the same, and assuming a 60 °C heat source temperature, the LCOE for the VCHP-ORC, the GEHP-ORC, and the AHT-ORC systems would be of 0.070, 0.094, and 0.061 USD/kWh. Table 4-6 also shows values for other temperatures. It can be noted that the cost of the ORC system has a moderate impact on the LCOE; and therefore the economic results improve when it decreases.

Table 4-6 The levelized cost of electricity (LCOE) of three systems

Heat source temperature (°C)	LCOE (USD/kWh)					
	VCHP-ORC		GEHP-ORC		AHT-ORC	
	ORC cost[1]	ORC cost[2]	ORC cost[1]	ORC cost[2]	ORC cost[1]	ORC cost[2]
60	0.084	0.070	0.101	0.094	0.068	0.061
62	0.069	0.058	0.090	0.083	0.069	0.062
64	0.059	0.050	0.079	0.073	0.069	0.062
66	0.052	0.043	0.069	0.062	0.069	0.062
68	0.046	0.039	0.058	0.052	0.070	0.063

ORC cost[1]; Cost of the ORC power plant of 2500 USD/ kW_e
ORC cost[2]; Cost of the ORC power plant of 1500 USD/ kW_e

4.5.4 Environment Assessment

To estimate CO_2 emissions in this study, the carbon dioxide intensity of electricity in Thailand is used. This value is calculated from the amount of fuel energy, such as Natural Gas (NG), Oil, and Coal/Lignite, that an electricity generation power plant requires in Thailand. In terms of the environmental impact, carbon dioxide intensity of electricity is referenced at 0.548 kg CO_2 eq./kWh [95] for CO_2 reduction of the three systems.

The capability to reduce CO_2 emissions of the system depends on the amount of the electricity that the system can generate and its energy consumption. Then, based on net power output and energy consumption of the system, in term of the environmental impact the results indicates that the tendency of CO_2 reduction of the VCHP-ORC and the GEHP-ORC systems increases when the heat source temperature increases. These results are shown in Figure 4-14. The AHT-ORC system has the highest potential to reduce CO_2 emission because of the low energy consumption in the system, followed by the VCHP-ORC system, and the GEHP-ORC system. For instance, when the temperature of heat source is around 60 °C, the AHT-ORC, the VCHP-ORC, and the GEHP-ORC systems reduce the CO_2 emissions in the order of 87.1, 43.4, and 20.7 Ton CO_2 eq./Year, respectively.

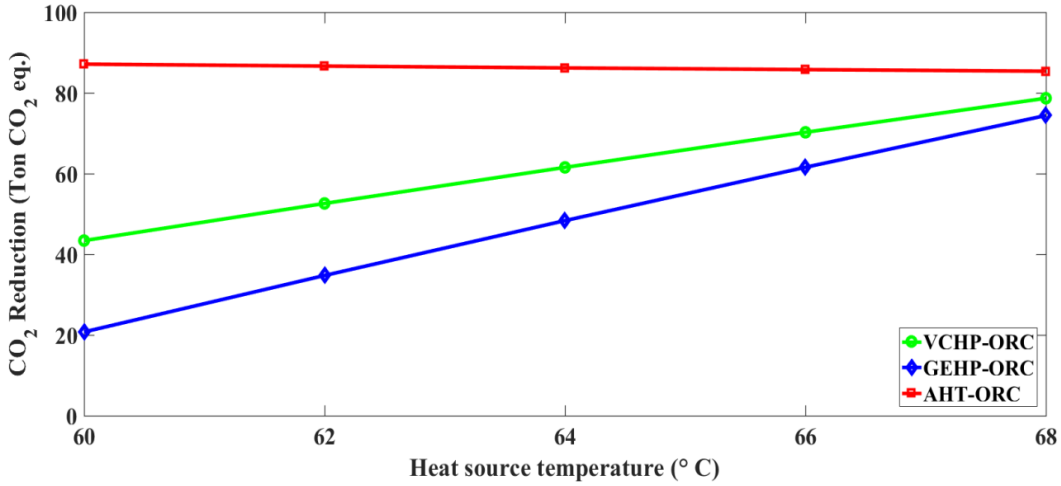

Figure 4-14 Effect of the heat source temperature (°C) on the CO_2 reduction (Ton CO_2 eq.)

4.6 Foot Print of the Heat Boosting Technologies

Dimension, installation, operation, and maintenance of the three different heat boosting technologies are taken into consideration. The data specification of each technology is shown in Table 4-7. The commercial products for these three heat boosting technologies are shown in Figure 4-15. The study finds that the VCHP system has the smallest foot print per heat capacity compared to that of the GEHP and the AHT systems (as shown in Figure 4-16). The VCHP system is compact for combination/integration, easy installation, and simply operation & maintenance. Moreover, the AHT system is more appropriate for large-scale waste heat recovery, because it needs more energy or heat sources to supply the system. On the other hand, an industrial installation that already uses fuel-gas in some of its equipment, would benefit more from the GEHP system, since the infrastructure can easily accommodate it.

Table 4-7 Data specification of three different heat boosting technologies [96-98]

Company	Model	Heat Capacity [kW_{th}]	Size [mm]			Total weight [Ton]	Foot print [kW_{th}/m^2]
			Length	Width	Height		
Vapor Compression Heat Pump (VCHP) system							
Mitsubishi Heavy Industries, Ltd. [96]	ETW-L	545	1550	1200	2065	2.7	293.01
Gas Engine-driven Heat Pump (GEHP) system							
Ilios dynamics [97]	HEWH-500-WS	220	1524	914.4	1829	1.6	157.87
Absorption Heat Transformer (AHT) system							
Hope Deepblue Air-conditioner Manufacture Co., Ltd [98]	RB II58	580	3480	1655	2100	6.4	100.70

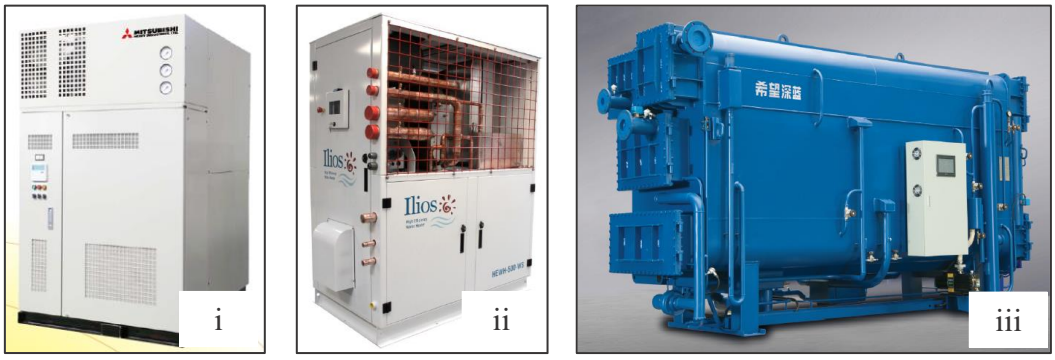

Figure 4-15 Heat boosting technologies, (i) Vapor compression heat pump (VCHP) system [96], (ii) Gas engine-driven heat pump (GEHP) system [97], and Absorption heat transformer (AHT) system [98]

4.7 Effect of the Heat Source Temperature

From the above results, it can be concluded that the heat source temperature has significant effect on the net power output and energy consumption, the economic, and the environmental impact of the system. However, when the three systems are compared, and focusing on the systems lifetime cost and the foot print of the heat boosting technologies, the results point out that, the VCHP-ORC system is the most appropriate because of its lowest the cost throughout the lifetime, compactness, easy installation, and simple operation & maintenance.

Moreover, when considering the results of the LCOE of the system, the VCHP-ORC system was the most appropriate when the temperature of heat source is around 63 °C. Figure 4-17 shows the effect of the heat source temperature (°C) on the LCOE, when the cost of the ORC system of 2500 USD/kW_e. The study suggests that when the heat sources temperature increases, the LCOE of the VCHP-ORC and the GEHP-ORC systems follow a downward trend. If the temperature of heat source is 63 °C, then the LCOE of the VCHP-ORC system is the lowest at 0.065 USD/kWh. Whereas, the LCOE of the GEHP-ORC and the AHT-ORC systems are 0.086, and 0.066 USD/kWh, respectively. Furthermore, Figure 4-18 shown the LCOE of three systems when the cost of the ORC system was set at 1500 USD/kW_e. It was found that the LCOE of the VCHP-ORC system is the lowest at 0.06 USD/kWh, when the temperature of heat source is around 61.5 °C. Or it can be said that the VCHP-ORC system becomes more interesting when the cost of the ORC system is reduced.

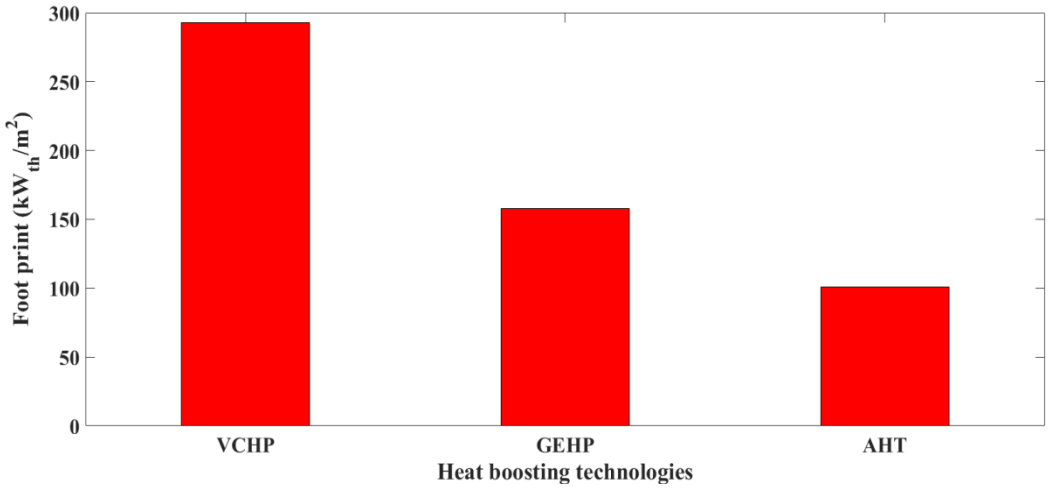

Figure 4-16 Comparisons of heat capacity per installation area (kW_{th}/m^2) of three heat boosting technologies

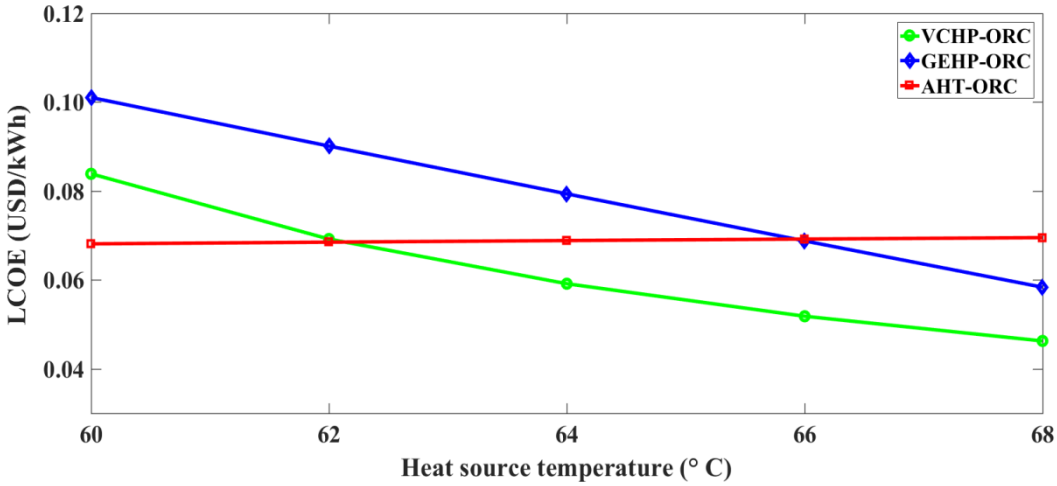

Figure 4-17 Effect of the heat source temperature (°C) on the LCOE, when cost of the ORC power plant of 2500 USD/kW_e

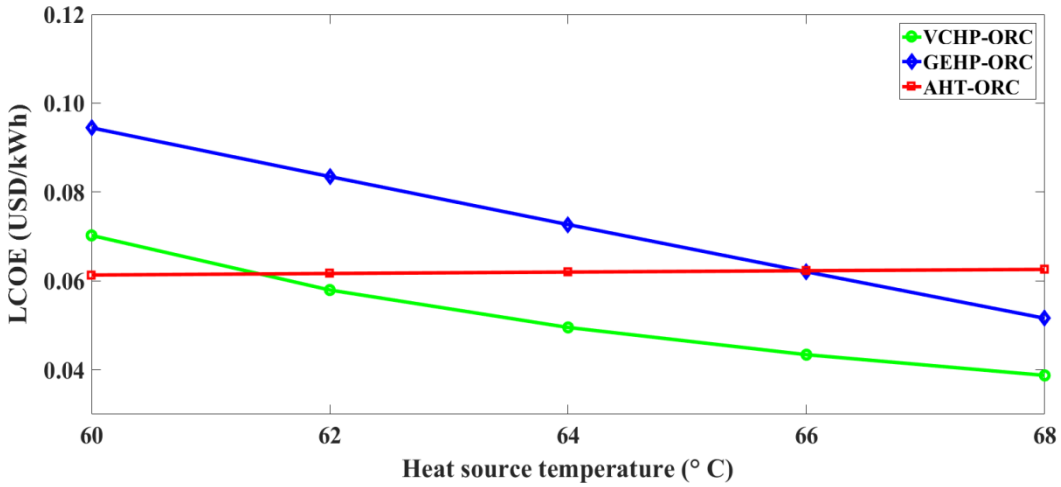

Figure 4-18 Effect of the heat source temperature (°C) on the LCOE, when cost of the ORC power plant of 1500 USD/kW$_e$

4.8 Conclusion

In this Chapter, a concept for an ORC power generation from low-grade IWH with temperature below 70 °C, combined with heat boosting technologies, was investigated. Three technologies consisting of Vapor compression heat pump (VCHP), Gas engine-driven heat pump (GEHP), and Absorption heat transformer (AHT) systems were compared in their capacity to rise the low-temperature heat source to the high-temperature heat sink/heat reservoir. The system was mathematically modeled and simulated to evaluate the net power output, the environmental impact, and the LCOE of the system. The conclusions are as follows:

1) The ORC power generation combined with the proposed heat boosters is applicable for below 70 °C heat source, which is available in large quantities from industrial processes. Moreover, it is a technically feasible solution for power generation from low-grade IWH recovery, which otherwise is wasted on releasing into the environment.
2) This technique may enable the industrial sector to reduce operating cost of the facilities by increasing their energy productivity, as well as help to reduce pollution (greenhouse gas emissions (GHG), and thermal pollution).
3) For the heat boosting technologies: the VCHP system is more appropriate when compared with the GEHP and the AHT systems, because of its compactness, easy to installation, and simple operation & maintenance.
4) For the ORC power generation combined with the heat boosting technologies; the VCHP-ORC system was appropriate, when the temperature of heat source was around at 63 °C:
    - Because of the LCOE of the VCHP-ORC system was the lowest at 0.065 USD/kWh, while the LCOE of the AHT-ORC and GEHP-ORC systems were 0.066, and 0.086 USD/kWh, respectively,

- And in term of the environmental impact of the VCHP-ORC, the AHT-ORC, and the GEHP-ORC systems, the CO_2 emission reduced were 63.0, 86.4, and 37.8 Ton CO_2 eq./Year, respectively.

5

Power Generation from Low-grade Heat Combined with Solar Water Heating System

In Chapter 5, we considered situations where apart from the solar water heating system (SWHS) in the factories [32], there is also waste heat produced by the processes. In this part, is presents simulation results of ORC power generation from industrial waste heat (IWH), which wasted and released into the environment, combined with the SWHS by using the vapor compression heat pump (VCHP) as a heating booster.

5.1 Introduction

Thailand is considered as one of the countries having the highest average total solar radiation with less annual direct normal solar radiation [28]. Thus, it is insufficient for the Concentrating Solar Power (CSP) technology [99, 100]. Therefore, the low-temperature heat, as a form of low-to-medium temperature hot water is consumed in industries. In the industrial sector, waste heat is one of the most abundant sources of energy, as it accounts for more than 2000 Ton BTU/Year of wasted energy [101]. Unfortunately, this heat cannot directly be converted into electricity by a steam Rankine cycle [9]. However, it is still productive for power generation by employing an ORC system [11-14].

Recently, many researchers are working on the design, analysis, and development of ORC systems for low-temperature heat conversion. For solar collectors combined with the ORC power generation, Bocci et al. [102] analyzed of a power plant producing electrical power, heat, cooling and fresh water needs for a house. The power plant included compound parabolic concentrator (CPC) solar collectors, the thermal storage tank, the ORC system, the absorption chiller system, and the reverse osmosis desalination unit. Delgado-Torres and García-Rodríguez [103] presented the theoretical analysis of the solar thermal driven seawater and brackish water reverse osmosis desalination technology. The system was analyzed of twelve substances as working fluids of the ORC system and four different models of stationary solar collectors (flat-plate, evacuated-tube, and CPC solar collectors) are taken into account. Baral and Kim [104] presented a solar ORC power plant for combined heat and power (CHP) application in Busan, Korea. Flat-plate solar collectors were analyzed for the ORC power plant with 90 ˚C as the hot fluid temperature, whereas vacuum tube solar collectors were analyzed for the ORC power plant with 125 ˚C as the hot fluid high temperature. Zhang et al. [105] presented of a transcritical CO_2 Rankine cycle for CHP application. The system included evacuated-tube solar collectors, the ORC system, the heat recovery system, and the feed pump. The results suggested that the cycle has a good potential

for distributed energy supply system. Freeman et al. [106] investigated the potential of a small-scale combined solar heat and power (CSHP) system based on an ORC for provision of hot water and power for domestic use in the UK.

Moreover, there is an ongoing research on ORC system for low-grade heat conversion from renewable resources (e.g. solar energy, geothermal, etc.) combined with low-grade IWH. Li et al. [107] proposed a cascade ORC and an optimization criterion for the hybridization of solar energy and liquefied natural gas (LNG) for power generation. In the system, energy from solar collectors drives the evaporation of the working fluid in the top cycle. The heat released by the top cycle facilitates the evaporation of the working fluid in the bottom cycle, and LNG is used for the cold source of the bottom cycle. Higgo and Zhang [26] designed and fabricated a small-scale ORC power generation by utilizing waste heat from high-concentration photovoltaic (HCPV) arrays, and solar energy from evacuated-tube solar collectors. Pikra et al. [108] analyzed the potential of ORC power generation from the hot springs in Indonesia, with heat source temperatures between 70 to 80 °C. Chaiyat [109] studied the possibility of power generation by using alternative energy in Thailand which are geothermal energy, solar energy and waste heat based on the energy and economy indicators. Sonsaree et al. [110] proposed a novel concept of ORC power generation from industrial waste heat recovery (IWHR) combined with the SWHS by using a VCHP as heating booster. It was found that the number of solar collectors affects the system in terms of the economic and the environmental impact.

From the literature review, there are only a few designed to utilize lower temperature thermal energy supplies on a small-scale ORC. If an ORC system can be applied for power generation at below 70 ºC heat sources, the industrial sector could benefit from this waste heat as well as reduction of the energy intensity, increase of energy efficiency of industrial processes [34], and reduce of pollutants. Moreover, In Thailand, a lot of solar collectors are available, operating in hotels, hospitals and industries. Their main function is to generate hot water, with temperatures in the range of 60 to 70 °C. Although it is used in various processes, not all the available heat can be exploited. If this hot water could be also used for power generation, adds another benefit to the installation of these collectors and also makes our system more interesting. Furthermore, in the future, the system can improve or refine the application or processes involved in generating electricity from low-temperature heat source. In this Chapter, such system is proposed with the use of the VCHP system modeled in Chapter 4, to rise the low-temperature heat source to the high-temperature heat sink before supplying it to the ORC power generation. The objectives of this research are:

- Mathematical modeling and simulating to evaluate the net power output, the environmental impact, and the levelized cost of electricity (LCOE) of the VCHP-ORC power generation from low-grade IWH combined with SWHS,
- The evaluation of three types of solar collectors consisting of flat-plate, heat pipe evacuated-tube, and compound parabolic concentrator (CPC) used for hot water generation,

- Test of the system in six representative areas of industrial estate in Thailand consisting of Chiang Mai, Bangkok, Ratchaburi, Songkhla, Nakhon Ratchasima, and Chon Buri by using their weather data during the simulations.

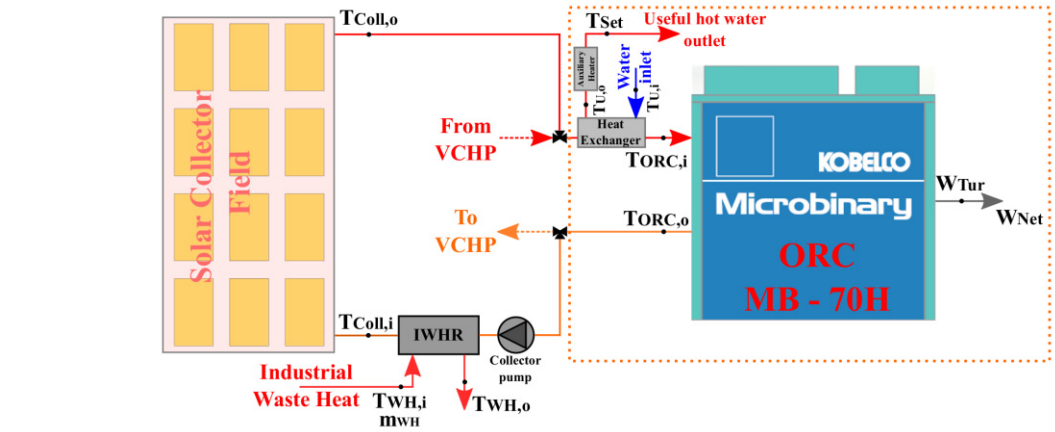

(a) Day time or sunrise

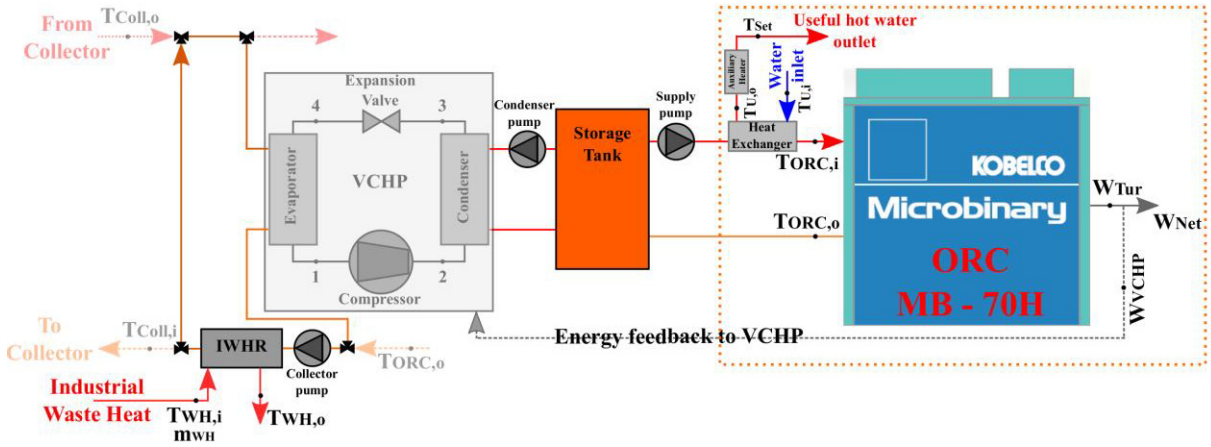

(b) Nighttime or sunset

Figure 5-1 Schematic diagram of the VCHP-ORC power generation from low-grade IWH combined with SWHS

5.2 System Description

A schematic diagram of the VCHP-ORC power generation from low-grade IWH combined with SWHS is shown in Figure 5-1. The main components of the system are: the solar collectors, the VCHP, and the ORC systems. In the system operation, during *the daytime or sunrise* as shown in Figure 5-1 (a): low-grade IWH at constant quantity ($\dot{m}_{WH,i}$) and quality ($T_{WH,i}$) is used to increase or maintain the outlet temperature of hot water from the ORC system ($T_{ORC,o}$) before supplying it to the solar collectors ($T_{Coll,i}$) for hot water production. In this step, if the outlet hot water temperature from solar collectors ($T_{Coll,o}$) is equal to or higher than 70 °C, one part of the heat is supplied for industrial usage and the other part is directly supplied to the ORC system ($T_{ORC,i}$) for power generation. Otherwise, the temperature is raised by the VCHP system as shown in Figure 5-1 (b), to an equal-to or higher temperature heat and then is stored in the heat reservoir/thermal storage tank. After

that, the heat from the thermal storage tank is supplied to the industrial process and the ORC system ($T_{ORC,i}$) to generate electricity. During *the nighttime or sunset* as shown in Figure 5-1 (b): low-grade IWH with the same quantity ($\dot{m}_{WH,i}$) and quality ($T_{WH,i}$) is directly supplied to the VCHP system where the temperature is raised before supplying it to the industrial process and the ORC power generation. Moreover, when the VCHP system was used to raise the low-temperature heat, the power generation from the ORC system (W_{Tur}), has feedback to the VCHP system (W_{VCHP}). After that, the net power output (W_{Net}) will be supplied for industrial usage.

5.3 Operating Conditions and Assumptions

5.3.1 Solar Water Heating System (SWHS)

Three types of solar collectors were compared, consisting of flat-plate, heat pipe evacuated-tubes, and CPC solar collectors of 300 to 700 units connected in parallel used for hot water generation. Which these numbers of solar collectors is appropriate as combined with a 60 kW_e ORC power generation. The characteristics of the solar collectors such as aperture area (m^2) *(Aperture area is defined as the unobstructed cover area or the total cover area less the area of cover supports [36])*, gross area (m^2) *(Gross area is defined as the total area occupied by a collector module, that is, the total area of a collector array divided by the number of modules in the array [36])*, optical efficiency ($F_R(\tau\alpha)_e$), and overall heat transfer coefficient ($F_R U_L$, W/m^2-K) are shown in Table 5-1 and Figure 5-2.

Table 5-1 Characteristic of three types of solar collectors: flat-plate, heat pipe evacuated-tube, and CPC solar collectors

Type	Aperture area	Gross area	$F_R(\tau\alpha)_e$	$F_R U_L$
	(m^2)	(m^2)	(−)	(W/m^2-K)
Flat-plate solar collectors [111]	1.966	2.081	0.740	3.620
Heat pipe evacuated-tube solar collectors [112]	1.671	2.369	0.572	0.750
CPC solar collectors [113]	1.890	2.160	0.718	0.974

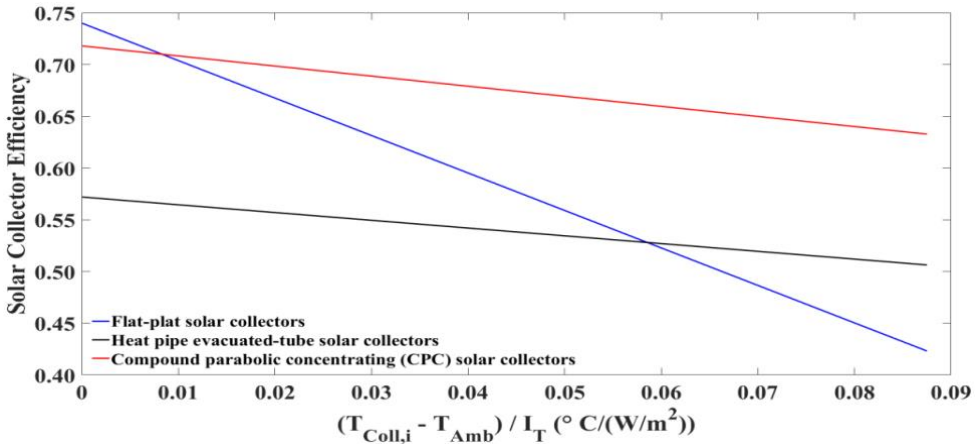

Figure 5-2 Efficiency comparison of three types of solar collectors: flat-plate, heat pipe evacuated-tube, and CPC solar collectors *($T_{Coll,i} = 30$ to $100\ °C, T_{Amb} = 30\ °C$, and $I_T = 800\ W/m^2$)*

5.3.2 Vapor Compression Heat Pump (VCHP)

A 400 kW thermal capacity of the VCHP system with R-365mfc as working fluid is used to increase the below 70 °C heat either from IWH or SWHS before supplying it to the ORC power generation. Moreover, the initial condition of the VCHP system consists of isentropic ($\eta_{Comp,VCHP,s}$), mechanical ($\eta_{Comp,ME}$) and motor ($\eta_{Comp,MO}$) compressor efficiency set at 90, 95, and 95%, respectively.

5.3.3 Organic Rankine Cycle (ORC)

A 60 kW_e ORC power generation with R-245fa as working fluid *(ORC model: MB-70H from KOBELCO Company [24])* was simulated to find a power generation of the system as shown in Figure 5-3 and Table 5-2.

Figure 5-3 MB-70H ORC power generation from KOBELCO Company *(60 kW_e electrical capacities and using R-245fa as working fluid)* [24]

Table 5-2 The performance characteristic of MB-70H ORC power generation from KOBELCO Company [24]

Hot water flow rate (Ton/h)	Cooling water temperature (°C)	Cooling water flow rate (120 Ton/h)					
		Hot water temperature (°C)					
		95	**90**	**85**	**80**	**75**	**70**
30	15	46	40	35	30	24	18
	20	45	38	31	25	20	15
	25	41	34	28	22	17	12
	30	36	29	24	19	14	9
25	15	43	38	33	28	22	17
	20	43	35	29	24	19	14
	25	38	31	26	20	16	11
	30	33	27	22	17	13	9

In Table 5-2, the hot water temperature (°C) is the outlet temperature from solar collectors during the daytime or sunrise, and is from the VCHP system during the nighttime or sunset. In addition, the cooling water temperature is from the cooling tower (°C) (equal to ambient temperature in this Chapter). Furthermore, to find out the power output from the performance characteristic of ORC model MB-70H from KOBELCO Company. For instance, when the hot water flow rate is 25 Ton/h, the cooling water, and the hot water temperature is 20 and 85 °C, respectively. The ORC system can generate the power of 29 kW_e.

5.3.4 Simulation Conditions

In this Chapter, six areas of industrial estate consisting of Chiang Mai (18.80 °N, 98.98 °E), Bangkok (13.75 °N, 100.52 °E), Ratchaburi (13.54 °N, 99.82 °E), Songkhla (7.21 °N, 100.56 °E), Nakhon Ratchasima (13.75 °N, 100.52 °E), and Chon Buri (13.40 °N, 101.00 °E) represent the north, central, west, south, north-east and east part of Thailand as shown in Figure 5-4. The weather data from these provinces was taken as input data for simulations consisting of ambient temperature (°C) and total average solar radiation on the tilted surface (kWh/m^2-day) [114] are shown in the APPENDIX B Solar Radiation and Ambient Temperature. Moreover, solar radiation in terms of the hourly global radiation is estimation as presented in the studies of Zhang et al. [115] and Duffie JA and Beckman WA [36], and it shown in Figure 2-4 calculation steps for evaluating the solar radiation on tilting plan.

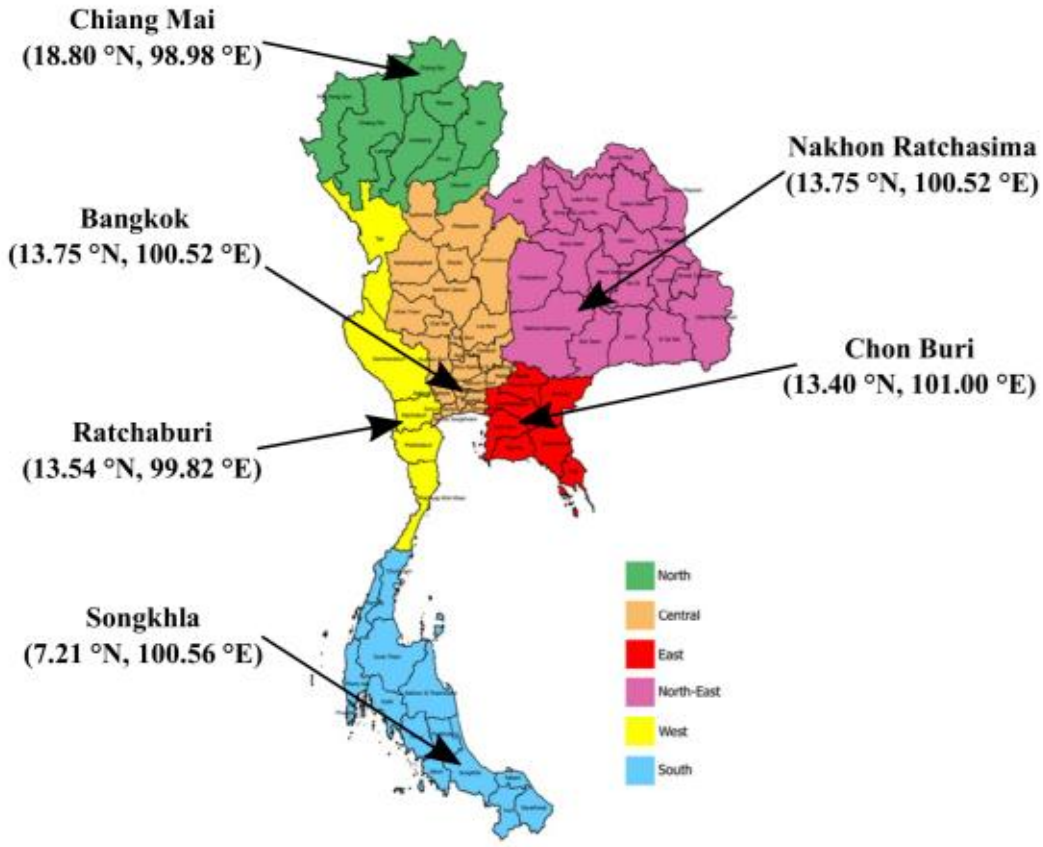

Figure 5-4 The location of Chiang Mai, Bangkok, Ratchaburi, Songkhla, Nakhon Ratchasima, and Chon Buri

The system was mathematically modeled based on steady state condition. Heat loss from the system components such as the evaporator, the condenser, and the piping system was neglected. Also, the power input for the water pump consists of the collector, the condenser, and the supply pump as shown in Figure 5-1 were neglected. The low-grade IWH, under the assumption of the waste heat temperature in the range of 60 to 70 °C, and constant waste heat flow rate were used as input to the systems. It is used to increase or maintain the outlet temperature of hot water from the ORC system before supplying it to the solar collectors for hot water production during the daytime or sunrise. Moreover, the low-grade IWH is directly supplied to the VCHP system during the nighttime or sunset. The water temperature stored in the heat reservoir/thermal storage tank is assumed to be 70 °C. In addition, the system normally produces 10 m^3/day of hot water at 70 °C as shown in the daily and annual hot water profile in Figure 5-7, and Figure 5-8, respectively. The degree of superheating (SH), sub-cooling (SC), and the pinch-point temperature (PT) difference was set at 5 °C. In addition, heat exchanger effectiveness (ε_{HX}) was assumed to be 90%. The thermodynamic properties of the VCHP system were calculated by REFPROP NIST7.0 [81].

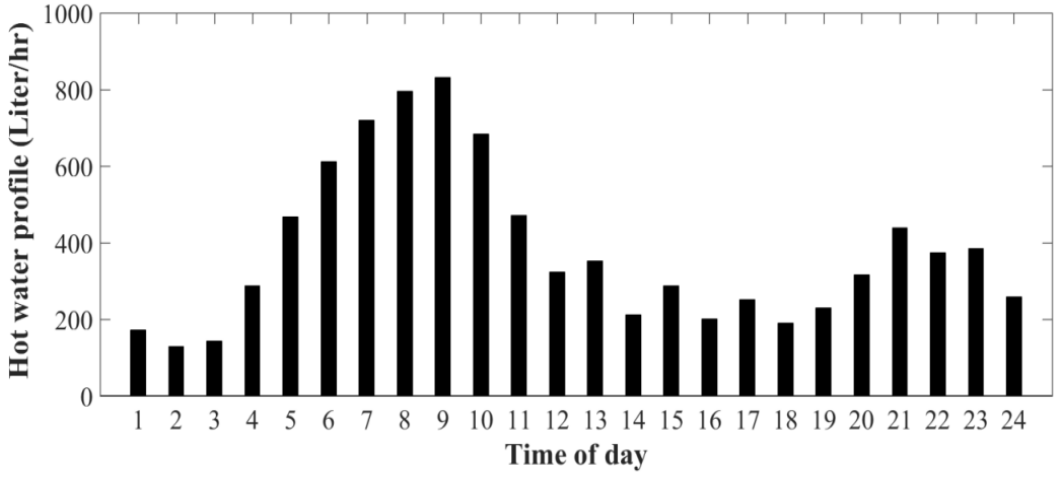

Figure 5-5 Daily hot water profile of the industrial process (Liter/hr)

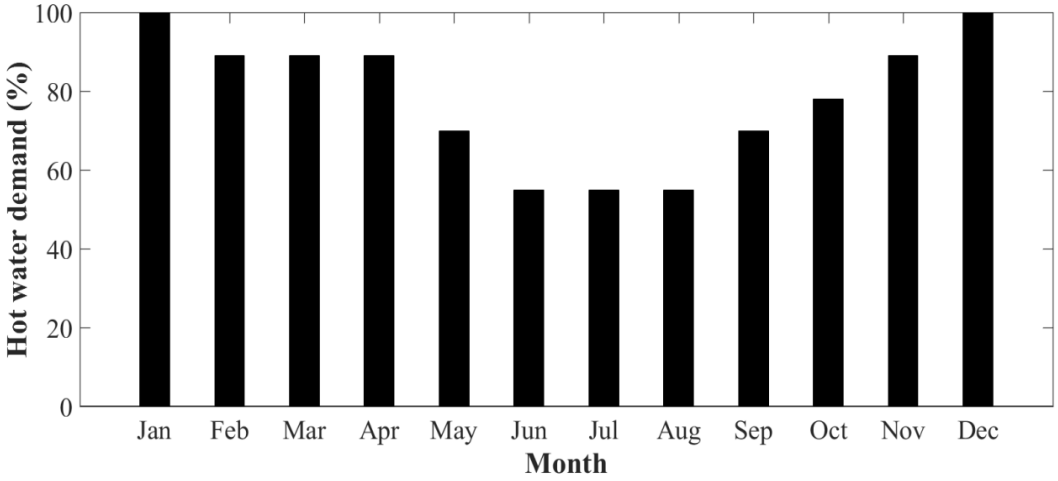

Figure 5-6 Annual hot water profile of the industrial process (%)

The calculation steps for evaluating the net power output of the VCHP-ORC power generation from low-grade IWH combined with SWHS are shown in Figure 5-7 and Figure 5-8. Inputs of the simulation were the low-grade IWH temperature ($T_{WH,i}$) that varies from 60 to 70 °C, and the heat reservoir/thermal storage tank ($T_{w1,i}$) was set at 70 °C. The working fluids of the VCHP system and the performance characteristic of the MB-70H ORC power generation from KOBELCO Company [24]. The given data is the fixed value of the calculation such as daily radiation (H), solar collector area (A_{Coll}), Optical efficiency ($F_R(\tau\alpha)_e$) and overall heat loss coefficient ($F_R U_L$) of solar collectors, heat exchanger effectiveness (ε_{HX}), isentropic VCHP compressor ($\eta_{VCHP,s}$), mechanical VCHP compressor ($\eta_{Me,Comp}$) and motor VCHP compressor ($\eta_{MO,Comp}$) efficiency, degree of sub-cooling (SC) and superheating (SH). For the step of calculations, the combinations of the systems were evaluated to find out the net power output at six areas of industrial estate of Thailand.

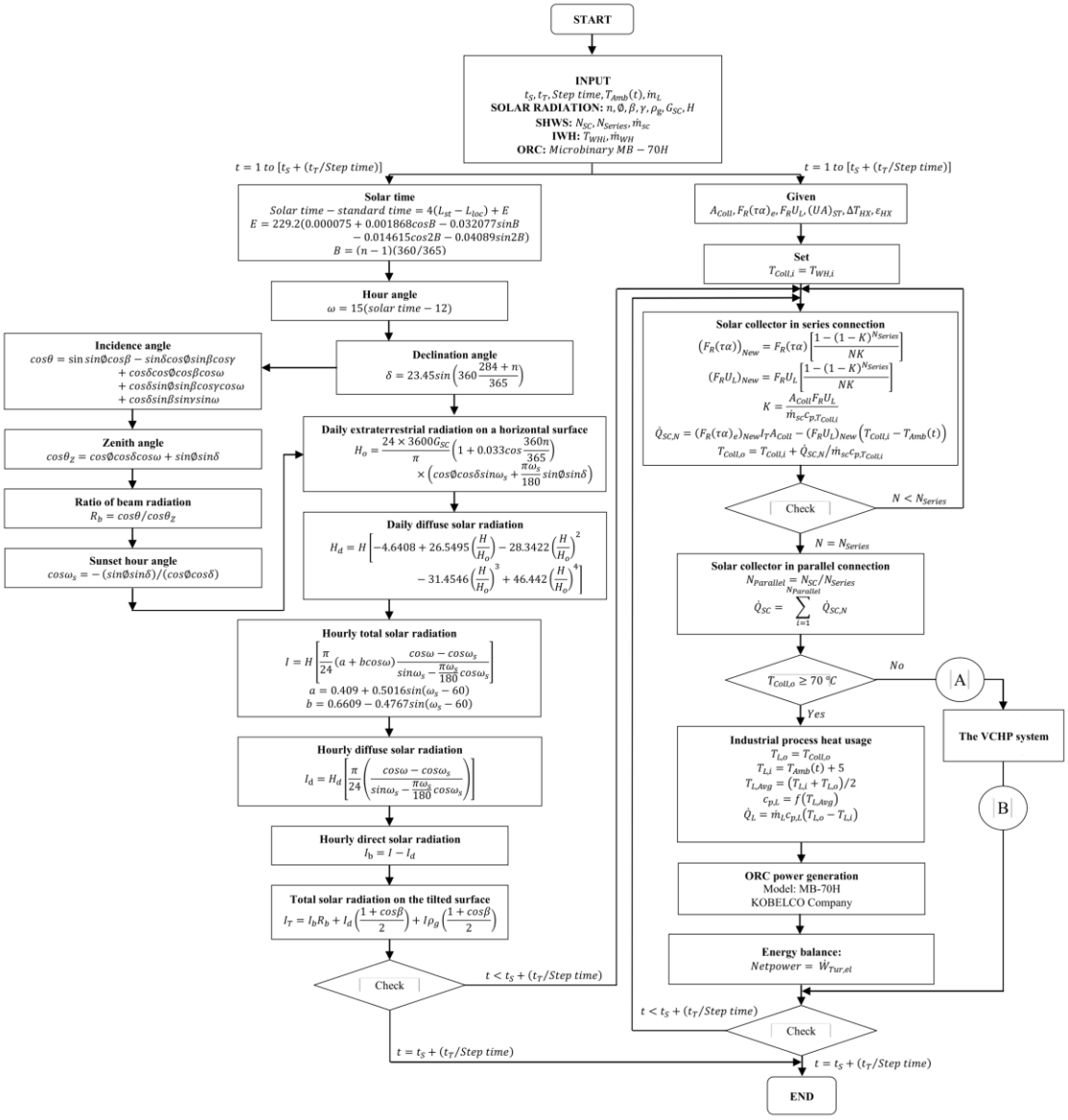

Figure 5-7 Flow chart of the simulation program for evaluating the net power output of the VCHP-ORC power generation from low-grade IWH combined with SWHS

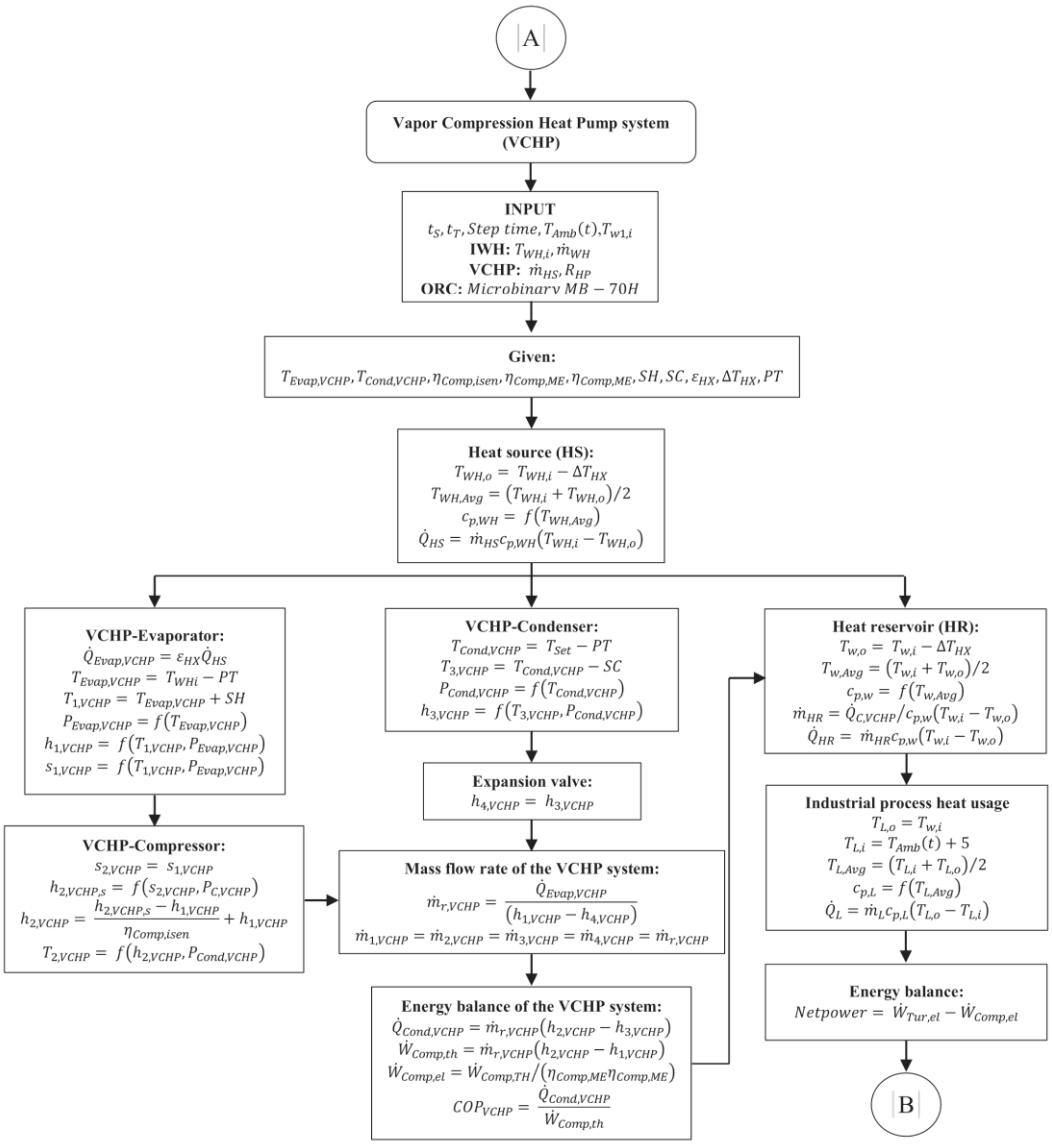

Figure 5-8 Flow chart of the simulation program for evaluating the net power output of the VCHP-ORC power generation from low-grade IWH combined with SWHS *(continuous)*

Table 5-3 Initial condition, and cost data used for the economic evaluation of the system

Descriptions	**Data**
Condition	
Operation time, (hour/day)	24
Operation day, (day/year)	353
Investment cost	
Surcharge for construction and engineering, (%)	10
Operation & maintenance (O&M) cost	
Operation & maintenance cost (% of investment cost per year)	0.5
Financial parameter	
Annual insurance rate, $k_{insurance}$ (%/year)	0.6
Real debt interest rate, i_d (%)	7.325
Depreciation period, n (year)	25

5.4 Economic Analysis

In the economic assessment, the initial condition and the commercial cost of the VCHP system was used to evaluate the capital cost of the system as shown in Table 4-4 and Table 5-3, respectively. Capital cost of the ORC power plant, this Chapter was also selected a small-scale ORC power plant at around 2500 USD/kW_e. The investment in solar collectors is not included in the calculation. As an assumption of the factories, the SWHS was already installed.

5.5 Results and Discussion

In this Chapter, a concept for a VCHP-ORC power generation from a low-grade IWH combined with SWHS was proposed and investigated. Three types of solar collectors consisting of flat-plate, heat pipe evacuated-tube, and CPC solar collectors were compared in their heat output at six areas of industrial estate in Thailand. The results were compared based on the net power output, the environmental impact, and the LCOE of the system as shown in the following:

5.5.1 Net Power Output of the Systems

The net power output (MWh/Year) of the system, when the number of solar collectors (Units) and the heat source temperature (°C) increases of Chiang Mai, Bangkok, Ratchaburi, Songkhla, Nakhon Ratchasima, and Chon Buri are shown in Figure 5-9 to Figure 5-14, respectively. The results showed that the more number of solar collectors are available and the higher the heat source temperature is the more electricity the system can generate. This means that the solar field can produce more thermal energy to supply to the ORC power generation. Moreover, when the heat source temperature increases, the power requirement of the VCHP system to increase the low-temperature heat source to the high-temperature heat sink/heat reservoir is reduced. Furthermore, as consider in location of Bangkok, the power output of the system, when the number of CPC solar collectors was higher than that 600 units, and the heat source temperature of 70 °C. It was found that the power output of the system had decreased due to the collector outlet temperature over the temperature limit of the ORC power generation (95 °C). From Figure 5-9 to Figure 5-14, it could be presented the factors that influence the power output by:

$$P = \eta_{ORC}(q_{IWH} + A_{Coll}I_T) \tag{5-1}$$

where P is the power output (kW_e). η_{ORC} is the ORC system efficiency, it depends on the temperature of IWH and the number of solar collectors (Unit). q_{IWH} is energy input from IWH (kW_{th}), it is constant in this study. And $A_{Coll}I_T$ is energy input from the solar collectors, A_{Coll} is increasing by the number of solar collectors (Unit).

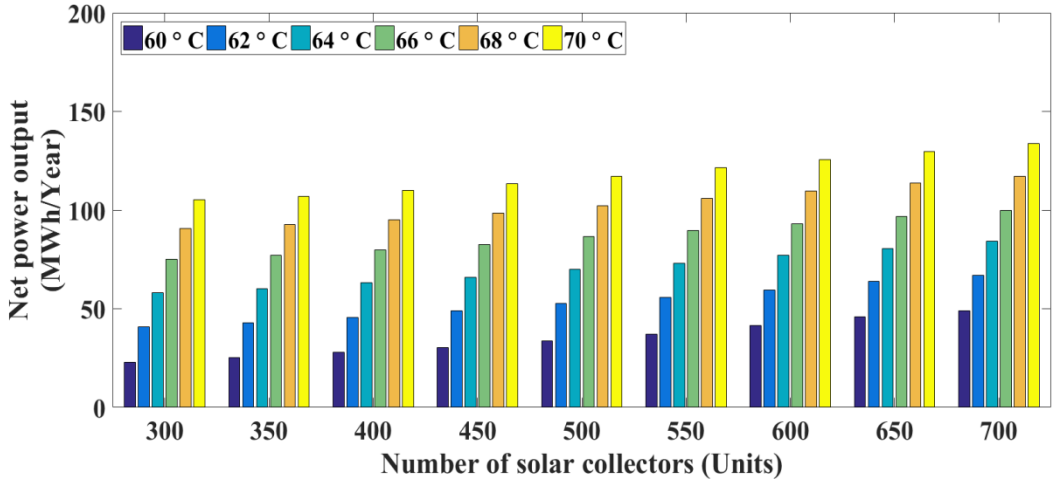

(a) Flat-plate solar collectors

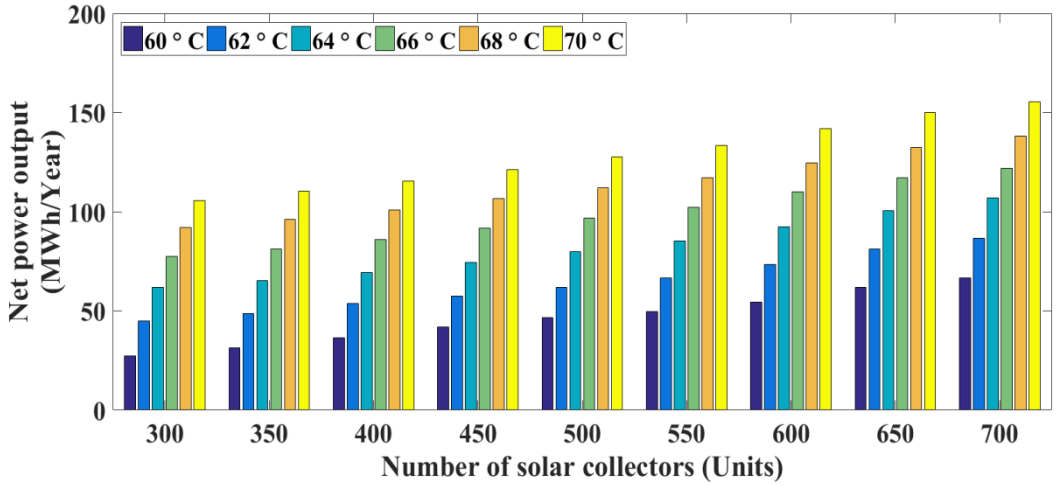

(b) Heat pipe evacuated-tube solar collectors

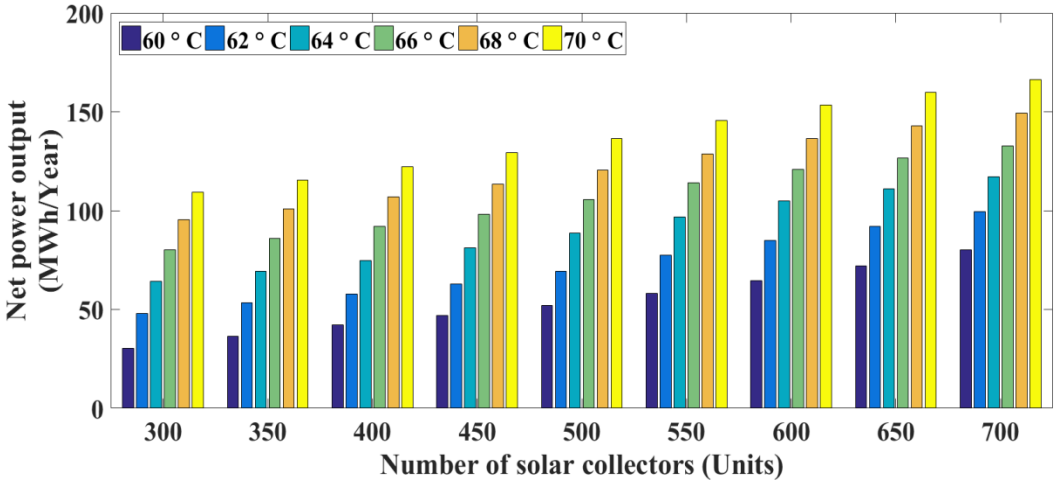

(c) Compound parabolic concentrator (CPC) solar collectors

Figure 5-9 Net power output (MWh/Year) of the systems *(Location: Chiang Mai)*, when the number of solar collectors of 300 to 700 units connected in parallel, and the heat source temperature increases from 60 to 70 °C *(Constant hot water flow rate)*

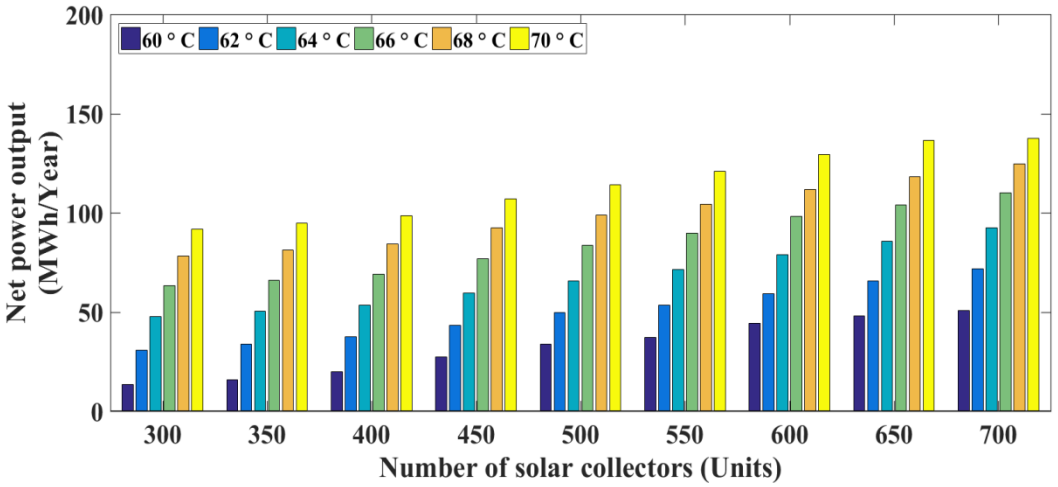

(a) Flat-plate solar collectors

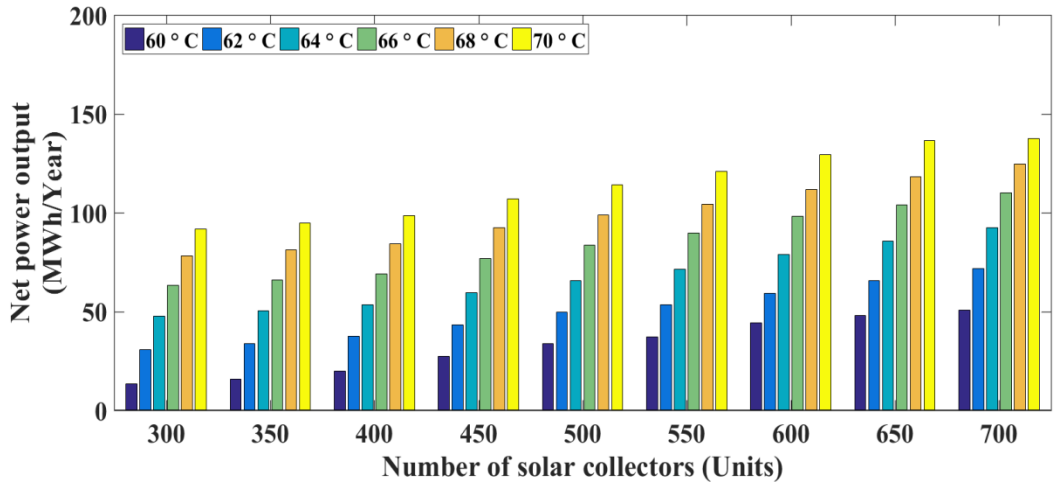

(b) Heat pipe evacuated-tube solar collectors

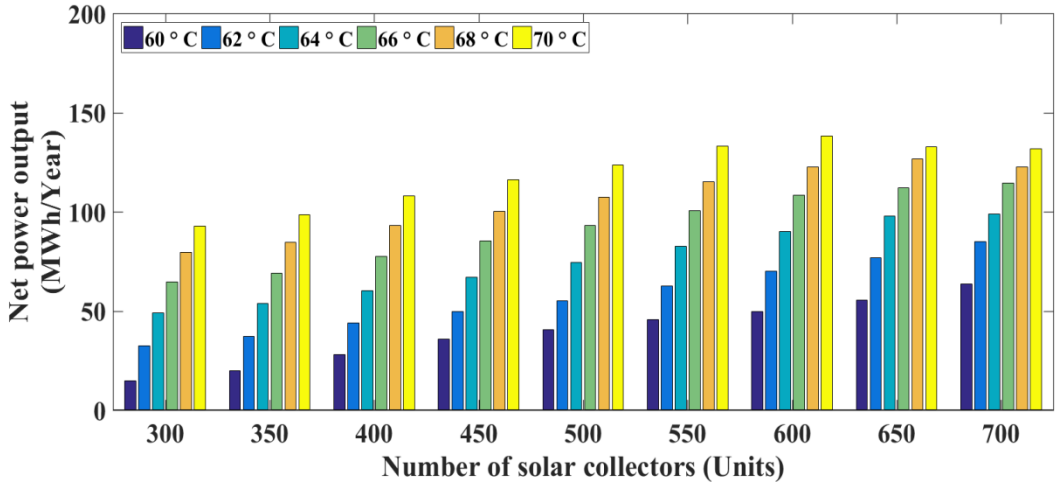

(c) Compound parabolic concentrator (CPC) solar collectors

Figure 5-10 Net power output (MWh/Year) of the systems *(Location: Bangkok)*, when the number of solar collectors of 300 to 700 units connected in parallel, and the heat source temperature increases from 60 to 70 °C *(Constant hot water flow rate)*

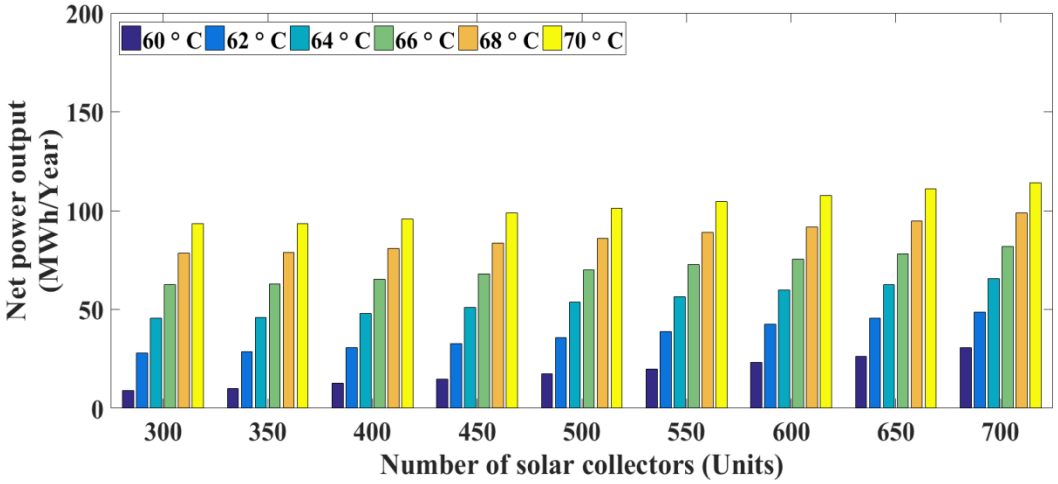

(a) Flat-plate solar collectors

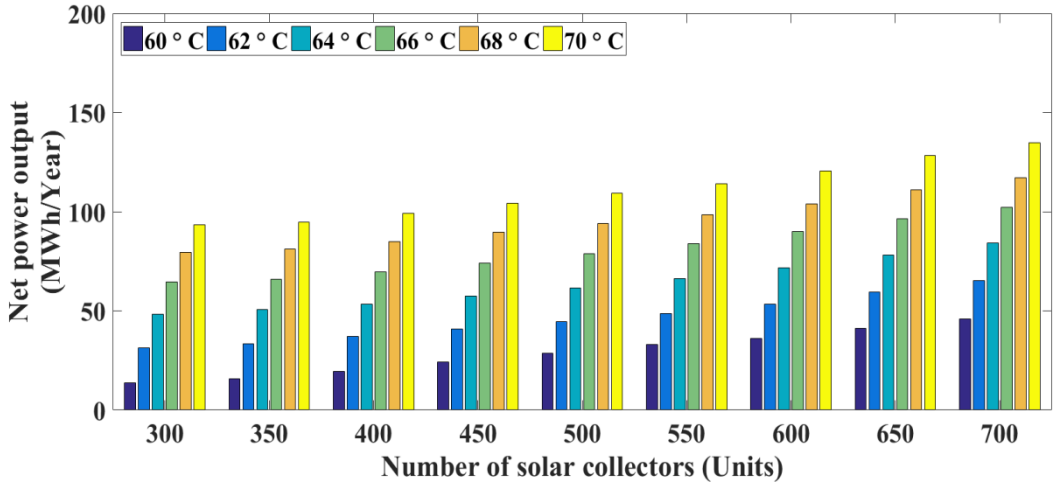

(b) Heat pipe evacuated-tube solar collectors

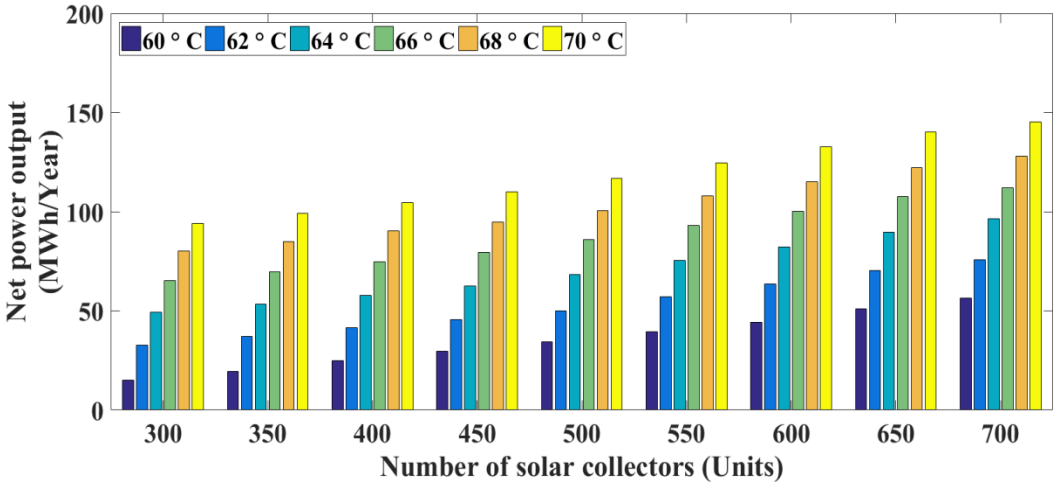

(c) Compound parabolic concentrator (CPC) solar collectors

Figure 5-11 Net power output (MWh/Year) of the systems *(Location: Ratchaburi)*, when the number of solar collectors of 300 to 700 units connected in parallel, and the heat source temperature increases from 60 to 70 °C *(Constant hot water flow rate)*

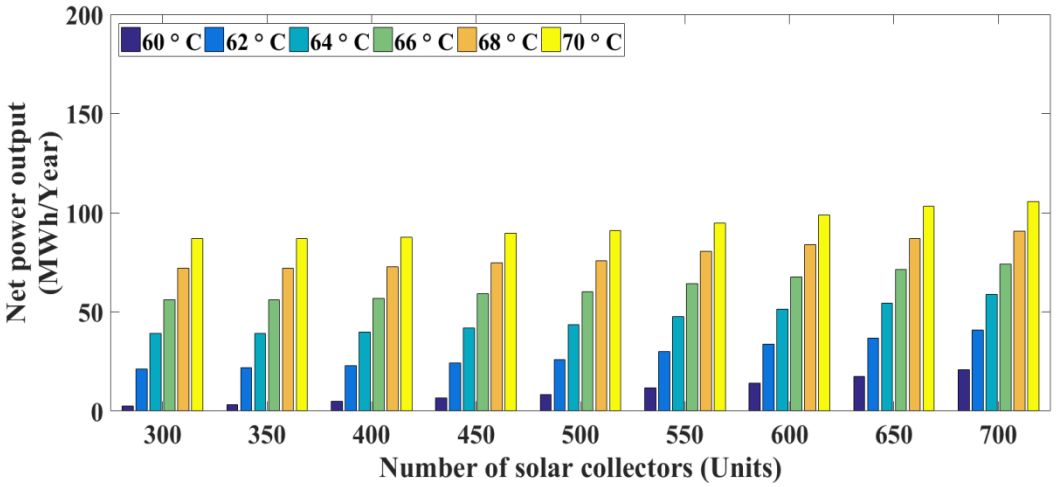

(a) Flat-plate solar collectors

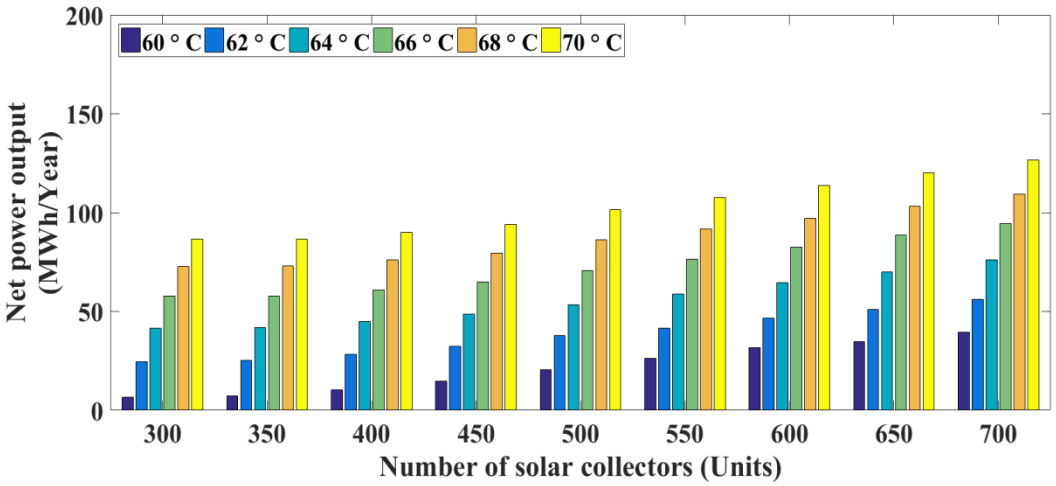

(b) Heat pipe evacuated-tube solar collectors

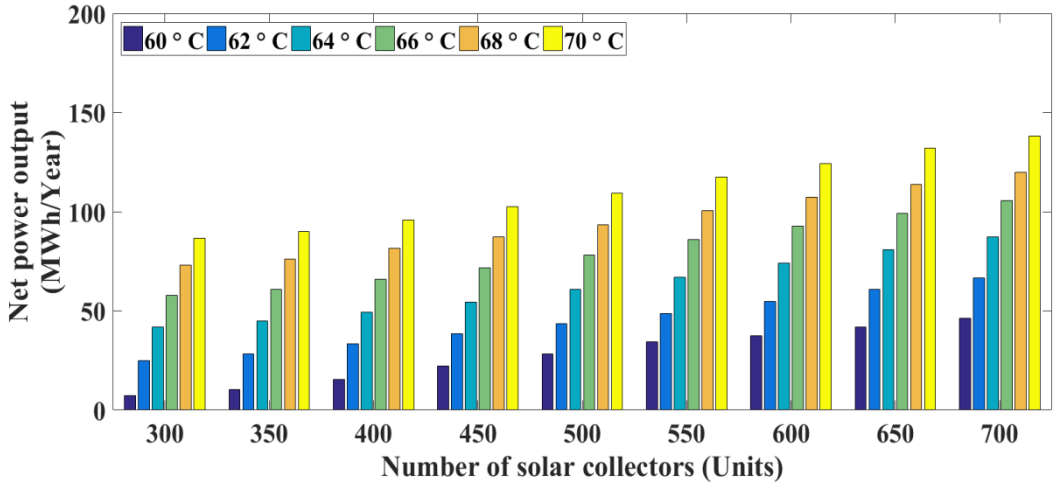

(c) Compound parabolic concentrator (CPC) solar collectors

Figure 5-12 Net power output (MWh/Year) of the systems *(Location: Songkhla)*, when the number of solar collectors of 300 to 700 units connected in parallel, and the heat source temperature increases from 60 to 70 °C *(Constant hot water flow rate)*

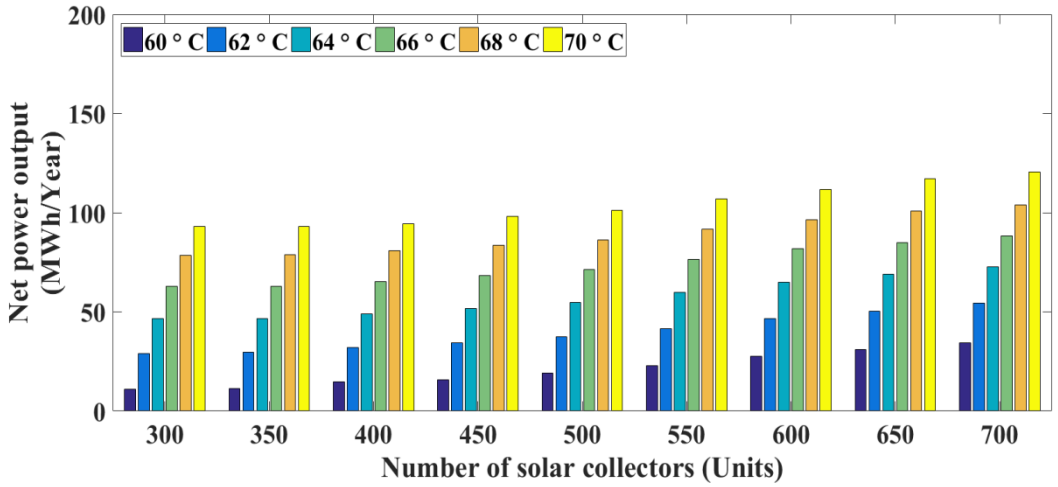

(a) Flat-plate solar collectors

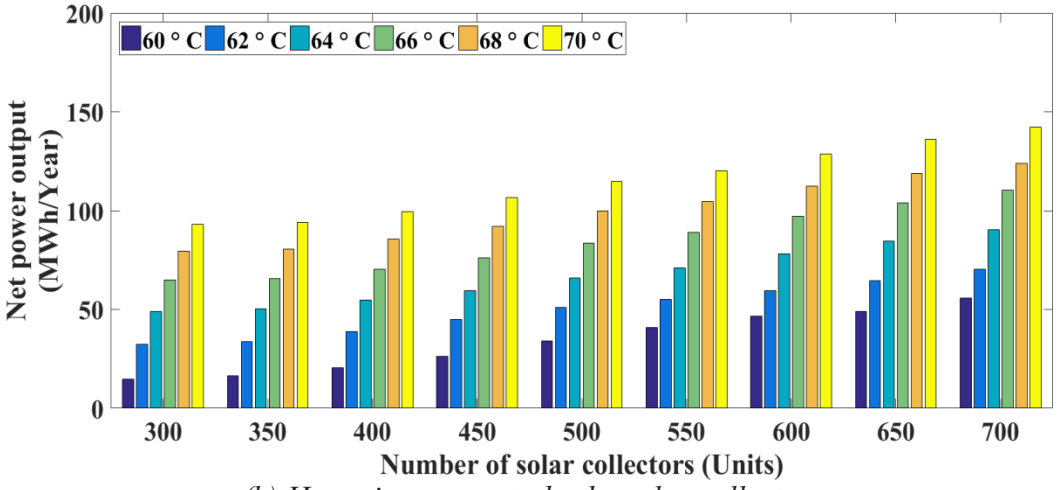

(b) Heat pipe evacuated-tube solar collectors

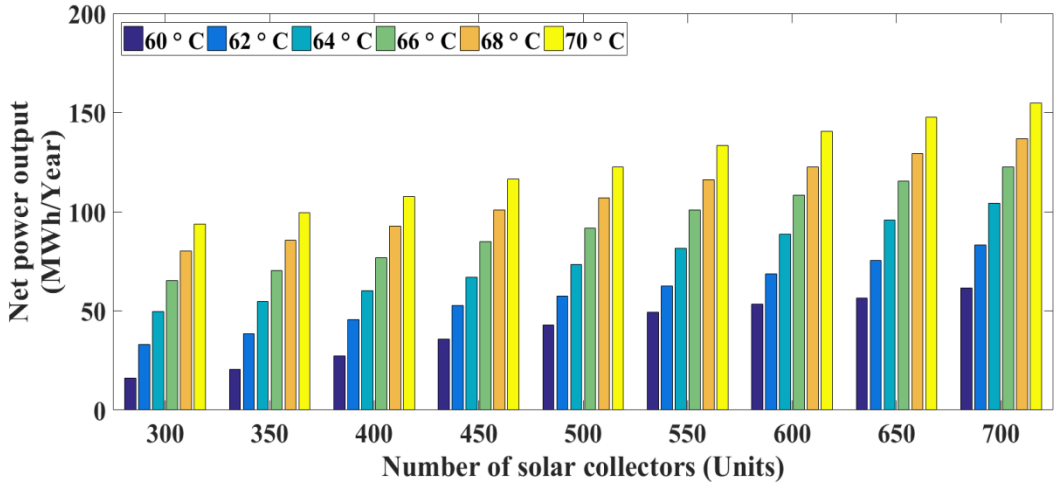

(c) Compound parabolic concentrator (CPC) solar collectors

Figure 5-13 Net power output (MWh/Year) of the systems *(Location: Nakhon Ratchasima)*, when the number of solar collectors of 300 to 700 units connected in parallel, and the heat source temperature increases from 60 to 70 °C *(Constant hot water flow rate)*

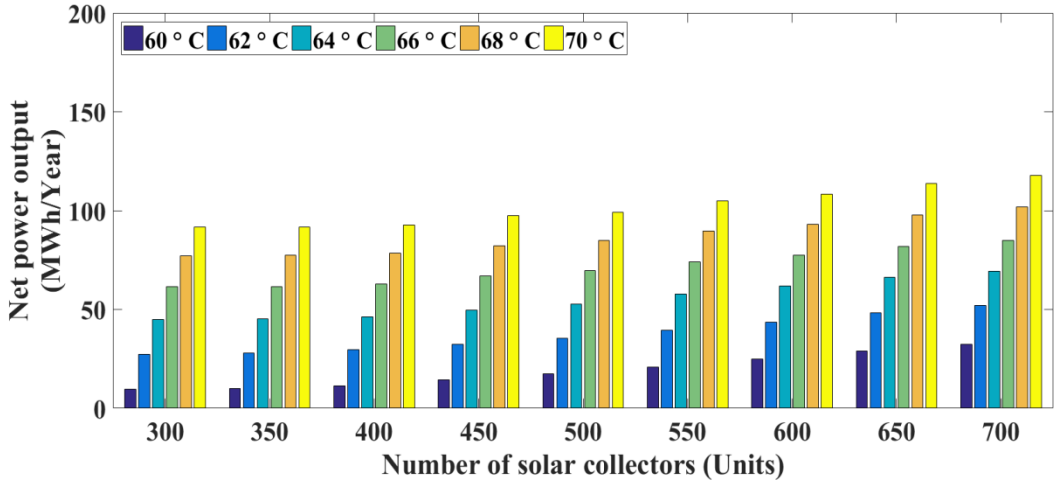

(a) Flat-plate solar collectors

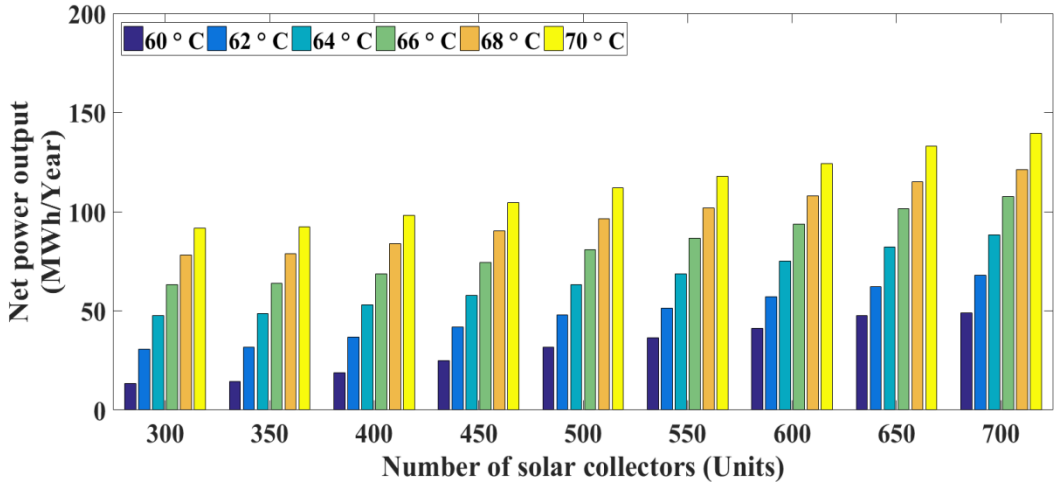

(b) Heat pipe evacuated-tube solar collectors

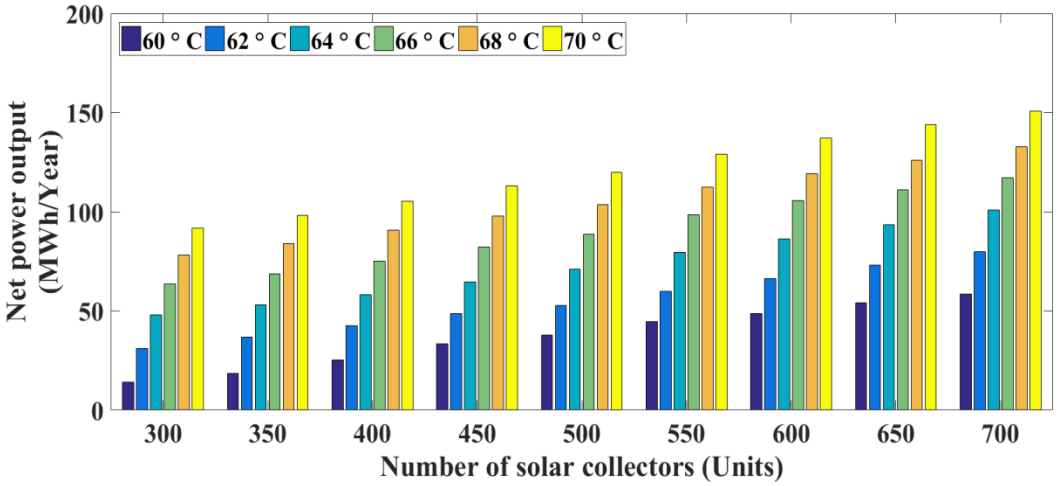

(c) Compound parabolic concentrator (CPC) solar collectors

Figure 5-14 Net power output (MWh/Year) of the systems *(Location: Chon Buri)*, when the number of solar collectors of 300 to 700 units connected in parallel, and the heat source temperature increases from 60 to 70 °C *(Constant hot water flow rate)*

- **Effect of the Heat Source Temperature:**

According to the concept developed in this study, the VCHP system was used to increase the low-temperature heat source to the high-temperature heat sink/heat reservoir before supplying to the ORC power generation. The VCHP system is a thermal upgrading device driven by electrical power, with its power requirement depending on the temperature difference between the heat source and heat sink/heat reservoir. Focusing on the heat source temperature, Figure 5-15 to Figure 5-23 shows the effect of the heat source on the hourly net power output of the system when the number of solar collectors varies from 300 to 700 units with 50 unit increments and the heat source temperature increases from 60 to 70 °C of Bangkok. The results showed that, the heat source temperature impacted on the net power output of the system. The system can be operated during day and night time or 24 hours per day, when the temperature of heat source is above 62 °C. This means that, at this temperature the power output of the VCHP-ORC system was higher than the power fed back to the VCHP system.

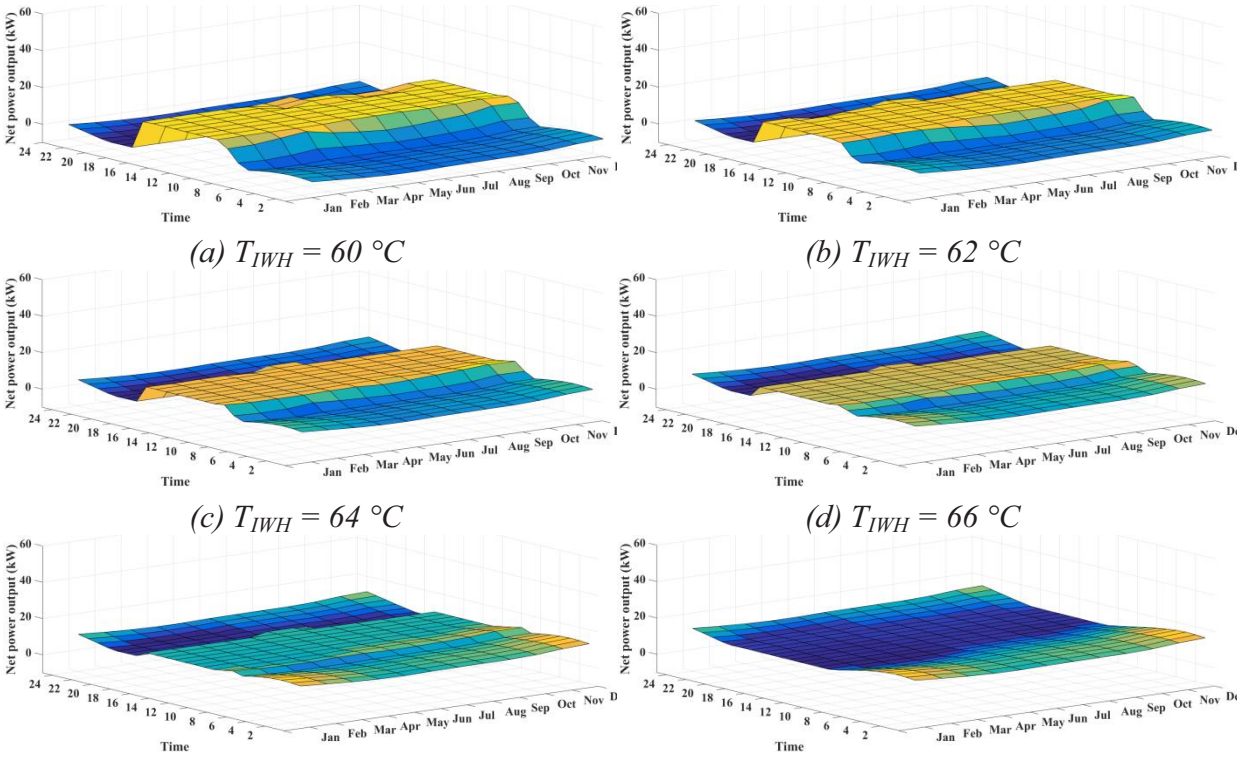

(a) T_{IWH} *= 60 °C* *(b)* T_{IWH} *= 62 °C*

(c) T_{IWH} *= 64 °C* *(d)* T_{IWH} *= 66 °C*

(e) T_{IWH} *= 68 °C* *(f)* T_{IWH} *= 70 °C*

Figure 5-15 Hourly net power output (kW_e) of the systems, when the number of solar collectors is 300 units *(Collector type: Flat-plate solar collectors and Location: Bangkok)*

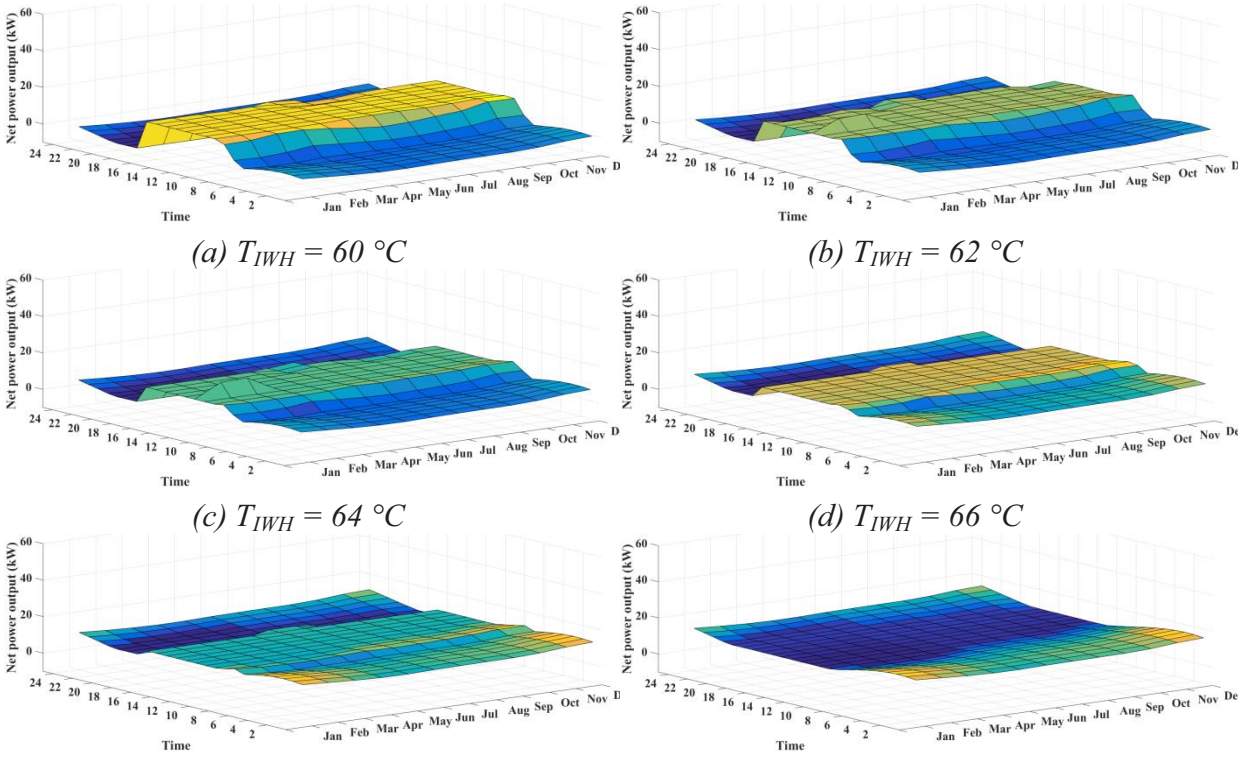

(a) T_{IWH} = 60 °C *(b) T_{IWH} = 62 °C*

(c) T_{IWH} = 64 °C *(d) T_{IWH} = 66 °C*

(e) T_{IWH} = 68 °C *(f) T_{IWH} = 70 °C*

Figure 5-16 Hourly net power output (kW_e) of the systems, when the number of solar collectors is 350 units *(Collector type: Flat-plate solar collectors and Location: Bangkok)*

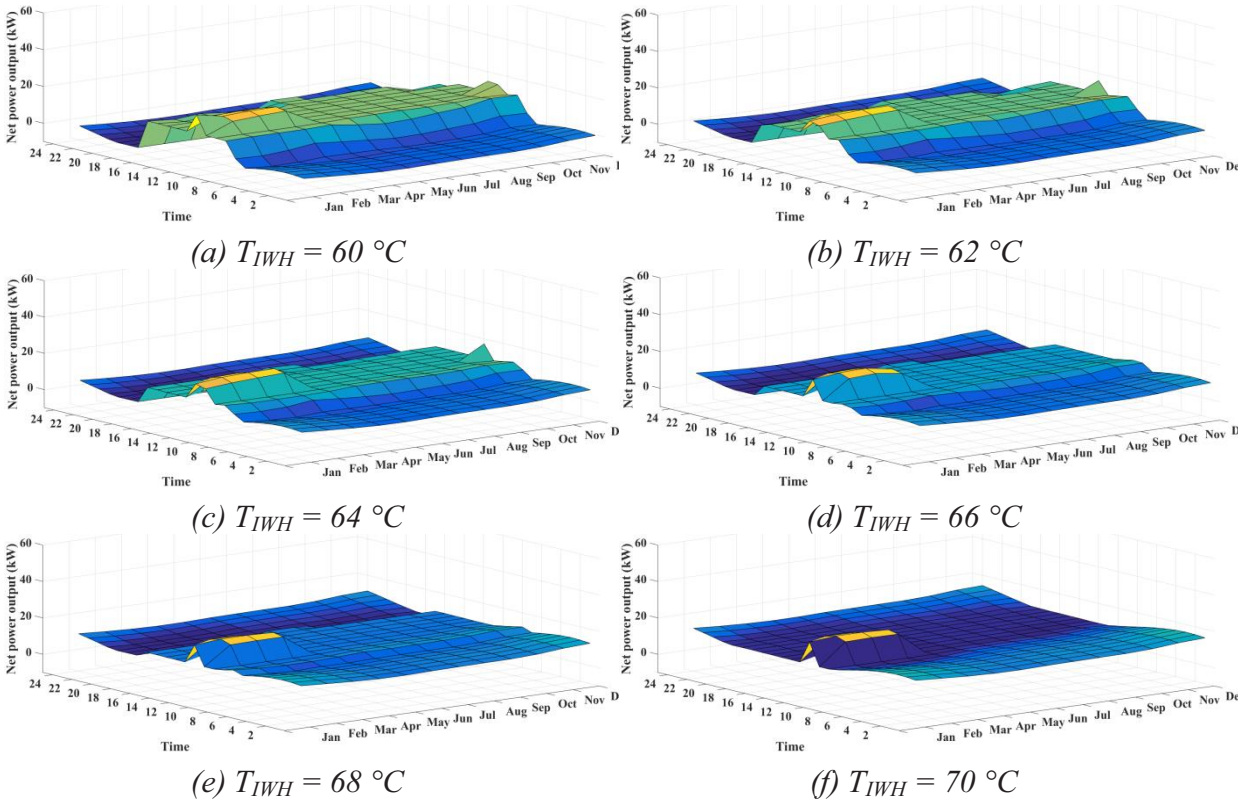

(a) T_{IWH} = 60 °C *(b) T_{IWH} = 62 °C*

(c) T_{IWH} = 64 °C *(d) T_{IWH} = 66 °C*

(e) T_{IWH} = 68 °C *(f) T_{IWH} = 70 °C*

Figure 5-17 Hourly net power output (kW_e) of the systems, when the number of solar collectors is 400 units *(Collector type: Flat-plate solar collectors and Location: Bangkok)*

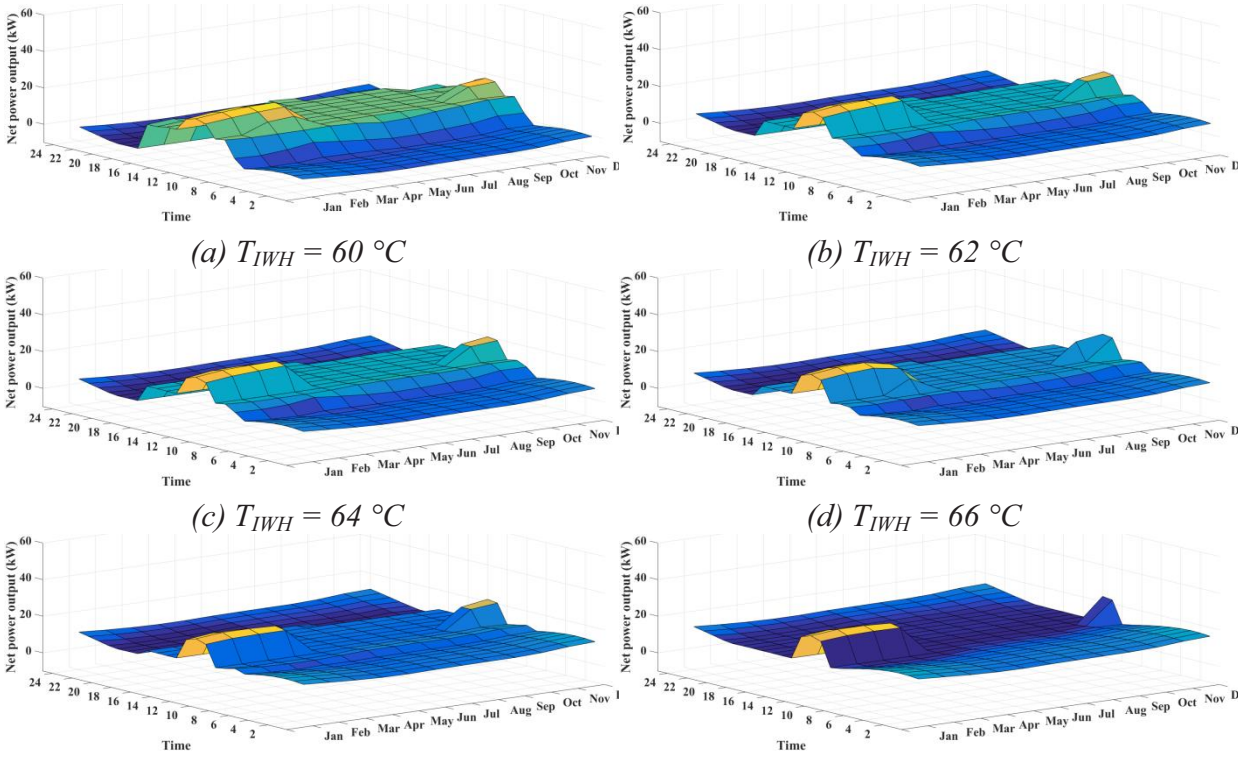

(a) T_{IWH} = 60 °C (b) T_{IWH} = 62 °C

(c) T_{IWH} = 64 °C (d) T_{IWH} = 66 °C

(e) T_{IWH} = 68 °C (f) T_{IWH} = 70 °C

Figure 5-18 Hourly net power output (kW_e) of the systems, when the number of solar collectors is 450 *(Collector type: Flat-plate solar collectors and Location: Bangkok)*

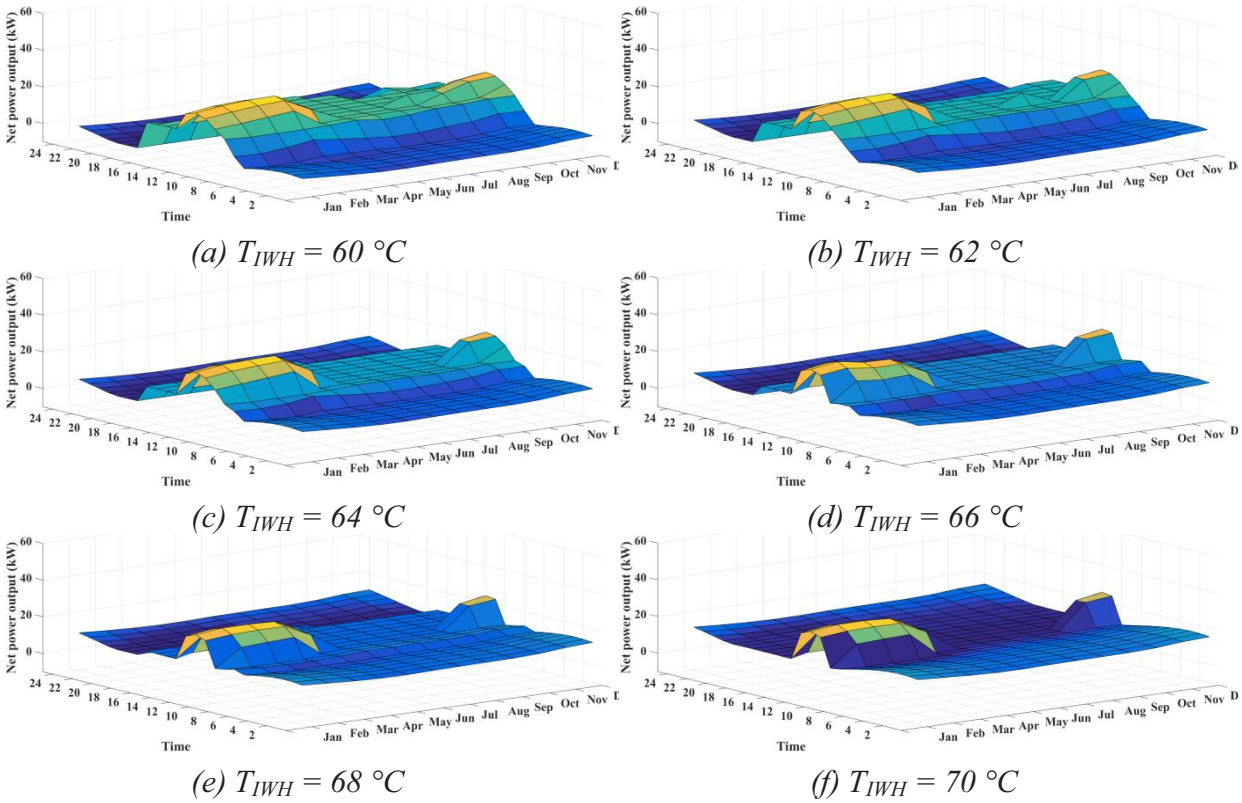

(a) T_{IWH} = 60 °C (b) T_{IWH} = 62 °C

(c) T_{IWH} = 64 °C (d) T_{IWH} = 66 °C

(e) T_{IWH} = 68 °C (f) T_{IWH} = 70 °C

Figure 5-19 Hourly net power output (kW_e) of the systems, when the number of solar collectors is 500 units *(Collector type: Flat-plate solar collectors and Location: Bangkok)*

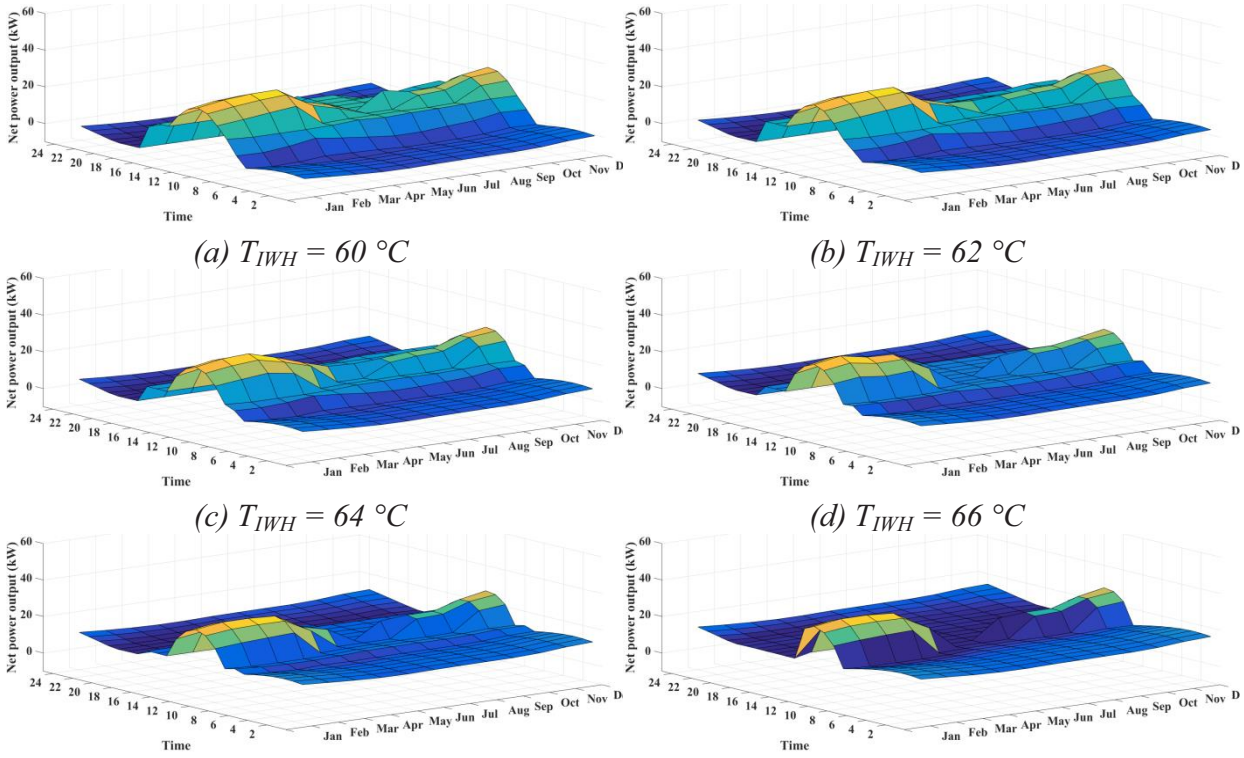

(a) T_{IWH} = 60 °C *(b)* T_{IWH} = 62 °C

(c) T_{IWH} = 64 °C *(d)* T_{IWH} = 66 °C

(e) T_{IWH} = 68 °C *(f)* T_{IWH} = 70 °C

Figure 5-20 Hourly net power output (kW_e) of the systems, when the number of solar collectors is 550 units *(Collector type: Flat-plate solar collectors and Location: Bangkok)*

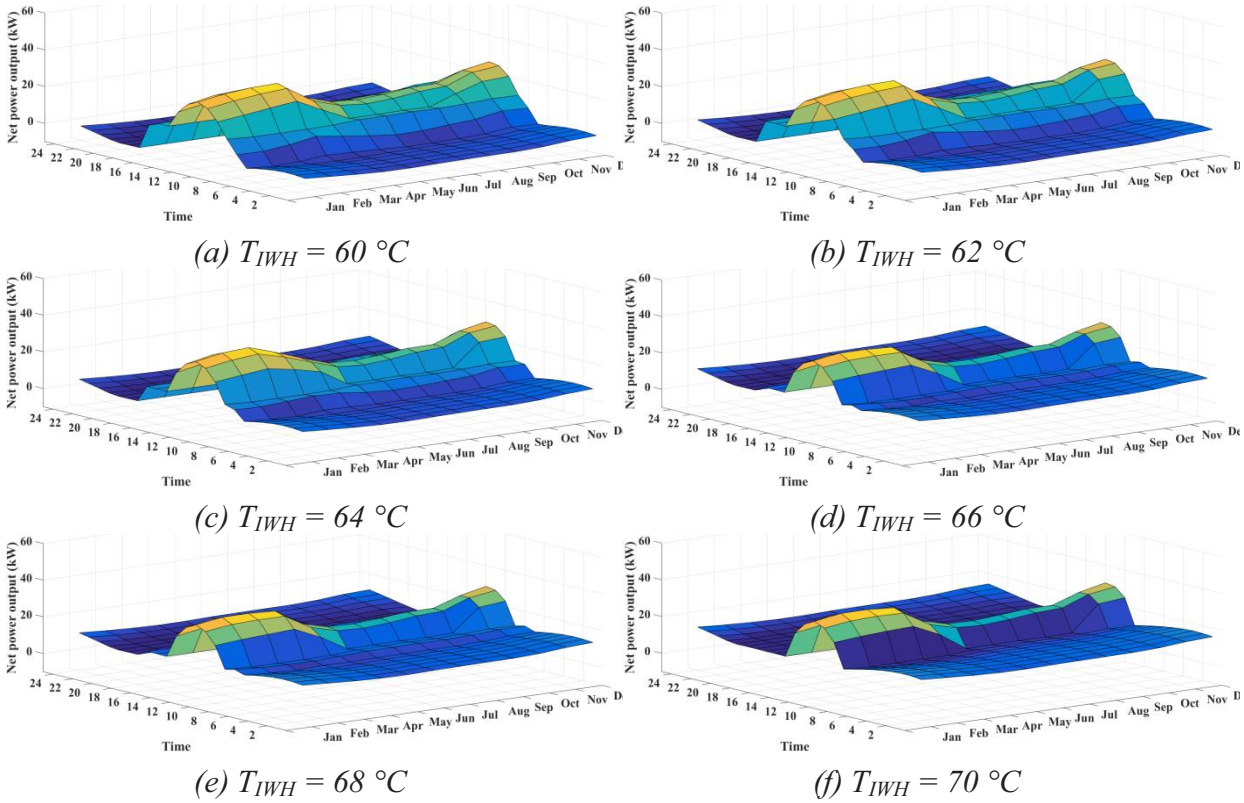

(a) T_{IWH} = 60 °C *(b)* T_{IWH} = 62 °C

(c) T_{IWH} = 64 °C *(d)* T_{IWH} = 66 °C

(e) T_{IWH} = 68 °C *(f)* T_{IWH} = 70 °C

Figure 5-21 Hourly net power output (kW_e) of the systems, when the number of solar collectors is 600 units *(Collector type: Flat-plate solar collectors and Location: Bangkok)*

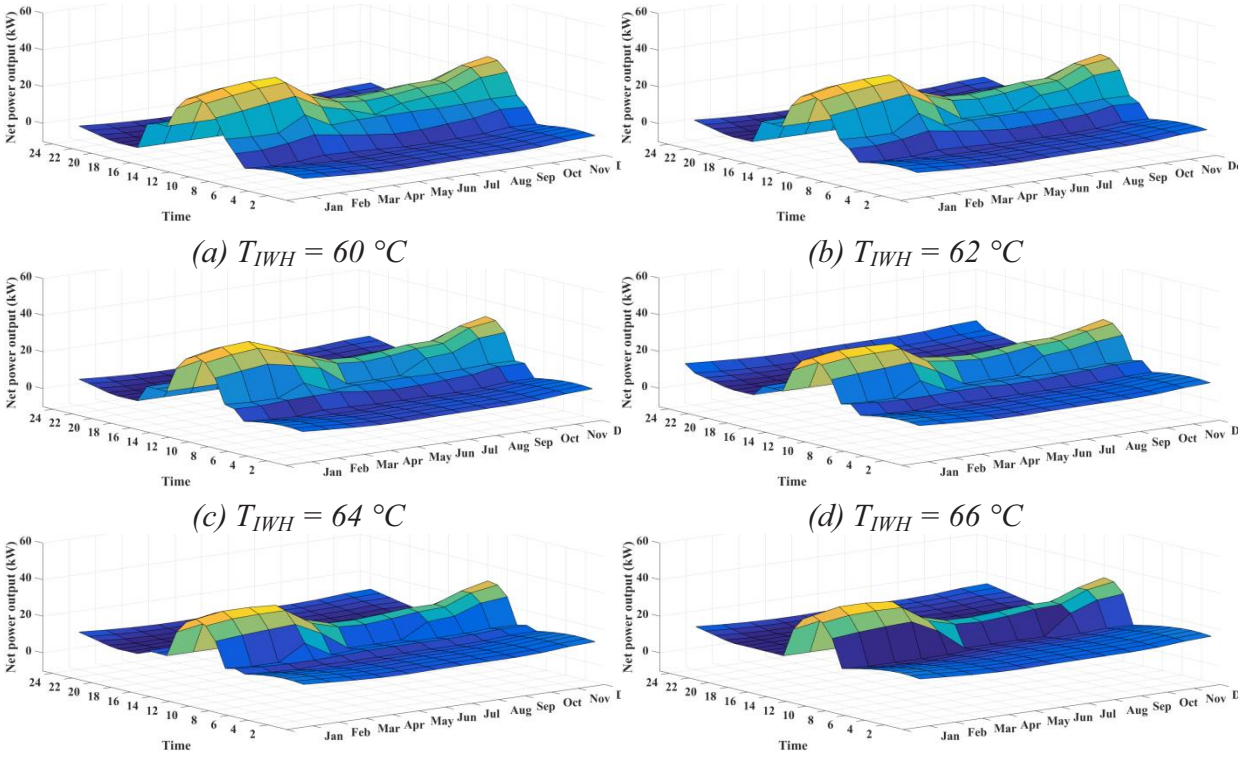

(a) T_{IWH} = 60 °C *(b)* T_{IWH} = 62 °C

(c) T_{IWH} = 64 °C *(d)* T_{IWH} = 66 °C

(e) T_{IWH} = 68 °C *(f)* T_{IWH} = 70 °C

Figure 5-22 Hourly net power output (kW_e) of the systems, when the number of solar collectors is 650 units *(Collector type: Flat-plate solar collectors and Location: Bangkok)*

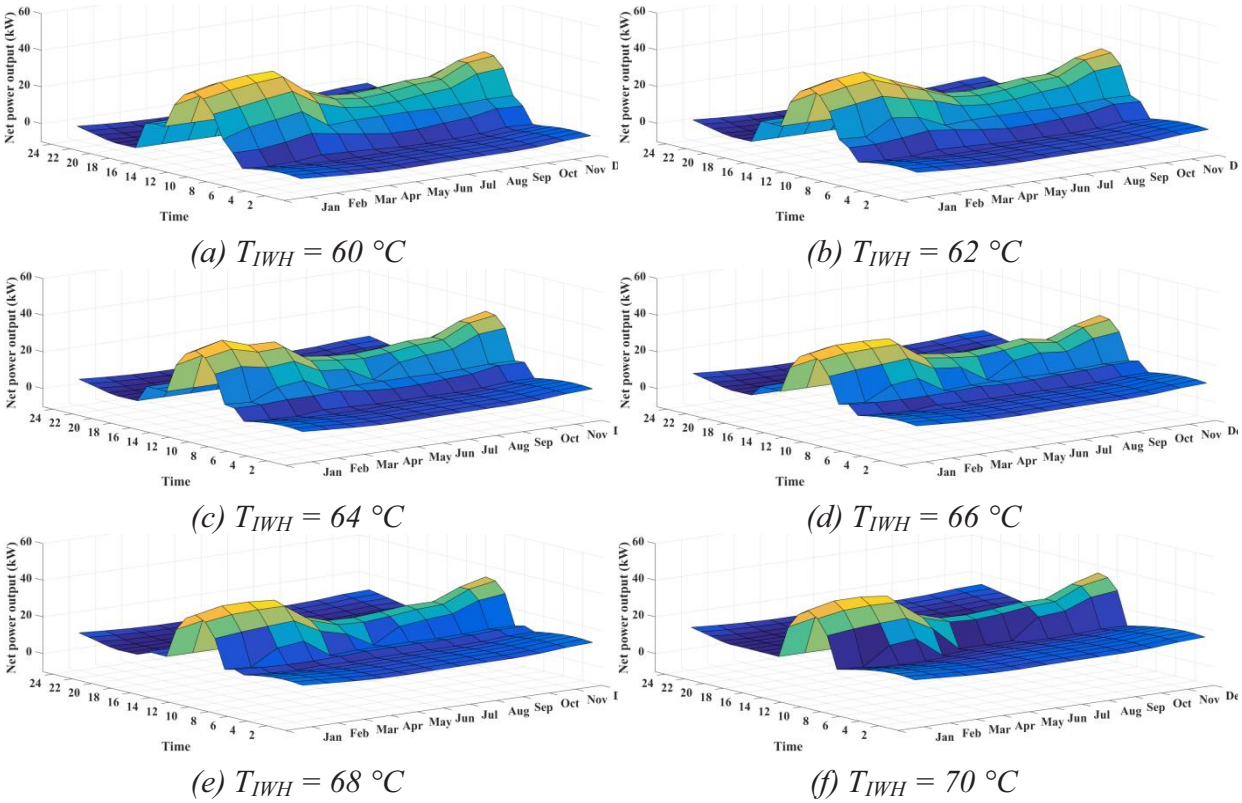

(a) T_{IWH} = 60 °C *(b)* T_{IWH} = 62 °C

(c) T_{IWH} = 64 °C *(d)* T_{IWH} = 66 °C

(e) T_{IWH} = 68 °C *(f)* T_{IWH} = 70 °C

Figure 5-23 Hourly net power output (kW_e) of the systems, when the number of solar collectors is 700 units *(Collector type: Flat-plate solar collectors and Location: Bangkok)*

An example for energy balance, from Figure 5-23 when the number of solar collectors is 700 units, it can be noted oscillation trends exist in the morning (7.00 ~ 10.00 a.m.) and the afternoon (14.00 ~ 18.00 p.m.). It can be explained in terms of the energy balance of the system with consists of rate of heat transfer from solar collectors ($\dot{Q}_{Coll}$) (day time or sunrise), rate of heat transfer from the VCHP system ($\dot{Q}_{Cond,VCHP}$) (night time or sunset), rate of heat transfer supply to the load ($\dot{Q}_{Load}$), power output from the ORC system ($\dot{W}_{ORC}$), and power input to the VCHP system ($\dot{W}_{VCHP}$) as shown in Figure 5-24. From the Figure, it seems that in the morning and the afternoon, the SWHS could maintain the thermal energy from the solar collectors ($\dot{Q}_{Coll}$) to supply the ORC power generation even though solar radiation was slightly low, because of the number of solar collectors available. In addition, at night time with the same quality and quantity of waste heat, the power output from the ORC system was higher when the ambient temperature was lower. In other words, the ORC system could produce the highest power at the lowest ambient temperature.

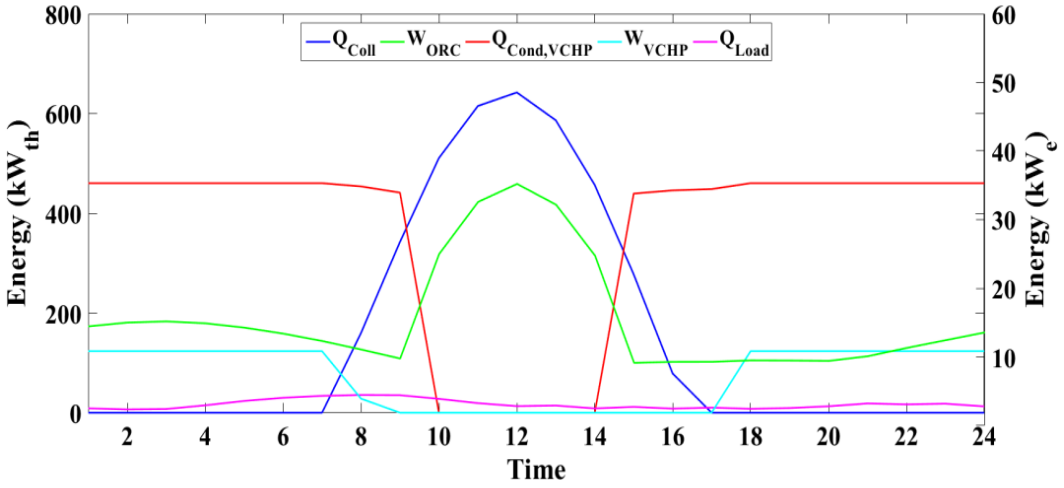

Figure 5-24 Energy balance of the systems on January, when the number of solar collectors is 700 units connected in parallel and the heat source temperature of 64 °C *(Collector type: Flat-plate solar collectors and Location: Bangkok)*

- **Net Power Output**

As mentioned above, Figure 5-25 shows a comparison of the net power output of three types of solar collectors, when the numbers of solar collectors were varied from 300 – 700 units connected in parallel, and the heat source temperature was around 64 °C (Location: Bangkok). The comparing results presented that with increment of 50 units, the system with CPC solar collectors provided the net power outputs of 48.8, 53.7, 60.1, 67.1, 74.5, 82.6, 90.0, 97.7, and 98.7 MWh/Year, respectively due to the highest thermal energy and collector outlet temperature of the collector. In addition, the system combined with heat pipe evacuated-tube solar collectors provided their net power output of 47.5, 50.2, 53.4, 59.6, 65.6, 71.3, 78.9, 85.8, and 92.2 MWh/Year, respectively and for flat-plate solar collectors provided 45.1, 45.6, 48.3, 51.0, 55.3, 60.1, 64.3, 69.4, and 72.6 MWh/Year, respectively.

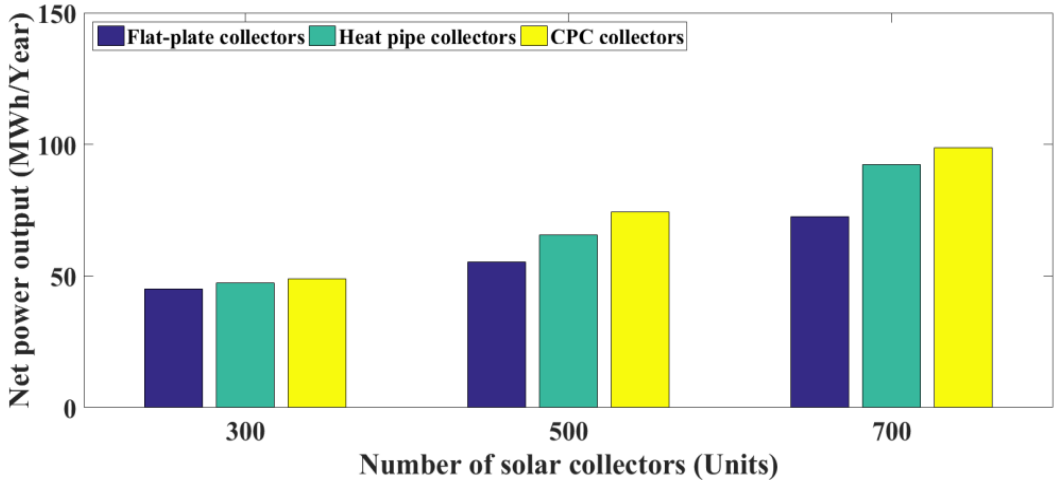

Figure 5-25 Comparison of the net power output (MWh/Year) of the systems *(Location: Bangkok)*, when the number of solar collectors increases from 300 to 700 units connected in parallel, the heat source temperature of 64 °C, and three types of solar collectors *(Constant hot water flow rate)*

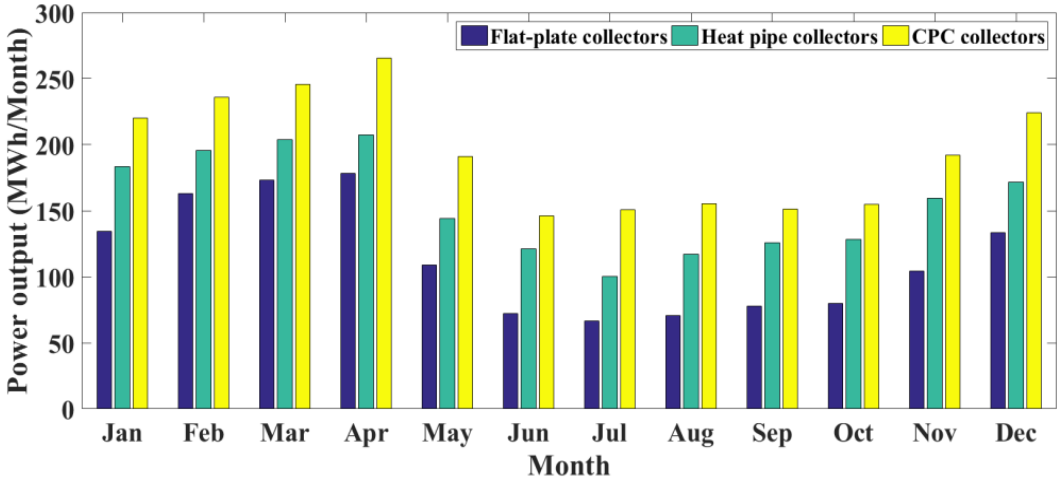

Figure 5-26 Average monthly net power output (kWh/Month) of the systems *(Location: Bangkok, and Daytime operations)*, when the number of solar collectors is 700 units connected in parallel, the heat source temperature of 60 °C, and three types of solar collectors *(Constant hot water flow rate)*

For average monthly net power output (kWh/Month) of the system with different types of the collector, it is shown in Figure 5-26 (Location: Bangkok). It shows that during daytime operations the highest electricity generation occurred in March and April or in the summer season *(Summer: March to May, Rainy: June to October, and Winter: November to February)*. In addition, the result indicates that the system can generate the highest amount of electricity depending on: (1) Rate of heat transfer from solar collectors, (2) ORC inlet hot water temperature or Collector outlet temperature, and (3) Ambient temperature or the weather of each season, as shown in Figure 5-27 to Figure 5-29, respectively.

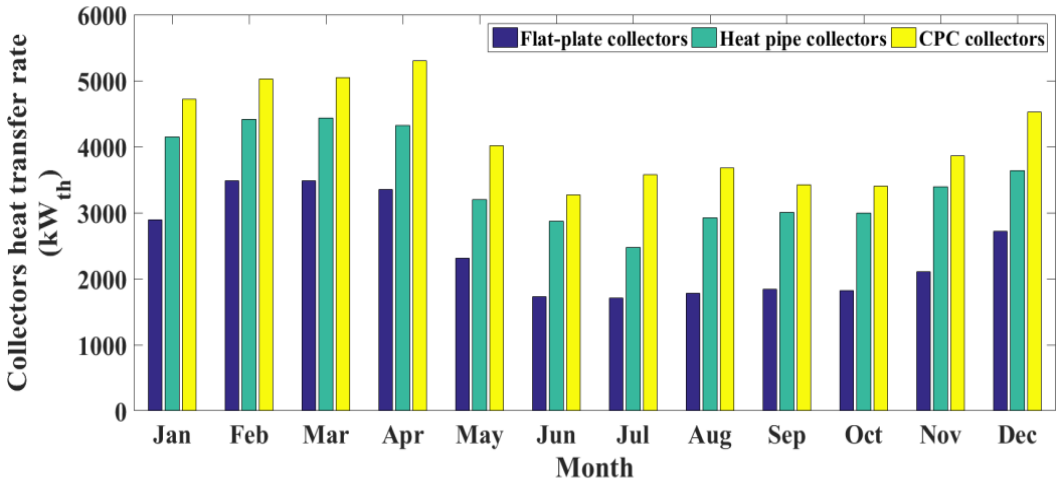

Figure 5-27 Average monthly rate of heat transfer from solar collectors (kW_{th}) of the systems, when the number of solar collectors is 700 units connected in parallel, the heat source temperature of 60 °C, and three types of solar collectors *(Location: Bangkok, and Daytime operations)*

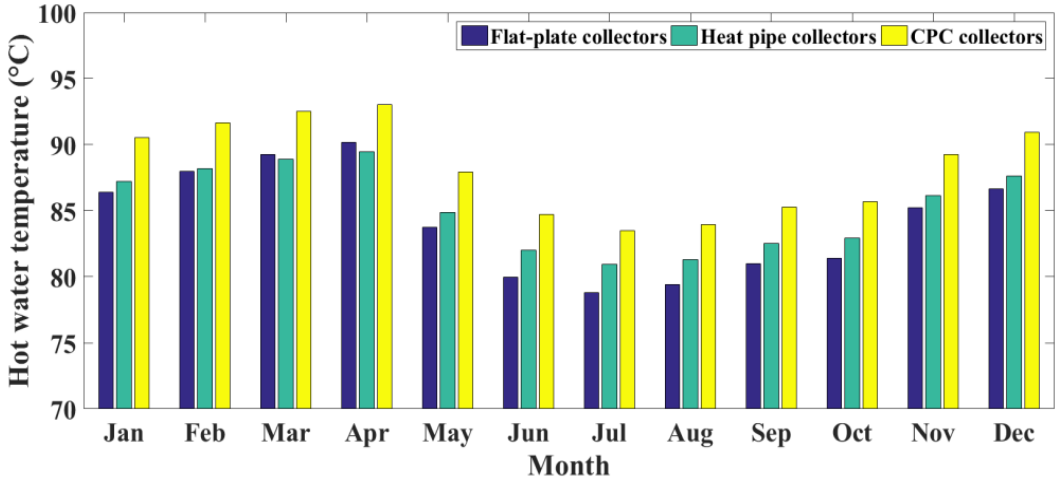

Figure 5-28 Maximum ORC inlet hot water temperature (°C), when the number of solar collectors is 700 units connected in parallels, the heat source temperature of 60 °C, and three types of solar collectors *(Location: Bangkok, and Daytime operations)*

Figure 5-30 shows the hourly ORC inlet hot water temperature (°C) of the system, when the number of solar collectors is 700 units connected in parallel and the heat source temperature is around 64 °C (Location: Bangkok). The results were found that the highest ORC inlet hot water temperature or collector outlet temperature can be produced when the system is combined with the CPC solar collectors. Although their efficiency can slightly decrease when the solar collector inlet temperature increases (as shown in Figure 5-2). These results are consistent with the highest power generation that the system could generate, when the system was combined with the CPC solar collectors.

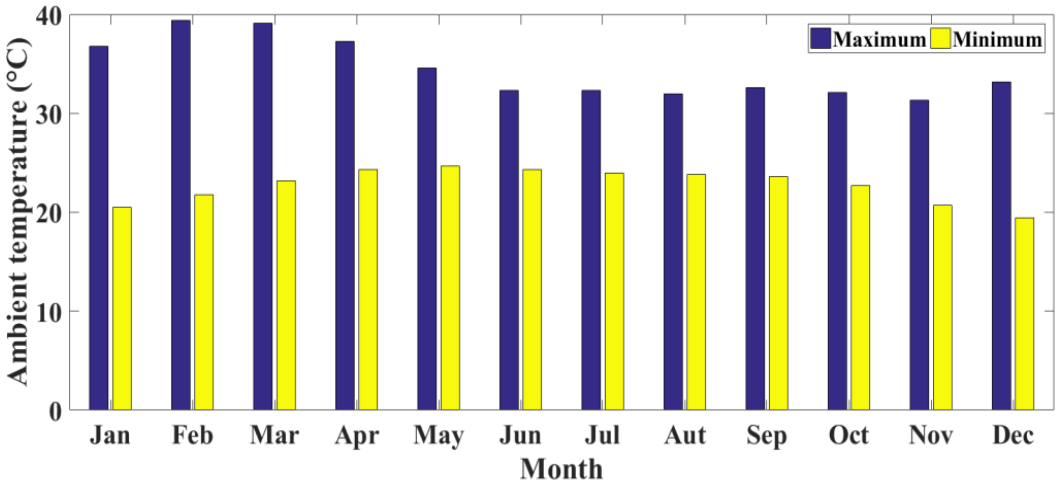

Figure 5-29 Maximum and minimum ambient temperature (°C) at Bangkok, Thailand

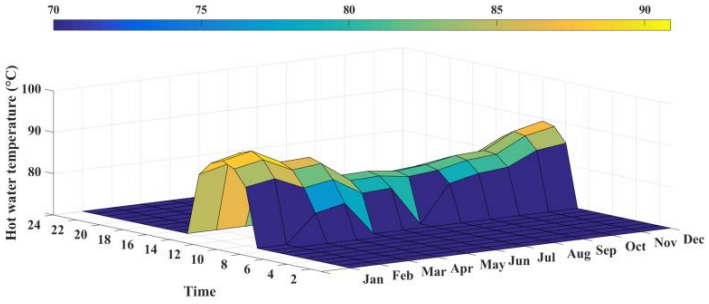

(a) Flat-plate solar collectors

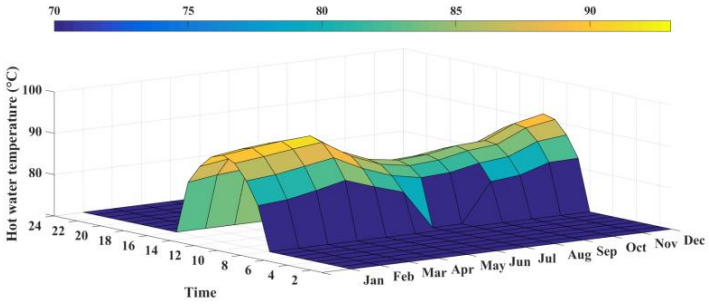

(b) Heat pipe evacuated-tube solar collectors

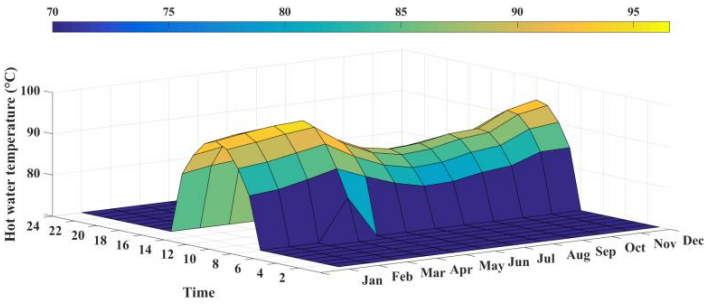

(c) Compound parabolic concentrator (CPC) solar collectors

Figure 5-30 Hourly ORC inlet hot water temperature (°C) of the systems *(Location: Bangkok)*, when the number of solar collectors is 700 units connected in parallels, the heat source temperature of 64 °C, and three types of solar collectors *(Constant hot water flow rate)*

5.5.2 Environment Assessment

The capability of reducing the CO_2 emission of the system depends on the amount of the electricity the system can generate, and it can be calculated from Eq. (5-2). Based on net power output of the system, it was found, that the tendency of CO_2 reduction by the system increases when the number of solar collectors and the heat source temperature increase.

$$CO_2\ Emission = [(Net\ power\ output) \times 0.548]/1000 \quad (5\text{-}2)$$

From Figure 5-31 (Location: Bangkok), it was shown that the CO_2 reduction by the system has the upward trend when the number of solar collector increases. When the number of solar collectors varies from 300 to 700 units with 50 unit increments, the system with CPC solar collectors can provide the lowest CO_2 emissions of 26.8, 29.4, 33.0, 36.8, 40.8, 45.3, 49.3, 53.5, and 54.1 Ton CO_2 eq./Year, respectively. In addition, the system with the heat pipe evacuated-tube solar collectors and the flat-plate solar collectors can decrease the CO_2 emission of 26.0, 27.5, 29.3, 32.6, 35.9, 39.1, 43.2, 47.0, and 50.4 Ton CO_2 eq./Year and 24.7, 25.0, 26.5, 28.0, 30.3, 33.0, 35.3, 38.0, and 40.0 Ton CO_2 eq./Year, respectively.

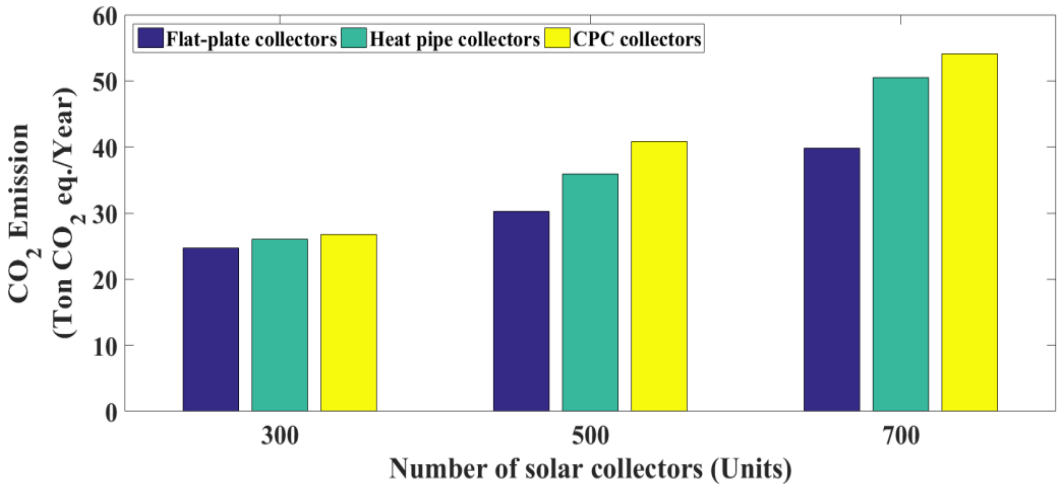

Figure 5-31 Effect of the number of solar collectors on the CO_2 reduction (Ton CO_2 eq./Year) *(Location: Bangkok)*, when the number of solar collectors increases from 300 to 700 units connected in parallel, and the heat source temperature was at around 64 °C

5.5.3 Economic Assessment

In this assessment, the investment of solar collectors was not included as mentioned in a previous section (5.4 Economic Analysis). The LCOE was selected to represent the economic results of the VCHP-ORC power generation from low-grade IWH combined with SWHS. The results found that, the LCOE of the system had decreased when the number of solar collectors and the heat source temperature were increasing. The LCOE of the system with three different types of solar collectors was shown in Figure 5-32 (Location: Bangkok). The results showed that the system with 50 unit increments of the CPC solar collectors provided the lowest LCOE of 0.604, 0.550, 0.491, 0.440, 0.396, 0.357, 0.328, 0.302, and 0.299 USD/kWh, respectively. Moreover, the system with the heat pipe evacuated-tube solar collectors and the flat-plate solar collectors provide the LCOE of 0.621, 0.587, 0.552, 0.495,

0.450, 0.414, 0.374, 0.344, and 0.320 USD/kWh and 0.654, 0.647, 0.611, 0.578, 0.534, 0.491, 0.459, 0.425, and 0.406 USD/kWh, respectively. Furthermore, the net power output (MWh/Year), the CO_2 reduction (Ton CO_2 eq./Year), and the LCOE (USD/kWh) of the system are shown in Table 5-4 (Location: Bangkok), when the number of solar collectors of 700 units is connected in parallel and the heat source temperature increase from 60 to 70 °C.

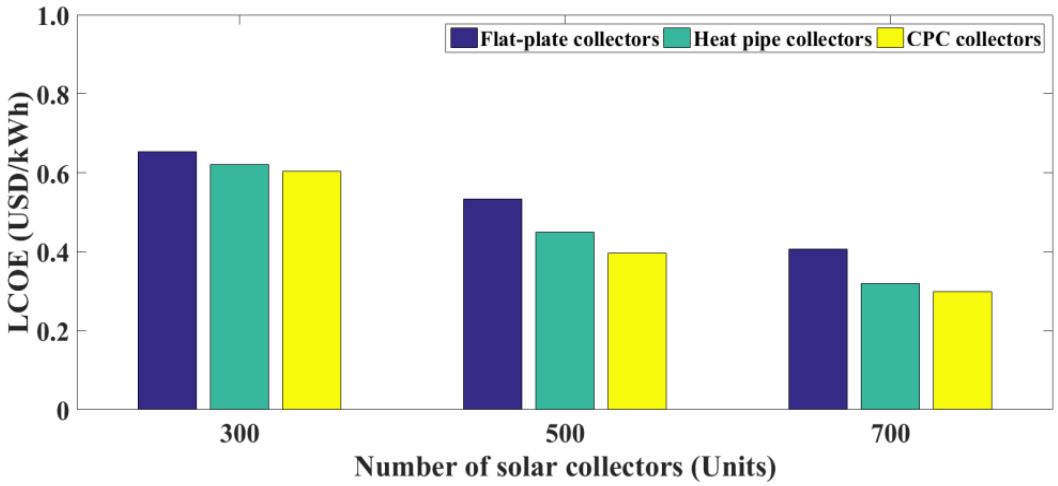

Figure 5-32 LCOE (USD/kWh) of the systems *(Location: Bangkok)*, when the number of solar collectors increases from 300 to 700 units connected in parallels, and the heat source temperature of 64 °C

Table 5-4 Net power output (MWh/Year), CO_2 Emission (Ton CO_2 eq./Year), and LCOE (USD/kWh) of the system *(Location: Bangkok)*, when the number of solar collectors of 700 units connected in parallel, and the heat source temperature increases from 60 to 70 °C, respectively

Collectors	Heat source temperature (°C)	60	62	64	66	68	70
Flat-plate	Net power output (MWh/Year)	36.9	55.1	72.6	88.5	104.8	121.4
	CO_2 Emission (Ton CO_2 eq./Year)	20.2	30.2	39.8	48.5	57.5	66.5
	LCOE (USD/kWh)	0.805	0.537	0.406	0.332	0.280	0.241
Heat pipe evacuated-tube	Net power output (MWh/Year)	50.6	71.8	92.2	110.0	124.5	137.5
	CO_2 Emission (Ton CO_2 eq./Year)	27.7	39.4	50.5	60.3	68.2	75.3
	LCOE (USD/kWh)	0.587	0.412	0.320	0.268	0.236	0.213
CPC	Net power output (MWh/Year)	63.4	85.0	98.7	114.5	122.4	131.7
	CO_2 Emission (Ton CO_2 eq./Year)	34.8	46.6	54.1	62.7	67.1	72.2
	LCOE (USD/kWh)	0.468	0.348	0.299	0.257	0.240	0.222

Therefore, it is noted that the VCHP-ORC power generation from a low-grade IWH combined with SWHS is an interesting system as the industries produce large amounts of low-grade wasted heat with temperatures above 62 °C. In addition, a large number of solar collectors already installed can assist the industries in terms of the economic and the environmental impact. Moreover, from the Table 5-4, when the heat source temperature is above 66 °C, it was found that the system with CPC solar collectors produced the lower net power output as compared with that of the heat pipe evacuated-tube solar collectors due to

the ORC inlet temperature or collector outlet temperature over the temperature limit of the ORC power generation (for this study 95 °C). In other word the ORC system cannot generate electricity.

5.5.4 System Evaluation in Difference Areas

The evaluation results of the system at different locations were compared. When the number of solar collectors is 700 units connected in parallel with the heat source temperature of 64 °C as shown in Table 5-5. It was found that in Chiang Mai province, as a representative of the north part of Thailand, generated the highest electricity because of the highest annual solar energy collected. With the same number of solar collectors Chiang Mai can produce the maximum thermal energy required for ORC power generation. In addition, the average maximum and minimum ambient temperatures of this province were the lowest compared to other areas *(the results are consistent with previous studies of Chakkraphan and Tanongkiat (2012) [28])*, followed by Nakhon Ratchasima, Chonburi, Bangkok, Ratchaburi, and Songkhla, respectively.

Table 5-5 Comparison of the net power output (MWh/Year), the CO_2 Emission (Ton CO_2 eq./Year), and the LCOE (USD/kWh) of the systems of six areas, when the number of solar collectors of 700 units connected in parallel, and the heat source temperature was at around 64 °C

Location	Net power output (MWh/Yar)			CO_2 Emission (Ton CO_2 eq./Year)			LCOE (USD/kWh)		
	FP	HPE	CPC	FP	HPE	CPC	FP	HPE	CPC
Chiang Mai	84.4	107.0	117.1	46.2	58.6	64.2	0.350	0.276	0.252
Bangkok	72.6	92.2	98.7	39.8	50.5	54.1	0.406	0.320	0.299
Ratchaburi	65.6	84.4	96.5	35.9	46.2	52.9	0.450	0.350	0.306
Songkhla	58.8	76.1	87.3	32.2	41.7	47.8	0.501	0.388	0.338
Nakhon Ratchasima	72.7	90.4	104.3	39.9	49.5	57.1	0.406	0.326	0.283
Chonburi	69.4	88.3	100.9	38.1	48.4	55.3	0.425	0.334	0.293

* FP: Flat-plate solar collectors,
* HPE: Heat pipe evacuated-tube solar collectors,
* CPC: Compound parabolic concentrator solar collectors.

From the evaluation results above, the weather data was only taken into account. However, these results can help the government to make a decision whether to support an industry based on the quality and quantity of low-grade waste heat, type and number of solar collectors, and the number of factories in the estate. Therefore, the larger number of factories in an industrial estate is, the more quantity of low-grade waste heat is available. Thus, it makes the system a good candidate for power generation from low heat waste. In this study, Bangkok province presented the highest number of factories, follow by Nakhon Ratchasima, Chonburi, Chiang Mai, Songkhla, and Ratchaburi, respectively [116]. Moreover, LCOE of each location is shown in Table 5-5. the VCHP-ORC power generation from a low-grade IWH combined with SWHS has a LCOE between 0.252 and 0.501 USD/kWh, while CSP technologies have a LCOE between 0.200 and 0.350 USD/kWh, and the solar photovoltaic has a LCOE between 0.140 and 0.470 USD/kWh [117]. Therefore, the VCHP-ORC system is the most interesting.

5.6 Conclusion

In this Chapter, a concept for a VCHP-ORC power generation from a low-grade IWH with temperature below 70 °C combined with SWHS was proposed and investigated. Three types of solar collectors consisting of flat-plate, heat pipe evacuated-tube, and compound parabolic concentrator (CPC) solar collectors were compared in terms of heat generation to feed the system. Six areas of industrial estate consisting of Chiang Mai, Bangkok, Ratchaburi, Songkhla, Nakhon Ratchasima, and Chon Buri that represent the north, central, west, south, north-east and east part of Thailand were taken as input weather data for the simulations. The system was mathematically modeled and simulated to evaluate the net power output, the environmental impact, and the LCOE of the system. The main conclusions can be summarized as follows:

1) The VCHP-ORC power system is applicable for the below 70 °C heat source from low-grade IWH combined with SWHS. Moreover, it is a technology solution for power generation from low-grade IWH, which is generally wasted and released into the environment.
2) This technology can help the industrial sector to reduce the energy intensity, increase the energy efficiency of the industrial processes, as well to reduce the pollution (greenhouse gas emissions (GHG), and thermal pollution).
3) Type and number of solar collectors, quality and quantity of low-grade IWH, and location and number of industries in industrial estates have an effect on the system in terms of the net power output, the environmental impact, and the LCOE of the system.
4) Chiang Mai province as a representative of the north part of Thailand provided the highest net power output and the lowest LCOE of the system due to the highest annual solar energy and the lowest average maximum and minimum ambient temperature compared to other areas. For instance, when the temperature of the heat source was around 64 °C with 700 units of solar collectors connected in parallel; the system combined with flat-plate, heat pipe evacuated-tube, and CPC solar collectors can produce 84.4, 107.0, and 117.1 MWh/Year with a LCOE of 0.350, 0.276, and 0.252 USD/kWh, respectively. In terms of the environmental impact, the system can reduce the CO_2 emissions by 46.2, 58.6, and 64.2 Ton CO_2 eq./Year, respectively.
5) In terms of the economics analysis, the LCOE of the VCHP-ORC system is in the LCOE range of the CSP and the solar photovoltaic technologies which makes it much interesting.
6) Moreover for the economic analysis, in currently, only two types of solar collectors consist of flat-plate, and heat pipe evacuated-tube were already installed in the factories. In the future work, the investment cost of CPC solar collectors must be included to evaluate the LCOE of the system. Besides, the government must should to promote and subsidies the CPC solar collectors for hot water production. Because of this type of the collectors can be generated highest thermal energy as compared to other two types with the same collector area.

6

Small-scale Solar ORC Power Plant

In Chapter 6, area where the only heat source is a solar water heating system (SWHS) were considered, particularly the case which would make the use of heat boosters lose their effectiveness. This was done taking into account that a system that only requires solar collectors, which are more common in Thailand, would be more interesting for the Department of Alternative Energy Department and Efficiency (DEDE) [32] and reduce the barrier from its implementation. In this part, is presents simulation results of small-scale solar Organic Rankine Cycle (SORC) power system with the heat source having temperature below 100 °C, from SWHS. Three types of non-concentrator solar collectors consisting of flat-plate, evacuated-tube, and compound parabolic concentrator (CPC) were used for hot water production.

6.1 Introduction

The utilization of fossil fuels for power generation has led to many environmental problems, e.g. Gagnon et al. [118] reported that greenhouse gas (GHG) emissions from natural gas and coal (with and without SO_2 scrubbing) power plants contributed 443, 1050, and 960 kt CO_2 eq./TWh, respectively. Environment problems could be decreased moving to renewable energy resources for power generation [119]. In recent years, solar energy is one of the renewables that has been gaining increasing attention and traction. It is a resource that never depletes, therefore its worth to develop and explore. Moreover, it can help to move from fossil fuel technologies to renewable ones [120]. For SWHS combined with the ORC power generation, Marion et al. [27] developed a model based on heat transfer equations to find out the potential of the system that combined a single glazed flat-plate solar collectors with a small-scale ORC system. Wang et al. [119] proposed a SORC system, with CPC solar collectors. The system was tested by changing the value of the environment temperature, and thermal oil mass flow rate that passes through the vapor generator. Calise et al. [13] analyzed a small-scale solar combined heat and power (SCHP) system by using evacuated flat-plate solar collectors for heat generation. Sonsaree et al. [110, 121] a combination of vapor compression heat pump (VCHP), solar collectors, and an ORC system were presented. The VCHP was used to upgrade heat either from the SHWS and waste heat from an industrial process. The results show the system can be applied in the industrial sector with large number of solar collectors and large amount of waste heat.

From the literature review, there are only a few designed with solar collectors in mind to utilize thermal energy with temperature lower than 100 °C. Moreover, only one type of solar collectors such as flat-plate, evacuated-tube, or CPC are considered for heat generation in a

very small-to-medium scale ORC power generation system with capacities lower than 20 kW_e, and higher than 250 kW_e, respectively. These capacities are not suitable to be applied on regionalized small-scale thermal power plants. Then in this Chapter, we define a small-scale ORC system for power generation if the capacity is between 20 and 60 kW_e. Furthermore, in terms of the economic analysis, there are also a few analyzed in terms of the levelized cost of electricity (LCOE), which is a good indicator that helps to compare other power technologies using electricity cost (USD/kWh). Additionally, if a SWHS can be integrated with an ORC power generation, the system will become more interesting to the Thailand government to achieve its goal of 30 percent reduction of energy intensity by 2036 [4]. The main objectives of this research are:

- Develop a mathematical model and simulate the performance of the small-scale SORC power generation system based on the power output, the CO_2 emission, and the economic analysis in terms of LCOE,
- Compare the performance of the power generation system integrated with three types of solar collectors consisting of, flat-plate (FP), evacuated-tube (ET), and compound parabolic concentrator (CPC) used for hot water production,
- Obtain the optimal flow rate of hot water for the maximum power output,
- Simulate the system performance based on weather data from Bangkok city (13.75 °N, 100.52 °E) having the highest number of factories *(in Chapter 5)*.

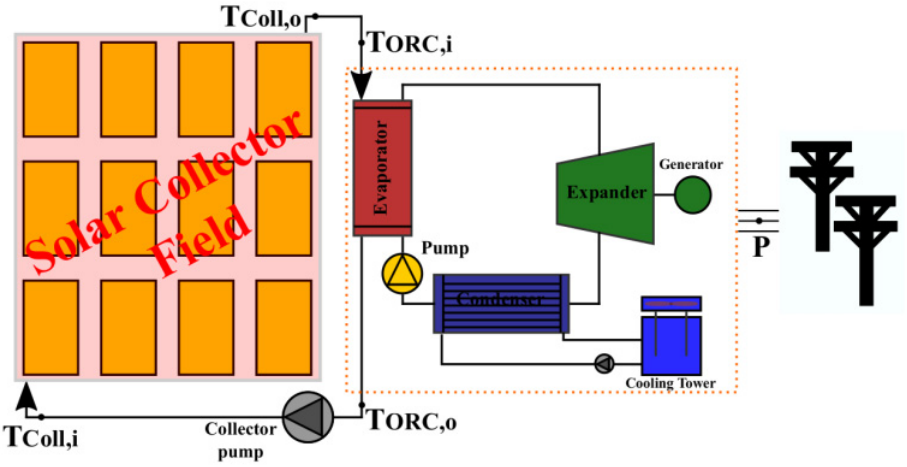

Figure 6-1 Schematic diagram of the small-scale SORC power system

6.2 Descriptions and Simulation Conditions of System

The main components of a small-scale SORC power system shown in Figure 6-1 are the solar collectors, the ORC system, the cooling tower, and the collector pump. In the system operation: the outlet hot water from the ORC system ($T_{ORC,o}$) is pumped by the collector pump, to the solar collector field to produce the high-temperature hot water. At this step, the hot water flow rate is adjusted to achieve a hot water temperature in the range of 70 to 95 °C (high-temperature hot water). After that, the outlet hot water from the solar collector field ($T_{Coll,o}$) is supplied to the ORC for power generation. In this Chapter, the system performance was analyzed based on two capacities for the ORC system (20 and 60 kW_e)

combined in four different configurations with three types of stationary solar collectors (FP, ET, and CPC solar collectors). The testing configuration consists of (i) solar collectors integrated with one unit of a 20 kW_e (SORC-I) *(total capacity of 20 kW_e)*, (ii) solar collectors integrated with two units of a 20 kW_e (SORC-II) *(total capacity of 40 kW_e)*, (iii) solar collectors integrated with three units of a 20 kW_e (SORC-III) *(total capacity of 60 kW_e)*, and (iv) solar collectors integrated with one unit of a 60 kW_e (SORC-IV) *(total capacity of 60 kW_e)* which are shown in Figure 6-2.

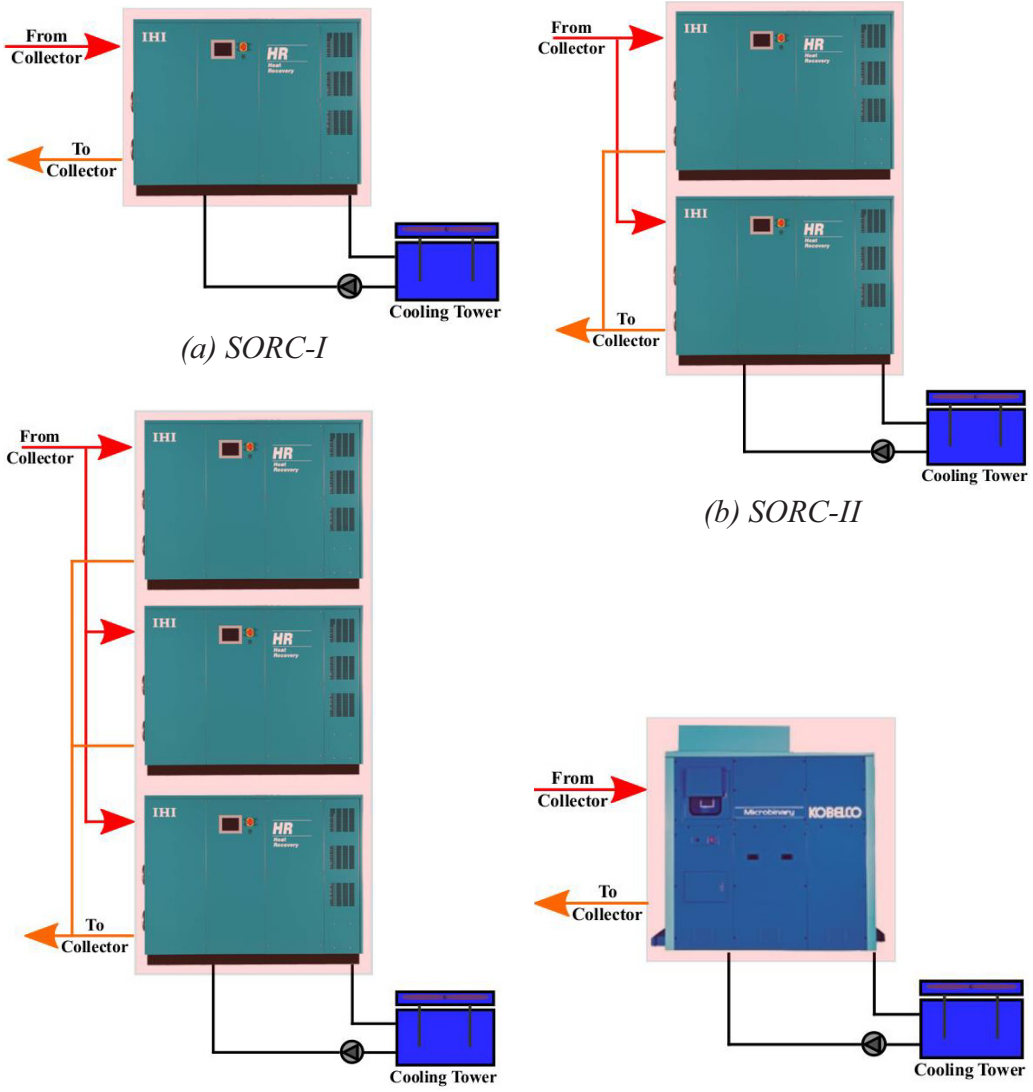

Figure 6-2 (a) Solar collectors integrated with one unit of a 20 kW_e (SORC-I), (b) Solar collectors integrated with two units of a 20 kW_e (SORC-II), (c) Solar collectors integrated with three units of a 20 kW_e (SORC-III), and (d) Solar collectors integrated with one unit of a 60 kW_e (SORC-IV)

In this Chapter, 100 to 1200 units (in 50 units increment) of FP, ET, and CPC solar collectors connected in parallel were used for hot water production as shown in Figure 6-3, having optical efficiency ($F_R(\tau\alpha)_e$) of 0.740, 0.572, 0.718, overall heat transfer coefficient ($F_R U_L$) of 3.620, 0.750, 0.974 W/m^2-K, and gross area of 2.081, 2.369, 2.160 m^2 per unit,

respectively *(in Chapter 5)*. Moreover, an ORC capacity of a 20 and 60 kW_e and R-245fa as working fluid *(ORC model: HR20W from IHI Company [25], and MB-70H from KOBELCO Company [24], respectively)* were simulated to find the power generation capabilities of the system as shown in Figure 6-4, Table 6-1, and Table 6-2.

(a) *(b)* *(c)*

Figure 6-3 (a) FP solar collectors; *Model: Superline M-1 FSB PU from Ezince Company [111]*, (b) ET solar collectors; *Model: DF120/6 from EuroSun Solarsystem GmbH [122]*, and (c) CPC solar collectors; *Model: CPC 12 from Solarbayer Company [113]*

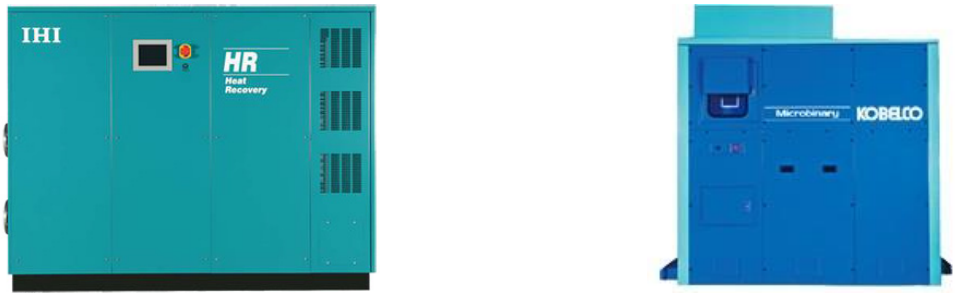

(a) *(b)*

Figure 6-4 (a) a 20 kW_e ORC; *model: HR20W from IHI Company [25]*, (b) a 60 kW_e ORC; *model: MB-70H from KOBELCO Company [24]*

Table 6-1 The performance characteristic of an ORC system, model: *HR20W from IHI Company* [25]

Hot water flow rate (Ton/h)	Cooling water temperature (°C)	Cooling water flow rate (40 Ton/h)			
		Hot water temperature (°C)			
		95	85	75	70
28	20	20	18	12	9
	25	20	16	10	7
	30	20	13	8	6
20	20	20	16	10	8
	25	20	14	9	7
	30	17	12	7	5
12	20	17	12	8	6
	25	15	10	6	5
	30	13	9	5	4

To find out the power output from the performance characteristic of an ORC system as shown in Table 6-1 and Table 6-2, the hot water flow rate (Ton/h), the hot water temperature

(°C), and the cooling water temperature (°C) (equal to ambient temperature in this Chapter) need to be known. For example, *ORC model: HR20W from IHI Company* as shown in Table 6-1, when the hot water flow rate is 12 Ton/h, the hot water and the cooling water temperature is 75 and 30 °C, respectively. The ORC system can generate the power of 5 kW_e.

Table 6-2 The performance characteristic of an ORC system, model: *MB-70H from KOBELCO Company* [24]

Hot water flow rate (Ton/h)	Cooling water temperature (°C)	Cooling water flow rate (120 Ton/h)					
		Hot water temperature (°C)					
		95	**90**	**85**	**80**	**75**	**70**
75	15	60	55	47	39	32	24
	20	60	52	44	35	28	21
	25	57	49	40	32	24	17
	30	52	45	36	27	20	14
70	15	59	54	46	38	31	24
	20	59	51	43	35	27	20
	25	56	48	40	31	24	16
	30	51	43	35	27	20	13
60	15	58	51	44	38	31	24
	20	57	49	41	33	26	19
	25	54	46	38	30	23	16
	30	49	41	33	26	19	13
50	15	56	48	42	37	30	23
	20	55	48	40	32	25	18
	25	52	44	36	29	22	15
	30	42	34	28	22	16	11
40	15	51	44	39	33	27	21
	20	50	43	36	29	23	17
	25	47	39	32	25	19	13
	30	42	34	28	22	16	11
30	15	46	40	35	30	24	18
	20	45	38	31	25	20	15
	25	41	34	28	22	17	12
	30	36	29	24	19	14	9
25	15	43	38	33	28	22	17
	20	43	35	29	24	19	14
	25	38	31	26	20	16	11
	30	33	27	22	17	13	9

6.3 Simulation Conditions

In this Chapter, Bangkok (13.75 °N, 100.52 °E) is chosen as a central city of Thailand with the highest number of factories *(in Chapter 5)*. Its weather data was taken as input data for system simulations, consisting of total average solar radiation on the tilted surface (kWh/m^2-day) and ambient temperature (°C) [114] which are shown in APPENDIX B Solar Radiation and Ambient Temperature. The system was modeled and evaluated for an optimal hot water flow rate passing through the SORC system when the maximum power output was achieved. The calculation step was presented in Figure 6-5. The hot water flow rate (Ton/h) from the performance characteristics of the ORC power generation shown in Table 6-1 (a 20

kW_e ORC from IHI Company) and Table 6-2 (a 60 kW_e ORC from KOBELCO Company) were obtained. In order to obtain the optimal hot water flow rate supplied to the collector field, it was varied between the minimum and maximum allowed by the ORC system (increments were in the order of 1 Ton/h). For the system at hand it would be a flow rate of 12 to 28 Ton/h for a 20 kW_e ORC from IHI Company, and 25 to 75 Ton/h for a 60 kW_e ORC from KOBELCO Company. At this step is also possible to calculate the heat input to the ORC system ($\dot{Q}_{ORC}$) and the collectors outlet ($T_{Coll,o}$) or the ORC inlet hot water temperature ($T_{ORC,i}$) from the hot water flow rate obtained. After that, to find out the power output (kW_e) of the system, interpolation on the data presented in the performance characteristics of the ORC power generation (Table 6-1 and Table 6-2) was used in combination to the hot water flow rate and temperature found in the previous step and the cooling water temperature (°C). Finally, the system simulation will select the hot water flow rate that achieves the highest power output during the system operation. In the system simulations heat loss from the system such as the piping system was neglected. Beside to that, the power input of the collector pump as shown in Figure 6-1 was neglected.

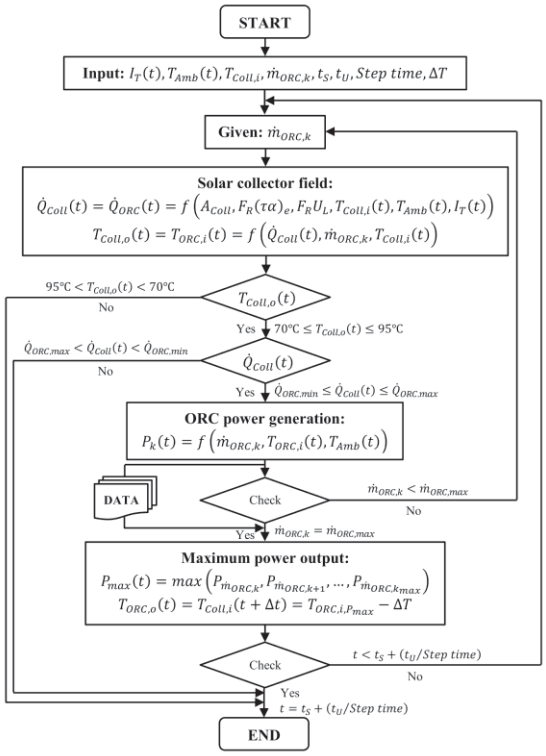

Figure 6-5 Step to evaluate the maximum power output on the optimal hot water flow rate

6.4 Economic Analysis

In this Chapter, also the economic analysis in terms of the LCOE was done as shown in Eq. (2-78) and (2-79). In this assessment, the initial conditions of the system are shown in Table 6-3. Investment cost of a small-scale ORC power plant was set at around 2500 USD/kW_e *(in Chapter 5)*. The economic analysis considered two cases; *(i) with initial investment of the collectors* that models a new consumer and *(ii) without initial investment of the collectors* in this case, the collectors were assumed to be partially subsidized by the government [32], as detailed in Section 5.4 Economic Analysis.

Table 6-3 Initial economic condition of the small-scale SORC power system

Descriptions	Data
Operation time *(6.00 am. to 6.00 pm.)*, (hour/day)	12
Operation day, (day/year)	353
Cost of solar collectors (USD/m^2)	
Flat-plate (FP) solar collectors	112.3
Evacuated-tube (ET) solar collectors	154.4
CPC solar collectors	196.5
Construction and engineering, (%)	10
O&M cost (% of investment cost per year)	5
Annual insurance rate, $k_{insurance}$ (%/year)	0.6
Real debt interest rate, i_d (%)	7.325
Depreciation period, n (year)	25

6.5 Results and Discussion

In this Chapter, a small-scale SORC power plant with low-temperature heat (<100 °C) was proposed and investigated. Four different ORC capacities with different collectors (FP, ET, and CPC) are designated as (i) SORC-I, (ii) SORC-II, (iii) SORC-III, and (iv) SORC-IV. Their performance in Bangkok, Thailand was mathematically evaluated in terms of power output, CO_2 reduction, and the LCOE as shown in the following:

6.5.1 Power Output

For the calculations of power output (MWh/Year) the solar collectors (from 100 to 1200 units) of each type were used for hot water production paired with each ORC configuration (SORC-I, SORC-II, SORC-III, and SORC-IV). The results are shown in Table 6-4, Figure 6-8 and Figure 6-9, *(the ORC system stops when the hot water temperature is over 95 °C)*. It found that the large amounts of the collectors were obtainable and higher the capacities of the ORC system, the more electricity of a system were generated. In addition, the maximum power output of ORC power system, it depend on the appropriated number of solar collectors. It also showed that each system configuration can produce the maximum power output based on the suitable numbers of the collectors as follows: 26.3, 53.2, 81.1, and 90.4 MWh/Year, which requires 400, 750, 1150, and 1050 units of FP collectors, 36.0, 72.3, 108.7, and 113.5 MWh/Year with 350, 700, 1050, and 950 units of ET collectors, and 35.2, 70.6, 106.2, and 111.4 MWh/Year, with 300, 600, 900, and 800 units of CPC collectors, respectively. However, when the power output of the same ORC power capacity (total capacity of 60 kW_e) with the same number of the collectors (the SORC-III and the SORC-IV) is compared, it was found that the SORC-IV generated more electricity than that of the SORC-III because of higher thermal efficiency of the ORC-IV as shown in Figure 6-7, *(the SWHS stops when the hot water temperature is over 95 °C)*. Moreover, as shown in Figure 6-6, with the same number of the collectors and without initial investment of them, the SORC power plant with CPC collectors can produce the highest power output. Moreover, from the above results, the power output of the SORC power system was the highest of 113.5 MWh/Year, when 950 units of ET collectors combined with a 60 kW_e ORC.

Table 6-4 Maximum and minimum power output (MWh/Year) of different ORC system capacity integrated by different collectors from 100 to 1200 units *(Inconstant hot water flow rate and the ORC stops when the hot water temperature is over 95 °C)*

Collectors (Units)	FP-SORC				ET-SORC				CPC-SORC			
	I	II	III	IV	I	II	III	IV	I	II	III	IV
100												
150									4.9			
200					10.1				17.5			
250	11.6				21.6				28.3			
300	18.8				31.2				**35.2**			8.5
350	23.8				**36.0**				27.8	20.3		20.1
400	**26.3**			10.1	27.3	20.4		20.3		35.4		39.4
450	23.1	16.3		17.1		33.8		37.3		46.0		52.6
500		23.3		26.6		43.7		53.7		56.9		66.6
550		32.4		37.3		53.6		63.0		64.7		79.1
600		37.7		43.6		62.6		73.6		**70.6**		85.8
650		43.3		48.8		67.4		82.1		63.1	64.2	91.5
700		47.9		56.1		**72.3**		88.0			76.3	97.7
750		**53.2**		63.2		62.3	65.7	93.0			85.5	105.0
800		52.8	46.2	67.3			77.3	98.2			96.5	**111.4**
850			52.1	71.5			83.5	104.9			100.3	104.2
900			56.7	77.2			94.2	110.0			**106.2**	
950			61.1	83.3			99.2	**113.5**			99.8	
1000			66.9	86.8			104.6	100.0				
1050			72.0	**90.4**			**108.7**					
1100			77.8	82.1			94.8					
1150			**81.1**									
1200			79.3									

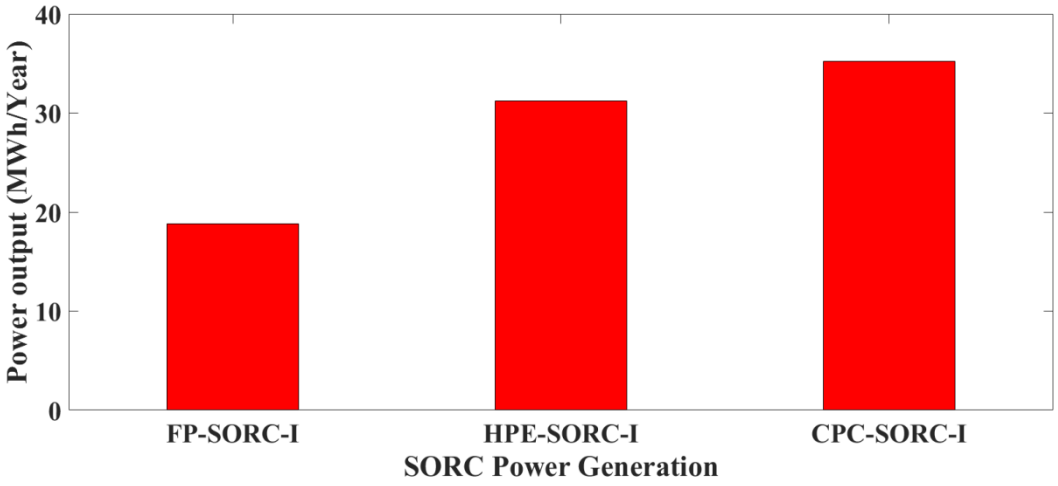

Figure 6-6 Comparisons of power output of FP-SORC-I, HPE-SORC-I, and CPC-SORC-I, when the number of solar collectors is 300 units *(Inconstant hot water flow rate)*

The results obtained showed that at each combination system all the systems had lower and higher limit numbers of solar collectors (see Table 6-4). For example, with one unit of a 20 kW_e ORC power generation (total capacity of 20 kW_e), the system can produce a minimum and maximum power output of 11.6 and 26.3 MWh/Year with 250 and 400 units of FP collectors, respectively. Another example, with one unit of a 60 kW_e ORC power generation (total capacity of 60 kW_e), the system can produce a minimum and maximum power output of 8.5 and 111.4 MWh/Year with 300 and 800 units of CPC collectors,

respectively. It was observed that the system cannot produce electricity when the numbers of solar collectors were at lower and higher limits. Furthermore, the large amount of solar collectors is not required when the number of solar collectors is at higher limit.

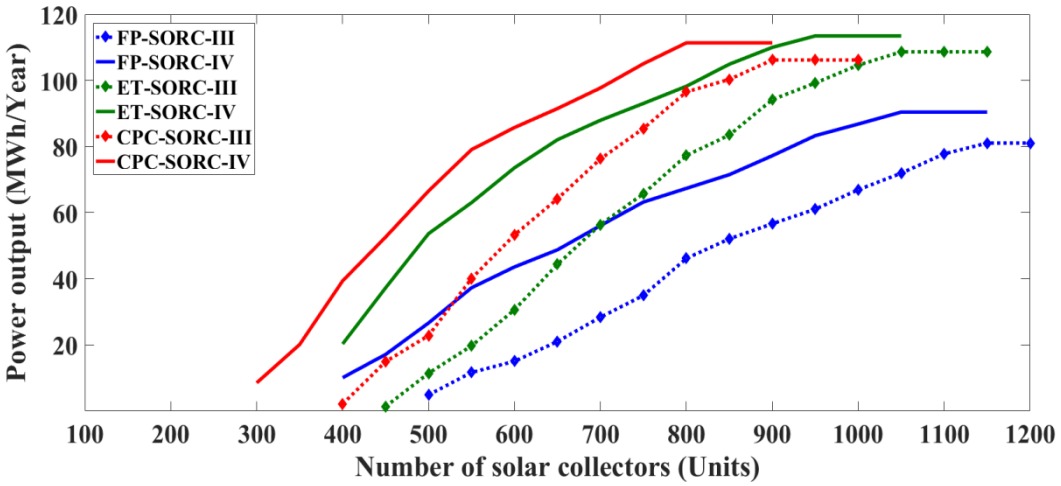

Figure 6-7 Power output (MWh/Year) of the SORC-III and the SORC-IV with increment of the collectors from 100 to 1200 units *(Inconstant hot water flow rate, and the SWHS stops when the hot water temperature is over 95 °C)*

In Figure 6-8 and Figure 6-9 *(M: Mathematical model and F: Fit curves)*, taking the data from Table 6-4, the power output (MWh/Year) of four different models of stationary solar collectors can be viewed. Using this information, a simplified formula to find out the power output of each model of stationary solar collectors can be created as shown in Eq. (6-1) to (6-12). Moreover, it can be further simplified into a single equation to estimate the power output of small-scale SORC power plant, as shown in Eq. (6-13).

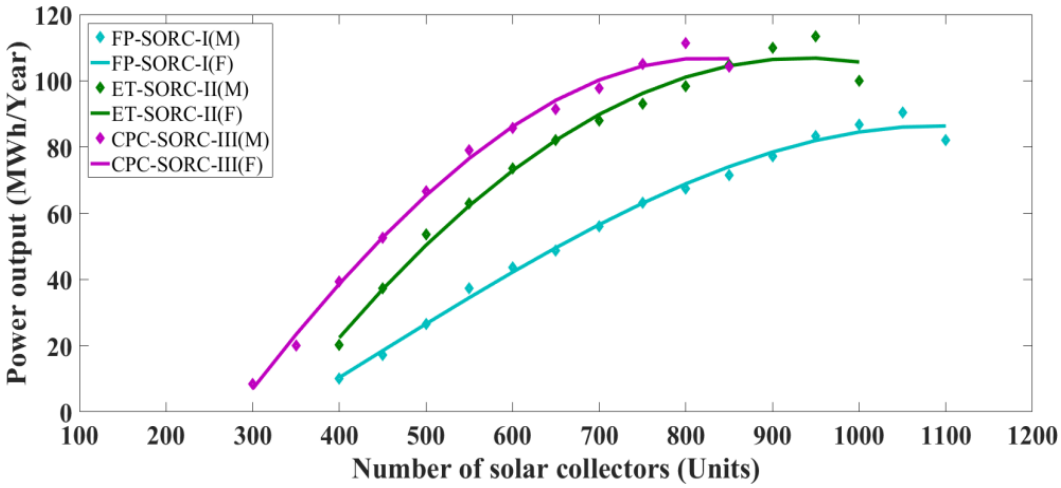

Figure 6-8 The highest power output (MWh/Year) of the SORC-IV *(M: Mathematical model and F: Fit curves)* when the number of solar collectors increases from 100 to 1200 units, with three different collectors (FP, ET, and CPC solar collectors) *(Inconstant hot water flow rate, and the ORC system stops when the hot water temperature is over 95 °C)*

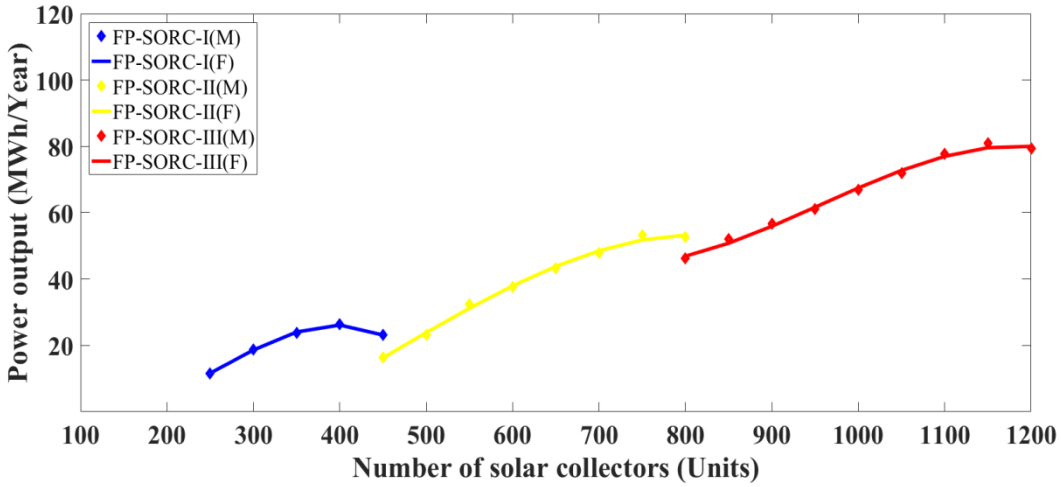

(a) FP-SORC power system

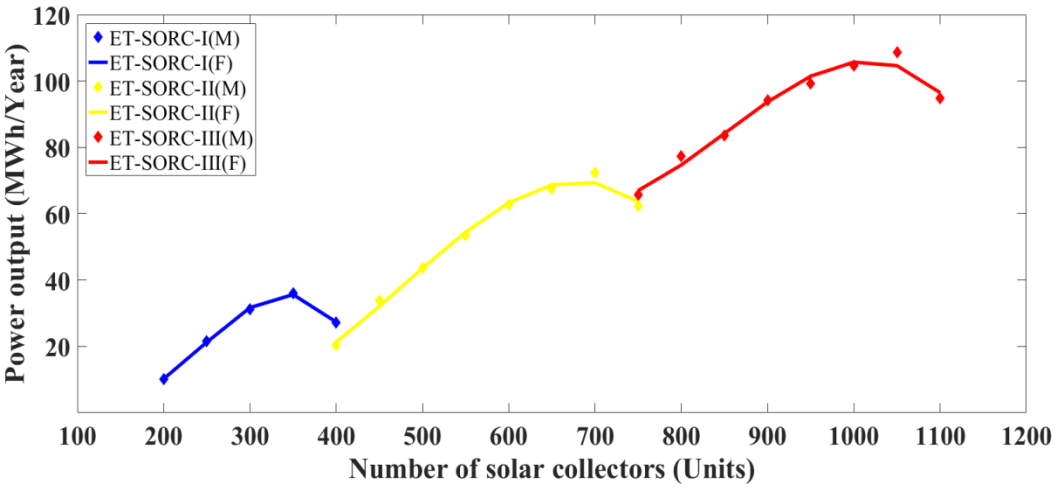

(b) ET-SORC power system

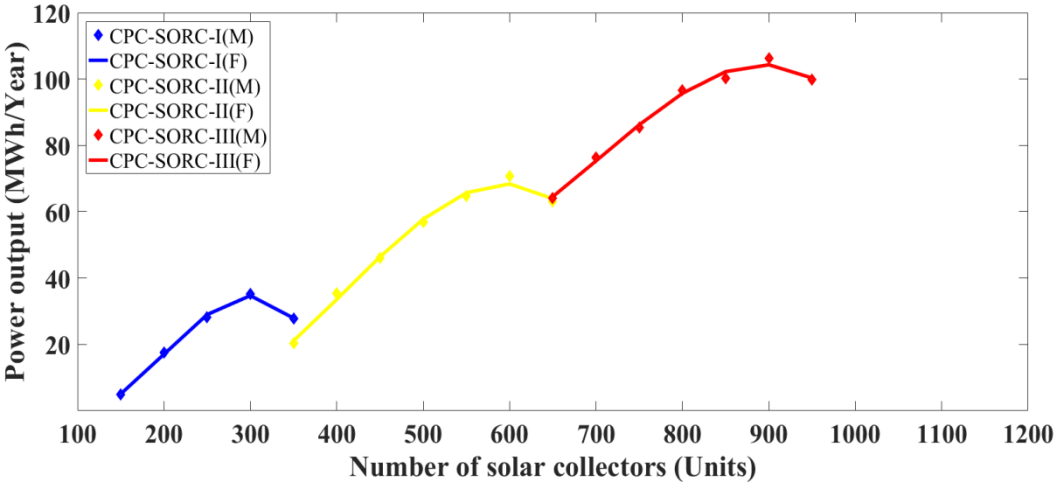

(c) CPC-SORC power system

Figure 6-9 The highest power output (MWh/Year) of the SORC-I, SORC-II, and SORC-III *(M: Mathematical model and F: Fit curves)* when the number of solar collectors increases from 100 to 1200 units, with three different collectors (FP, ET, and CPC solar collectors) *(Inconstant hot water flow rate, and the ORC system stops when the hot water temperature is over 95 °C)*

- **SORC-I, SORC-II, and SORC-III**

FP-SORC power generation ($P_{FP-SORC}$):

$$P_{FP-SORC-I} = (-2.3738 \times 10^{-6})N_{Coll}^3 + (0.001825)N_{Coll}^2 + (-0.32383)N_{Coll} + (15.606) \quad (6\text{-}1)$$

$$P_{FP-SORC-II} = (-3.9758 \times 10^{-7})N_{Coll}^3 + (0.00054118)N_{Coll}^2 + (-0.092643)N_{Coll} + (-15.4) \quad (6\text{-}2)$$

$$P_{FP-SORC-III} = (-7.5296 \times 10^{-7})N_{Coll}^3 + (0.0021586)N_{Coll}^2 + (-1.9454)N_{Coll} + (607.23) \quad (6\text{-}3)$$

ET-SORC power generation ($P_{ET-SORC}$):

$$P_{ET-SORC-I} = (-7.715 \times 10^{-6})N_{Coll}^3 + (0.0056534)N_{Coll}^2 + (-1.1462)N_{Coll} + (75.046) \quad (6\text{-}4)$$

$$P_{ET-SORC-II} = (-1.8618 \times 10^{-6})N_{Coll}^3 + (0.0026659)N_{Coll}^2 + (-1.041)N_{Coll} + (130.32) \quad (6\text{-}5)$$

$$P_{ET-SORC-III} = (-2.3557 \times 10^{-6})N_{Coll}^3 + (0.0060082)N_{Coll}^2 + (-4.9119)N_{Coll} + (1365.1) \quad (6\text{-}6)$$

CPC-SORC power generation ($P_{CPC-SORC}$):

$$P_{CPC-SORC-I} = (-8.3274 \times 10^{-6})N_{Coll}^3 + (0.0049954)N_{Coll}^2 + (-0.73862)N_{Coll} + (31.564) \quad (6\text{-}7)$$

$$P_{CPC-SORC-II} = (-2.5091 \times 10^{-6})N_{Coll}^3 + (0.0030848)N_{Coll}^2 + (-1.0037)N_{Coll} + (102.06) \quad (6\text{-}8)$$

$$P_{CPC-SORC-III} = (-2.0482 \times 10^{-6})N_{Coll}^3 + (0.0043263)N_{Coll}^2 + (-2.8242)N_{Coll} + (634.91) \quad (6\text{-}9)$$

- **SORC-IV**

FP-SORC-IV power generation ($P_{FP-SORC-IV}$):

$$P_{FP-SORC-IV} = (-1.2346 \times 10^{-7})N_{Coll}^3 + (0.0001581)N_{Coll}^2 + (0.094835)N_{Coll} - 44.952 \quad (6\text{-}10)$$

ET-SORC-IV power generation ($P_{ET-SORC-IV}$):

$$P_{ET-SORC-IV} = (-3.1012 \times 10^{-8})N_{Coll}^3 + (-0.00022158)N_{Coll}^2 + (0.49732)N_{Coll} - 139.07 \quad (6\text{-}11)$$

CPC-SORC-IV power generation ($P_{CPC-SORC-IV}$):

$$P_{CPC-SORC-IV} = (-1.5106 \times 10^{-7})N_{Coll}^3 + (-6.704 \times 10^{-5})N_{Coll}^2 + (0.41958)N_{Coll} - 108.8 \quad (6\text{-}12)$$

- **SORC Power system**

SORC power generation (P_{SORC}):

$$P_{SORC} = a + bN_{Coll} + cN_{Coll}^2 + dN_{Coll}^3 + eN_{Coll}^4 + fN_{Coll}^5 \quad (6\text{-}13)$$

when

$$a = (A_0) + (A_1)\eta_{Sys} + (A_2)\eta_{Sys}^2 + (A_3)\eta_{Sys}^3 + (A_4)\eta_{Sys}^4 + (A_5)\eta_{Sys}^5$$

$$b = (B_0) + (B_1)\eta_{Sys} + (B_2)\eta_{Sys}^2 + (B_3)\eta_{Sys}^3 + (B_4)\eta_{Sys}^4 + (B_5)\eta_{Sys}^5$$

$$c = (C_0) + (C_1)\eta_{Sys} + (C_2)\eta_{Sys}^2 + (C_3)\eta_{Sys}^3 + (C_4)\eta_{Sys}^4 + (C_5)\eta_{Sys}^5$$

$$d = (D_0) + (D_1)\eta_{Sys} + (D_2)\eta_{Sys}^2 + (D_3)\eta_{Sys}^3 + (D_4)\eta_{Sys}^4 + (D_5)\eta_{Sys}^5$$

$$e = (E_0) + (E_1)\eta_{Sys} + (E_2)\eta_{Sys}^2 + (E_3)\eta_{Sys}^3 + (E_4)\eta_{Sys}^4 + (E_5)\eta_{Sys}^5$$

$$f = (F_0) + (F_1)\eta_{Sys} + (F_2)\eta_{Sys}^2 + (F_3)\eta_{Sys}^3 + (F_4)\eta_{Sys}^4 + (F_5)\eta_{Sys}^5$$

where P_{SORC} is the power output (MWh/Year). η_{Sys} is overall system efficiency (%), which is the maximum power output that the system can generate divided by the thermal energy input depends on the number of solar collector (Unit), solar collectors area (A_{Coll}), and solar radiation (I_T). In the Eq. (6-13), the overall system efficiency (η_{Sys}) and the

number of solar collectors (N_{Coll}) varies from 11.6 to 22.8, and 200 to 1200 units, respectively. The variables A, B, C, D and F are shown in Table 6-5.

Table 6-5 The variables value of A, B, C, D and F

	A	B	C
0	$2862.91\times10^{+05}$	$-2828.88\times10^{+03}$	$1454.53\times10^{+01}$
1	$-8394.99\times10^{+04}$	$8221.99\times10^{+02}$	$-4287.40\times10^{+00}$
2	$9605.96\times10^{+03}$	$-9305.24\times10^{+01}$	4942.58×10^{-01}
3	$-5364.89\times10^{+02}$	$5126.53\times10^{+00}$	-2787.77×10^{-02}
4	$1464.44\times10^{+01}$	-1375.93×10^{-01}	7703.61×10^{-04}
5	-1565.56×10^{-01}	1440.68×10^{-03}	-8357.12×10^{-06}

	D	E	F
0	-3119.89×10^{-02}	2841.70×10^{-05}	-9158.99×10^{-09}
1	9282.96×10^{-03}	-8501.79×10^{-06}	2749.42×10^{-09}
2	-1082.79×10^{-03}	9983.24×10^{-07}	-3241.50×10^{-10}
3	6195.16×10^{-05}	-5757.19×10^{-08}	1878.04×10^{-11}
4	-1741.07×10^{-06}	1632.69×10^{-09}	-5353.87×10^{-13}
5	1925.77×10^{-08}	-1824.22×10^{-11}	6016.18×10^{-15}

Figure 6-10 to Figure 6-21 presents the fluctuation of the hourly hot water flow rate (kg/s), hot water temperature (°C), and power output (kW_e) versus the time and months of each system that can generate the highest electricity. The FP-SORC-I, the FP-SORC-II, the FP-SORC-III, and the FP-SORC-IV can generate the highest electricity with 400, 750, 1150, and 1050 units of the FP collectors, respectively. The ET-SORC-I, the ET-SORC-II, the ET-SORC-III, and ET-SORC-IV can generate the highest electricity with 350, 700, 1050, and 950 units of the ET collectors, respectively. The CPC-SORC-I, the CPC-SORC-II, the CPC-SORC-III, and the CPC-SORC-IV can generate the highest electricity with 300, 600, 900, and 800 units of the CPC collectors, respectively.

It can be seen that when the CPC collectors are combined with the ORC system, the collectors outlet temperature or the ORC inlet hot water temperature could be maintained at around 95 °C during the system operation, due to the efficiency of CPC collectors a slight decrease occurs when the collector inlet hot water increases *(in Chapter 5)*, nevertheless it can be concluded that the highest power generation achievable occurs when using this kind of collectors are used.

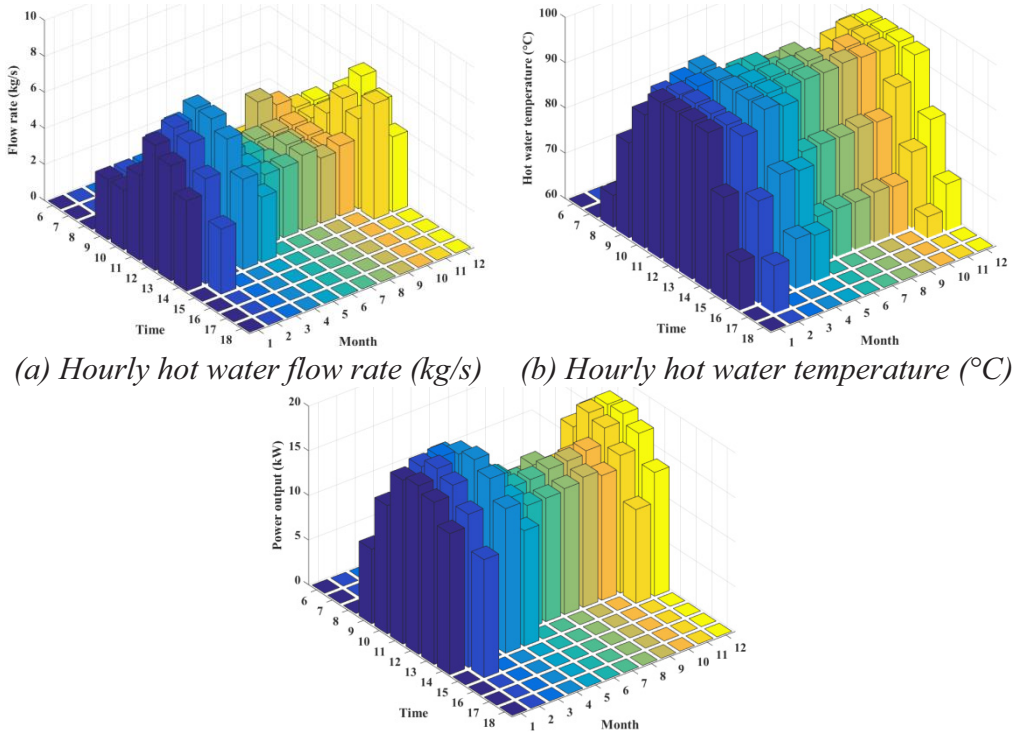

(a) Hourly hot water flow rate (kg/s) *(b) Hourly hot water temperature (°C)*

(c) Hourly power output (kW_e)

Figure 6-10 Hourly hot water flow rate, hot water temperature, and power output of the FP-SORC-I: *400 units of FP collectors combined with a 20 kW_e ORC system*

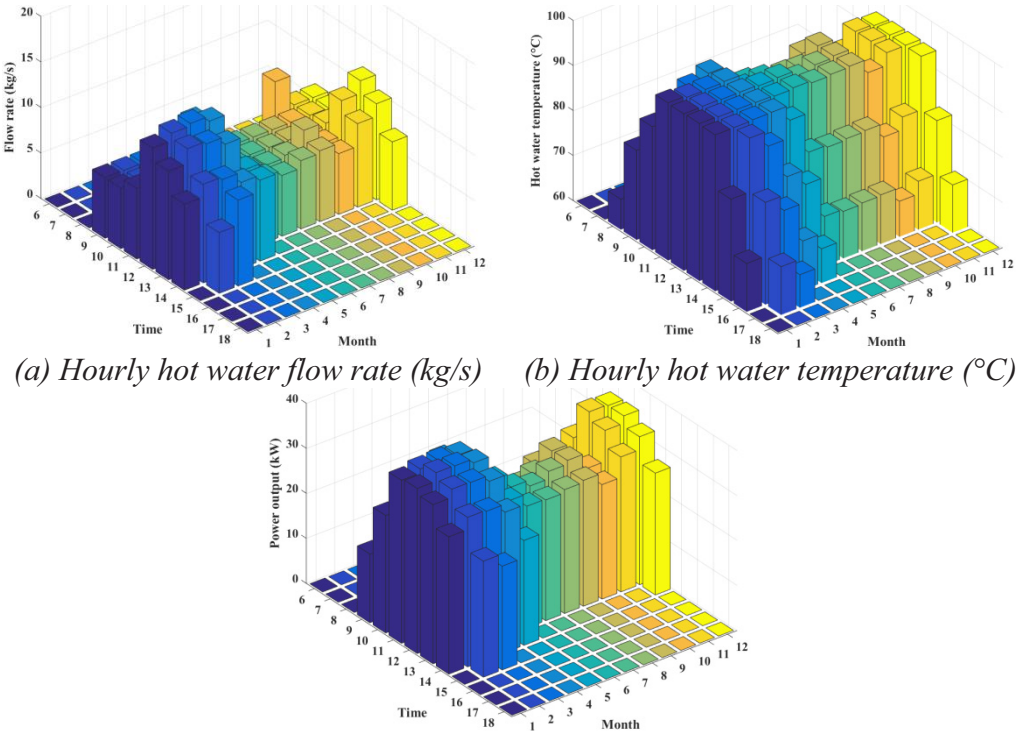

(a) Hourly hot water flow rate (kg/s) *(b) Hourly hot water temperature (°C)*

(c) Hourly power output (kW_e)

Figure 6-11 Hourly hot water flow rate, hot water temperature, and power output of the FP-SORC-II: *750 units of FP collectors combined with two unit of a 20 kW_e ORC system*

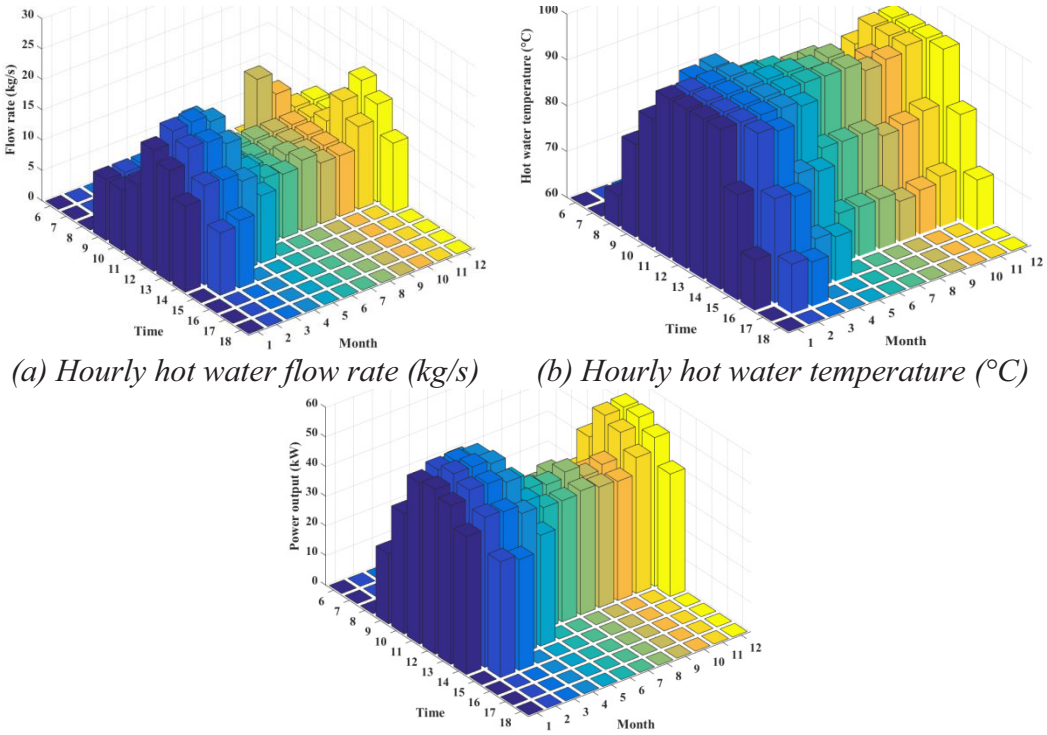

(a) Hourly hot water flow rate (kg/s) *(b) Hourly hot water temperature (°C)*

(c) Hourly power output (kW_e)

Figure 6-12 Hourly hot water flow rate, hot water temperature, and power output of the FP-SORC-III: *1150 units of FP collectors combined with three unit of a 20 kW_e ORC system*

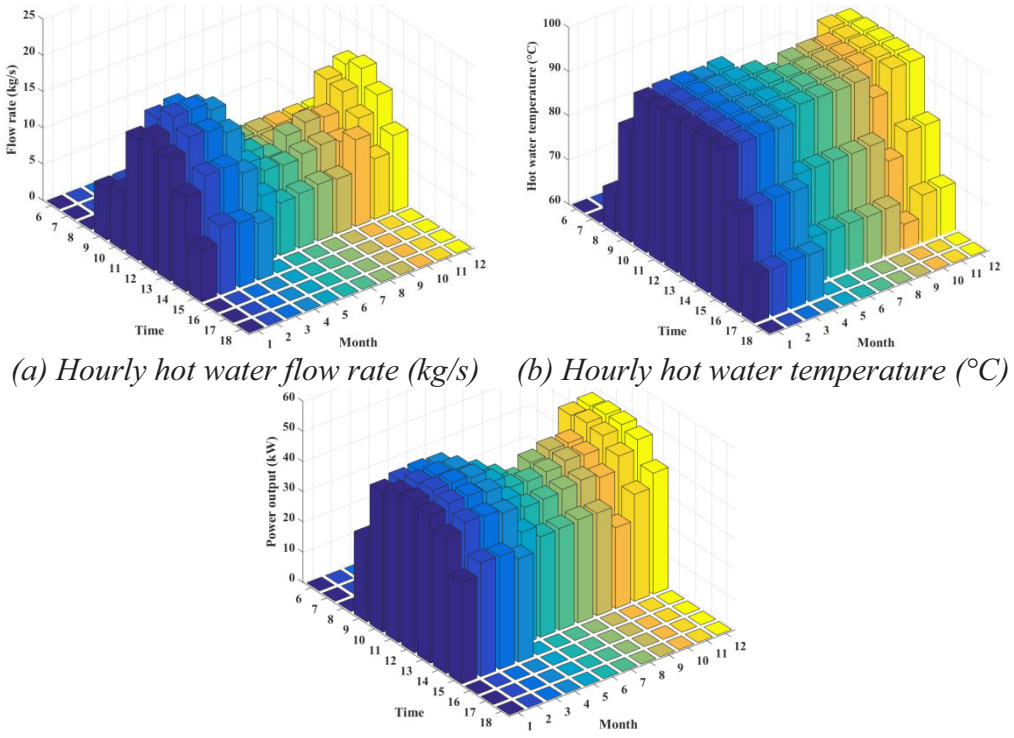

(a) Hourly hot water flow rate (kg/s) *(b) Hourly hot water temperature (°C)*

(c) Hourly power output (kW_e)

Figure 6-13 Hourly hot water flow rate, hot water temperature, and power output of the FP-SORC-IV: *1050 units of FP collectors combined with a 60 kW_e ORC system*

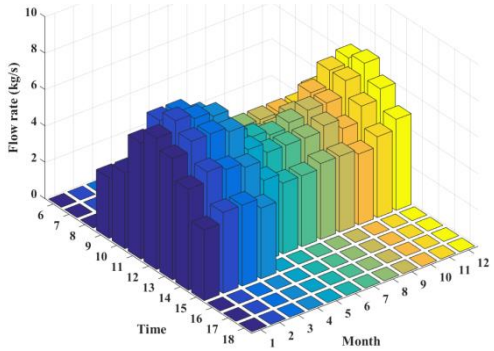

(a) Hourly hot water flow rate (kg/s)

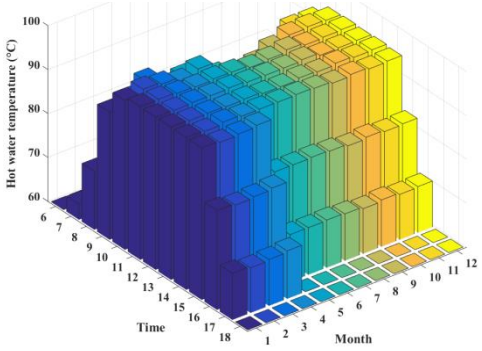

(b) Hourly hot water temperature (°C)

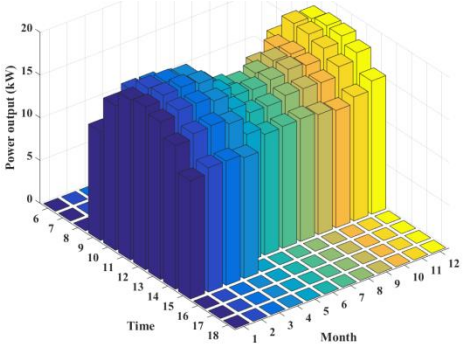

(c) Hourly power output (kW_e)

Figure 6-14 Hourly hot water flow rate, hot water temperature, and power output of the ET-SORC-I: *350 units of ET collectors combined with a 20 kW_e ORC system*

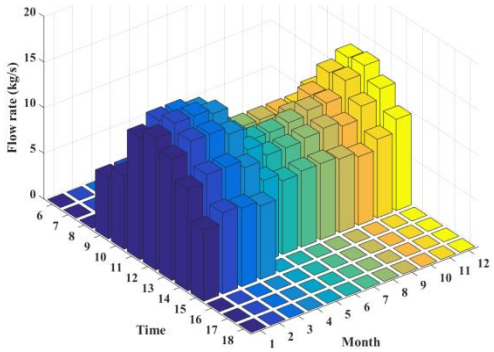

(a) Hourly hot water flow rate (kg/s)

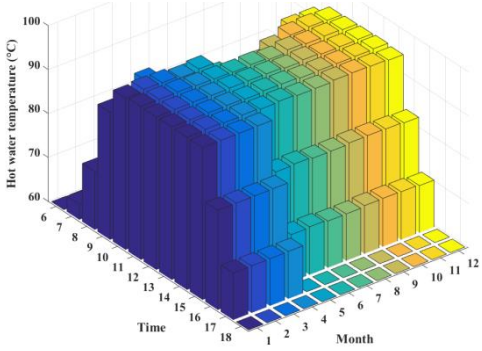

(b) Hourly hot water temperature (°C)

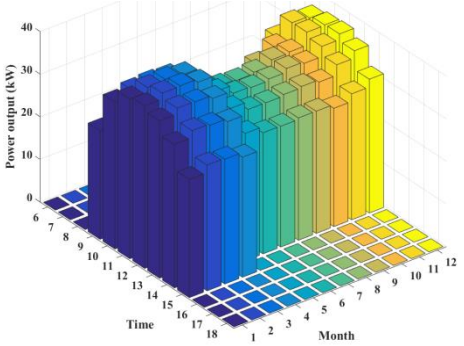

(c) Hourly power output (kW_e)

Figure 6-15 Hourly hot water flow rate, hot water temperature, and power output of the ET-SORC-II: *700 units of ET collectors combined with two units of a 20 kW_e ORC system*

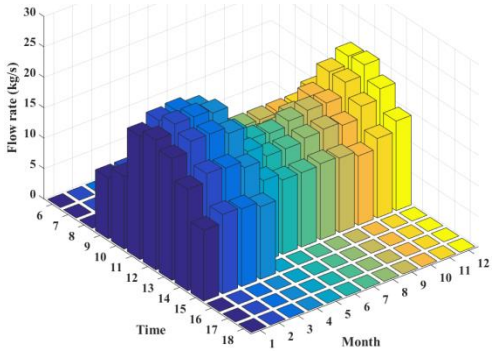

(a) Hourly hot water flow rate (kg/s)

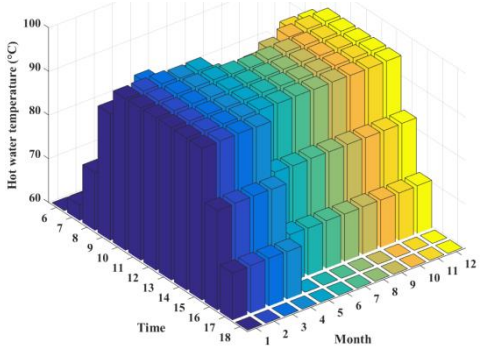

(b) Hourly hot water temperature (°C)

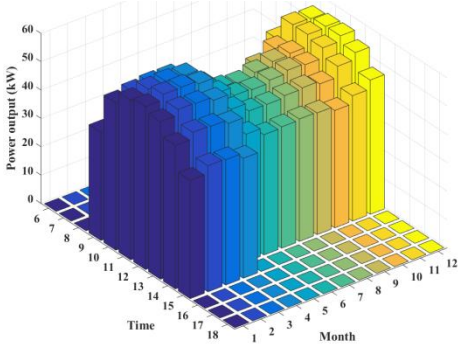

(c) Hourly power output (kW_e)

Figure 6-16 Hourly hot water flow rate, hot water temperature, and power output of the ET-SORC-III: *1050 units of ET collectors combined with three units of a 20 kW_e ORC system*

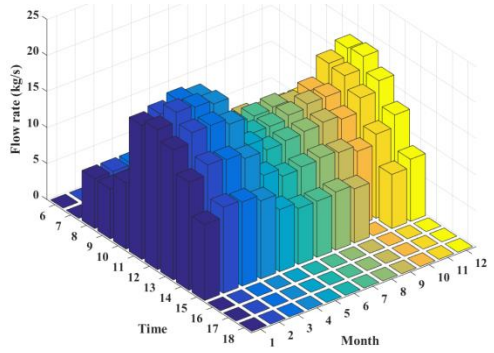

(a) Hourly hot water flow rate (kg/s)

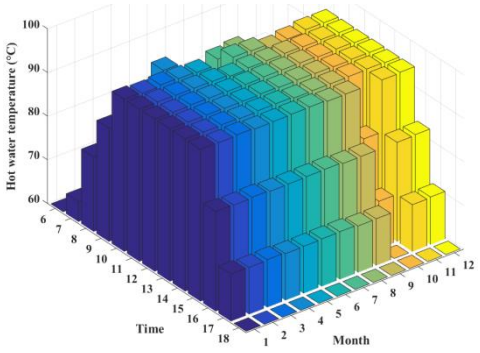

(b) Hourly hot water temperature (°C)

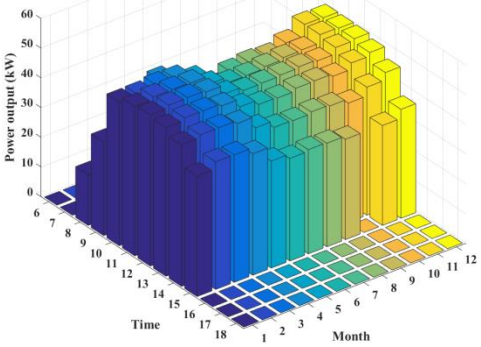

(c) Hourly power output (kW_e)

Figure 6-17 Hourly hot water flow rate, hot water temperature, and power output of the ET-SORC-IV: *950 units of ET collectors combined with a 60 kW_e ORC system*

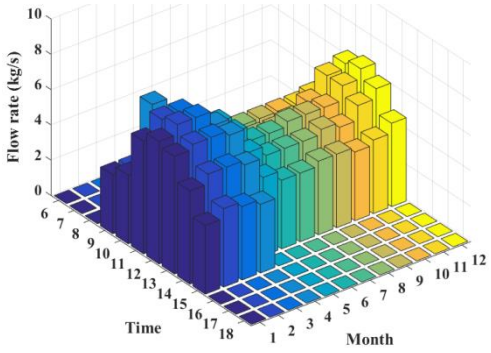

(a) Hourly hot water flow rate (kg/s)

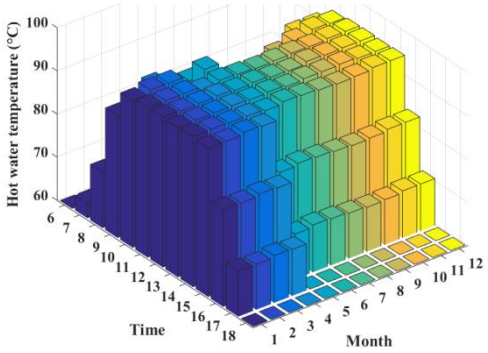

(b) Hourly hot water temperature (°C)

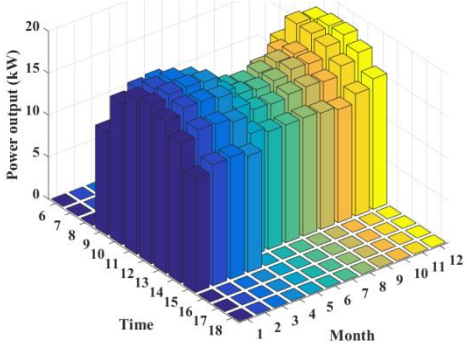

(c) Hourly power output (kW_e)

Figure 6-18 Hourly hot water flow rate, hot water temperature, and power output of the CPC-SORC-I: *300 units of CPC collectors combined with a 20 kW_e ORC system*

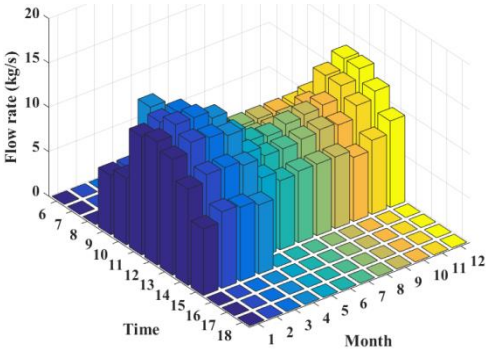

(a) Hourly hot water flow rate (kg/s)

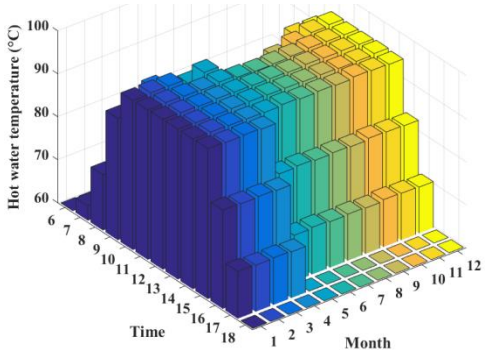

(b) Hourly hot water temperature (°C)

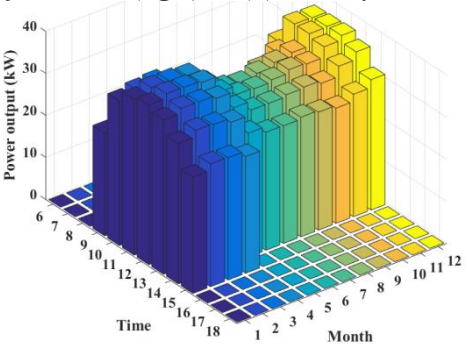

(c) Hourly power output (kW_e)

Figure 6-19 Hourly hot water flow rate, hot water temperature, and power output of the CPC-SORC-II: *600 units of CPC collectors combined with two units of a 20 kW_e ORC system*

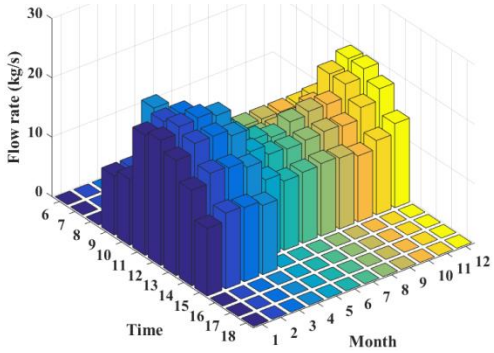

(a) Hourly hot water flow rate (kg/s)

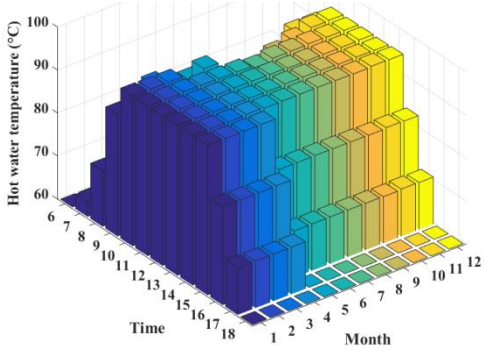

(b) Hourly hot water temperature (°C)

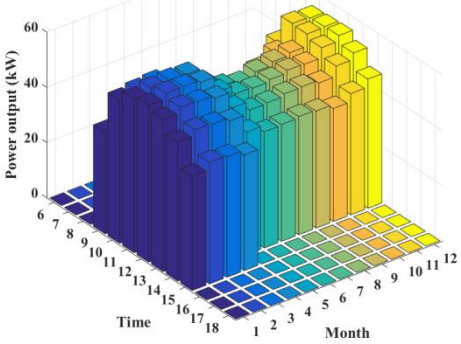

(c) Hourly power output (kW_e)

Figure 6-20 Hourly hot water flow rate, hot water temperature, and power output of the CPC-SORC-III: *900 units of CPC collectors combined with three units of a 20 kW_e ORC system*

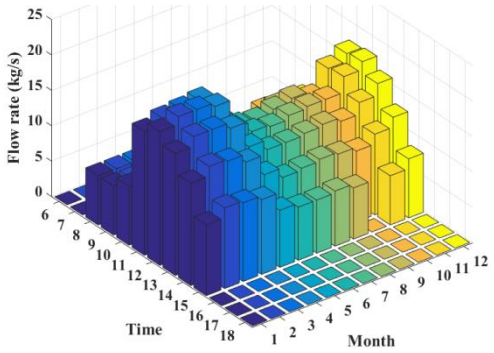

(a) Hourly hot water flow rate (kg/s)

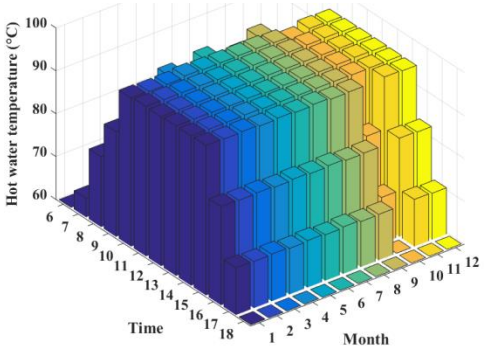

(b) Hourly hot water temperature (°C)

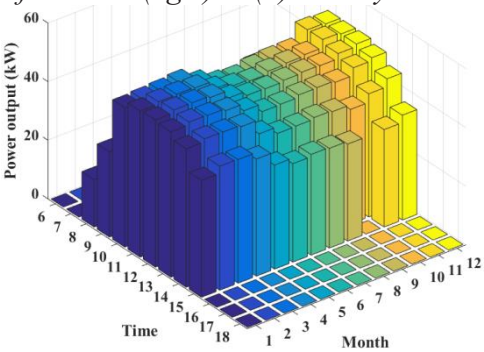

(c) Hourly power output (kW_e)

Figure 6-21 Hourly hot water flow rate, hot water temperature, and power output of the CPC-SORC-IV: 8*00 units of CPC collectors combined with a 60 kW_e ORC system*

Figure 6-22 showed examples of the ORC power output (P_{ORC}), and collector input energy ($\dot{Q}_{Coll}$) of the corresponding combined systems from Figure 6-10 (FP-SORC-I), Figure 6-15 (ET-SORC-II), and Figure 6-21 (CPC-SORC-IV). *In case (a) FP-SORC-I:* the power generated slightly increases in the morning due to the lower numbers of the collectors. *In case (b) ET-SORC-II and (c) CPC-SORC-IV*: the power was generated in both morning and afternoon even though the solar radiation was slightly low due to high numbers of the collectors. Moreover, in case *(c) CPC-SORC-IV*, the power was generated for the longest hours as compared to other systems from 8:00 hs. to 15:00 hs. or 7 hours.

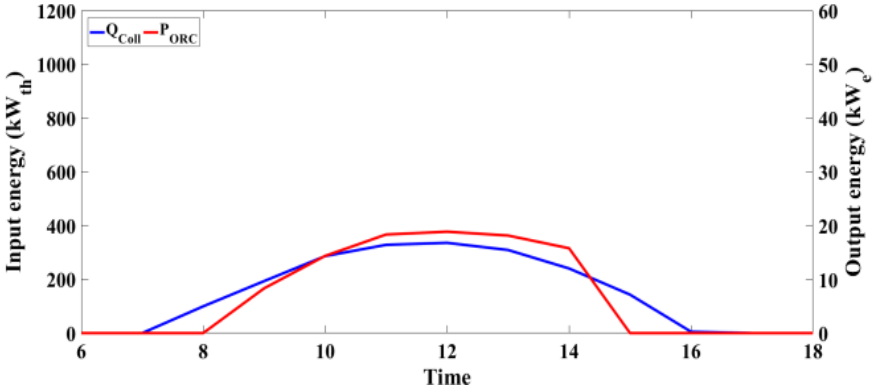

(a) FP-SORC-I (400 units of FP collectors)

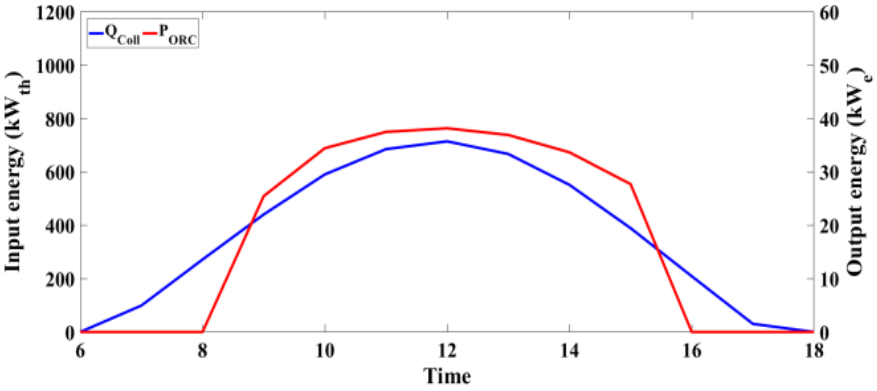

(b) ET-SORC-II (700 units of ET collectors)

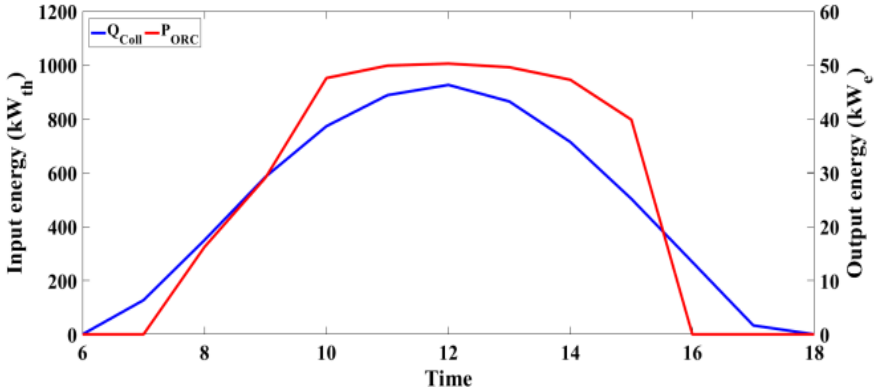

(c) CPC-SORC-IV (800 units of CPC collectors)

Figure 6-22 Power output and Input energy of three systems (FP-SORC-I, ET-SORC-II, and CPC-SORC-IV) on January, Bangkok city, Thailand

6.5.2 Environment Assessment

The results found that, the quantity of CO_2 reduction the system can decrease depends on the electricity production. It can be calculates from Eq. (5-2), where, $Power\ output$ is the electricity (MWh/Year) generated from each system configuration, as shown in Table 6-4, and can be calculated from Eq. (6-1) to Eq. (6-13). It was found, the CO_2 reduction is continuously decreasing when the power output of the system increases as well as the numbers of the collectors, are shown in Figure 6-23 to Figure 6-25, the CO_2 reduction of the FP-SORC, ET-SORC, and CPC-SORC systems, respectively.

Based on the type and the numbers of collectors, power output (MWh/Year) and the CO_2 reduction (Ton CO_2 eq./Year) above, it was found that when the numbers of the collectors are constrained, the system with CPC collectors generated the highest power and achieved the highest reduction of CO_2 emissions as compared with that of other two types of the collectors. For example, when a 20 kW_e ORC power system is combined with 250 units of each collector type (FP, ET, and CPC) having the occupied area of 540.0, 592.5, and 520.0 m^2, respectively, the system can produce electricity of 11.6, 21.6, and 28.3 MWh/Year, and reduce CO_2 emission by 6.4, 11.8, and 15.5 Ton CO_2 eq./Year. With two units of a 20 kW_e ORC power system is combined with 450 units of each collector type (FP, ET, and CPC) having the occupied area of 972.0, 1066.5, and 936.0 m^2, respectively, the system can produce electricity of 16.3, 33.8, and 46.0 MWh/Year, and reduce CO_2 emission by 8.9, 18.5, and 25.2 Ton CO_2 eq./Year. With three units of a 20 kW_e ORC power system is combined with 800 units of each collector type (FP, ET, and CPC) having the occupied area of 1728.0, 1896.0, and 1664.0 m^2, respectively, the system can produce electricity of 46.2, 77.3, and 96.5 MWh/Year, and reduce CO_2 emission by 25.3, 42.4, and 52.9 Ton CO_2 eq./Year. Finally with a 60 kW_e ORC power system is combined with 400 units of each collector type (FP, ET, and CPC) having the occupied area of 864, 948, and 832 m^2, respectively, the system can produce electricity of 10.1, 20.3, and 39.4 MWh/Year, and reduce CO_2 emission by 5.5, 11.1, and 21.6 Ton CO_2 eq./Year.

6.5.3 Economic Assessment

The LCOE was assessed in two cases: with and without initial investment of the collectors explained below:

- **Without Initial Investment of the Collectors**

In this assessment, the objective of this Chapter is to determine the ORC capacity when the maximum power is generated without taking the collector investment into account. The results are shown in Figure 6-26 (a), Figure 6-26 (c) and Table 6-6. An analytical summary of each system configurations with varying the number of collectors is discussed as follows:

FP-SORC power system: when the numbers of FP collectors is between 250 and 600 units, they should be combined with a 20 kW_e ORC because its LCOE was lower as compared with other ORC capacities. The lowest LCOE of the system obtained was 0.292 USD/kWh, with 400 collectors. From 600 to 800 collectors, they should be combined with two units of a 20 kW_e ORC. The lowest LCOE of the system obtained was 0.289 USD/kWh, with 750 collectors. Finally from 800 to 1200 collectors, the system should be combined with

one unit of a 60 kW_e ORC. The lowest LCOE of the system obtained was 0.255 USD/kWh, with 1050 collectors.

ET-SORC power system: when the numbers of ET collectors is between 200 and 450 units, they should be combined with a 20 kW_e ORC because its LCOE was lower as compared with other ORC capacities. The lowest LCOE of the system obtained was 0.214 USD/kWh, with 350 collectors. From 450 to 750 collectors, they should be combined with two units of a 20 kW_e ORC. The lowest LCOE of the system obtained was 0.213 USD/kWh, with 700 collectors. Finally from 750 to 1200 collectors, the system should be combined with one unit of a 60 kW_e ORC. The lowest LCOE of the system obtained was 0.203 USD/kWh, with 950 collectors.

CPC-SORC power system: when the numbers of CPC collectors is between 150 and 400 units, they should be combined with a 20 kW_e ORC because its LCOE was lower as compared with other ORC capacities. The lowest LCOE of the system obtained was 0.218 USD/kWh, with 300 collectors. From 400 to 650 collectors, they should be combined with two units of a 20 kW_e ORC. The lowest LCOE of the system obtained was 0.218 USD/kWh, with 600 collectors. Finally from 650 to 1200 collectors, the system should be combined with one unit of a 60 kW_e ORC. The lowest LCOE of the system obtained was 0.207 USD/kWh, with 800 collectors.

As mentioned, the LCOE of the SORC power plant was the lowest of 0.203 USD/kWh, when 950 units of ET collectors combined with one unit of a 60 kW_e ORC. It can also be concluded into three cases; *Case I: if 100 to 400 units of collectors are available,* the maximum power output can be obtained when combined with a 20 kW_e ORC power generation. *Case II: if 400 to 800 units of collectors are available,* two units of a 20 kW_e ORC power generation are required. *Case III: if 800 to 1200 units of collectors are available,* one unit of a 60 kW_e ORC power unit is the most appropriate. Moreover, it should be noted that a small-scale SORC power plant with lower temperature less than 100 °C is an interesting system in Thailand.

- **With Initial Investment of the Collectors**

In this economic, the initial investment of the collectors is considered for a small-scale SORC power system. From Figure 6-26 (b), Figure 6-26 (c), and Table 6-7, the results was found that, with *FP-SORC power system configuration:* the LCOE of the FP-SORC-I, the FP-SORC-II, the FP-SORC-III, and FP-SORC-IV was at the lowest of 0.839, 0.796, 0.794, and 0.672 USD/kWh, with 400, 750, 1150, and 1050 units of collectors, respectively. With *ET-SORC power system configuration:* the LCOE of the ET-SORC-I, the ET-SORC-II, the ET-SORC-III, and the ET-SORC-IV was at the lowest of 0.761, 0.757, 0.756, and 0.670 USD/kWh, with 350, 700, 1050, and 900 units of collectors, respectively. With *CPC-SORC power system configuration:* the LCOE of the CPC-SORC-I, the CPC-SORC-II, the CPC-SORC-III, and the CPC-SORC-IV was at the lowest of 0.774, 0.772, 0.770, and 0.676 USD/kWh, with 300, 600, 900, and 800 units of collectors, respectively. Based on the results above, it can be concluded that the LCOE of the SORC power plant was the lowest of 0.670 USD/kWh, when 900 units of ET collectors combined with one unit of a 60 kW_e ORC.

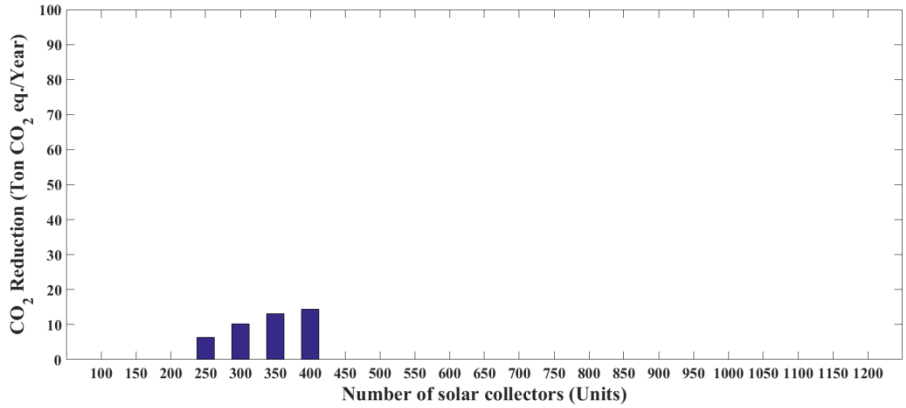

(a) FP-SORC-I

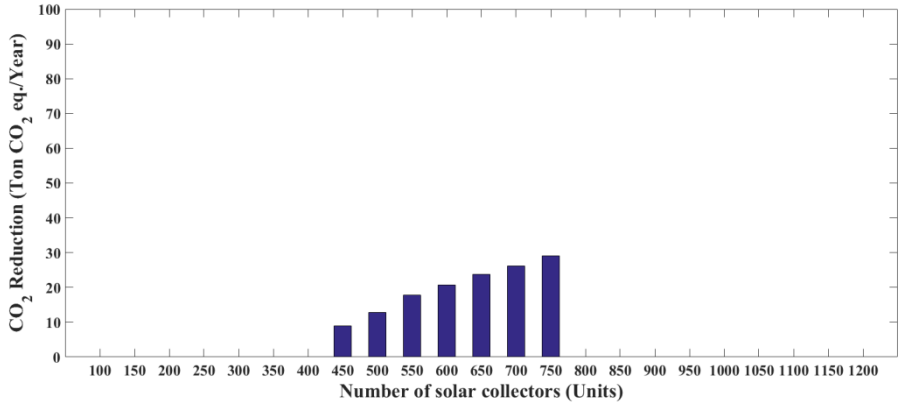

(b) FP-SORC-II

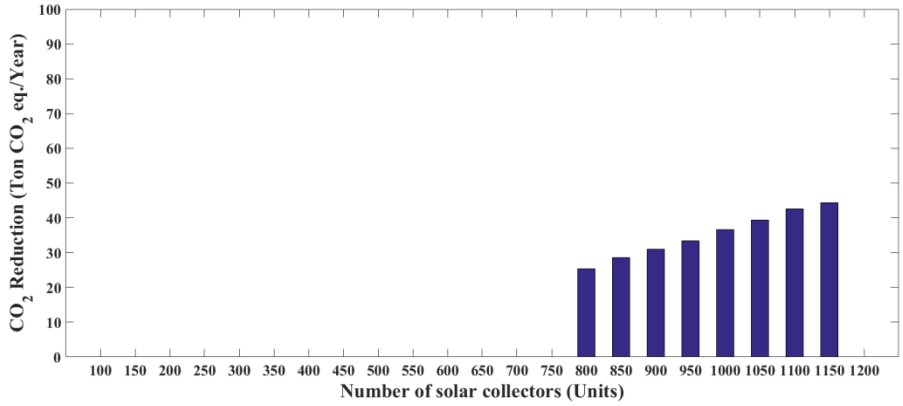

(c) FP-SORC-III

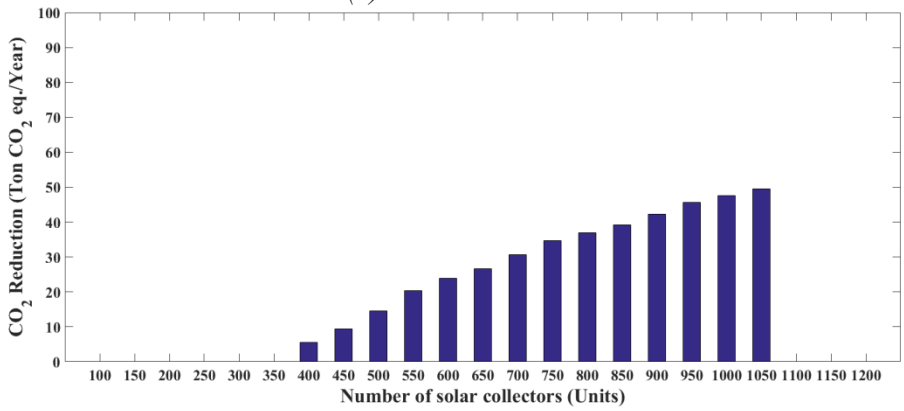

(d) FP-SORC-IV

Figure 6-23 CO_2 reduction of the FP-SORC power system

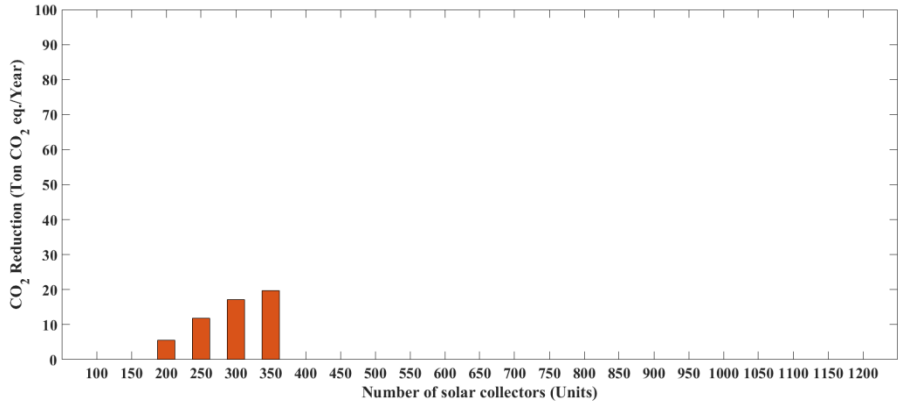

(a) ET-SORC-I

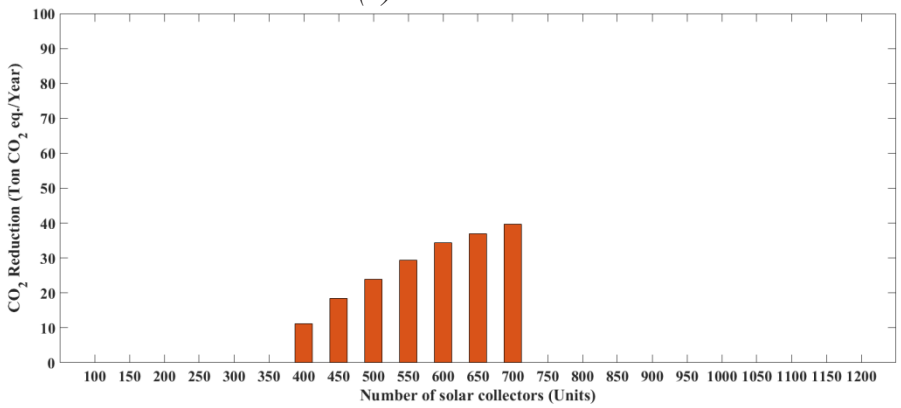

(b) ET -SORC-II

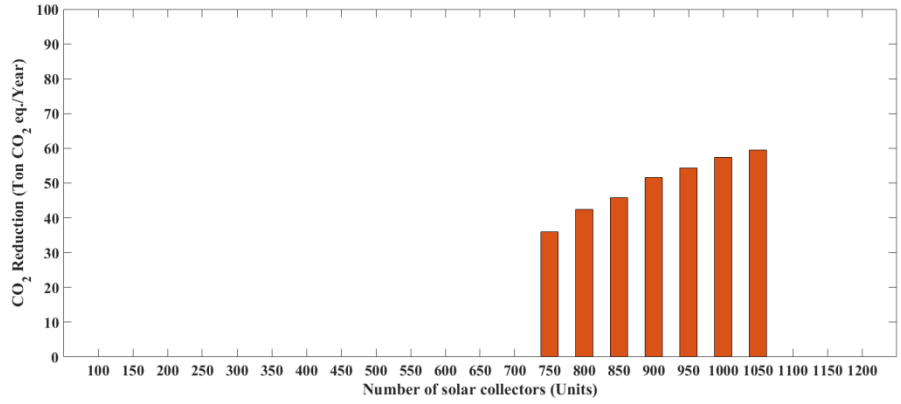

(c) ET -SORC-III

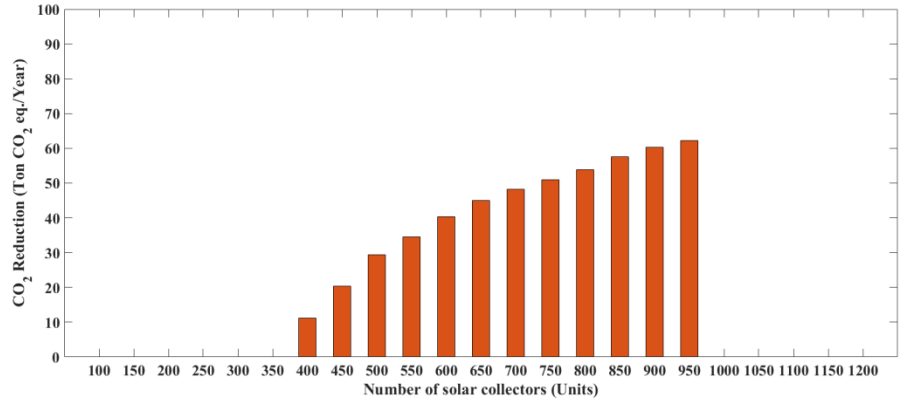

(d) ET -SORC-IV

Figure 6-24 CO_2 reduction of the ET-SORC power system

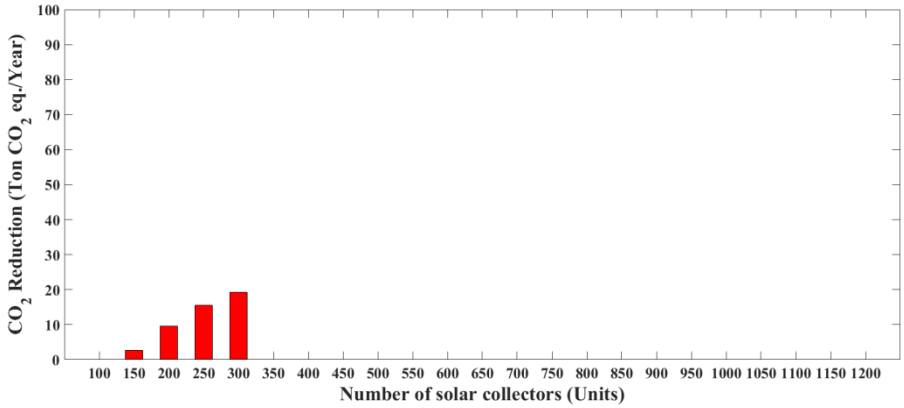

(a) CPC-SORC-I

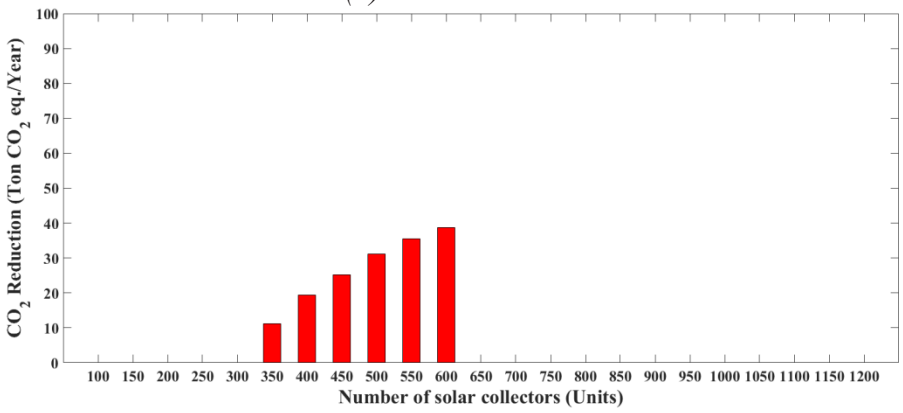

(b) CPC-SORC-II

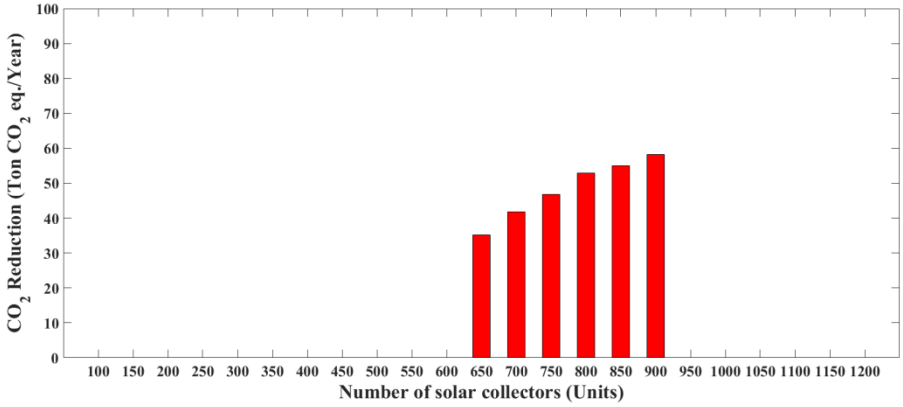

(c) CPC-SORC-III

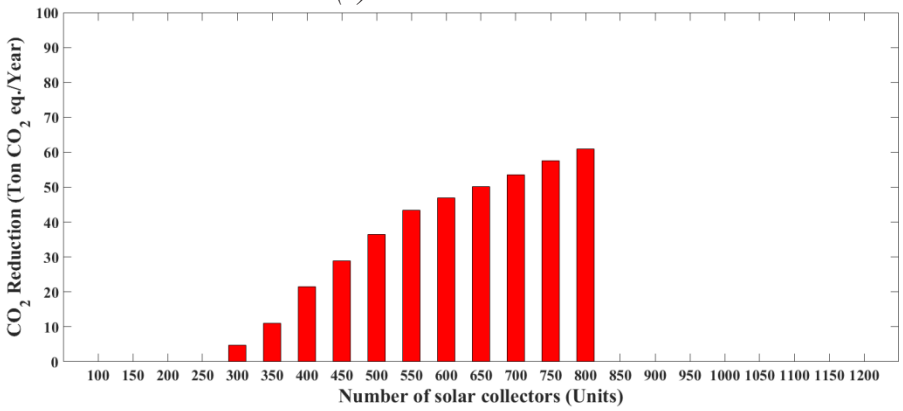

(d) CPC-SORC-IV

Figure 6-25 CO_2 reduction of the CPC-SORC power system

Table 6-6 LCOE (USD/kWh) of the systems *(without initial investment of the collectors)*

Collector (Units)	LCOE (USD/kWh)											
	FP-SORC				ET-SORC				CPC-SORC			
	I	II	III	IV	I	II	III	IV	I	II	III	IV
100												
150									1.556			
200					0.759				0.439			
250	0.664				0.355				0.272			
300	0.410				0.247				**0.218**			2.706
350	0.323				**0.214**				0.276	0.756		1.146
400	**0.293**			2.287	0.282	0.755		1.137	0.316	0.435		0.586
450	0.333	0.942		1.347	0.287	0.455		0.619	0.423	0.335		0.438
500	0.335	0.661		0.866	0.389	0.352		0.430		0.270		0.347
550	0.370	0.475		0.619		0.287		0.366		0.238		0.292
600	0.411	0.408		0.529		0.246		0.313		**0.218**		0.269
650		0.355		0.473		0.228		0.281		0.244	0.359	0.252
700		0.321		0.411		**0.213**		0.262		0.275	0.302	0.236
750		**0.289**		0.365		0.247	0.351	0.248		0.293	0.270	0.220
800		0.292	0.500	0.343		0.281	0.298	0.235			0.239	**0.207**
850		0.316	0.443	0.323			0.276	0.220			0.230	0.222
900		0.332	0.407	0.299			0.245	0.210			**0.217**	
950			0.378	0.277			0.232	**0.203**			0.231	
1000			0.345	0.267			0.221	0.231				
1050			0.321	**0.256**			**0.212**					
1100			0.297	0.281			0.243					
1150			**0.285**									
1200			0.291									

Table 6-7 LCOE (USD/kWh) of the systems *(with initial investment of the collectors)*

Collector (Units)	LCOE (USD/kWh)											
	FP-SORC				ET-SORC				CPC-SORC			
	I	II	III	IV	I	II	III	IV	I	II	III	IV
100												
150									3.538			
200					1.869				1.184			
250	1.439				1.005				0.849			
300	0.985				0.788				**0.774**			5.003
350	0.850				**0.761**				1.097	1.879		2.282
400	**0.839**			3.712	1.107	1.860		2.245	1.392	1.173		1.249
450	1.033	1.933		2.292	1.232	1.205		1.298		0.973		0.997
500	1.118	1.433		1.541		0.995		0.954		0.844		0.837
550	1.321	1.084		1.149		0.865		0.857		0.792		0.746
600		0.980		1.024		0.784		0.772		**0.772**		0.726
650		0.895		0.952		0.770		0.726		0.916	1.020	0.716
700		0.846		0.860		**0.757**		0.710		1.094	0.901	0.703
750		**0.796**		0.791		0.923	0.993	0.701			0.843	0.686
800		0.836	1.122	0.769		1.102	0.880	0.693			0.780	**0.676**
850		0.943	1.029	0.750			0.849	0.676			0.783	0.754
900		1.028	0.978	0.717			0.782	**0.670**			**0.770**	
950			0.937	0.687			0.771	0.674			0.853	
1000			0.881	0.680			0.758					
1050			0.845	**0.672**			**0.756**					
1100			0.805	0.762			0.896					
1150			**0.794**									
1200			0.835									

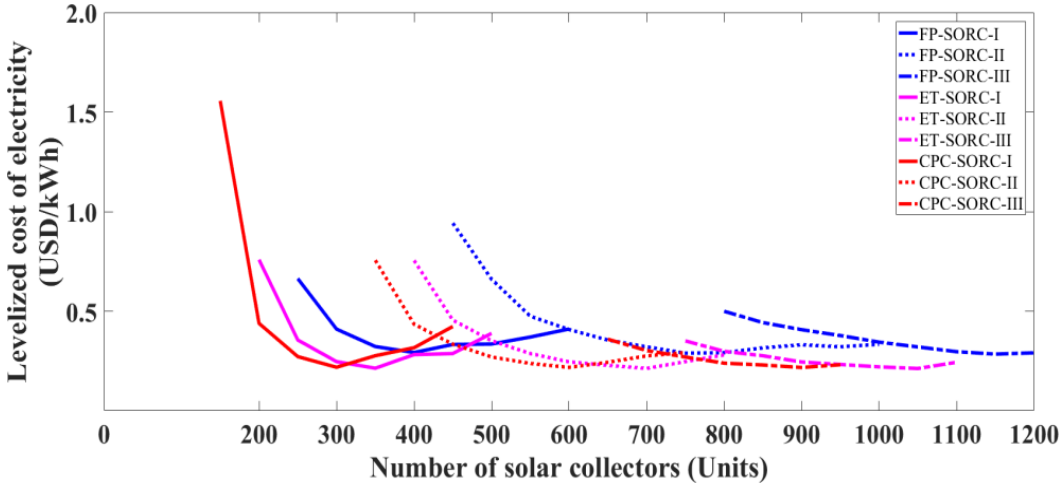

(a) SORC-I, SORC-II, and SORC-III (without initial investment of the collectors)

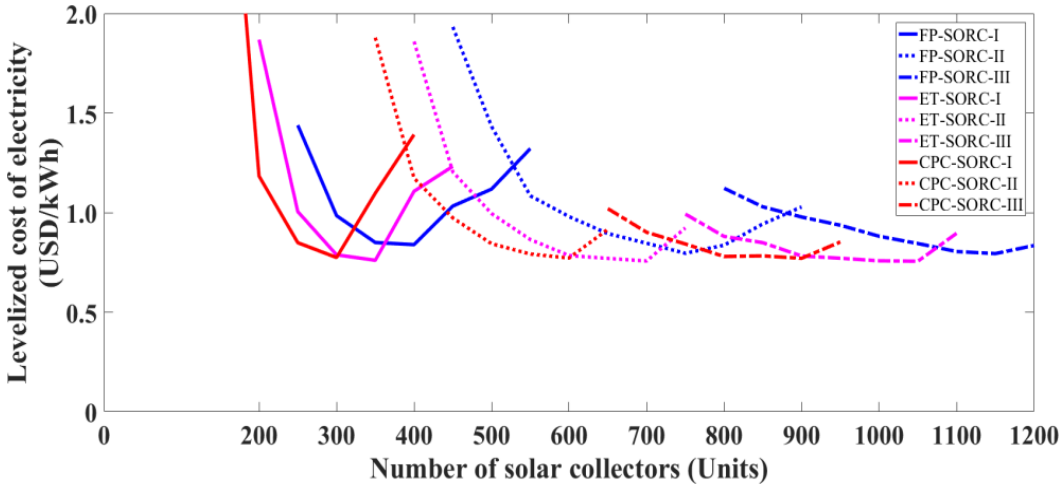

(b) SORC-I, SORC-II, and SORC-III (with initial investment of the collectors)

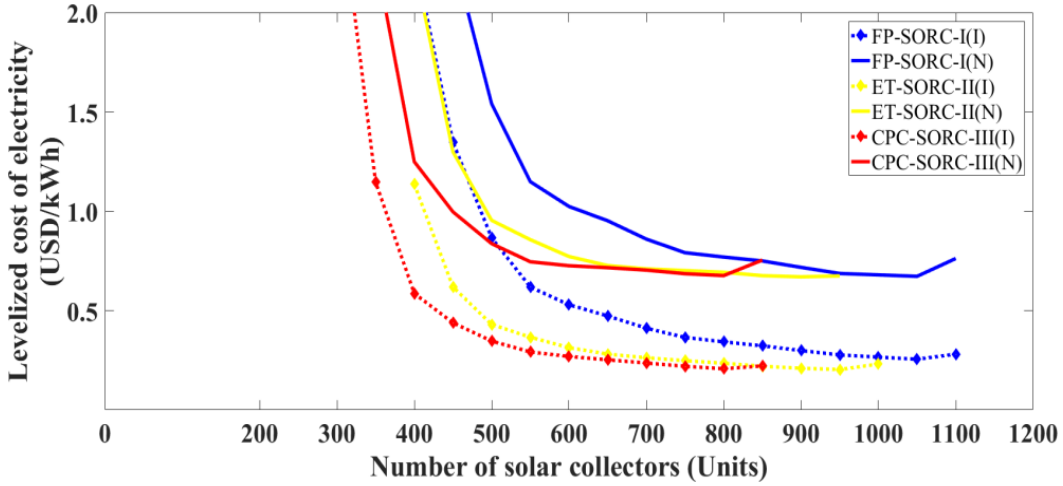

(c) SORC-IV power plant (with (I) and without (N) initial investment of the collectors)

Figure 6-26 LCOE (USD/kWh) of different system configurations (SORC-I, SORC-II, SORC-III, and SORC-IV) with different collectors (FP, ET, and CPC solar collectors)

Table 6-8 LCOE (USD/kWh) of the systems *(without initial investment of the collectors and capital cost of the ORC power plant was set at 1500 USD/kW$_e$)*

Collector (Units)	LCOE (USD/kWh)											
	FP-SORC				ET-SORC				CPC-SORC			
	I	II	III	IV	I	II	III	IV	I	II	III	IV
100												
150									0.934			
200					0.455				0.263			
250	0.398				0.213				0.163			
300	0.246				0.148				**0.131**			1.624
350	0.193				**0.128**				0.166	0.454		0.688
400	**0.175**			1.372	0.169	0.453		0.682	0.190	0.261		0.352
450	0.200	0.565		0.808	0.172	0.273		0.371	0.254	0.201		0.263
500	0.201	0.396		0.520	0.233	0.211		0.258		0.162		0.208
550	0.222	0.285		0.371		0.172		0.220		0.143		0.175
600	0.246	0.245		0.318		0.147		0.188		**0.131**		0.161
650		0.213		0.284		0.137		0.169		0.146	0.216	0.151
700		0.193		0.247		**0.128**		0.157		0.165	0.181	0.142
750		**0.173**		0.219		0.148	0.211	0.149		0.176	0.162	0.132
800		0.175	0.300	0.205		0.168	0.179	0.141			0.143	**0.124**
850		0.190	0.266	0.194			0.166	0.132			0.138	0.133
900		0.199	0.244	0.179			0.147	0.126			**0.130**	
950			0.227	0.166			0.139	**0.122**			0.139	
1000			0.207	0.159			0.132	0.138				
1050			0.192	**0.153**			**0.127**					
1100			0.178	0.169			0.146					
1150			**0.171**									
1200			0.175									

Table 6-9 LCOE (USD/kWh) of the systems *(with initial investment of the collectors: subsidized by 50 percent of total cost of collectors and capital cost of the ORC power plant is set at 1500 USD/kW$_e$)*

Collector (Units)	LCOE (USD/kWh)											
	FP-SORC				ET-SORC				CPC-SORC			
	I	II	III	IV	I	II	III	IV	I	II	III	IV
100												
150									1.924			
200					1.010				0.636			
250	0.786				0.538				0.452			
300	0.533				0.419				**0.409**			2.772
350	0.457				**0.402**				0.576	1.015		1.255
400	**0.449**			2.084	0.582	1.005		1.236	0.727	0.630		0.683
450	0.550	1.061		1.281	0.645	0.648		0.711		0.520		0.542
500	0.593	0.782		0.857	0.944	0.533		0.520		0.449		0.453
550	0.698	0.590		0.636		0.461		0.465		0.420		0.402
600		0.531		0.565		0.417		0.417		**0.408**		0.390
650		0.483		0.523		0.408		0.391		0.482	0.546	0.383
700		0.455		0.471		**0.400**		0.381		0.574	0.481	0.375
750		**0.427**		0.432		0.486	0.531	0.375			0.448	0.365
800		0.447	0.611	0.419		0.579	0.470	0.370			0.414	**0.359**
850		0.503	0.559	0.407			0.452	0.360			0.414	0.399
900		0.547	0.530	0.389			0.416	**0.356**			**0.407**	
950			0.506	0.371			0.409	0.357			0.449	
1000			0.475	0.366			0.401					
1050			0.454	**0.362**			**0.399**					
1100			0.432	0.409			0.472					
1150			**0.426**									
1200			0.447									

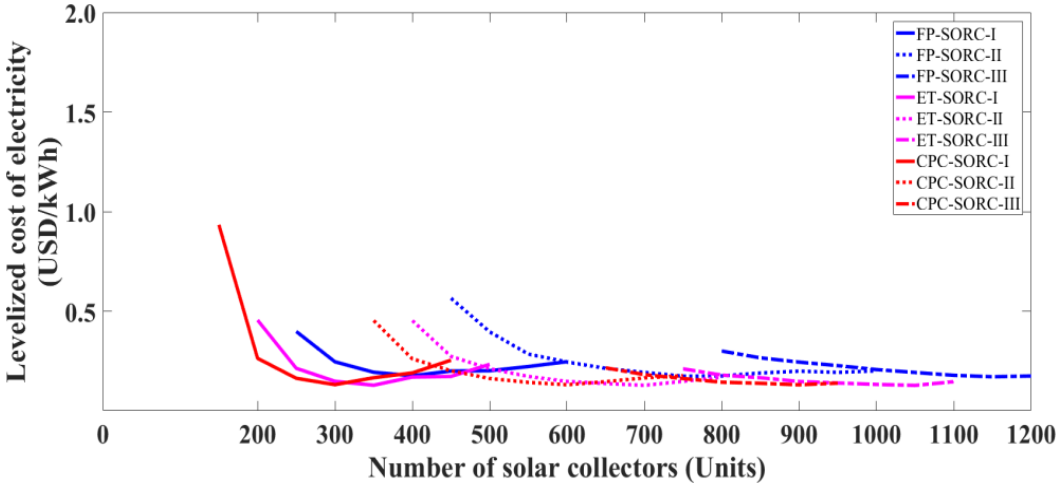

(a) SORC-I, SORC-II, and SORC-III (without initial investment of the collectors)

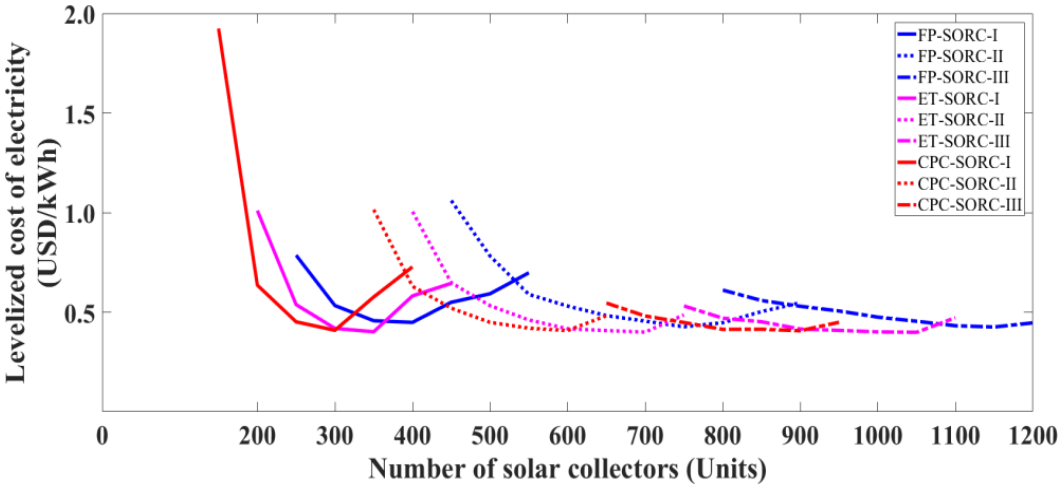

(b) SORC-I, SORC-II, and SORC-III (with initial investment of the collectors)

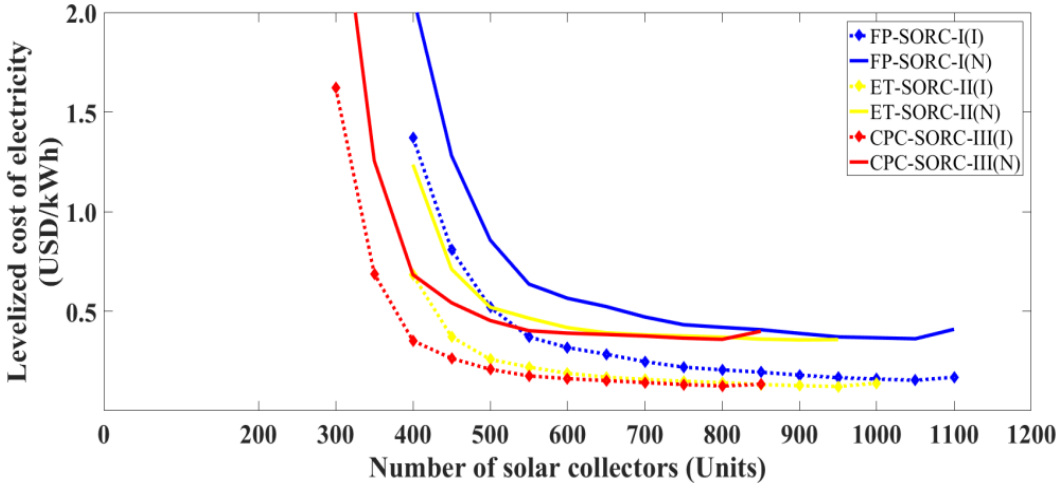

(c) SORC-IV power plant (with (I) and without (N) initial investment of the collectors)

Figure 6-27 LCOE (USD/kWh) of different system configurations (SORC-I, SORC-II, SORC-III, and SORC-IV) with different collectors (FP, ET, and CPC solar collectors), *by assumed 50 percent of total cost of solar collectors subsidized by the government as shown in* Table 6-3*, with 1500 USD/kW$_e$ of the ORC power plant)*

From the previous evaluations, when the initial investment of the collectors for ORC power systems is included, their LCOE can be achieved between 0.670 and 0.839 USD/kWh. While CSP and Photovoltaic technologies are applied for electrical power, the LCOE is between 0.140 and 0.360 USD/kWh [123], and between 0.250 and 0.710 USD/kWh [124], respectively. Therefore, the small-scale SORC power system with initial investment of the collectors is not interesting due to the highest value of LCOE. However, when the investment of the collectors is not included, their LCOE can be achieved between 0.203 and 0.293 USD/kWh, which is interesting. In other words, the system becomes more interesting, when the systems are subsidized by the government.

If the investment cost of FP, ET, and CPC collectors is subsidized by 50 percent of their total cost, their initial investment cost will be 56.14, 77.19, and 98.25 USD/m^2, respectively and capital cost of the ORC power plant is set at around 1500 USD/kW_e, then the economic evaluation can be redone as shown in Table 6-8, Table 6-9 and Figure 6-27 with both previous considered cases (with and without initial investment of the collectors). From this analysis is found that the system becomes more interesting in both cases. Furthermore, in the case without initial investment of the collectors, the system has a LCOE between 0.122 and 0.175 USD/kWh. And in remaining case the system has a LCOE between 0.356 and 0.449 USD/kWh.

6.6 Conclusions

In this Chapter, a concept of a small-scale SORC power system applied for low-temperature heat (< 100 °C) was proposed and investigated. The solar collectors consisting of flat-plate, evacuated-tube, and compound parabolic concentrator (CPC) solar collectors are used to upgrade the heat before supplying to the system. The system was mathematically modeled and simulated under the climate of Bangkok, to investigate the maximum power output, the impact on the environment, and the economic analysis in terms of levelized cost of electricity (LCOE). It can be summarized as follows:

1) A small-scale SORC power plant is suitable for below 100 °C heat sources. This technology is a good solution for power generation from low-temperature heat, in particular thermal solar energy, which is a resource that never depletes.
2) This technology can help achieving the strategy of the Thailand government of energy intensity reduction around 30 percent by 2036.
3) The CPC-SORC power system can produce the highest power output, in comparison to using the same number of collectors from the other two technologies.
4) The system become more interesting, when the government support or subsidies the investment of collectors, and the ORC system.

6.7 Information and Suggestions

For more understanding of the number limit of solar collectors used in the combination systems, this section provides a brief explanation. The steps in calculating hot water flow rate per unit of collectors ($\dot{m}_{Coll}$), rate of heat transfer ($\dot{Q}_{Coll}$), and the outlet hot water ($T_{Coll,o}$) from the SWHS are shown below.

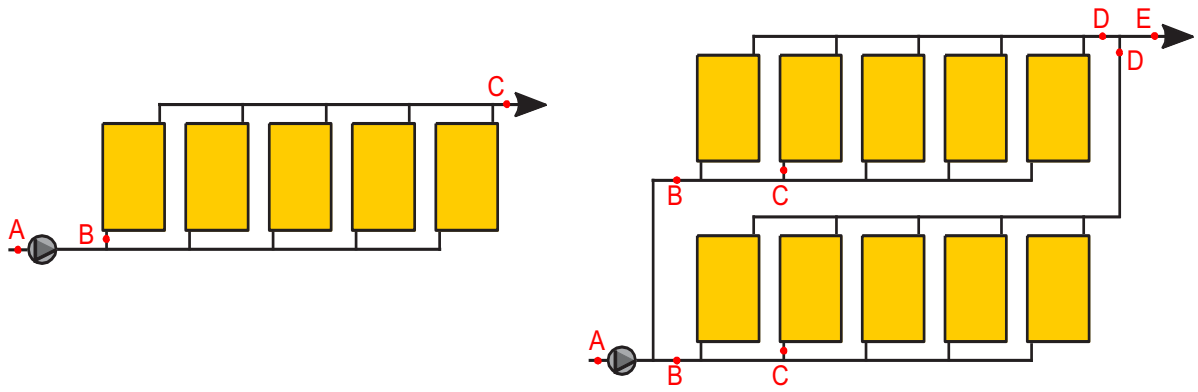

(a) Five units of solar collectors *(b) Ten units of solar collectors*

Figure 6-28 Solar collectors field connected in parallel

Example: Finding the rate of heat transfer ($\dot{Q}_{Coll}$) and outlet hot water temperature ($T_{Coll,o}$) from solar collectors field with flat-plate collectors of five and ten units connected in parallel (as shown in Figure 6-28). Assuming the collectors have the area (A_{Coll}) of 2.081 m^2 per unit, the optical efficiency ($F_R(\tau\alpha)_e$) and the overall heat transfer coefficient ($F_R U_L$) of 0.740 and 3.620 W/m^2-K, respectively. When calculated, the assumed solar energy is at 800 W/m^2, the total hot water flow rate ($\dot{m}_{Total}$) of 10 kg/s (flow rate supply to the solar collectors field), the collectors inlet hot water ($T_{Coll,i}$) of 70 °C, and ambient temperature (T_{Amb}) of 35 °C.

Eq. (2-18); $\dot{Q}_{Coll} = \dot{m}_w c_{p,w}\left(T_{Coll,o} - T_{Coll,i}\right)$

Eq. (2-19); $\dot{Q}_{Coll} = A_{Coll} F_R\left[I_T(\tau\alpha)_e - U_L\left(T_{Coll,i} - T_{Amb}\right)\right]$

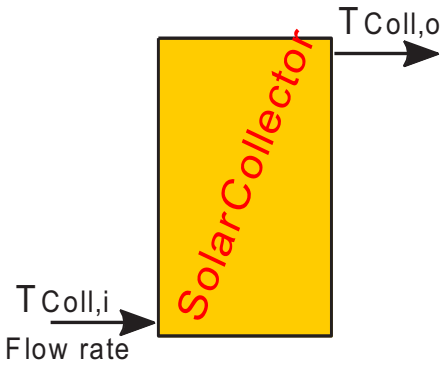

Figure 6-29 Position of the variable on the solar collectors

Case I: Five units of solar collectors *(parallel connection)* as shown in Figure 6-28 (a)

Solution

- Rate of heat transfer from the solar collectors ($\dot{Q}_{Coll}$):

Eq. (2-19) $\dot{Q}_{Coll} = (2.081\ m^2)\left[(0.740)\left(800\ \frac{W}{m^2}\right) - \left(3.620\ \frac{W}{m^2 - K}\right)(70 - 35\ K)\right]$

$\dot{Q}_{Coll} = 968.29\ W = 0.97\ kW$ *(One unit of solar collectors)*

$$\dot{Q}_{Coll} = (968.29\ W)(5) = 4841.45\ W = 4.84\ kW$$ *(Five units of solar collectors)*

- Hot water flow rate ($\dot{m}_{Coll}$):

$$\dot{m}_{Coll} = \frac{\dot{m}_{Total}}{N_{Coll}} = \frac{10\ kg/s}{5\ units} = 2\ kg/s$$ *(per unit of solar collectors)*

From Figure 6-28 (a)

$Point\ A = Point\ C = 10\ kg/s$

$Point\ B = 2\ kg/s$ *(Hot water flow rate per unit of solar collectors)*

- Collector outlet hot water temperature ($T_{Coll,o}$):

Eq. (2-18) $$\dot{Q}_{Coll} = \dot{m}_w c_{p,w}\left(T_{Coll,o} - T_{Coll,i}\right)$$

$$0.97\ kW = \left(2\frac{kg}{s}\right)\left(4.18\ \frac{kJ}{kg-K}\right)\left(T_{Coll,o} - 70\right)$$

$T_{Coll,o} = 70.12$ ℃ Ans

Case II: Ten units of solar collectors *(parallel connection)* as shown in Figure 6-28 (b)

Solution

- Rate of heat transfer from the solar collectors ($\dot{Q}_{Coll}$):

Eq. (2-19) $$\dot{Q}_{Coll} = (2.081\ m^2)\left[(0.740)\left(800\ \frac{W}{m^2}\right) - \left(3.620\ \frac{W}{m^2-K}\right)(70 - 35\ K)\right]$$

$$\dot{Q}_{Coll} = 968.29\ W = 0.97\ kW$$ *(One unit of solar collectors)*

$$\dot{Q}_{Coll} = (968.29\ W)(10) = 9682.89\ W = 9.68\ kW$$ *(Ten units of solar collectors)*

- Hot water flow rate ($\dot{m}_{Coll}$):

$$\dot{m}_{Coll} = \frac{\dot{m}_{Total}}{N_{Coll}} = \frac{10\ kg/s}{10\ units} = 1\ kg/s$$ *(per unit of solar collectors)*

From Figure 6-28 (b)

$Point\ A = Point\ E = 10\ kg/s$

$Point\ B = Point\ D = 5\ kg/s$

$Point\ C = 1\ kg/s$ *(Hot water flow rate per unit of solar collectors)*

- Collector outlet hot water temperature ($T_{Coll,o}$):

Eq. (2-18) $$\dot{Q}_{Coll} = \dot{m}_w c_{p,w}\left(T_{Coll,o} - T_{Coll,i}\right)$$

$$0.97\ kW = \left(1\frac{kg}{s}\right)\left(4.18\ \frac{kJ}{kg-K}\right)\left(T_{Coll,o} - 70\right)$$

$T_{Coll,o} = 70.23$ ℃ Ans

The abovementioned results in *Case I* and *II* show the rate of heat transfer from the solar collectors ($\dot{Q}_{Coll}$), hot water flow rate ($\dot{m}_{Coll}$), and collector outlet hot water temperature ($T_{Coll,o}$). The hot water flow rate ($\dot{m}_{Coll}$) was constant, but the number of solar collectors in

the two cases was not same. The collector outlet hot water temperature ($T_{Coll,o}$) increased when the number of solar collectors increased because the hot water flow rate per unit of solar collectors was low. Moreover, when a large number of solar collectors were installed, the system could generate high rates of heat transfer from the solar collectors ($\dot{Q}_{Coll}$). Based on these findings, it can be concluded that the highest value of hot water flow rate, as shown in Table 6-1 and Table 6-2, was selected to operate with the large amount of solar collectors. This is larger than the number limit of solar collectors used in the combination system. The collector outlet hot water temperature from the SWHS may be higher than 95 °C. In this situation, it means the system cannot generate electricity.

Accordingly, the following suggestions to improve the system operation are provided: (1) Put the thermal storage tank into the systems, as shown in Figure 6-30. The hot water flow rate that supplies the solar collectors field and the ORC system can be controlled by the collector pump and the ORC pump. (2) Design the numbers of solar collectors in each loop for the operation of the SWHS system, as shown in Figure 6-31. For instance, in the morning solar energy is low. Four loops operation for the SWHS system as shown in Figure 6-31 (a) becomes helpful for producing the needed hot water. However, at noon, solar energy is high. Three loops operation for the SWHS system as shown in Figure 6-31 (b) becomes helpful for producing the hot water.

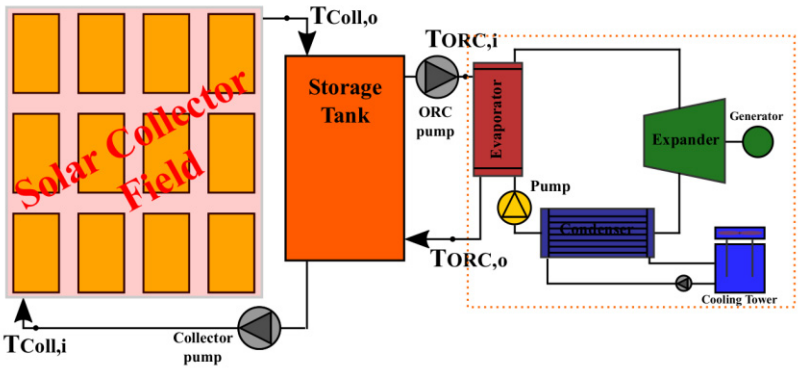

Figure 6-30 The SORC power system with thermal energy storage tank

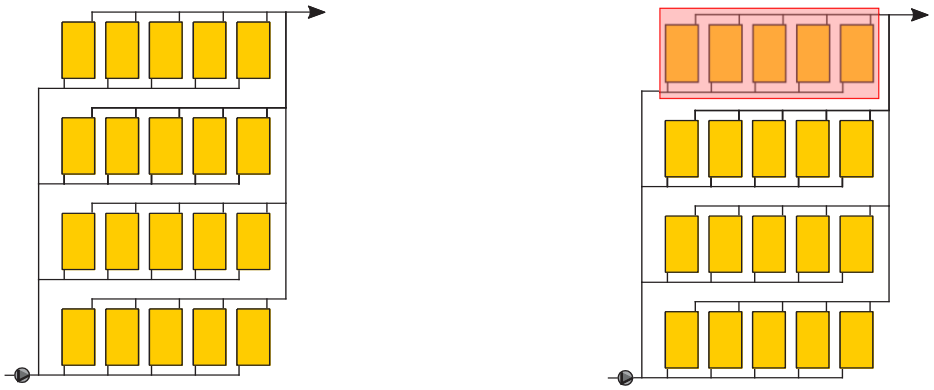

(a) Four loops operation (20 units) *(b) Three loops operation (15 units)*

Figure 6-31 Design for loop operation of the SWHS system

7

Conclusion & Future Works

In this thesis, were presented Organic Rankine Cycle (ORC) for power generation systems that take low-temperature heat from industrial waste heat (IWH) or solar water heating system (SWHS) and modeled according to Thailand's weather. A suitable working fluid for both the ORC and Vapor Compression Heat pump (VCHP) were considered. Mathematical models for all the systems have been created to find power output, CO_2 emission, and perform an economic analysis in term of levelized cost of electricity (LCOE). The main conclusions of this work can be summarized as follows:

7.1 Selection of Working Fluid for the Organic Rankine Cycle (ORC) and the Vapor Compression Heat Pump (VCHP) Systems

19 different refrigerants were considered in the selection of a suitable working fluid for each system. The simulations results showed that for the proposed ORC system, R-365mfc, R-245ca, R-245fa, and R-1234zez are valid options due to their low mass flow rate, low evaporating pressure and high thermal efficiency. In addition their low global warming potential (GWP), toxicity and non-flammable properties make them a safe and more ecological choice. As for the VCHP system, R-365mfc was the most appropriate choice due to its lower maximum temperature and pressure for the VCHP compressor, while giving a high coefficient of performance (COP) when supplies heat in the range of 70 to 90 ºC, which complies with the requirements of the proposed system.

7.2 Low-temperature Upgrading Technologies for an ORC Power Generation

In order to achieve a ORC power generation system capable of using industrial waste heat (IWH) with temperature below 70 °C different heat boosting technologies were considered, Vapor Compression Heat Pump (VCHP), Gas Engine-driven Heat Pump (GEHP), and Absorption Heat Transformer (AHT). The results indicate that the ORC power generation system combined with these proposed heat boosting technologies are applicable, in particular the most appropriate is the VCHP which its compactness, easy installation and simple operation and maintenance make its an overall great choice. This particular system performs better when the heat source is above 63 °C, giving the lowest LCOE when compared to the other technologies considered.

7.3 Power Generation from Low-grade Heat Combined with Solar Water Heating System (SWHS)

A variation on the previous system was also proposed which now considers the use of a solar water heating system (SWHS). Three types of solar collectors consisting of flat-plate, heat pipe evacuated-tube, and compound parabolic concentrator (CPC) were compared in terms of heat generation to feed the system. The results shown that, the VCHP-ORC power system is applicable for the below 70 °C heat source from low-grade IWH combined with SWHS. Type and number of solar collectors, quality and quantity of low-grade IWH, location or weather condition and number of industries in industrial estates have an effect on the system in terms of the power output, the environmental impact, and the LCOE of the system.

7.4 Small-scale Solar Organic Rankine Cycle (SORC) Power Plant

The last system presented here focuses on a small-scale type of plant, where the source temperature is below 100 °C and uses solar energy. For this three types of solar collectors consisting of flat-plate, evacuated-tube, and compound parabolic concentrators (CPC) were compared, in terms of heat generation to feed the proposed system. The results indicated that, the small-scale SORC power plant is viable for the below 100 °C heat source, making it a good technological solutions for power generation in this circumstances. It could also be determined that the type and number of solar collectors has an effect on the system in terms of the power output, the environmental impact, and the LCOE of the system. Moreover, if there is no need to invest in solar collectors since a deployment is already available, the best type in this case would be the CPC solar collectors when compared to the other two types.

7.5 Recommendation for Future Works

An extension of this work could start with the development of a dynamic version of the proposed system, including the heat boosting technologies and considering industrial waste heat or solar energy. This would lead not only to a better understanding of the system, but improvements can be made applying the knowledge gained. Another point to focus would be to exploit other available renewable sources such as geothermal and biomass. Moreover, a study in terms of exergy of the different systems proposed would be the most interesting path to continue. Additionally, the experiment of the system such the VCHP-ORC and the SORC power systems under the real condition should be carried out to compare the simulation results.

8

Appendixes

8.1 APPENDIX A Properties of Lithium Bromide-Water (LiBr-H_2O) Solutions

8.1.1 Enthalpy-Concentration and Temperature for Lithium Bromide-water (LiBr-H_2O) Solutions [86]

For concentration X < 40%LiBr, and solution temperature range 15 < t < 165 °C.

$$h = 21.4817157 - 2.38366711X + 3.90458186t + 0.03625001X^2 + 5.25010607 \times 10^{-4}t^2 - 0.0369249939tX, kJ/kg$$

For concentration 40 ≤ X < 70%LiBr, and solution temperature range 15 < t < 165 °C.

$$h = \sum_0^4 A_n X^n + t\sum_0^4 B_n X^n + t^2\sum_0^4 C_n X^n,\ kJ/kg$$

Table of coefficients A_n, B_n and C_n

A_0 = -2024.33	B_0 = 18.2829	C_0 = -3.7008214E^{-2}
A_1 = 163.309	B_1 = -1.1691757	C_1 = 2.8877666E^{-3}
A_2 = -4.88161	B_2 = 3.248041E^{-2}	C_2 = -8.1313015E^{-5}
A_3 = 6.302948E^{-2}	B_3 = -4.034184E^{-4}	C_3 = 9.9116628E^{-7}
A_4 = -2.913705E^{-4}	B_4 = 1.8520569E^{-6}	C_4 = -4.4441207E^{-9}

8.1.2 Entropy-Concentration and Temperature for Lithium Bromide-water (LiBr-H_2O) Solutions [88]

For concentration 40 ≤ X ≤ 65%LiBr, and solution temperature range 40 ≤ t ≤ 210 °C.

$$S = \sum_{i=0}^{3}\sum_{j=0}^{3} B_{ij}X^jT^i$$

Table of coefficients B_{ij}

i/j	0	1	2	3
0	5.127558E^{-1}	-1.393954E^{-2}	2.924145E^{-5}	9.035697E^{-7}
1	1.226780E^{-2}	-9.156820E^{-5}	1.820453E^{-8}	-7.991806E^{-10}
2	-1.364895E^{-5}	1.068904E^{-7}	-1.381109E^{-9}	1.529784E^{-11}
1	1.021501E^{-8}	0	0	0

8.1.3 Solution Temperature-Refrigerant Temperature and Saturation Pressure [86]

For refrigerant -15 < t′ < 110 °C, solution temperature range 5 < t < 175 °C, and concentration 45 < X < 70%LiBr.

$$t = \sum_0^3 B_n X^n + t' \sum_0^3 A_n X^n \,,\ °C$$

$$t' = \left(t - \sum_0^3 B_n X^n\right) \Big/ \left(\sum_0^3 A_n X^n\right), °C$$

$$logP = C + D/T' + E/T'^2 \,, P = kPa;\ T' = K$$

$$T' = \frac{-2E}{D + [D^2 - 4E(C - logP)]^{0.5}}$$

Table of coefficients A_n, B_n, C, D and E

A_0 = -2.00755	B_0 = 124.937	C = 7.05
A_1 = 0.16976	B_1 = -7.71649	D = -1596.49
A_2 = -3.133362E^{-3}	B_2 = 0.152286	E = -104095.5
A_3 = 1.97668E^{-5}	B_3 = -7.9509E^{-4}	

8.1.4 Density of Lithium Bromide-water (LiBr-H_2O) Solution [87]

For solution temperature range t < 250 °C, and concentration 30 < X < 65%LiBr.

$$\tilde{n}(t,m) = \tilde{n}_o(t)[1 + d_o(t)m + d_1(t)m^{1.5} + d_2(t)m^2], kg/m^3$$

$$m = w/M_s(1-w)\,, mole/kg$$

$$d_j(t) = \sum_{i=0}^{4} C_{ji} t^i$$

$$\tilde{n}_o(t) = Density\ of\ pure\ water, kg/m^3$$

$$M_s = 0.086845\ kg/mole$$

Table of coefficients $\boldsymbol{C_{ji}}$

j/i	0	1	2	3	4
0	6.9979E^{-2}	-9.36591E^{-5}	1.1770035E^{-6}	-2.829722E^{-9}	7.963374E^{-12}
1	-7.30855E^{-3}	1.78947E^{-5}	-3.458841E^{-8}	-8.88725E^{-10}	1.085224E^{-12}
2	1.811867E^{-4}	-1.9292E^{-6}	-1.565022E^{-8}	2.082693E^{-10}	-3.761121E^{-13}

8.1.5 Heat Capacity of Lithium Bromide-water (LiBr-H_2O) Solutions [88]

For solution temperature range 40 < t < 210 °C, and concentration 40 < X < 65%LiBr.

$$C_p = (A_0 + A_1 X) + (B_0 + B_1 X)t, kJ/kg - °C$$

Table of coefficients A and B

A_0 = 3.462023	B_0 = 1.3499E^{-3}
A_1 = -2.679895E^{-2}	B_1 = -6.55E^{-6}

8.1.6 Equilibrium Chart for Aqueous Lithium Bromide Solutions [86]

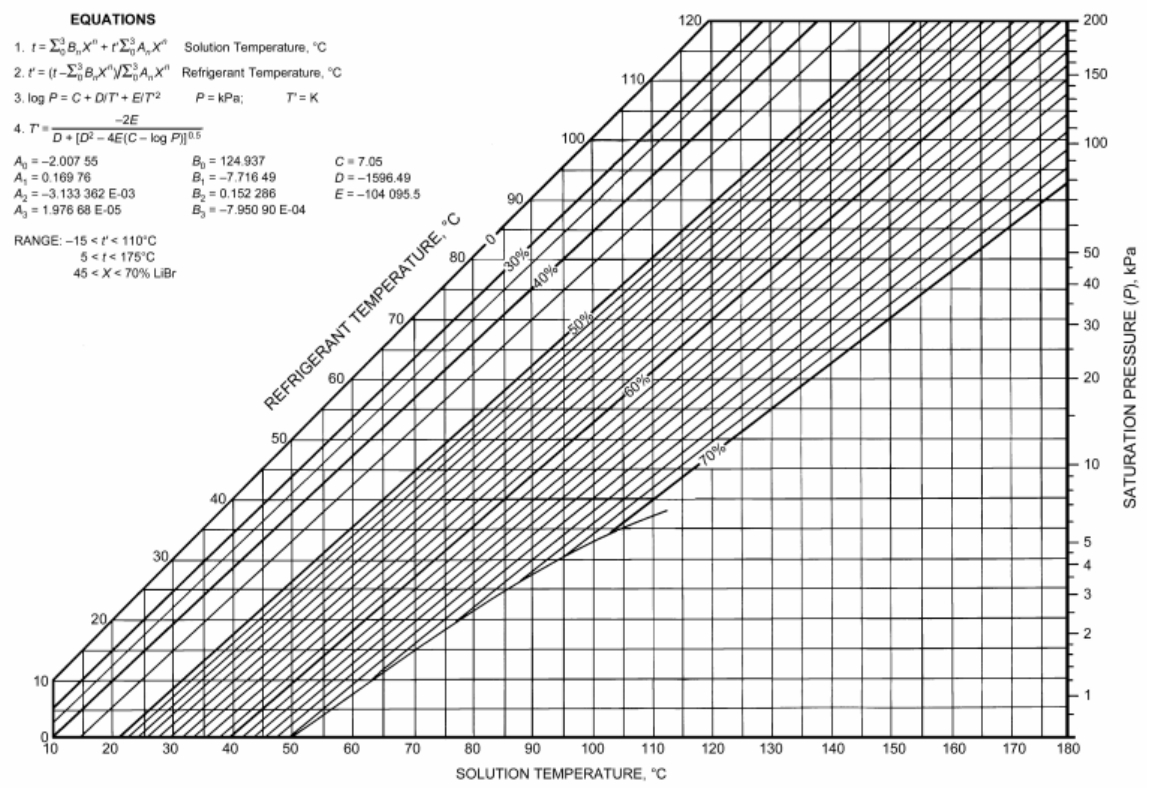

8.2 APPENDIX B Solar Radiation and Ambient Temperature

The total solar radiation on the tilted surface at Chiang Mai, Bangkok, Ratchaburi, Songkhla, Nakhon Ratchasima, and Chonburi as shown in Figure B. 1 to Figure B. 6 . And Figure B. 7 shows the total solar radiation for a day on the tilted surface.

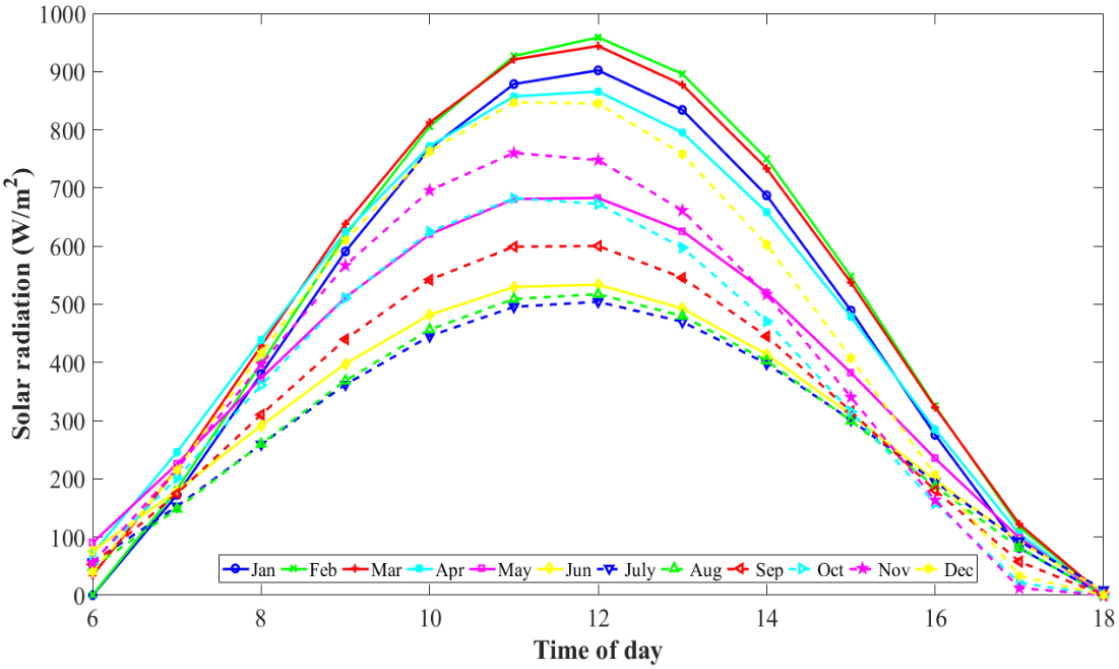

Figure B. 1 The total solar radiation on the tilted surface at Chiang Mai

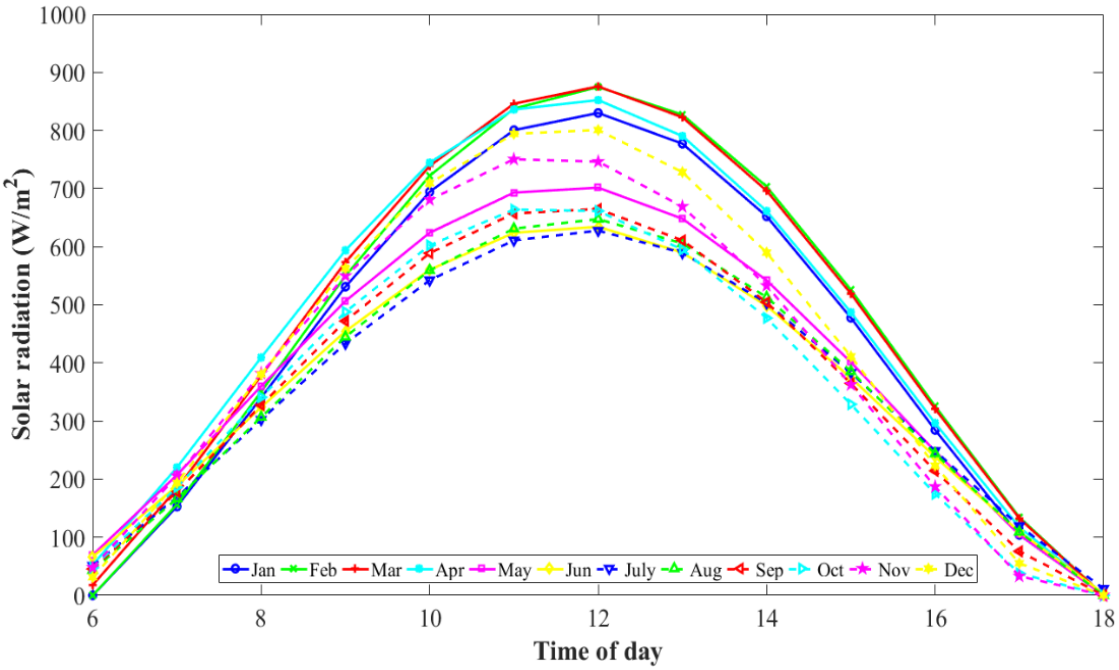

Figure B. 2 The total solar radiation on the tilted surface at Bangkok

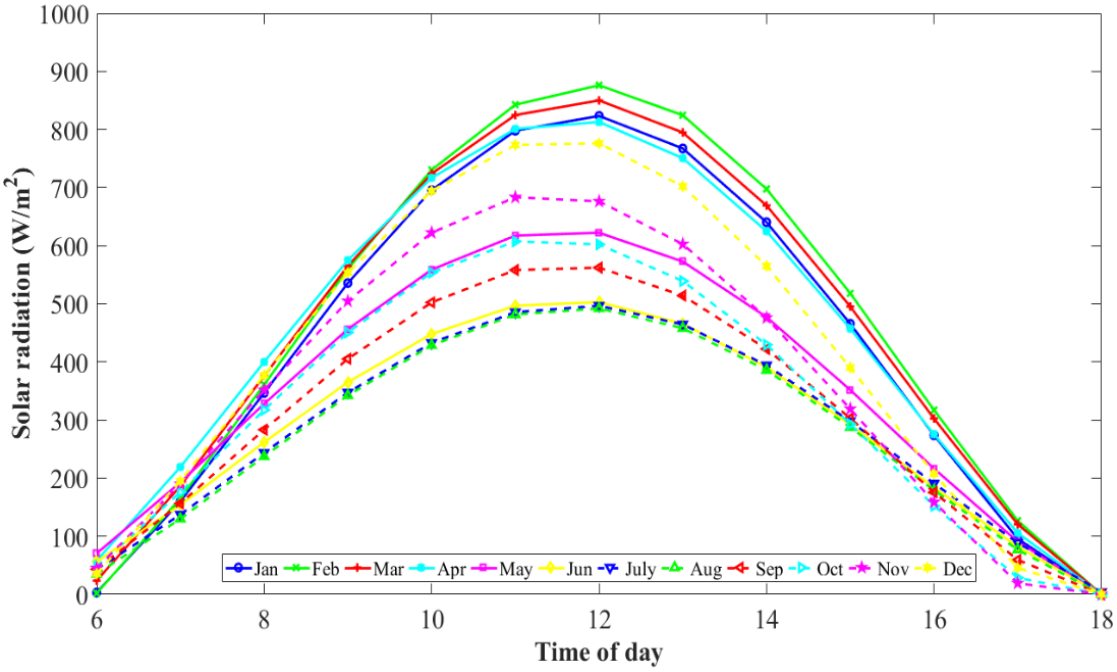

Figure B. 3 The total solar radiation on the tilted surface at Ratchaburi

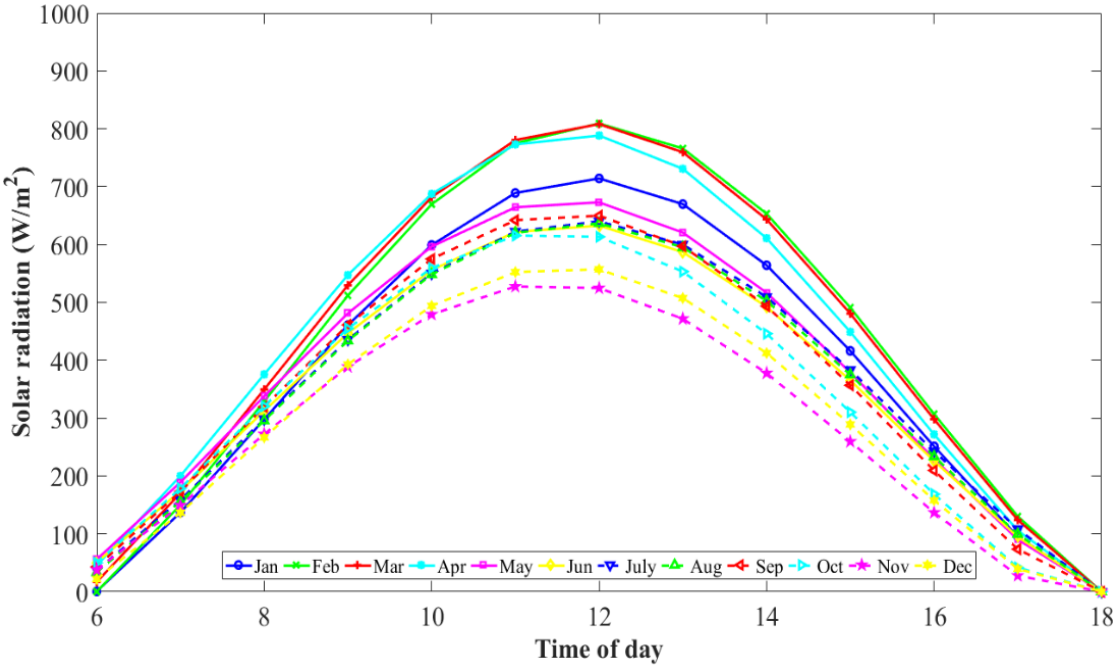

Figure B. 4 The total solar radiation on the tilted surface at Songkhla

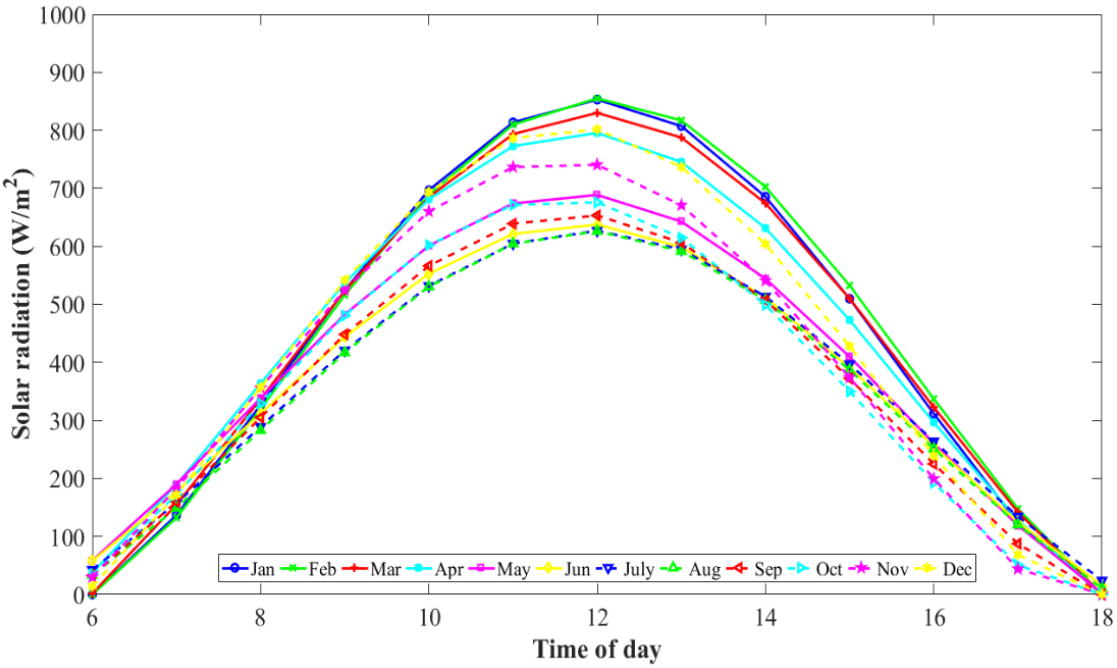

Figure B. 5 The total solar radiation on the tilted surface at Nakhon Ratchasima

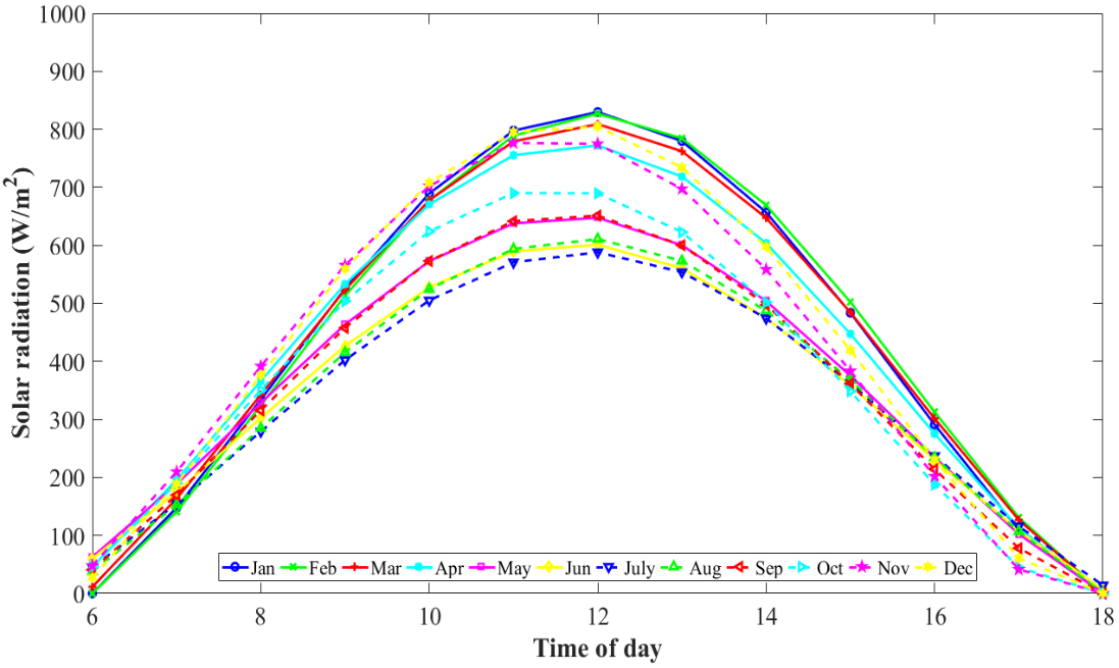

Figure B. 6 The total solar radiation on the tilted surface at Chon Buri

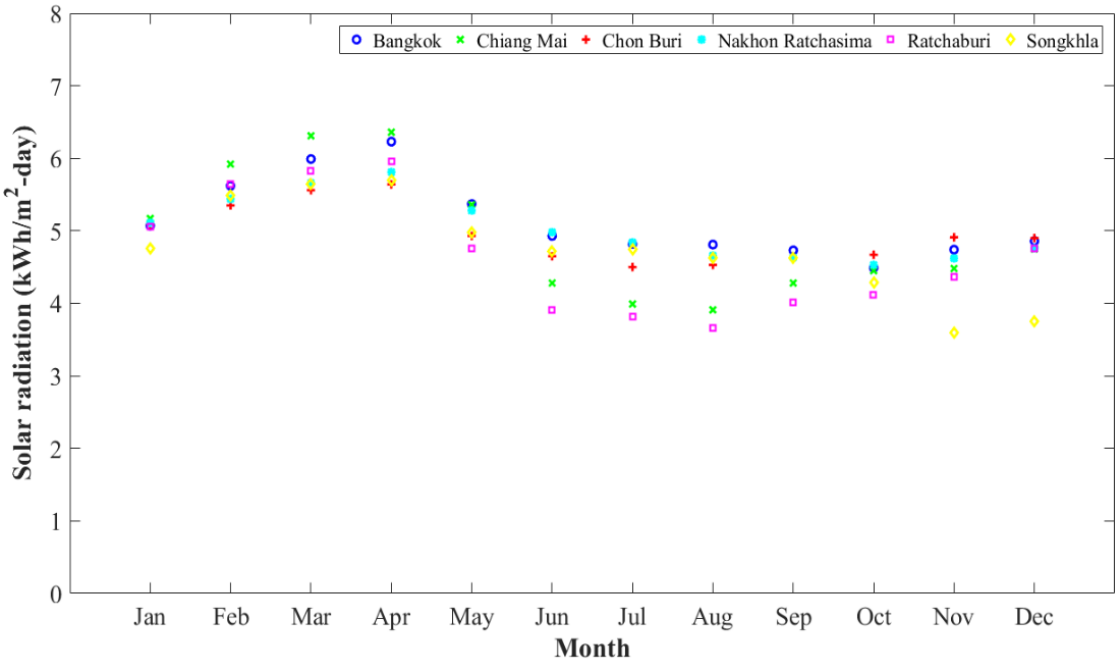

Figure B. 7 The total solar radiation (kWh/m^2-day) for a day on the tilted surface [114]

Table B 1. The average maximum-minimum temperature [114]

	Jan	Feb	Mar	Apr	May	Jun	Jul	Aug	Sep	Oct	Nov	Dec
Chiang Mai												
T_{max} $(°C)$	30.3	35.7	39.7	41.8	36.0	30.7	30.0	30.0	30.0	28.6	27.1	26.5
T_{min} $(°C)$	13.4	15.3	18.8	22.5	22.6	21.7	21.2	20.9	20.4	18.9	15.9	12.9
Bangkok												
T_{max} $(°C)$	36.8	39.4	39.1	37.3	34.6	32.3	32.3	32.0	32.6	32.1	31.3	33.2
T_{min} $(°C)$	20.5	21.8	23.2	24.3	24.7	24.3	24.0	23.8	23.6	22.7	20.7	19.4
Ratchaburi												
T_{max} $(°C)$	36.3	39.0	39.2	37.4	34.1	31.6	31.7	31.4	32.0	31.7	31.1	32.6
T_{min} $(°C)$	19.9	20.9	22.4	23.7	24.2	23.9	23.6	23.4	23.1	22.4	20.3	18.9
Songkhla												
T_{max} $(°C)$	31.1	33.4	34.3	33.9	32.6	32.1	31.9	31.8	31.8	31.5	30.5	29.9
T_{min} $(°C)$	24.0	24.4	25.3	26.3	26.7	26.4	26.1	26.0	26.0	26.0	25.6	24.5
Nakhon Ratchasima												
T_{max} $(°C)$	37.6	40.3	38.8	35.8	33.8	31.8	31.5	31.3	31.9	31.2	30.5	32.8
T_{min} $(°C)$	20.1	21.8	23.2	24.1	24.5	24.0	23.7	23.5	23.3	22.1	19.9	18.8
Chonburi												
T_{max} $(°C)$	37.4	39.3	38.4	36.4	34.2	32.2	32.0	31.7	32.3	32.0	31.3	33.6
T_{min} $(°C)$	20.8	22.1	23.4	24.3	24.7	24.3	24.0	23.8	23.6	22.6	20.6	19.5

9

Bibliography

[1] "BP Energy Outlook 2017 edition," BP Energy, 2017.

[2] "BP Statistical Review of World Energy: June 2017," BP Energy, 2017.

[3] "BP Energy Outlook 2016 edition," BP Energy, 2016.

[4] EPPO, "Alternative Energy Development Plan: AEDP2015," Department of Renewable Energy Development and Energy Efficiency (DEDE), Ministry of Energy, Thailand2015.

[5] "Thailand Alternative Energy Situation 2015," Department of Alternatve Energy Development and efficiency (DEDE), Ministry of Energy, Thailand, 2015.

[6] VV. Viswanathan, RW. Davies, and J. Holbery, "Opportunity Analysis for Recovering Energy from Industrial Waste Heat and Emissions," Pacific Northwest National Laboratory, 2006.

[7] Z. Söğüt, Z. Oktay, and H. Karakoç, "Mathematical modeling of heat recovery from a rotary kiln," *Applied Thermal Engineering,* vol. 30, pp. 817-825, 2010.

[8] "Energy Use, Loss and Opportunities Analysis: U.S. Manufacturing & Mining," U.S. Department of Energy Office of Energy Efficiency and Renewable Energy, 2004.

[9] "Waste Heat Recovery: Technology and Opportunities in U.S. Industry," BSC Incorporated, 2008.

[10] B. L. Blaney, "Project Summary: Industrial Waste Heat Recovery and the Potential for Emissions Reduction," United States Environmental Protection Agency, 1984.

[11] G. Pei, J. Li, and J. Ji, "Analysis of low temperature solar thermal electric generation using regenerative Organic Rankine Cycle," *Applied Thermal Engineering,* vol. 30, pp. 998-1004, 2010.

[12] H.-C. Jung, L. Taylor, and S. Krumdieck, "An experimental and modelling study of a 1 kW organic Rankine cycle unit with mixture working fluid," *Energy,* vol. 81, pp. 601-614, 2015.

[13] F. Calise, M. D. d'Accadia, M. Vicidomini, and M. Scarpellino, "Design and simulation of a prototype of a small-scale solar CHP system based on evacuated flat-plate solar collectors and Organic Rankine Cycle," *Energy Conversion and Management,* vol. 90, pp. 347-363, 2015.

[14] J. J. Bao, L. Zhao, and W. Z. Zhang, "A novel auto-cascade low-temperature solar Rankine cycle system for power generation," *Solar Energy,* vol. 85, pp. 2710-2719, 2011.

[15] K. Rahbar, S. Mahmoud, R. K. Al-Dadah, N. Moazami, and S. A. Mirhadizadeh, "Review of organic Rankine cycle for small-scale applications," *Energy Conversion and Management,* vol. 134, pp. 135-155, 2017.

[16] P. Garg, M. S. Orosz, and P. Kumar, "Thermo-economic evaluation of ORCs for various working fluids," *Applied Thermal Engineering,* vol. 109, pp. 841-853, 2016.

[17] Q. Sylvain and L. Vincent, "Technological and Economical Survey of Organic Rankine Cycle Systems," presented at the 5th EUROPEAN CONFERENCE

ECONOMICS AND MANAGEMENT OF ENERGY IN INDUSTRY, Hotel D. Pedro Golf Resort, Vilamoura, Algarve, Portugal, 2009.
[18] S. Quoilin, M. V. D. Broek, S. Declaye, P. Dewallef, and V. Lemort, "Techno-economic survey of Organic Rankine Cycle (ORC) systems," *Renewable and Sustainable Energy Reviews,* vol. 22, pp. 168-186, 2013.
[19] F. Campana, M. Bianchi, L. Branchini, A. De Pascale, A. Peretto, M. Baresi, A. Fermi, N. Rossetti, and R. Vescovo, "ORC waste heat recovery in European energy intensive industries: Energy and GHG savings," *Energy Conversion and Management,* vol. 76, pp. 244-252, 2013.
[20] H. Liu, Q. Zhou, H. Zhao, and P. Wang, "Experiments and thermal modeling on hybrid energy supply system of gas engine heat pumps and organic Rankine cycle," *Energy and Buildings,* vol. 87, pp. 226-232, 2015.
[21] N. Chaiyat, "Upgrading of Low Temperature Heat with Absorption Heat Transformer for Generating Electricity by Organic Rankine Cycle," *Global Advanced Research Journal of Engineering, Technology and Innovation,* vol. 3, pp. 235-247, November 2014.
[22] S. Sonsaree, T. Asaoka, S. Jiajitsawat, H. Aguirre, and K. Tanaka, "Application of low-grade industrial waste heat for power generation using organic Rankine cycle power generator combined with gas engine-driven heat pump," in *The Asian Conference on Sustainability, Energy & the Environment 2016*, 2016, pp. 443-451.
[23] B. F. Tchanche, M. Pétrissans, and G. Papadakis, "Heat resources and organic Rankine cycle machines," *Renewable and Sustainable Energy Reviews,* vol. 39, pp. 1185-1199, 2014.
[24] (1 July 2015). *KOBE STEEL, LTD, "Microbinary"*. Available: http://www.kobelco.co.jp/products/standard_compressors/microbinary/
[25] (1 January 2017). *HR Heat Recovery, "IHI Corporation"*. Available: http://www.ihi.co.jp/compressor/binary/index.html
[26] A. R. Higgo and T. J. Zhang, "Characterization of a Compact Organic Rankine Cycle Prototype for Low-grade Transient Solar Energy Conversion," *Energy Procedia,* vol. 69, pp. 1113-1122, 2015.
[27] M. Marion, I. Voicu, and A.-L. Tiffonnet, "Study and optimization of a solar subcritical organic Rankine cycle," *Renewable Energy,* vol. 48, pp. 100-109, 2012.
[28] C. Thawonngamyingsakul and T. Kiatsiriroat, "Potential of a Solar Organic Rankine Cycle with Evacuated-Tube Solar Collectors as Heat Source for Power Generation in Thailand," *Energy Science and Technology,* vol. 4, pp. 25-35, 2012.
[29] "Guide to renewable energy development and investment, Series 2: Solar Energy," Department of Alternatve Energy Development and efficiency (DEDE), Ministry of Energy, Thailand.
[30] S. Janjai, J. Laksanaboonsong, and T. Seesaard, "Potential application of concentrating solar power systems for the generation of electricity in Thailand," *Applied Energy,* vol. 88, pp. 4960-4967, 2011.
[31] I. Purohit and P. Purohit, "Techno-economic evaluation of concentrating solar power generation in India," *Energy Policy,* vol. 38, pp. 3015-3029, 2010.
[32] DEDE. (2017, 1 January 2017). *Department of Alternative Energy Development and Efficiency (DEDE), Ministry of Energy, "SOLAR HOT WATER"*. Available: http://www.solarhotwaterdede.com/en/
[33] (1 August 2017). *SOLARGIS, "Solar resource maps for Thailand"*. Available: http://solargis.com/products/maps-and-gis-data/free/download/Thailand

[34] F. Huang, J. Zheng, J. M. Baleynaud, and J. Lu, "Heat recovery potentials and technologies in industrial zones," *Journal of the Energy Institute,* vol. 90, pp. 951-961, 2017.
[35] F. Xiao-Wei, Z. Xian-Ping, J. Fu-Jun, and W. Fang, "Theoretical study of heat pump system using CO_2/Dimethylether as refrigerant," *Thermal Science,* vol. 17, pp. 1261-1268, 2013.
[36] A. Duffie Jone and A. Beckman William, *Solar Engineering of Thermal Process (4th Edition)*: John Wiley& Sons Inc, 2013.
[37] (22 November 2017). *Environmental Systems Research Institute, Inc., "Modeling solar radiation"*. Available: http://desktop.arcgis.com/en/arcmap/10.3/tools/spatial-analyst-toolbox/modeling-solar-radiation.htm
[38] S. A. Kalogirou, "Solar thermal collectors and applications," *Progress in Energy and Combustion Science,* vol. 30, pp. 231-295, 2004.
[39] Y. Tian and C. Y. Zhao, "A review of solar collectors and thermal energy storage in solar thermal applications," *Applied Energy,* vol. 104, pp. 538-553, 2013.
[40] (22 November 2017). *Alternative Energy Tutorials, "Flat Plate Collector"*. Available: http://www.alternative-energy-tutorials.com/solar-hot-water/flat-plate-collector.html
[41] (11 November 2017). *Zhejiang Gaodele New-Energy Co., Ltd, "Products"*. Available: http://www.gaodele.com/en/index.php?ac=article&at=list&tid=180
[42] (22 November 2017). *Zhejiang Sidite New Energy Co., Ltd., "Heat Pipe Solar Collector"*. Available: http://www.sidite-solar.com/product_1_heatpipesolarcollector.html
[43] (22 November 2017). *Building Services Index, "Solarmat CPC solar thermal unit"*. Available: https://www.buildingservicesindex.co.uk/entry/37016/MHG-Heating/Solarmat-CPC-solar-thermal-unit/
[44] (22 November 2017). *Power From The SUN, "Concentrating Collectors"*. Available: http://www.powerfromthesun.net/Book/chapter09/chapter09.html
[45] (22 November 2017). *Renewable Energy Sources, "Solar Power Tower"*. Available: https://newenergyportal.wordpress.com/category/solar-energy/
[46] (11 November 2017). *Four Peaks Technologies, "CONCENTRATED SOLAR POWER (CSP)"*. Available: http://solarcellcentral.com/csp_page.html
[47] S. Sonsaree, T. Asaoka, S. Jiajitsawat, H. Aguirre, and K. Tanaka, "VCHP-ORC power generation from low-grade industrial waste heat combined with solar water heating system: Power generation and CO_2 emission in industrial estate of Thailand," *Cogent Engineering,* vol. 4, 2017.
[48] R. L. Oonk, D. E. Jones, and B. E. Cole-Appel, "Calculation of performance of N collectors in series from test data on a single collector," *Solar Energy,* vol. 23, pp. 535-536, 1979.
[49] C. Chaichana, T. Kiatsiriroat, and A. Nuntaphan, "Comparison of conventional flat-plate solar collector and solar boosted heat pump using unglazed collector for hot water production in small slaughterhouse," *Heat Transfer Engineering,* vol. 31, pp. 419-429, 2010.
[50] J. Bonilla, J. Blanco, L. Lopez, and J. Sala, "Technological recovery potential of waste heat in the industry of the Basque Country," *Applied Thermal Engineering,* vol. 17, pp. 283-288, 1997.
[51] P. J. Mago, L. M. Chamra, K. Srinivasan, and C. Somayaji, "An examination of regenerative organic Rankine cycles using dry fluids," *Applied Thermal Engineering,* vol. 28, pp. 998-1007, 2008.
[52] B. Saleh, G. Koglbauer, M. Wendland, and J. Fischer, "Working fluids for low-temperature organic Rankine cycles," *Energy,* vol. 32, pp. 1210-1221, 2007.

[53] C. Thawonngamyingsakul, "Performance Analysis of an Organic Rankine Cycle with Solar Collectors and Biomass for Electricity Generation," Ph.D., Faculty of Engineering, Chiang Mai University, 2013.
[54] L. Aye, W. Charters, and C. Chaichana, "Solar heat pump systems for domestic hot water," *Solar Energy,* vol. 73, pp. 169-175, 2002.
[55] A. Hepbasli, Z. Erbay, F. Icier, N. Colak, and E. Hancioglu, "A review of gas engine driven heat pumps (GEHPs) for residential and industrial applications," *Renewable and Sustainable Energy Reviews,* vol. 13, pp. 85-99, 2009.
[56] A. Hepbasli and Y. Kalinci, "A review of heat pump water heating systems," *Renewable and Sustainable Energy Reviews,* vol. 13, pp. 1211-1229, 2009.
[57] O. Ibrahim, F. Fardoun, R. Younes, and H. Louahlia-Gualous, "Air source heat pump water heater: Dynamic modeling, optimal energy management and mini-tubes condensers," *Energy,* vol. 64, pp. 1102-1116, 2014.
[58] N. Chaiyat and T. Kiatsiriroat, "Improvement of an absorption heat transformer performance for upgrading low temperature heat by coupling with a vapor compression heat pump," *Chiang Mai University Journal of Natural Sciences, 10 (2),* pp. 315-333, 2011.
[59] S. Sanaye, M. A. Meybodi, and M. Chahartaghi, "Modeling and economic analysis of gas engine heat pumps for residential and commercial buildings in various climate regions of Iran," *Energy and Buildings,* vol. 42, pp. 1129-1138, 2010.
[60] N. Chaiyat and T. Kiatsiriroat, "Analysis of combined cooling heating and power generation from organic Rankine cycle and absorption system," *Energy,* vol. 91, pp. 363-370, 2015.
[61] N. Chaiyat, "Sustainability of alternative energy for organic rankine cycle power plant in Thailand," *Naresuan University Journal: Science and Technology,* vol. 23, pp. 45-62, 2015.
[62] R. Pitz-Paal, J. Dersch, and B. Milow, "European concentrated solar thermal road-mapping (ECOSTAR)," *European Commission, Coordinated action sustainable energy systems SES6-CT-2003-502578, Cologne,* 2005.
[63] N. Chaiyat, "Performance analysis of an absorption heat transformer with assisted vapor compression heat pump," Chiang Mai: Graduate School, Chiang Mai University, 2011.
[64] J. Bao and L. Zhao, "A review of working fluid and expander selections for organic Rankine cycle," *Renewable and Sustainable Energy Reviews,* vol. 24, pp. 325-342, 2013.
[65] L. Bo-Tau, C. Kuo-Hsiang, and W. Chi-Chuan, "Effect of working fluids on organic Rankine cycle for waste heat recovery," *Energy,* vol. 29, pp. 1207-1217, 2004.
[66] F. Heberle and D. Brüggemann, "Exergy based fluid selection for a geothermal Organic Rankine Cycle for combined heat and power generation," *Applied Thermal Engineering,* vol. 30, pp. 1326-1332, 2010.
[67] B. F. Tchanche, G. Papadakis, G. Lambrinos, and A. Frangoudakis, "Fluid selection for a low-temperature solar organic Rankine cycle," *Applied Thermal Engineering,* vol. 29, pp. 2468-2476, 2009.
[68] X. D. Wang and L. Zhao, "Analysis of zeotropic mixtures used in low-temperature solar Rankine cycles for power generation," *Solar Energy,* vol. 83, pp. 605-613, 2009.
[69] J. L. Wang, L. Zhao, and X. D. Wang, "A comparative study of pure and zeotropic mixtures in low-temperature solar Rankine cycle," *Applied Energy,* vol. 87, pp. 3366-3373, 2010.

[70] X. D. Wang, L. Zhao, J. L. Wang, W. Z. Zhang, X. Z. Zhao, and W. Wu, "Performance evaluation of a low-temperature solar Rankine cycle system utilizing R245fa," *Solar Energy,* vol. 84, pp. 353-364, 2010.
[71] M. Wang, J. Wang, Y. Zhao, P. Zhao, and Y. Dai, "Thermodynamic analysis and optimization of a solar-driven regenerative organic Rankine cycle (ORC) based on flat-plate solar collectors," *Applied Thermal Engineering,* vol. 50, pp. 816-825, 2013.
[72] F. de'Rossi, R. Mastrullo, and P. Mazzei, "Working fluids thermodynamic behavior for vapor compression cycles," *Applied Energy,* vol. 38, pp. 163-180, 1991.
[73] C. Chaichana, L. Aye, and W. W. S. Charters, "Natural working fluids for solar-boosted heat pumps," *International Journal of Refrigeration,* vol. 26, pp. 637-643, 2003.
[74] A. Schuster, S. Karellas, E. Kakaras, and H. Spliethoff, "Energetic and economic investigation of Organic Rankine Cycle applications," *Applied Thermal Engineering,* vol. 29, pp. 1809-1817, 2009.
[75] A. Stoppato, "Energetic and economic investigation of the operation management of an Organic Rankine Cycle cogeneration plant," *Energy,* vol. 41, pp. 3-9, 2012.
[76] C. Invernizzi, P. Iora, and P. Silva, "Bottoming micro-Rankine cycles for micro-gas turbines," *Applied Thermal Engineering,* vol. 27, pp. 100-110, 2007.
[77] J. S. Brown, C. Zilio, and A. Cavallini, "The fluorinated olefin R-1234ze(Z) as a high-temperature heat pumping refrigerant," *International Journal of Refrigeration,* vol. 32, pp. 1412-1422, 2009.
[78] S. Fukuda, C. Kondou, N. Takata, and S. Koyama, "Low GWP refrigerants R1234ze(E) and R1234ze(Z) for high temperature heat pumps," *International Journal of Refrigeration,* vol. 40, pp. 161-173, 2014.
[79] J. Li, J. Z. Alvi, G. Pei, J. Ji, P. Li, and H. Fu, "Effect of working fluids on the performance of a novel direct vapor generation solar organic Rankine cycle system," *Applied Thermal Engineering,* vol. 98, pp. 786-797, 2016.
[80] M. T. Nasir and K. C. Kim, "Working fluids selection and parametric optimization of an Organic Rankine Cycle coupled Vapor Compression Cycle (ORC-VCC) for air conditioning using low grade heat," *Energy and Buildings,* vol. 129, pp. 378-395, 2016.
[81] "REFPROP Version 7, Thermodynamic Properties of Refrigerants and Refrigerant Mixtures Software," ed: National Institute of Standards and Technology (NIST), U.S. Department of Commerce.
[82] A. Hepbasli, "A study on estimating the energetic and exergetic prices of various residential energy sources," *Energy and Buildings,* vol. 40, pp. 308-315, 2008.
[83] B. F. Tchanche, G. Lambrinos, A. Frangoudakis, and G. Papadakis, "Low-grade heat conversion into power using organic Rankine cycles – A review of various applications," *Renewable and Sustainable Energy Reviews,* vol. 15, pp. 3963-3979, 2011.
[84] D. M. van de Bor, C. A. Infante Ferreira, and A. A. Kiss, "Low grade waste heat recovery using heat pumps and power cycles," *Energy,* vol. 89, pp. 864-873, 2015.
[85] H. Fang, J. Xia, K. Zhu, Y. Su, and Y. Jiang, "Industrial waste heat utilization for low temperature district heating," *Energy Policy,* vol. 62, pp. 236-246, 2013.
[86] "The 2001 ASHRAE Hanbook: American Society of Heating, Refrigerating and Air Conditioning Engineers," ed: ASHRAE, 2001, p. 892.
[87] R. Khairulin, V. Gruzdev, S. Stankus, and O. Verba, "Experimental study of the density of aqueous solutions of lithium bromide at temperature of up to 250 °C in the range of mass concentrations from 30 to 65%," *Thermophysics and Aeromechanics,* vol. 13, pp. 575-583, 2006.

[88] Y. Kaita, "Thermodynamic properties of lithium bromide–water solutions at high temperatures," *International Journal of Refrigeration,* vol. 24, pp. 374-390, 2001.
[89] C. Kondou and S. Koyama, "Thermodynamic assessment of high-temperature heat pumps using Low-GWP HFO refrigerants for heat recovery," *International Journal of Refrigeration,* vol. 53, pp. 126-141, 2015.
[90] R. Rowshanzadeh, "Performance and cost evaluation of Organic Rankine Cycle at different technologies," Master, Department Of Energy Technology, KTH Royal Institute of Technology, 2010.
[91] P. Arvay, M. R. Muller, V. Ramdeen, and G. Cunningham, "Economic implementation of the organic Rankine cycle in industry," in *ACEEE Summer Study on Energy Efficiency in Industry*, 2011, pp. 12-22.
[92] S. Sénéchal, "Turboden ORC: Recent developments and new applications in organic rankine cycle technology," 21 May 2014, 2014.
[93] B. Soroka, "Application note: industrial heat pumps," *ECI Publication No. Cu0118, European Copper Institute (ECI), Brussels, Belgium,* 2015.
[94] (25 February 2016). *PTT Public Company Limited, Thailand, "Oil price in Bangkok and Vicinity"*. Available: http://www.pttplc.com/th/media-center/oil-price/pages/bangkok-oil-price.aspx
[95] EPPO, "ENERGY STATISTICS OF THAILAND 2015," Energy Forecast and Information Technology Center, Energy Policy and Planning (EPPO), Ministry of Energy, Thailand2015.
[96] (6 September 2017). *Mitsubishi Heavy Industries Air Conditioning Europe, "ETW Brochures"*. Available: http://www.mhiae.com/support-downloads/brochures
[97] (6 September 2017). *Tecogen, Inc, "Ilios Water-Source Heat Pump"*. Available: https://www.tecogen.com/heat-pumps/ilios-water-source-heat-pump
[98] (6 September 2017). *Continental Hope Singapore, "Hot Water Type LiBr Absorption Chiller"*. Available: http://www.dlhope.com.sg/our-products/hope-deepblue/hot-water-type-libr-absorption-chiller/
[99] IEA, "RENEWABLES FOR POWER GENERATION Status & Prospects: 2003 Edition," International Energy Agency (IEA)2003.
[100] J. Domínguez Bravo, X. García Casals, and I. Pinedo Pascua, "GIS approach to the definition of capacity and generation ceilings of renewable energy technologies," *Energy Policy,* vol. 35, pp. 4879-4892, 2007.
[101] D. P. Guillen and J. Zia, "Final Report: Modifications and Optimization of the Organic Rankine Cycle to Improve the Recovery of Waste Heat," Idaho National Laboratory, 2013.
[102] E. Bocci, M. Villarini, L. Vecchione, D. Sbordone, A. Di Carlo, and A. Dell'Era, "Energy and Economic Analysis of a Residential Solar Organic Rankine Plant," *Energy Procedia,* vol. 81, pp. 558-568, 2015.
[103] A. M. Delgado-Torres and L. García-Rodríguez, "Analysis and optimization of the low-temperature solar organic Rankine cycle (ORC)," *Energy Conversion and Management,* vol. 51, pp. 2846-2856, 2010.
[104] S. Baral and K. C. Kim, "Thermodynamic modeling of the solar organic Rankine cycle with selected organic working fluids for cogeneration," *Distributed Generation & Alternative Energy Journal,* vol. 29, pp. 7-34, 2014.
[105] X. R. Zhang, H. Yamaguchi, D. Uneno, K. Fujima, M. Enomoto, and N. Sawada, "Analysis of a novel solar energy-powered Rankine cycle for combined power and heat generation using supercritical carbon dioxide," *Renewable Energy,* vol. 31, pp. 1839-1854, 2006.

[106] J. Freeman, K. Hellgardt, and C. N. Markides, "An assessment of solar-powered organic Rankine cycle systems for combined heating and power in UK domestic applications," *Applied Energy,* vol. 138, pp. 605-620, 2015.
[107] P. Li, J. Li, G. Pei, A. Munir, and J. Ji, "A cascade organic Rankine cycle power generation system using hybrid solar energy and liquefied natural gas," *Solar Energy,* vol. 127, pp. 136-146, 2016.
[108] G. Pikra, N. Rohmah, R. I. Pramana, and A. J. Purwanto, "The Electricity Power Potency Estimation from Hot Spring in Indonesia with Temperature 70-80°C Using Organic Rankine Cycle," *Energy Procedia,* vol. 68, pp. 12-21, 2015.
[109] N. Chaiyat, "Assessment alternative energy for organic Rankine cycle power plant in Thailand," *International Journal of Engineering and Technology (IJET),* vol. 7, pp. 317-326, Feb-Mar 2015.
[110] S. Sonsaree, S. Jiajitsawat, T. Asaoka, H. Aguirre, and K. Tanaka, "Organic Rankine Cycle power generation from industrial waste heat recovery integrated with solar hot water system by using vapor compression heat pump as heating booster in Thailand," in *International Conference on Cogeneration, Small Power Plants and District Energy (ICUE)*, 2016, pp. 1-6.
[111] (1 Fabruary 2017). *Institute for Solar Technology (SPF), "Solar Collector Factsheet: Ezinc Superline M-1 FSB PU"*. Available: http://www.spf.ch/fileadmin/daten/reportInterface/kollektoren/factsheets/scf1623en.pdf
[112] (1 February 2017). *Institute for Solar Technology (SPF), "Solar Collector Factsheet: Eurosun DF120-6"*. Available: www.spf.ch/fileadmin/daten/reportInterface/kollektoren/factsheets/scf1655en.pdf
[113] (1 February 2017). *Solarbayer, "Vacuum Tube Collectors CPC"*. Available: www.solarbayer.com/Vacuum-tube-collector-CPC.html
[114] (1 January 2017). *Atmospheric Science Data Center, "NASA Surface meteorology and Solar Energy – Location"*. Available: eosweb.larc.nasa.gov/cgi-bin/sse/grid.cgi?email=skip@larc.nasa.gov
[115] J. Zhang, L. Zhao, S. Deng, W. Xu, and Y. Zhang, "A critical review of the models used to estimate solar radiation," *Renewable and Sustainable Energy Reviews,* vol. 70, pp. 314-329, 2017.
[116] (6 September). *Department of Industrial Works*. Available: www.diw.go.th/hawk/content.php?mode=spss59
[117] "RENEWABLE POWER GENERATION COSTS IN 2014," International Renewable Energy Agency (IRENA), 2014.
[118] L. Gagnon, C. Belanger, and Y. Uchiyama, "Life-cycle assessment of electricity generation options: The status of research in year 2001," *Energy policy,* vol. 30, pp. 1267-1278, 2002.
[119] J. Wang, Z. Yan, P. Zhao, and Y. Dai, "Off-design performance analysis of a solar-powered organic Rankine cycle," *Energy Conversion and Management,* vol. 80, pp. 150-157, 2014.
[120] A. Giostri, M. Binotti, M. Astolfi, P. Silva, E. Macchi, and G. Manzolini, "Comparison of different solar plants based on parabolic trough technology," *Solar Energy,* vol. 86, pp. 1208-1221, 2012.
[121] S. Sorawit, A. Tatsunori, J. Somchai, A. Hernan, and T. Kiyoshi, "Feasible Study of VCHP-ORC Power Generation from Low-Grade Industrial Waste Heat Combined with Solar Water Heating System in Thailand," presented at the SOLARIS 2017 Conference, Brunel University London, 2017.

[122] (1 July 2017). *GlobalMarket Group, "EuroSun DF 120 Direct flow vacuum collector"*. Available: http://www.globalmarket.com/product-info/eurosun-df-120-direct-flow-vacuum-collector-3430521.html
[123] IRENA, "RENEWABLE ENERGY TECHNOLOGIES: COST ANALYSIS SERIES: Concentrating Solar Power," International Renewable Energy Agency (IRENA)2012.
[124] IRENA, "RENEWABLE ENERGY TECHNOLOGIES: COST ANALYSIS SERIES: Solar Photovoltaics," International Renewable Energy Agency (IRENA)2012.

10

Publications

- **JOURNAL:**

[1] S. Sonsaree, T. Asaoka, S. Jiajitsawat, H. Aguirre, and K. Tanaka, "Analysis of Low-Heat Upgrading Technologies for Organic Rankine Cycle Power Generation," NU. International Journal of Science, vol. 14, pp. 43-57, 2017.

[2] S. Sonsaree, T. Asaoka, S. Jiajitsawat, H. Aguirre, and K. Tanaka, "VCHP-ORC power generation from low-grade industrial waste heat combined with solar water heating system: Power generation and CO_2 emission in industrial estate of Thailand," Cogent Engineering, vol. 4, 2017.

[3] S. Sonsaree, T. Asaoka, S. Jiajitsawat, H. Aguirre, and K. Tanaka, "A Small-scale Solar Organic Rankine Cycle Power Plant in Thailand: Three Types of Non-Concentrating Solar Collectors," Solar Energy 162C (2018), pp. 541-560.

- **INTERNATIONAL CONFERENCE:**

[4] S. Sonsaree, T. Asaoka, S. Jiajitsawat, H. Aguirre, and K. Tanaka, "Application of low-grade industrial waste heat for power generation using organic Rankine cycle power generator combined with gas engine-driven heat pump," in The Asian Conference on Sustainability, Energy & the Environment 2016, 2016, pp. 443-451.

[5] S. Sonsaree, S. Jiajitsawat, T. Asaoka, H. Aguirre, and K. Tanaka, "Organic Rankine Cycle power generation from industrial waste heat recovery integrated with solar hot water system by using vapor compression heat pump as heating booster in Thailand," in International Conference on Cogeneration, Small Power Plants and District Energy (ICUE) 2016, 2016, pp. 1-6.

[6] S. Sorawit, A. Tatsunori, J. Somchai, A. Hernan, and T. Kiyoshi, "Feasible Study of VCHP-ORC Power Generation from Low-Grade Industrial Waste Heat Combined with Solar Water Heating System in Thailand," presented at the SOLARIS 2017 Conference, Brunel University London, 2017, ISBN: 9781908549334, pp. 1-6.